

AD A 052046

AD No. ~~1~~
DDC FILE COPY

2

SOLID PROPELLANT IGNITION AND OTHER UNSTEADY
COMBUSTION PHENOMENA INDUCED BY RADIATION

[Handwritten signature]

TECHNICAL REPORT

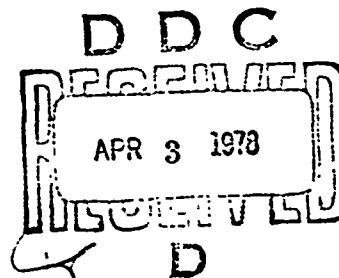
L. DELUCA, T. J. OHLEMILLER, L. H. CAVENY
AND M. SUMMERFIELD

NOVEMBER 1976

U. S. ARMY RESEARCH OFFICE
GRANTS DA-ARO-D-31-124-71-G51
DA-ARO-D-31-124-71-G184
DA-ARO-D-31-124-71-G109
DAHCO4-74-G-0125
DAHCO4-75-G-0124
DAA629-76-G-0270

DEPARTMENT OF AEROSPACE AND MECHANICAL SCIENCES
PRINCETON UNIVERSITY
PRINCETON, NEW JERSEY

APPROVED FOR PUBLIC RELEASE:
DISTRIBUTION UNLIMITED.



THE FINDINGS IN THIS REPORT ARE NOT TO BE
CONSTRUED AS AN OFFICIAL DEPARTMENT OF THE
ARMY POSITION, UNLESS SO DESIGNATED BY
OTHER AUTHORIZED DOCUMENTS.

UNCLASSIFIED

SECURITY CLASSIFICATION OF THIS PAGE (When Data Entered)

AMS-TR-1192-T

REPORT DOCUMENTATION PAGE		READ INSTRUCTIONS BEFORE COMPLETING FORM
1. REPORT NUMBER	2. GOVT ACCESSION NO.	3. RECIPIENT'S CATALOG NUMBER AMS Report No. 1192-T
4. TITLE (and Subtitle) SOLID PROPELLANT IGNITION AND OTHER UNSTEADY COMBUSTION PHENOMENA INDUCED BY RADIATION.		5. TYPE OF REPORT & PERIOD COVERED Technical rept.
7. AUTHOR(s) L./DeLuca, T. J./Ohlemiller, L. H./Caveny M./Summerfield		6. PERFORMING ORG. REPORT NUMBER
9. PERFORMING ORGANIZATION NAME AND ADDRESS Dept. of Aerospace and Mechanical Sciences, Princeton University Princeton, N.J. 08540		10. PROGRAM ELEMENT, PROJECT, TASK AREA & WORK UNIT NUMBERS 12/264p.
11. CONTROLLING OFFICE NAME AND ADDRESS U.S. Army Research Office Post Office Box 12211 Research Triangle Park, N.C. 27709		12. REPORT DATE Nov 1976
14. MONITORING AGENCY NAME & ADDRESS (if different from Controlling Office)		13. NUMBER OF PAGES 264
		15. SECURITY CLASS. (of this report) Unclassified
		15a. DECLASSIFICATION/DOWNGRADING SCHEDULE NA
16. DISTRIBUTION STATEMENT (of this Report) Approved for public release; distribution unlimited.		
17. DISTRIBUTION STATEMENT (of the abstract entered in Block 20, if different from Report) NA		
18. SUPPLEMENTARY NOTES The findings in this report are not to be construed as an official Department of the Army position, unless so designated by other authorized documents.		
19. KEY WORDS (Continue on reverse side if necessary and identify by block number) Solid Propellant Ignition Arc Image Furnace Heating Radiative Ignition Nonsteady Combustion Double Base Propellants Linear Stability Analysis Composite Propellants Nonlinear Stability Analysis CO ₂ Laser Heating		
20. ABSTRACT (Continue on reverse side if necessary and identify by block number) Experimental and analytical investigations were conducted to understand the ignition and nonsteady burning processes that occur at and near the propellant surface, to determine the connection between the ignitability of a propellant and its other nonsteady combustion characteristics, to quantify the peculiarities of radia- tive ignition, and to develop a means of ranking propellant ignit- ability. As a result of these investigations, radiative ignition processes have been explained for a wide variety of propellant and		

DD FORM 1 JAN 73 1473

EDITION OF 1 NOV 65 IS OBSOLETE

UNCLASSIFIED

SECURITY CLASSIFICATION OF THIS PAGE (When Data Entered)

288 475

JUL

UNCLASSIFIED

SECURITY CLASSIFICATION OF THIS PAGE(When Data Entered)

20. Abstract - continued

test conditions. The stability properties of heterogeneous combustion waves were considered for linear and nonlinear situations. Nonlinear (large disturbances) solid propellant stability boundaries can be immediately defined from the knowledge of the associated restoring function. The restoring function is a property strictly dependent on the nature of the solid propellant.

UNCLASSIFIED

SECURITY CLASSIFICATION OF THIS PAGE(When Data Entered)

ACKNOWLEDGMENTS

This study was conducted under the sponsorship of the U.S. Army Research Office under Grants DA-ARO-D-31-124-71-G51, DA-ARO-D-31-124-71-G184, DA-ARO-D-31-124-73-G109, DAHCO4-74-G-0124, DAHCO4-75-G-0125, and DAAG29-76-G-0270. Dr. James J. Murray, U.S. Army Research Office and Drs. Ingo W. May and Kevin J. White of the Ballistic Research Laboratories, Aberdeen Proving Ground, MD, were the technical monitors. Their technical contributions materially aided the research.

The authors thank Professors William A. Sirignano, Sau Hai Lam, and Irvin Glassman, of Princeton University for their constructive review of this research.

The performance of the experimental work was accomplished with the capable and careful assistance of the staff of the Research Group. In particular, the author is very grateful to Messrs. E. Roy Crosby, Chris R. Felsheim, James H. Semler, and Samuel O. Morris.

Warm thanks are extended to Mrs. Anne M. Chase and Miss Bridget A. Maisto for their patient and skillful typing of this report.

The first author wishes to express his gratitude to Professor Corrado Casci of Centro Nazionale di Propulsione of Politecnico di Milano for encouragement and for providing funds for the use of the computer facilities at Politecnico di Milano.

This report is also the Ph.D. Thesis of Luigi DeLuca and carries number 1192-T in the records of the Department of Aerospace and Mechanical Sciences.

White Section	<input checked="" type="checkbox"/>
Blue Section	<input type="checkbox"/>
Yellow Section	<input type="checkbox"/>
Green Section	<input type="checkbox"/>
Red Section	<input type="checkbox"/>
Black Section	<input type="checkbox"/>
A	

ABSTRACT

Ignition and transient combustion characteristics of several ammonium perchlorate composite propellants and several nitrocellulose double-base propellants were classified by their responses to strong radiant heating (5 to 100 cal/cm²-s) from laser and arc sources. The minimum exposure time to the external radiant flux required for ignition was measured in the pressure range from 5 to 21 atm using either nitrogen or air as the pressurizing gas. The experimental portion of this investigation shows that radiative sources are not suitable for rating solid rocket propellant ignitability due to the interfering effects of solid propellant optical transparency, slow chemical kinetics in the cool gas phase near the surface, combustion dynamics during the radiation termination interval, and nonuniform spatial distribution of impinging radiation. In particular, the results obtained show that addition of carbon powder may strongly decrease the required exposure time for ignition both for composite and double-base propellants (e.g., by a factor of 30 when 1% carbon is added to a double-base propellant tested in the arc image apparatus at 21 atm). Non-self-sustaining reactions are observed for the double-base propellants both in the arc image and laser ignition apparatus. Extinction of well-developed flames is observed for noncatalyzed double-base propellants following fast removal (e.g., 0.001 s at 5 - 21 atm) of the impinging radiant flux in the laser ignition apparatus.

These effects, unwanted in a routine test device, however, make radiative ignition tools particularly suitable for understanding the basic phenomena connected with unsteady heterogeneous flames. This is shown in the theoretical developments of this thesis. Analytical and numerical studies prompted by the variety of phenomena found in the experimental investigation have generated new knowledge of heterogeneous flame behavior. The theory developed to elucidate these phenomena assumes a quasi-steady gas phase; it employs properly posed flame models of the heat feedback for the specific propellant type being analyzed. With it, stability properties of heterogeneous combustion waves have been studied both for linear (small disturbance) and nonlinear (large disturbance) situations.

The linearized approach is considered first. The work by Mihlfeith on pressure and radiation driven frequency response function (acoustic admittance) has been reviewed. Improvements in the consistency of the data (the integral energy balance has to be satisfied) and in the choice of the gas phase model (a diffusion flame for composite propellants) have been made. When a diffusion flame is adopted, the nondimensional admittance function for opaque propellants is shown to be the same for variable pressure or radiation driven mechanisms. This confirms the validity of the suggestion made by Mihlfeith of testing the stability of a propellant by its response to a radiative stimulus.

However, linearized theories are intrinsically of limited value in large burning rate excursions (e.g., extinction).

The nonlinear governing set of equations is based on a parabolic partial differential equation describing the heat conduction in the condensed phase of the burning propellant. In order to ascertain general properties of this set of equations, an approximate formulation of the problem in terms of an ordinary differential equation has been derived by means of an integral method. This permits a detailed nonlinear stability analysis of solid propellant burning. Use is made of a flame model developed by Merkle-Turk-Summerfield (MTS) primarily for analysis of composite propellant unsteady burning behavior. In this model, the gas phase flame is controlled by a proper combination of mass diffusion and chemical kinetics. An algebraic function is derived that contains the basic properties (equilibrium and stability) of the burning solid propellant; this is called restoring function. It does not depend on time but only on the nature of the particular solid propellant. It is noted that the alternative approach of Zeldovich, requiring steady-state experiments, is useful in establishing intrinsic stability boundaries but cannot be extended to obtain dynamic stability boundaries. By analysis of the restoring function, it is found that, in the low burning rate region (e.g., less than 0.1 cm/s at 30 atm), both static and dynamic stability boundaries can be determined in a burning rate vs heat feedback plot. The former is defined as the line of separation between a region where stable steady state solutions are allowed and a region where only unstable steady state solutions are found; the latter is defined as that ultimate burning condition beyond which (dynamic) extinction necessarily follows. The restoring function shows that static and dynamic stability boundaries may be determined also in the high burning rate region (e.g., above 2 cm/s at 30 atm). This (upper) dynamic stability boundary is defined as that ultimate burning condition beyond which vigorous acceleration of the heterogeneous combustion wave occurs (the burning rate may increase by orders of magnitude), possibly followed by dynamic extinction. The restoring function also shows that between the two (lower and upper) static stability boundaries, the stable steady solution is either stationary (for sufficiently low values of the surface heat release, e.g., 150 cal/g at 30 atm) or of a self-sustained oscillating nature (for larger values of the surface heat release, e.g., 200 cal/g at 30 atm). A simple procedure for predicting the existence of self-sustained oscillations, based on the shape of the restoring function, is suggested.

The variety of phenomena discovered in the nonlinear stability analysis is shown to be not necessarily related to heat losses from the solid propellants. Stability boundaries hold true for both pressure and radiation timewise changes. The effects of several parameters on the stability properties (restoring function)

of burning solid propellants are classified; for example, it is shown that large pressure, residual radiant flux intensity and low surface energy release favor stability.

Numerical results, obtained by integration of the original governing partial differential equation and based on the MTS flame model, show very good agreement (generally 5 - 10% with regard to extinction condition) with the nonlinear stability analysis predictions. Computer-simulated tests yield dynamic extinction due to fast deradiation as well as the widely known dynamic extinction due to fast depressurization. The optical transparency of the propellant to radiation is shown to have a stabilizing effect on fast transients via radiant flux penetration. The importance of radiation scattering in the condensed phase is discussed and an approximate way of accounting for it is shown. For fast pressurizations, stationary equilibrium or self-sustained oscillations are observed, consistent with the theory. Dynamic extinction following fast pressurization is also observed when the surface heat release is very large (e.g., 230 cal/g at 30 atm).

In conclusion, nonlinear (large disturbances) solid propellant burning stability boundaries can be immediately defined from the knowledge of the associated restoring function. The restoring function is a property strictly dependent on the nature of the solid propellant.

TABLE OF CONTENTS

	Page
Title Page	i
Acknowledgments	ii
Abstract	iii
Table of Contents	vi
Nomenclature	ix
List of Tables	xv
List of Figures	xvii
 <u>CHAPTER 1 OBJECTIVES, BACKGROUND AND PLAN OF PRESENTATION</u>	 1
1.1 Motivations of Radiative Ignition Research	1
1.2 Background on Solid Propellant Ignition	3
1.3 Historical Background on Solid Propellant Radiative Ignition	5
1.4 Subjects Treated	8
1.5 Objectives and Plan of Presentation	9
 <u>CHAPTER 2 CRITICAL REVIEW OF RADIATIVE IGNITION EXPERIMENTAL WORK</u>	 11
2.1 Experimental Results at Low Radiant Flux	11
2.2 Experimental Results in the Arc Image Ignition Apparatus	13
2.3 Experimental Results in the Laser Ignition Apparatus	17
2.4 Summary of the Results Obtained from Radiative Ignition Experiments	18
 <u>CHAPTER 3 EXPERIMENTAL APPARATUS AND PROCEDURE</u>	 20
3.1 Description of Experimental Apparatus	20
3.2 Description of Experimental Procedure	21
 <u>CHAPTER 4 EXPERIMENTAL RADIATIVE IGNITION RESULTS</u>	 23
4.1 Comparisons Between Propellant Classes	23
4.2 Effect of Catalyst Addition in Double-Base Propellants	26
4.3 Effect of Carbon Powder Addition	28
4.4 Dynamic Extinction	29
4.5 Effect of Atmosphere in Chamber	31
4.6 Effect of Radiation Source	32
4.7 Pre-Ignition Events and Qualitative Observations in the Laser Ignition Apparatus	34
 <u>CHAPTER 5 DISCUSSION OF EXPERIMENTAL RESULTS</u>	 37
5.1 Phenomenological Description of Radiant Ignition Transients	37
5.2 A Generalized Radiant Ignition Map	38

<u>CHAPTER 6 THEORETICAL BACKGROUND ON UNSTEADY COMBUSTION OF SOLID PROPELLANTS</u>	42
6.1 The Quasi-Steady State Gas Phase Assumption	42
6.2 The MTS Flame Model	43
6.3 Matching of the Deflagration Wave at the Inter- face of the Condensed and Gas Phases	45
6.4 Further Relationships Required by the Presence of an External Radiant Flux	47
6.5 Formulation of the General Quasi-Steady Transient Problem	49
6.6 An Alternative Approach for the Gas Phase: The Mechanistic Approach of Ya. B. Zeldovich	53
<u>CHAPTER 7 LINEARIZED BURNING STABILITY ANALYSIS</u>	55
7.1 Background and Nomenclature	55
7.2 Response Function of a Burning Propellant Surface	57
<u>CHAPTER 8 NONLINEAR BURNING STABILITY ANALYSIS</u>	70
8.1 Current Status of the Theory of Nonlinear Dynamic Stability of Solid Propellant Combustion	70
8.2 Nonlinear Static Stability Analysis	72
8.3 Nonlinear Dynamic Stability Analysis (Dynamic Extinction)	85
8.4 The Question of the Critical Conditions for Dynamic Extinction	92
8.5 Lower and Upper Dynamic Stability Analysis	93
8.6 Self-Sustained Oscillations of Burning Solid Propellants	95
8.7 Further Considerations Regarding the Dynamic Burning Regime	96
8.8 Summary and Conclusions	98
<u>CHAPTER 9 NUMERICAL RESULTS</u>	101
9.1 Numerical Schemes	101
9.2 Organization of the Numerical Program	103
9.3 Checks on the Numerical Approach	105
9.4 Numerical Results from Quasi-Steady Fast Transients	105
9.5 Check of the Dynamic Stability Analysis by Computer-Simulated Tests	110
<u>CHAPTER 10 CONCLUSIONS</u>	113
10.1 Major Observations and Results	113
10.2 Conclusions	116
10.3 Suggestions for Future Work	119

References	121	
Tables	136	
Figures	149	
APPENDIX A	THE INFLUENCE OF RADIATION ON THE STEADY CONDENSED PHASE THERMAL PROFILE AND THE QUASI- STEADY GAS PHASE ASSUMPTION	210
A.1	Qualitative Picture	210
A.2	Stationary Thermal Profiles in Presence of Radiation	211
A.3	The Quasi-Steady State Gas Phase Assumption	213
APPENDIX B	RADIATION SCATTERING: EFFECT OF DISTRIBUTION FUNCTION IN THE CONDENSED PHASE	217
B.1	Description of the Physical Problem	217
B.2	Approximate Solutions of the Radiative Transfer Equation	223
B.2.1	Diffuse Irradiation in an Arc Image Furnace	223
B.2.2	Collimated Irradiation with a Laser	227
B.3	Experimental Determination of Optical Properties	228
References		232
Nomenclature		232a
List of Figures in Appendix B		233
Figures		234

NOMENCLATURE

a	= constant in ballistic mass burning rate law (see p.66) also: volume absorption coefficient, cm^{-1}
A	= constant defined in Eq. 7.2.24
A_M	= constant used in MTS flame model (see Eq. 6.2.2)
b	= constant used in KTSS surface pyrolysis law (see Eq. 6.3.5)
B	= pre-exponential factor (see Eq. 7.2.16)
B_M	= constant used in MTS flame model (see Eq. 6.2.3)
B_p	= depressurization rate coefficient (see Eq. 8.3.13)
B_r	= deradiation rate coefficient (see Eq. 8.3.14)
C	= specific heat, cal/g-K
$C_{1...5}$	= constants defined in Eq. 7.2.26
E	= activation energy, cal/mole
F	= nondimensional radiant flux intensity
H	= nondimensional surface heat release
I	= radiant flux intensity, $\text{cal/cm}^2\text{-s}$
I_o	= radiant flux intensity impinging at the propellant surface, $\text{cal/cm}^2\text{-s}$
ℓ	= nondimensional layer thickness
m	= mass flow rate, $\text{g/cm}^2\text{-s}$
n	= exponent in ballistic mass burning rate law (see p. 66)
n_s	= pressure coefficient in surface pyrolysis law (see Eq. 7.2.20)
N_t	= transparency factor (see Eq. 6.3.6)
P	= pressure, atm
PP	= nondimensional pressure
\dot{q}	= energy flux intensity, $\text{cal/cm}^2\text{-s}$
\dot{q}_f	= dimensional heat feedback from the gas phase, $\text{cal/cm}^2\text{-s}$
\dot{q}_g	= nondimensional heat feedback from the gas phase

q.s.	= quasi-steady state
Q	= heat release, cal/g
r	= surface reflectivity
r	= universal gas constant, cal/mole-K
R	= burning rate, cm/s
R_b	= response function (see Eqs. 7.2.1 and 7.2.2)
RR	= nondimensional burning rate
s	= exponent in KTSS surface pyrolysis law (see Eq. 6.3.5); also, scattering coefficient, cm^{-1}
s.s.	= steady state
t	= time, s
T	= temperature, K
TT	= nondimensional temperature (see Eq. 6.5.1b)
u	= nondimensional finite size disturbance of temperature (see Eq. 8.2.1)
u_x	= nondimensional finite size disturbance of thermal gradient (see Eq. 8.2.4)
U	= gas velocity, cm/s
W	= mass reaction rate, $\text{g/cm}^3\text{-s}$; <u>also, constant defined in Eq. 7.2.18.</u>
W_c	= mass reaction rate for a sharp flame model (see Eq. 7.2.16), $\text{g/cm}^3\text{-s}$
W_d	= mass reaction rate for a distributed flame model (see Eq. 7.2.13), $\text{g/cm}^3\text{-s}$
x	= space variable, cm
X	= nondimensional space variable

Greek Symbols:

- α = thermal diffusivity, cm^2/s ;
also, flame temperature coefficient (see Eq. 7.2.16)
- β = nondimensional parameter defined in Eq. 6.4.1
- δ = thermal layer penetration, cm ;
also, Dirac delta function
- Δ = finite difference of a quantity evaluated between
 $X=0$ and $X=-\delta$ (see Eq. 8.2.9)
- ϵ = small quantity
- $\dot{\epsilon}$ = rate of product generation, s^{-1}
- θ = nondimensional temperature
- λ = thermal conductivity, $\text{cal}/\text{cm-s-K}$; also, wavelength, μm
- Λ = constant defined in Eq. 7.2.24
- μ = microns (measurement of length), 10^{-4}cm
- ν = reaction order (see Eq. 7.2.16)
- ρ = density, g/cm^3
- τ = nondimensional time
- τ' = nondimensional time parameter defined in Eqs. 6.2.2-6.2.4
- ω = frequency, rad/s
- Ω = nondimensional frequency

Subscripts and Superscripts:

- a = ambient value
- b = burning
- c = condensed phase value
- D = dynamic
- δ = penetration depth
- f = final value;
also, flame

g	= gas
i	= initial value; also, used in finite difference scheme (see §9.1)
j	= used in finite difference scheme (see §9.1)
p	= pressure
r	= radiant
s	= surface value
S	= static
ch	= chemical
co	= conduction
di	= diffusion
op	= opaque condensed phase
re	= reaction
th	= thermal
ext	= external
rad	= radiant
ref	= reference value
-	= steady state or average value of a parameter
'	= perturbed value of a parameter
0^-	= condensed phase side of the propellant surface
0^+	= gas phase side of the propellant surface
s^-	= condensed phase side of the propellant surface fluctuating range (see Fig. 22c)
s^+	= gas phase side of the propellant surface fluctuating range (see Fig. 22c)
$-\infty$	= condition far upstream
$+\infty$	= condition far downstream

Abbreviations:

AFSC	= Air Force System Command
AIAA	= American Institute of Aeronautics And Astronautics
AN	= ammonium nitrate
AP	= ammonium perchlorate
BC	= boundary condition
BC1	= boundary condition at $x = 0$
BC2	= boundary condition at $x = -\infty$
BL-MVP	= butadiene-methylvinylpyridine
BRL	= Ballistic Research Laboratory
BUTAREZ	= carboxy-terminated polybutadiene with magnetite (see p. 10 of Ref. 85)
CC	= copper chromite
CPIA	= Chemical Propulsion Information Agency
CTPB	= carboxy-terminated polybutadiene
DB	= double base
DSC	= differential scanning calorimeter
DTA	= differential thermal analysis
GDF	= granular diffusion flame (model of steady state burning)
HMX	= Octahydro-1,3,5,7-tetranitro-1,3,5,7-tetrazocine ($C_4H_8O_8N_8$)
JSR	= Journal of Spacecraft and Rockets
KP	= potassium perchlorate
KTSS	= Krier-T'sien-Sirignano-Summerfield
MTS	= Merkle-Turk-Summerfield
NC	= nitrocellulose
NOTS	= Naval Ordnance Test Station
NWC	= Naval Weapons Center
ODE	= ordinary differential equation

ONERA = Office National d'Etudes et de Recherches Aéronautiques
PBAA = polybutadiene-acrylic acid
PBAN = polybutadiene-acrylic acid acrylonitrile
PDE = partial differential equation
PIB = polyisobutylene
PMTF = Journal of Applied Mechanics and Technical Physics
PS = polysulfide
PU = polyurethane
SRI = Stanford Research Institute
UTC = United Technology Center
UTREZ = polyisobutylene

LIST OF TABLES

Table No.	Title	Page
1	Propellants used in ignition experiments.	136
2	Scope of tests described in Chapter 4.	137
3	Summary of experimental radiative ignition works.	138
4	Measured slopes of ignition boundaries at 21 atm N_2 showing dependence of results on radiative energy source and optical properties of propellants.	139
5	Surface reflectivity and volumetric absorption of some of the tested propellants showing strong dependence on wavelength. (Values taken from Ref. 103).	140
6	Measured rates of pre-ignition gasification showing the occurrence of a stationary radiation sustained deflagration wave.	141
7	Properties of composite propellant AP/PBAA #941 used as datum case for nonlinear analysis.	142
8	Properties of the datum case used for linearized frequency response function analysis. (Values taken from Ref. 126).	143
9	Stability "measurements", according to Lyapunov, of steady state burning opaque strands of AP/PBAA #941. Results show beneficial effect of large ambient pressure and radiant flux but destabilizing effect of large surface heat release and heat loss.	144
10	Roots associated with the nonlinear static restoring function for an adiabatic opaque strand of AP/PBAA #941 deflagrating at $P = 30$ atm and $T_a = 300$ K. For all cases root C, corresponding to the trivial solution $\theta_s = 0$, is also found. The stationary unreacting configuration (root C) is always stable, while the stationary reacting configuration (root A) becomes unstable after coalescence with root D ($Q_s = -190$ cal/g).	145

Table No.	Title	Page
11	Critical values of surface heat release, at which upper dynamic instability shows up (appearance of D-E roots in Fig. 31b), in function of pressure for an adiabatic opaque strand of AP/PBAA #941 deflagrating at $T_a = 300$ K. For larger $ Q_s $, upper dynamic instability effects are manifested as vigorous accelerations of the combustion wave possibly followed by dynamic extinction. Cf. Fig. 56.	146
12	Range of values of surface heat release for which self-sustained oscillating combustion waves are expected as a function of pressure for an adiabatic opaque strand of AP/PBAA #941 deflagrating at $T_a = 300$ K. Cf. Fig. 57.	147
13	Computer simulated go/no-go tests showing strong dependence of dynamic extinction on the initial conditions and very good agreement with the lower dynamic but not the static stability boundary. Compare with Figs. 52 and 53.	148

LIST OF FIGURES

<u>Fig.</u>	<u>Caption</u>	<u>Page</u>
1a	Typical radiative ignition transient of a solid propellant showing importance of dynamic burning. Note initial burning rate overshoot and consequent undershoot.	149
1b	Representative burning rate transient due to deradiation showing possible occurrence of dynamic extinction.	149
2a	Schematic diagram of arc image ignition apparatus.	150
2b	Typical illumination profile on sample showing radiant flux intensity decreasing of about 15% from the peak value at the center of the sample toward the boundary.	150
3a	Schematic diagram of laser ignition apparatus.	151
3b	Typical illumination profile on sample showing + 20% fluctuation of radiant flux intensity on either side of the average value.	151
4	Spectral range (not to scale) of energy sources showing complicate wavelength dependence of the arc beam structure and strong relative response of the IR detection system in the 2-7 μ range.	152
5	Arc image ignition limits at 21 atm N_2 of several propellant classes showing correlation with the optical data given in Table 5.	153
6	Ignition of AP composite propellants #1, 2, 3, and 4 in the laser ignition apparatus demonstrating independence of pressure in the range 5-21 atm of N_2 or air.	154
7	Ignition of AP composite propellants #1, 2, and 4 in the arc image ignition apparatus demonstrating independence of pressure in the range 11 - 21 atm of N_2 and marked effect of radiation penetration.	155
8	Catalyzed DB propellants #9 and 10 tested in the laser ignition apparatus showing pressure dependence of ignition boundaries in the range 5 - 21 atm N_2 .	156

<u>Fig.</u>	<u>Caption</u>	<u>Page</u>
9	Dynamic extinction of noncatalyzed DB propellants #5 and #6 tested in the laser ignition apparatus. (No such boundaries noted in arc image tests.)	157
10	Arc image ignition data for HMX composite propellants #11, 12, and 13 in nitrogen and in air showing resistance to ignition.	158
11	High speed shadowgraph movie illustrating flame development of an AP composite propellant and closely coupled flame.	159
12	High speed shadowgraph movie illustrating flame development of a noncatalyzed DB propellant and large stand-off distance of the luminous zone.	160
13	High speed shadowgraph movie showing carbonaceous-appearing layer formation on the surface of a catalyzed DB propellant.	161
14	Testing of catalyzed DB propellant #10 in the arc image and laser ignition apparatus showing similarity of the two ignition maps and that pressure dependence is characteristic of the propellant not the ignition apparatus.	162
15	Addition of carbon reducing dynamic extinction domain of noncatalyzed DB propellants #7 and #8.	163
16	Arc image ignition data showing decrease of ignition delay with increase of carbon content and absence of dynamic extinction for noncatalyzed DB propellants #6, 7, and 8. (Contrast with Figs. 8 and 14).	164
17	Noncatalyzed DB propellants #6, 7, and 8, and catalyzed DB propellant #10, ignited in air, showing elimination of pressure dependence in the range 5 - 21 atm when air is the ambient gas.	165
18	Pressure dependence of strong IR signal for noncatalyzed DB propellant #6. (Weak signal is independent of pressure and ambient atmosphere.)	166

<u>Fig.</u>	<u>Caption</u>	<u>Page</u>
19	Spreading of gasification process over the surface of a catalyzed DB propellant subjected to laser heating showing presence of hot spots. Compare with Figs. 13 and 21.	167
20	Pre-ignition ablation of a catalyzed DB propellant subjected to laser radiation showing occurrence of stationary gasification process prior to the self-sustained flame. See also Table 6.	168
21	Generalized ignition map showing event limits or signals that occur during radiant heating of solid propellants.	169
22a	Schematic diagram of the physical problem.	170
22b	Schematic diagram of energy balance at the surface.	170
22c	Schematic diagram of Culick's nomenclature for the acoustic admittance function determination.	170
23a	Energy balance in differential form at the interior of a slab subjected to conductive and radiative heating.	171
23b	Steady state thermal profile in a slab subjected to conductive and radiative heating.	171
24	Determination of gas phase constants required in the MTS flame model.	172
25	Quasi-steady burning rate vs heat feedback plot according to MTS flame model.	173
26	Construction of the quasi-steady thermal gradient at the condensed/surface boundary according to Ya. B. Zeldovich.	174
27	Response function of a propellant strongly affected by the assumed flame model.	175
28	Response function of a propellant strongly affected by the pressure dependence of surface pyrolysis law and by energy release in gas phase (sharp flame model).	176

Fig.	Caption	Page
29	Response function of a propellant showing that the pressure and radiation driven frequency behavior of an opaque propellant is the same for a distributed flame model.	177
30	Destabilizing effect of large surface energy release (distributed flame model).	178
31a	Qualitative sketch of the nonlinear static restoring function, for different pressure values, illustrating the existence of three equilibrium configurations: A_i and B_i (for the reacting mode), C (for the unreacting mode). Roots B_i are statically unstable.	179
31b	Qualitative sketch of the nonlinear static restoring function, for increasing surface heat release values, illustrating the appearance of a second pair of roots, D and E , for the reacting mode (upper dynamic instability).	180
32	Influence of pressure on nonlinear static restoring function for $Q_s = -158.2$ cal/g showing upper dynamic instability at $P = 10$ atm.	181
33	Stabilizing effect of residual radiant flux intensity on lower dynamic stability boundary.	182
34a	Destabilizing effect of large surface energy release on upper dynamic stability boundary.	183
34b	Coalescence of A-D roots at $Q_s = -190.$ cal/g; the steady reacting mode is stationary for $ Q_s < 190.$ cal/g and self-sustained oscillating for $ Q_s > 190.$ cal/g. See Fig. 57.	184
35	Negligible influence of ambient temperature on nonlinear static restoring function (for the indicated range of values).	185
36	Construction of the static stability line and its meaning.	186
37a	Representative time histories of burning rate during deradiation showing possible occurrence of dynamic extinction.	187
37b	Corresponding trajectories in burning rate vs heat feedback plane.	187
37c	Nomenclature used for deradiation transients.	187
37d	Nature of nonautonomous function considered in this study.	187

<u>Fig.</u>	<u>Caption.</u>	<u>Page</u>
38	The range of possible unstable equilibrium points in dynamic burning regime is limited by the no-return point M (the unstable root associated to the static restoring function for $\tau \rightarrow \infty$).	188
39	Lower dynamic stability boundary on a burning rate vs heat feedback plane showing a sensible increase of burning region as compared with static burning regime.	189
40	Numerical molecules used in the computer solution.	190
41	Flow chart of the numerical program.	191-193
42	Destabilizing effect of large initial radiant flux intensity on dynamic burning rate. (cf. Fig. 46).	194
43	Occurrence of dynamic extinction following fast deradiation.	195
44	Sensitivity of the burning propellant to the initial conditions in the region near the lower dynamic stability.	196
45	Occurrence of damped oscillations in the dynamic burning rate following fast deradiation. (cf. Fig. 47).	197
46	Destabilizing effect of large depressurization rate on dynamic burning rate. (cf. Fig. 42).	198
47	Occurrence of damped oscillations in the dynamic burning rate following fast depressurization. (cf. Fig. 45).	199
48	Trajectories in the burning rate vs heat feedback (or MTS) plane showing that deradiation and depressurization transients follow different paths.	200
49	Radiation penetration making more difficult dynamic extinction due to fast deradiation.	201
50	Radiation penetration decreasing the intensity of the undershoot following fast deradiation.	202

<u>Fig.</u>	<u>Caption</u>	<u>Page</u>
51	Radiation penetration favoring damped oscillations of the dynamic burning rate following fast deradiation.	203
52	Go/no-go computer simulated deradiation tests in the MTS plane showing very good agreement with the predicted lower dynamic stability boundary.	204
53	Go/no-go computer simulated deradiation tests in the MTS plane showing that radiation penetration does not affect the lower dynamic stability boundary. See also Table 13 and Fig. 52.	205
54	Go/no-go computer simulated depressurization tests showing very good agreement with the predicted lower dynamic stability boundary. See also Table 13.	206
55	Computer simulated pressurization tests showing no upper dynamic instability for $ Q_s < 170$ cal/g. (cf. Tables 10 and 11.)	207
56	Computer simulated pressurization tests showing upper dynamic instability for $ Q_s > 170$ cal/g. (cf. Tables 10 and 11.)	208
57	Computer simulated pressurization tests showing self-sustained surface temperature oscillations. (cf. Tables 10 and 12).	209

CHAPTER 1

OBJECTIVES, BACKGROUND AND PLAN OF PRESENTATION

This chapter describes the purpose of the study and its connection with other studies performed at Princeton University and, more generally, with the broad field of solid propellant ignition and combustion. An introductory background to the problems investigated is offered both from a technical and historical point of view. Finally, the overall plan of presentation is given. Note that phenomena associated with solid propellant burning will be denoted throughout this study as heterogeneous combustion, since they usually involve the presence of condensed and gas phases.

1.1 Motivations of Radiative Ignition Research

This study concentrates on the ignition and nonsteady burning of solid rocket propellants. A successful ignition process is a necessary condition for a solid rocket propellant powered device to achieve the objectives of its mission. Unfortunately, even today the initiation of the deflagration wave and the subsequent transients are among the less understood and less predictable combustion phenomena. Solid propellant rocket motor ignition transients include a number of processes occurring in succession or simultaneously in a combustion chamber due to the action of some igniter: in particular, the induction interval required for the appearance of a first flame somewhere along a grain, the flame spreading over the entire surface of the grain, and the chamber filling with gaseous products. However, the ignition transient cannot be considered complete at this point since pressure overshoots following chamber filling can imperil the motor casing, sometimes causing rupture. Furthermore, a number of severe requirements on reproducibility, short ignition delays, capability of ignition in various unfavorable conditions (e.g., low temperature and vacuum), etc., are usually made for solid propellant powered devices. To ascertain the basic factors in the above processes and to avoid expensive and time consuming large scale tests, broadly-based ignition and nonsteady combustion research has evolved.

The ultimate goal of solid propellant ignition research is to predict with confidence the ignition responses of solid propellants under any set of operating conditions. From this point of view, the (propellant, combustion chamber) system should be considered.¹⁻³ However, this study emphasizes the propellant and does not consider the fluid dynamic interactions between the propellant and chamber. This means that the flame spreading and chamber filling phenomena are neglected and concentration is placed on the first ignition event and on nonsteady burning.

In practice, the ignition of solid propellants is frequently due to the action of a pyrotechnic igniter emitting hot combustion products both solid and gaseous. The ignition response of the

propellant depends on the rate of energy transfer from the pyrotechnic igniter combustion products to the mass of the initially cool solid propellant. These responses are complicated to determine, since the heat transfer occurs by simultaneous convection from the flowing hot gas, conduction from impinging incandescent particles, and by radiation both from gas and particles. Other heat sources, such as atom recombination and condensation of saturated vapors, are also present. Since each of the above modes of energy transfer is complicated greatly by the actual geometrical and physical configuration of the propellant and of the igniter combustion products, it is often advisable to restrict experimental or theoretical analysis to just one mode of energy transfer. Sources of radiant energy allow both a wide range of excursion and an accurate control of the intensity of the heat input and of the exposure time of the propellant under examination. Accordingly, this study is concerned with the ignition and non-steady burning of solid propellant by purely radiative heat transfer.

A typical radiative ignition transient is shown in Fig. 1a. The history of the burning rate illustrates the abrupt passage from an initially negligible gasification rate to a vigorous burning regime. It is apparent from Fig. 1a that the steady state (s.s.) burning rate value may be strongly exceeded (overshoot) during the ignition transient by the instantaneous burning rate peak; on the other hand, dynamic effects associated with this overshoot may involve the instantaneous burning rate following the peak value falling well below (undershoot) the s.s. value. Usually, the entire transient converges toward the s.s. burning rate after some oscillations with a period of the order of magnitude of the solid phase thermal layer characteristic time (see §9.4). A second and distinct phenomenon which will also be dealt with in this thesis is illustrated in Fig. 1b. It is shown that the abrupt (in a sense to be specified in §A.3) passage from an initial to a final burning configuration corresponding to different values of radiant flux (occurring, for example, at the end of the ignition event), may involve a precipitous undershoot leading to extinction depending on how fast the change of radiant flux is accomplished. This phenomenon is referred to as dynamic extinction (see §2.3) and may be associated with either an initially unperturbed s.s. burning regime (Fig. 1b) or a not yet completed ignition transient (Fig. 1a). Accordingly, a radiative ignition transient in its most general form includes the presence of phenomena (for example, the possibility of extinction of the sample just ignited following the cut off of the radiant source) not found in other ignition transients. Changes in any of the several parameters related either to the radiant source (level of the radiant flux, time for cutting off the radiant source, etc.) or to the propellant sample (addition of chemical additives, transparency of the propellant, etc.) affect the entire transient.

A radiant ignition transient contains a wide variety of combustion phenomena: an induction interval, starting of surface regression, fast acceleration of the burning rate, overdriven deflagration wave, undershoot of burning rate following radiant source cut off, extinction or recovery, and oscillations. This study is concerned with all these aspects (for details see §1.4) of unsteady combustion phenomena induced by radiation. In particular, detailed analysis is offered of the stability conditions for burning propellant subjected to variable pressure and/or radiant flux level.

1.2 Background on Solid Propellant Ignition

Comprehensive reviews of this subject have been offered by Summerfield⁴ in 1963, Price⁵ in 1966, Baxrère⁶ in 1969, and Merzhanov⁷ in 1971. In this section, the basic concepts are presented; a detailed review of radiant ignition research is made in the next chapter. The most recent comprehensive review on radiative ignition is contained in the work by Ohlemiller and Summerfield.⁸

The first quantitative ignition theory for a reactable substance was written by Frank-Kamenetski⁹⁻¹⁰ in his classical work on combustion in 1939. Although it later evolved in two different forms, his model can be considered the beginning of a long line of ignition research, known as thermal ignition theory, mainly developed in the Soviet Union (see Refs. 11-18, for example) in its various aspects. This theory has been adapted in several ways by many investigators. The basic hypothesis is that ignition occurs once a purely thermal condition has been satisfied. Frank-Kamenetski considered ignition to have occurred when the rate of heat production by chemical reaction exceeds the rate of heat loss to the surroundings, so that a very rapid reaction would be subsequently triggered. This idea was also used later for propellants by Hicks¹⁹⁻²⁰ and Bradley²¹ among others. Another ignition criterion is the achievement of a critical temperature at the propellant surface. This was used by Altman and Grant.²² Of particular interest to us (see §6.6) is the approach by Zeldovich,²³ later followed by other Soviet investigators, prominent among them is Librovich.²⁴⁻²⁵ Zeldovich recognizes that solid propellant ignition requires triggering chemical activity in both the gas and solid phases and the formation of a thermal layer in the condensed phase thick enough to sustain the deflagration wave. However, in the spirit of the thermal theory, Zeldovich²³ argues that the critical step is the heating of this inert layer. Other criteria of this nature are possible. Parallel to this, similar criteria may be adopted for experimental work. Commonly accepted (and often erroneous) are the first flame appearance or the achievement of a critical surface temperature.

In the search for more complete models, the ignition process has been considered to result from a critical chemical reaction whose occurrence provides the chemical activity and the thermal

energy required for starting the deflagration wave in the propellant. The complications inherent in any chemical kinetics are such that, as yet, only single one-step reactions are considered. Much controversy exists as to where to assign this single, controlling reaction. Thus, depending on the beliefs of the individual investigator, the ignition process is seen as being triggered by a single one-step reaction in the condensed phase, in the gas phase, or at the solid/gas interface.

Solid phase ignition theory assumes the triggering reaction occurs in the condensed phase. Since the ignition criteria are necessarily the same as in the thermal theory, the distinction is by no means sharp. Work along this line has been done by Baer and Ryan,²⁶ Price,^{27,28} Rosser,²⁹ Gray and Harper,³⁰⁻³² and some Soviet investigators.³³⁻³⁵ A fundamental shortcoming of thermal and solid phase theories is an inherent inability to predict the pressure dependence of the ignition process seen in experimental results. An approximate way to include these effects is indicated by Baer and Ryan.³⁶ They assume that the energy input cannot be larger than the final steady-state heat feedback which, in turn, depends on the pressure. Similar considerations were introduced by Von Elbe³⁷ and Pantoflicek.³⁸

Gas phase ignition theory assumes the triggering reaction occurs in the gas phase between decomposition products of the fuel and oxidizer. This line of research³⁹⁻⁴³ is due mainly to Summerfield and was prompted by the necessity of explaining the observed effects of pressure and oxygen presence on ignition delay. Contrary to most solid phase ignition theories, the gas phase theory predicts a continuous path from the initially cool propellant to the final steady state combustion configuration.

Heterogeneous ignition theory assumes the triggering reaction occurs between the strongly oxidizing gas products of a crystalline oxidizer (e.g., ammonium perchlorate) decomposition and the fuel surface. This line of research⁴⁴⁻⁵⁰ is due mainly to Anderson.

Because of the necessarily oversimplified assumptions in all the above models and of the many interacting processes, it has not been possible to achieve a single theory for ignition of all propellants in all situations. Indeed, a single theory is not necessary; as in other fields of research, a good understanding of a few representative cases which include the important processes may suffice for the clarification of many other cases. Accordingly, in the experimental part of this study, we have sought propellant formulations and test conditions that emphasize particular ignition events.

For the sake of completeness and to avoid confusion, notice that the above solid, gas, and heterogeneous phase ignition theories are all specific models in the area of the heterogeneous

combustion phenomena associated with solid propellants. A similar expression, "initiation of fast reactions in solids", denotes that wide branch of applied science which studies the ignition processes in the solid state. An excellent account of this subject is given in the books by Bowden and Yoffe⁵¹⁻⁵² and by Johansson and Persson.⁵³ It is shown there that the triggering mechanism may be heat, shock, light, ionizing radiation and some not yet understood internal process confined to the explosive crystal. It is of interest that the development of fast reactions in a solid, initiated by one or more of the above mechanisms, occurs in "hot spots" (definite regions of decomposition of the solid compound) which then develop into a deflagration or detonation. In this report the concepts of thermal explosion, photochemical effects, and initiation by hot spots will be occasionally borrowed.

Likewise notice that the expression "gas phase ignition theory" also denotes that specialized branch of homogeneous combustion which studies the initiation of reactions in a gas mixture. Excellent accounts of this subject are given in the classical books by Jost,⁵⁴ Lewis and Von Elbe,⁵⁵ Gaydon and Wolfhard,⁵⁶ and Williams.⁵⁷ However, no confusion should arise with the Summerfield gas phase ignition model proposed for the initiation of combustion reactions in a solid propellant (e.g., Ref. 39); the terminology is similar but the physical situations are distinctly different.

1.3 Historical Background of Solid Propellant Radiative Ignition

The well defined and easily controlled heat outputs obtainable from radiative energy sources have made the use of such devices quite popular both in rating solid propellant ignitability and in investigating the basic laws of heterogeneous combustion. However, this particular experimental tool has several inherent difficulties which initially were unsuspected; these difficulties will be discussed later. Now, a brief historical survey of the subject is given.

Possibly the first experimental data on radiative ignition were obtained by focusing sunlight on a propellant surface. This was done by Anderson and Shook⁵⁸ in 1949. Basic shortcomings of this type of experiment are the nonreproducibility of the radiative source conditions and the scattering of the data due to propellant smoking. About this same time, 1950, the theoretical analysis by Avery⁵⁹ dealing with the effect of radiation penetration on the burning rate of a tubular grain of JPT propellant was published. Avery demonstrated that in-depth absorption of radiation could lead to subsurface reactions (referred to as "wormholing"). An improvement over the original sunlight furnace for radiative ignition experiments was made by Baer, Ryan and co-workers.^{36,60-62} During a research program started in 1957 at the University of Utah, they systematically tested ammonium perchlorate (AP) and ammonium nitrate (AN) based composite propellants in a black body type of radiator obtained by electrical heating of a metallic core.

Also, they performed experiments at pressures other than one atmosphere and were the first to recognize that radiative, convective, or conductive ignition tests give, in general, different results. The details of this and of all the various other experimental works concerning radiative ignition are summarized in Chapter 2.

A decisive improvement in the experimental technique is due to Beyer and Fishman⁶³ of SRI. They adapted an arc image furnace to radiative ignition tests and, in 1960, published results on AP-based composite propellants. This was the first of a large number of papers entirely dedicated to radiative ignition research conducted using an arc image ignition apparatus.

In particular, attention is called to the work by Price,²⁷⁻²⁸ who first recognized the existence of steady gasification processes at the surface of the strand prior to ignition. Price also tested double-base (DB) propellants and examined the effect of modifiers on the ignition delay of AP propellants. Later he offered a review⁵ on the entire subject of propellant ignition.

From the beginning it was clear that some unique factors were involved in the radiative ignition experiments. For example, the presence of a cold environmental gas is not found in an actual rocket motor ignition. Likewise, several factors due to the physics of the radiation are not found in the usual convective or conductive ignition experiments. To elucidate the unique consequences of this experimental technique and also to resolve some controversies concerning the experimental procedures, a round-robin study was initiated in 1964.⁶⁴⁻⁶⁵ Due to several difficulties, a brochure was not published until 1973. The important points are that:

- (1) the arc image has certain advantages: supply of energy in a form independent of the test sample's environment; environment can be controlled over a wide range of pressure; evolved gas may be analyzed; energy flux is easily controlled and reproducible over a wide range; sample may be continuously observed by means of a transparent cell; and limitations (radiation penetration and cold, chemically-inert atmosphere are not typical of rocket motor ignition).
- (2) the report suggests suitable factors in apparatus design (maximum transmission of energy, accuracy of positioning of test sample, ease of flushing out combustion products, etc.), experimental procedure (ignition criterion, time delay measurement, calibration of focal volume, etc.) and data reduction (statistical treatment for each ignition criterion).

- (3) the difficulty in relating arc image ignition test data to ignition in solid propellant powered devices (radiation absorption, heterogeneous optical properties and effect of cold atmosphere) is discussed.

Even though no standard test procedures are recommended, this brochure helps to systemize radiant ignition experimentation.

A number of papers were published dealing more with specific effects of the radiation/propellant interaction than with furnishing further ignition data. Bastress⁶⁶⁻⁶⁷ made progress in this direction. Measurements of cut propellant reflectivities in the arc image wavelength range indicated that at least the AP composite propellant surface is, to a good approximation, a diffuse reflector. Ignition delay results were shown to be independent of the wavelength. Additional values for propellant reflectivity were given by Sutton and Wellings,⁶⁸ who also discuss the use of opacifiers at the surface of the strand to concentrate in a thin layer the absorption of radiation. Absorption in depth was also considered at SRI.^{29,69} Further comments were given by Fleming and Derr.⁷⁰ Unfortunately, radiation scattering has been generally neglected and, therefore, the results are strongly suspect. For example, the data collected at SRI were obtained from experiments performed on pressed samples so that the unusually large values of absorption coefficient measured are very likely due to scattering. Other peculiar effects, such as bubbling of the binder or quicker vaporization of the binder as compared with AP, have also been observed⁷¹⁻⁷² in radiative ignition tests. For a critical review of these and other unique factors, the reader is referred to Ohlemiller and Summerfield (see pp. 6-10 of Ref. 8a).

Other papers⁷³⁻⁷⁵ distilled unifying concepts from the large amount of experimental data which were being collected. Anderson⁷³ at UTC offered an interpretation of the data in terms of his heterogeneous phase ignition theory. Baer and Ryan³⁶ gave an approximate model for the ignition response of a solid propellant in the framework of solid phase theory. A comprehensive critical analysis of the arc image as a radiative source for ignition tests was offered by Summerfield and Ohlemiller⁷⁵ in 1968.

In an effort to overcome the difficulties inherent in the use of the arc image, a laser ignition apparatus was developed at Princeton University. The laser radiation, being collimated and monochromatic, allows a much simpler interpretation of the results. The first results obtained in the laser ignition apparatus were for tests of polymeric materials in an oxidizing atmosphere. Reference 8 also contains a complete description of the experimental apparatus used in this study. Several effects peculiar to ignition experiments performed with the laser source were investigated at Princeton in a series of works⁷⁶⁻⁷⁹ and are partly discussed in this report.

Further papers concerning wholly or partly radiative ignition research, both from experimental and theoretical points of view, are given in Refs. 80-89. The relevant details of the experimental works are discussed and summarized in Chapter 2.

1.4 Subjects Treated

Ignition characteristics of several classes of solid propellants ignited by radiative heating differ markedly depending not only on the differences in their chemical reactions but also on the radiative ignition device. This study summarizes the ignition responses of several propellants and offers interpretations of certain radiative ignition characteristics and the effects of various propellant additives on the ignition events. As new propellants and new propellant ingredients arise, their ignition characteristics are of interest. Although the ignition data are useful in themselves, the main purpose of our radiative ignition experiments was to elucidate the mechanism of ignition and combustion in terms of the gas phase, surface, and condensed phase processes and not to provide a direct means of rating propellant ignitability for particular applications. Indeed, we show that relating radiative ignition data to the convective and conductive conditions prevalent in most applications is questionable because of: (1) distorting effects of solid propellant transparency and reflectivity, (2) slow chemical kinetics in the cool gases near the surface, (3) combustion dynamics during the stop-radiation interval, and (4) spatial distribution of impinging radiation.

This work goes beyond a previous analysis⁷⁵ of radiative ignition (which covered in-depth radiation penetration and cool gas phase considerations) since the effects of spatial and time distributions of radiation and radiation sources are treated as well. Also, our recent theory⁷⁷ of extinguishment following rapid deradiation (i.e., removal of the radiant flux from the propellant surface) is applied to propellants in this work by relating the flame dynamics following deradiation to the global combustion characteristics.

In previous studies, ignition maps with complex boundaries have stimulated discussion and analyses of the underlying combustion mechanisms. For example, Price and co-workers²⁸ developed ignition maps which showed interactions between condensed phase reactions, gas phase reactions, free convection, and dilution of the flame zone by chamber gases. Also, Lenchitz and co-workers⁸⁷ discovered several difficult to explain ignition trends during their examination of thin nitrocellulose films. In the spirit of this work, complex interactions of the ignition trends are welcomed because they are often useful in deducing information about the ignition and transient burning processes.

Particular attention has been given to the phenomena of dynamic extinction, since it encompasses several problems of heterogeneous flame theory. As such, the dynamic extinction might provide an easy and meaningful way of testing the stability properties of a propellant when subjected to disturbances. This idea has already been suggested by Mihlfeith and is more fully discussed in this report. To show peculiarities of radiative-controlled combustion versus pressure-controlled combustion, computer simulated tests were performed. This required the numerical integration of a parabolic partial differential equation (PDE). In the computer simulated tests it was noted that, in a transient, the propellant is able to burn even beyond the static stability line as defined by Zeldovich or by other intrinsic stability analyses. This fact generated further interest in the dynamics of heterogeneous flames. It is shown that the use of a static stability boundary is not only wrong in principle but also might give a bad approximation of the actual dynamic stability boundary. A method is offered for evaluating separately both the static and the dynamic stability boundaries in conditions of nonlinear behavior. The quasi-steady assumption has been required for all analytical and numerical treatments. The granular diffusion flame (GDF) theory, in its quasi-steady version known as (MTS) Merkle-Turk-Summerfield flame model,⁹⁰ has been adopted as a gas phase model and has been extended to the deradiation situation. Theoretical results, both analytical and numerical, are given mostly for the specific case of an AP-based composite propellant. The MTS flame model can, however, be specialized to DB propellants, as shown by Merkle (see Ref. 90b).

A critical review of the quasi-steady assumption has been offered by Krier and Summerfield.⁹¹ A critical analysis of deradiation tests will be offered in Chapter 2 of this work. The reader is assumed to be familiar with the Zeldovich analysis of unsteady heterogeneous flames as presented in Ref. 92. Such familiarity will aid in appreciating the utility of gas phase models when dealing with complex aspects of unsteady combustion.

All of the above theoretical results have been found within the context of the simplifying assumptions that the distribution of radiant flux in the condensed phase can be described by Beer's law. This is generally untrue, as already mentioned. Therefore, a background in radiation scattering is offered in Appendix B of this work. It will be shown how to account for this effect in the mathematical model and some results will be given.

1.5 Objectives and Plan of Presentation

In the experimental part of this study a general characterization of the radiative ignition process will be sought. The following are specific objectives:

1. characterization of solid propellant radiative ignition trends through systematic experimental testing (see Table 1 and 2) in various operating conditions;
2. characterization of radiative energy source through a comparison of arc image versus laser (see §3.1 and 4.6);
3. ascertaining the relevance of radiative ignition research to actual rocket motor configuration;
4. deduction of a generalized radiative ignition map accounting for the wide variety of phenomena experimentally observed (see §5.2).

In the theoretical part of this study a deeper understanding of dynamic burning will be sought. The following are specific objectives:

1. definition of a nonlinear static stability boundary (see §8.2);
2. definition of a nonlinear dynamic stability boundary (see §8.3);
3. comparison of dynamic extinction due to depressurization with dynamic extinction due to deradiation;
4. review of previous works on radiation driven response function as a tool for studying linearized instability of solid propellant combustion (see Chapter 7).

The overall plan of presentation is the following. A critical review of radiative ignition experimental work (Chapter 2) introduces the reader to the experimental part of this investigation (apparatus is described in Chapter 3, results are given in Chapter 4, and discussions are offered in Chapter 5). A background on unsteady combustion of solid propellants (Chapter 6) introduces the reader to the theoretical part of this investigation. The linearized approach is discussed in Chapter 7 and the nonlinear approach is presented in Chapter 8. Results by numerical integration of the governing equations are shown in Chapter 9. A summary of major observations, conclusions and suggestions for future work are given in Chapter 10. Finally, some problems associated with radiation interaction with the condensed phase are discussed in Appendices A and B. The propellants used in experimental tests are listed in Table 1. The experiments performed are summarized in Table 2. Some details of the experiments in the radiative ignition area performed by previous investigators, including some Soviet, are discussed in the next chapter and are summarized in Table 3.

CHAPTER 2

CRITICAL REVIEW OF RADIATIVE IGNITION EXPERIMENTAL WORK

This chapter is a review of the results obtained in experimental investigations specifically dedicated to radiative ignition. An historical background on the overall question of radiative ignition research has been given in §1.3. The experimental details of the papers mentioned in this chapter are summarized in Table 3.

In §2.1 the results obtained testing solid propellant at low (up to about $15 \text{ cal/cm}^2\text{-sec}$) radiant flux are discussed. The results obtained with a strong (up to about $150 \text{ cal/cm}^2\text{-sec}$) radiant flux are discussed in §2.2 (arc image furnace) and in §2.3 (laser furnace). Finally, some comments about the organization of Table 3 are given in §2.4.

2.1 Experimental Results at Low Radiant Flux

This section discusses results obtained using several types of radiation heat sources. They have in common only the fact that the level of the incident radiant fluxes is less than about $15 \text{ cal/cm}^2\text{-sec}$. This is an arbitrary but useful distinction. Indeed, virtually all of the experimental investigating performed prior to the advent of arc image and laser ignition apparatus fall in this category of "low radiant flux" tests. Researchers resorted to many of the possible means to obtain radiative energy sources, but several of these early works are simply out of date in view of the current level of sophistication.

The experiments by Anderson and Shook⁵⁸ already mentioned in §1.3 have only historical interest. The use of sunlight is too uncontrollable for scientific purposes. Some experiments by Altman and Nichols (p. 2 of Ref. 80), although rough, first tested whether in the wavelength range from 0.18 to 0.58μ (UV to orange light) the radiation effect is purely thermal. This was checked by testing disks of ammonium nitrate (AN) based composite propellants in a 50 lb thrust motor started by gasless igniters containing metallic constituents. The considerable radiation emission of the igniting mixture in the UV was suspected as a possible source of photo-chemical activation, but no evidence could be found in support of this hypothesis.

The first radiative furnace purposely designed for testing solid propellant ignition trends is the black-body type of radiator developed by Baer and Ryan of the University of Utah and used extensively both in this country^{26,60-62,84} and the Soviet Union.⁹³⁻⁹⁵ Although much less flexible than the arc image and the laser apparatus, this electrical furnace was used with excellent results by Baer and Ryan in particular.

The first systematic analysis of solid propellant radiative ignition was started at the University of Utah in 1957 as a part of a broader program on combustion transients of solid rocket propellants. Results, partially published in Refs. 60-61, are summarized in Ref. 62. The radiative source was a black body type of radiator energized by electrically heating the furnace core. The level of the radiant flux could be changed by varying the current to the heating element. Four composite propellants were tested: three containing AP with different polymeric binders and one containing AN. Pressure (0.2 - 11 atm), type of pressurizing gas (air, nitrogen, or oxygen), and initial sample temperature (-60 to +60 C) were the basic variables whose effects were checked. These and other experimental details are summarized in Table 3. This type of experiment is relatively unsophisticated compared to succeeding works. For example, the radiant flux intensity was evaluated by means of the Stefan-Boltzmann law once the furnace temperature had been measured with a thermocouple; the optical properties were only roughly approximated. The low intensity of the radiant flux ($\leq 15 \text{ cal/cm}^2\text{-sec}$) resulted in relatively long exposure times, i.e., several seconds are required for ignition. Subsequently, pressure effects on ignition were observed only in few tests at sub-atmospheric pressure. The ignition criterion was the appearance of first light emission as detected by a photocell. This method often led to erroneous interpretation of ignition results (see §2.2). Probably this error did not occur because low radiant flux intensities produced non-pressure-sensitive ignitions. The conclusions reached by Baer and Ryan are therefore in agreement with succeeding works. Within the experimental range of their investigations, they established that:

1. change of binder has no noticeable affect on AP propellant radiative ignition;
2. the nature of the pressurizing gas has no affect on AP propellant radiative ignition (this is true only as far as the flame appearance is concerned);
3. pressure dependence is observed only at sub-atmospheric pressure;
4. ignition temperature does not depend on the initial temperature of the strand;
5. AN propellants are more difficult to ignite than AP propellants.

This early work, although relatively unrefined, is basically correct. It is noteworthy that so many correct predictions could be reached in such a simple experimental apparatus.

In a 1965 paper, Baer and Ryan²⁶ presented a more complete account of their work. The beneficial effects of carbon black and burning rate catalyst addition to the tested propellants was experimentally verified. However, no major experimental result was given besides those listed above. The authors themselves recognized

"Although the high pressure, high convective heat flux data of Baer, Ryan and Salt [Ref. 61] are reasonably consistent with the results of the low flux ignition tests, most data obtained by use of the high radiant fluxes of arc image furnaces [Ref. 63a] show significant differences, particularly with respect to the effect of pressure. Thus, the simple model for low flux ignition probably represents a special case of the general ignition processes." (p. 888 of Ref. 26)

The question of the convective vs radiative ignition results will be dealt with in more detail in Chapter 5.

The few results concerning radiative ignition reported by Soviet investigators⁹³⁻⁹⁵ have been obtained in somewhat similar furnaces. The black body type of radiative source was a graphite plate electrically heated. The purpose of the experiment was not to rate propellant ignitability but rather to check the model based on a solid phase thermal theory proposed by Koval'skii³³ for solid propellant ignition. The testing was restricted to DB propellants and only a limited amount of data was generated. Some of the available experimental details are summarized in Table 3 (entries 1 - 6).

This area of experimental research at low radiant fluxes shows valid propellant ignition trends. However, there are several limitations on these experiments and their results. The level of the energy flux ($\leq 15 \text{ cal/cm}^2\text{-sec}$) is not comparable to that observed in actual igniters (usually greater than $50 \text{ cal/cm}^2\text{-sec}$). Moreover, the experimental apparatus does not allow refined tests useful for basic understanding of heterogeneous flame processes (see Chapter 5). Finally, most of the experimental parameters are poorly known and controlled.

2.2 Experimental Results in the Arc Image Ignition Apparatus

The first experimental data with "high" radiation fluxes (order of $100 \text{ cal/cm}^2\text{-sec}$) were obtained by Beyer and Fishman (see Ref. 63a) at SRI by using a carbon arc image ignition apparatus. Two composite propellants, respectively containing AP and AN as oxidizer, were tested up to $75 \text{ cal/cm}^2\text{-sec}$ in the range 0.006 - 35 atm of a controlled O_2/N_2 mixture. The time delay to first light emission was measured by a photocell, but the ignition was considered to occur on a go/no-go basis (see below

for discussion of the go/no-go criterion). An inconvenience of this SRI experimental study is the time dependence of the radiant pulse, which is approximately one-half a sine wave; this implies nonuniform intensity in time of the radiant flux and, therefore, lessened the possibility of dynamic extinction. The facts ascertained in the above study are:

1. a distinction was made between a self-sustained and a radiation-sustained flame (boundary at 0.06 atm N_2 for AP/PS type of propellant);
2. a pressure dependence for the self-sustained flame was observed (starting at about 5 atm N_2 for AP/PS type of propellant);
3. a requirement of a minimum amount of energy for self-sustained flame was found (1 cal/cm² for AP/PS type of propellant at 1 atm N_2);
4. a solid phase ignition mechanism is the controlling factor at high pressure (above 5 atm N_2 for AP/PS type of propellant);
5. ignition energy decreases with increase of initial temperature of the propellant;
6. there is an ignition-accelerating effect of the O_2 presence since it decreases ignition energy at atmospheric pressure;
7. delay times between the end of the exposure pulse and ignition from 50 to 100 msec and surface temperatures at ignition of 200 - 250 C were measured at atmospheric pressure for AP/PS type of propellant. (This relatively low value of the ignition surface temperature might depend on the measurement technique.)

Further work at SRI is summarized in Ref. 63b. Among the improvements realized in the experimental procedure, a trapezoidal radiant pulse was used instead of the original sinusoidal pulse. A large amount of data was provided, but only a few new conclusions were reached:

1. the minimum pressure for self-sustained flame depends on the nature of the binder;
2. domains (large pressure and/or low radiant flux intensity) which appear to be controlled by a solid phase ignition mechanism are described by a straight line of slope -2 in an ($\log I_0$) vs ($\log t$) plot, except when transparency effects are appreciable.

For other details see Table 3. The main theme of this SRI report consisted of attempts to relate ignitability to steady-state burning rate of propellants and has not been proved correct.

Price, et al,²⁷ in 1963, tested a JPN type of DB propellant in a carbon arc image furnace in the range of pressures from about 1 to 15 atm. The ambient gases were N₂, He, or air. The ignition criterion was the go/no-go method. For further experimental details consult Table 3. Among other things, Price recorded the weight loss of a series of samples exposed for varying lengths of time to the arc image radiation. On the basis of the results obtained, he first gave evidence of the:

1. existence of steady gasification processes sustained by radiation at the surface of the strand prior to ignition;
2. existence of different regimes of ignition according to the level of the incident radiant flux;
3. dependence of the gas phase regime (in which energy liberated in the gas phase is necessary to sustained combustion) on the nature and state of the environmental atmosphere.

In a subsequent paper, Price, et al²⁸ confirmed the above findings concerning DB propellants and, moreover, presented further experimental results concerning AP-based composite propellants. Evidence was given for the following:

1. at low heating rates the solid phase decomposition of AP is the limiting mechanism for ignition;
2. lowering the ambient pressure (e.g., toward 1 atm) or increasing the radiant flux (e.g., above 40 cal/cm²-sec) shifts the ignition process from the condensed phase toward a gas phase reaction controlled regime;
3. carbon powder or catalyst addition may strongly decrease the minimum amount of energy required for ignition;
4. a fine particle size of AP crystals reduces the minimum amount of energy required for ignition, if no additive is present.

For further experimental details consult Table 3.

The arc-image results discussed above lead to an excellent body of data, and virtually no new experimental findings of major significance were reported after these works in the area of solid propellant ignition by arc image radiation.

Price^{27,28} also clearly discussed the question as to the experimental definition of ignition.

"A series of samples is tested as near to the ignition time as possible, and the exposure time leading to a 50-50 probability of ignition is determined. This go/no-go criterion for ignition does not depend on detection of self-luminosity of the test sample nor on assumptions regarding the relevance of self-luminosity to a state of ignitedness." (p. 8 of Ref. 27)

Although subsequently proposed as a standard method (see Ref. 64a) for determining ignition, the go/no-go criterion has not always been adopted and this is the reason for a great deal of confusion in the field. Indeed, even at sub-atmospheric pressure

"Results of those facilities using light detection methods agreed among themselves and showed no pressure effects, while go/no-go test results agreed relatively well but did demonstrate considerable influence of pressure." (p. 16 of Ref. 74)

The reason for this will be clear after reading Chapters 5 and 6. For the time being, the suggestion of Price that ignition has to be experimentally detected through a go/no-go criterion is accepted.

Extensive experimental investigations were performed at SRI,^{74,85} at UTC,^{71-73,79} at NWC,⁸ at A. D. Little,^{66,67} and at BRL.⁸⁷ The details of these experiments are summarized in Table 3 (entries 7-23). Consistent trends can be found from this literature:

1. a solid phase mechanism dominates when the pressure is large and/or the radiant flux low;
2. a gas phase mechanism dominates when the pressure is low and/or the radiant flux large;
3. the gas phase regime is affected by the nature, the pressure, and the fluid dynamics of the ambient gas;
4. addition of opacifiers at the propellant surface is effective in decreasing the minimum energy required for sustained ignition;
5. DB and AP based composite propellants show similar behavior but for different values of pressure and radiant flux;

6. the first appearance of luminosity is independent of pressure and does not imply that sustained ignition will follow;
7. steady radiation-induced gasification occurs in the region of nonsustained ignition.

It will be shown in this study (see Chapter 4) that similar trends are observed when propellants are tested in the laser ignition apparatus. In addition, laser ignition tests can produce the dynamic extinction phenomenon observed for noncatalyzed DB tested in an inert ambient atmosphere.

Notice, finally, that today the arc image ignition apparatus is by far the most widely used radiative source not only in research programs but also for practical applications. Indeed,

"A common use of the arc image furnace is to determine the ignition energy requirements of a propellant or pellet sample (usually 3/8 inch diameter) under conditions of various heat flux levels, pressure, environmental gases, propellant surface conditions, aging, and initial temperature." (p. 12 of Ref. 96)

Moreover, use has been made of

"An arc ignition system to provide multiple ignition of solid propellant grains." (p. 1 of Ref. 97)

in an actual rocket regime.

However, it has already been mentioned (see §1.4) that rating of propellant ignitability by radiative energy devices is questionable. On the other hand, radiative ignition tools are particularly apt for obtaining a deeper understanding of the basic phenomena connected with unsteady heterogeneous flames. From this point of view, the laser ignition apparatus offers substantial improvements (the improvements are indicated in §3.1) with respect to other radiative sources. In conclusion, it is felt that the use of the arc image device should be restricted in the future to those practical situations where a simple panchromatic and non-collimated but relatively controllable and powerful energy source can be tolerated.

2.3 Experimental Results in the Laser Ignition Apparatus

Most of the laser ignition work has been performed at Princeton University. Kondrikov (see Ref. 76a), in 1970, proved that a catalyzed DB propellant (N5 composition) tested in an inert atmosphere shows the same qualitative ignition characteristics in the arc image and laser ignition apparatus. Ohlemiller (see Ref. 76b) proved that this is not so for a non-catalyzed DB propellant (NG

composition). The dynamic extinction phenomenon found in the latter case, although initially surprising, has been confirmed by a large body of experimental evidence⁷⁷⁻⁷⁹ and has been theoretically explained in the framework of the Zeldovich theory.⁷⁷ Some details of the experimental work completed to date in the laser ignition apparatus are summarized in Table 3 (entries 24-27).

However, the results mentioned above are limited to a few representative propellants and operating conditions. This study is directed at solving specific problems associated with the radiative ignition experiments performed in the laser apparatus by offering a systematic analysis of ignition trends of several classes of solid propellants. One of the main questions which still needs to be answered is the following: how do the results obtained in the laser ignition apparatus compare to those obtained in the arc ignition apparatus? This question is fully treated in Chapter 4. Moreover, new experimental facts (see §4.4) concerning dynamic extinction and its theoretical interpretation (see Chapters 8 and 9) in terms of the MTS flame model are given. Likewise, the unique aspects connected with the use of the laser as a radiative energy source are treated in §4.7. Some details of the experimental work done in this investigation are summarized in Table 3. Further details are given in Tables 1, 2, 4, and 5.

2.4 Summary of the Results Obtained from Radiative Ignition Experiments

Some of the details of the experimental works previously mentioned and of other papers directly or partly connected with radiative ignition experiments are summarized in Table 3. The papers have been listed in order of time of publication for each category: low radiant flux (entries 1 - 6), arc image (entries 7 - 23), and laser source (entries 24 - 27). The nature of the radiation source and its power output characteristics have been indicated. The criterion adopted for deciding about the occurrence of ignition is given, since different results are expected from different criteria. The type of history of the radiative energy stimulus and/or the type of shutters are listed, since they are important in data comparisons and in the occurrence or non-occurrence of dynamic extinction. The nature of the propellants tested, the operating pressure, and the nature of the ambient atmosphere are the basic factors affecting the ignition experiments. It is considered useful to know which parameters have been varied during each experimental investigation. Finally, a concise summary of the main experimental results is given and the purpose of the research is specified.

The above information was not always explicitly stated in the original papers. Therefore, sometimes it is either missing in the table or has been inferred from other sources. Except

the work by Ohlemiller and Summerfield⁸ in 1969, reporting for the first time a systematic analysis of ignition trends (of polymeric fuels in oxidizing atmosphere) as observed in the laser ignition apparatus, only papers dealing with solid propellants have been listed.

CHAPTER 3

EXPERIMENTAL APPARATUS AND PROCEDURE

In this chapter, the experimental apparatus used in the present investigation is only briefly described, since it was fully discussed in previous reports.⁸ Likewise, the experimental procedure is only briefly described. Tables are given of the experiments performed and of the solid propellants tested.

3.1 Description of Experimental Apparatus

The two radiative sources used in the study are an arc image furnace and a CO₂ laser. Similar arc image ignition apparatus have been described in detail in Refs. 63, 73, and 83, for example. Its schematic diagram is depicted in Fig. 2a. A xenon lamp provides the arc whose image is focused at the surface of the propellant sample. The average intensity of the radiant flux on the target is not larger than 120 cal/cm²-sec and is controlled in a discontinuous manner by inserting attenuation screens (stainless steel mesh) into the optical path. A typical illumination profile along a diameter of the sample is also depicted in Fig. 2b. It shows a decrease of about 15% of radiant flux intensity from the peak value at the periphery of the sample. For data concerning the spatial structure of the arc beam, see Ref. 98. The holder of the sample is designed so that no side exposure to radiation is allowed. The fast action shutters are the same shutters as those used in the laser ignition apparatus.

The laser ignition apparatus has been described in detail in Ref. 8. Its schematic diagram is depicted in Fig. 3a. The CO₂ laser tube provides a continuous emission at 10.6 μ with a maximum average radiant flux intensity on the propellant sample of 100 cal/cm²-sec. Continuous control of the radiant flux intensity is obtained by varying the regulated discharge current through the plasma tube. The spatial nonuniformity of the radiant beam depends on the oscillating modes of the laser optical cavity and on the subsequent optical system. Intensity fluctuations of 20% on either side of the average value have been detected at the target surface. However, the spacing and sharpness of the beam nonuniformities (see Fig. 3b) are so small that conductive processes in the sample solid phase are expected to appreciably smooth the peaks of radiant flux in a fraction of the typical ignition delay time. For details concerning the spatial structure of the laser beam, see p. 41 of Ref. 8a and also §4.7 of this work. In any event, it is worthwhile to note that to obtain the maximum power output the laser must be run in a multi-mode configuration yielding a nonuniform flux distribution; the subsequent optical system improves this somewhat. This also is shown in Fig. 3b. The spot size at the propellant surface is about 2.5 × 2.5 mm and (usually) no side exposure to the perpendicularly impinging radiation is possible because the sides of the sample are nearly parallel to the laser beam.

The laser is, generally speaking, far superior to the arc as a radiative source for ignition tests. The laser beam is spectrally monochromatic and geometrically collimated; its intensity can be controlled with continuity. In principle, any power output requested for combustion experiments may be provided and, moreover, one has the choice of the most convenient wavelength (by changing the laser source). Again, the reader may consult the work by Ohlemiller (see Ref. 8a) for full discussions on this matter. The basic difference in the spectral emissions between the xenon arc lamp (polychromatic) and the CO₂ laser (monochromatic) is shown in Fig. 4.

In most experiments to be discussed, both in the laser and arc image ignition apparatus, a standard sample geometry was used. This was a cylinder approximately 2.6 mm in diameter and 10 mm long. The reason behind this choice is explained on p. 34 of Ref. 8a; the reader might wish to consult Ref. 99, also. (Some tests were conducted with larger diameter samples to investigate flame spreading away from the heated region.) The sample surface was completely illuminated by the arc image radiant beam but not totally covered by the laser radiant beam. The duration and rate of termination of the radiant pulse are controlled by two high speed, iris-type shutters, which operate within less than 1 msec. The speed of the shutter system is known to be a very important parameter from previous studies of the Princeton group.⁷⁷

3.2 Description of Experimental Procedure

It follows from discussions of previous chapters (§2.2) and from literature review that the appropriate experimental method for rating the ignitability of propellants is the go/no-go type of test rather than the detection of a flame during the continuous radiation type of test, since the appearance of the incipient flame (as indicated by IR, photo detectors, or high-speed movies) is often only a step in the overall ignition transient. The point-by-point nature of the go/no-go data are illustrated on Fig. 5 and figures in subsequent chapters. A statistical treatment was not applied to the data. Uncertainties concerning a boundary were reduced by conducting additional tests in the vicinity of the boundary. A typical boundary is defined with some tens of tests; double or triple additional tests might be required for defining boundaries with complex shapes. The results are plotted as the log of radiative heating time vs log of intensity of the incident radiant flux (i.e., intensity before beam is attenuated by scattering and absorption in a smoke layer, reflection from surface, etc.). To permit direct comparisons, all of the results are plotted on the same grid.

Most of the propellants considered were tested in both of the ignition apparatus at 5, 11, and 21 atm (either air or N₂) and at radiant flux intensities up to 100 cal/cm²-sec. The response of the propellant to the radiant pulse is observed both in

terms of a global result of ignition/no ignition and in terms of detailed processes of gasification, incipient flame, and well-developed flame. For selected tests, high-speed (1000 frames/sec) shadowgraph and color movies were used to record the ignition sequence.

The surfaces of the propellants were freshly cut with a razor blade a few minutes before the test. The solid propellants for which ignition maps were obtained are listed in Table 1. They include both nitrate ester and AP-based composite propellants. (For a detailed description of propellants #5 through #10, see Ref. 100). Propellants #9 and #10 are referred to as catalyzed DB propellants since they contain lead and copper salts that produce increased burning rates.¹⁰⁰ A summary of the experimental tests performed is given in Table 2.

A complete interpretation of the ignition trends requires detailed studies of the radiation properties of each propellant. In general, all of the propellants are relatively opaque to the 10.6μ radiation from the laser. The fraction of the polychromatic arc image radiation that is transmitted below the propellant surface is very dependent on composition and particulate additives such as carbon and metal fuel. An extensive study (see §4.1.1) of the radiation properties of the propellants listed in Table 1 is being completed and some of the results are shown in Table 4.

Overall IR emissions from the propellant surface region were observed during continuous irradiation ignition experiments carried out in the laser apparatus for the same experimental parameters as used for the go/no-go type of experiments. For each test, two times were noted during the ignition transient: (1) the time at which the IR detector senses a first faint emission of radiation (somewhere near the surface), and (2) the time at which a given (specified below) level of IR emission is reached due to strong surface gasification and combustion reactions. The IR detector is a resistive type of photoconductor made of gold-doped germanium as the semi-conducting material. The IR detector is positioned so that it detects radiation from the surface region through an optical path consisting of two IRTAN 2 windows and a front surface aluminum-coated mirror. As shown in Fig. 4, the spectral range of the overall IR detector system encompasses the range of wavelengths emitted by the surface, even at relatively low temperatures, but it responds very weakly to the 10.6μ emission of the laser. In order to evaluate the rapidity and the intensity of the flame development during the ignition transient, a reference level of IR emission producing a response of 20 mV from the IR detector was arbitrarily chosen. This value is usually achieved by all of the propellants tested during the present investigation. It corresponds to an early stage of the flame development for the AP-based composite propellants, but to a late stage for the noncatalyzed DB propellants; the catalyzed DB propellants range in the middle.

CHAPTER 4

EXPERIMENTAL RESULTS

Results concerning ignition of a number of solid propellants tested both in the arc image ignition apparatus and in the laser ignition apparatus are presented. For a general discussion of these results read Chapter 5. An "ignition map" is introduced there accounting for all experimental observations made in this chapter.

4.1 Comparisons Between Propellant Classes

Since the objective of this section is to present data from a wide variety of propellants and test conditions, the detailed comparisons require that the reader make repeated references to the figures. Some of the observations are repeated in the next sections for the sake of clarity.

4.1.1 Relative Ignitability in the Arc Image Ignition Apparatus

A comparison of the relative ignitability (under arc image heating) of the several propellant classes is given in Fig. 5. Under the 21 atm N_2 conditions shown in Fig. 5, the ignition limits are straight lines over the indicated range of heat fluxes. At lower pressures (e.g., 5 atm), the limit lines are not straight and a direct comparison of the propellants would be more difficult. The results in Fig. 5 show that the HMX/PU propellants are the most resistant to ignition. The next most resistant propellants are the AP composite propellants. The opacified NC double-base propellants (i.e., propellants containing particulate carbon) are clearly the easiest to ignite. These trends are consistent with the burning surface temperatures of the three propellant types (i.e., 260 to 340 C for NC,¹⁰⁰ 700 to 800 C for AP composite,¹⁰¹ and 1050 C for HMX composite¹⁰²) and with their optical properties (surface reflectivity and volumetric absorption) as measured in Ref. 103. The ignition trends could not be correlated with the temperature of runaway exothermic reactions as measured in slow decomposition experiments, such as DTA and DSC. Data from such experiments are apparently not indicative of the high-temperature decomposition processes that occur at the propellant surface during rapid ignition; the slow heating rate in the DTA and DSC is not comparable to the fast energy input due to the radiative source during an ignition transient. Such differences in heating rate can shift the relative orders of the exothermic reactions.

A list of the high pressure (> 21 atm of N_2) ignition boundary slopes obtained in the laser and in the arc image ignition apparatus is given in Table 4.

4.1.2 AP Composite Propellants

In order to deduce information concerning the combustion processes of the propellant classes, several ignition experiments were performed under various testing conditions. The results concerning AP-based composite propellants are shown in Fig. 6 (laser heating) and in Fig. 7 (arc image heating). In the laser ignition apparatus (Fig. 6) no pressure dependence is discernible in the range from 5 to 21 atm of N₂ or air. Moreover, with the laser, neither the addition of 1% carbon (propellant #2) nor the simultaneous change of AP particle granularity and mixture ratio (propellant #3) appreciably affect the ignitability of the AP composite propellants. Likewise, the very fuel-rich propellant #4 has ignition times comparable to the conventional AP composite propellant #1, #2 and #3 when tested in the laser ignition apparatus in the range from 5 to 21 atm of N₂ or air. The value of the slope (-2) indicates that penetration of radiation below the surface is negligible. Thus, in the tested conditions, boron appears to act as an inert opacifier with no major effect on the ignition behavior of the propellant. In the arc image ignition apparatus (Fig. 7), in the range 5 to 21 atm of N₂, no pressure dependence is discernible, but the influence of carbon addition in reducing the minimum exposure time to radiation required for obtaining a self-sustaining flame is marked in the whole range of radiant flux intensity. Again the slope -2 of the ignition boundary for propellant #4 in the range from 11 to 21 atm of N₂ indicates that boron acts as an efficient inert opacifier. From all this it is inferred that in the range of investigation, AP composite propellant ignition with the arc is essentially controlled by radiation penetration below the propellant surface. However, it is expected (and it has been confirmed by some experiments at 1.3 and 2 atm of N₂ in the laser ignition apparatus for propellants #1 and #4) that lowering the pressure of N₂ in the combustion chamber will make the ignition data pressure dependent.

4.1.3 DB Catalyzed Propellants

The results concerning catalyzed DB propellants #9 and #10, both tested in the laser ignition apparatus, are shown in Fig. 8. For both propellants, the pressure dependence of the ignition data in the range 5 to 21 atm of N₂ is increased when the pressure is lowered (toward 5 atm) and/or when the radiant flux intensity is increased (toward 100 cal/cm²-sec). The slightly different slope of the high pressure boundary may depend on the radiation penetration below the propellant surface. Later, other results will prove that this type of behavior does not depend on the specific ignition apparatus used for the experiments. More detailed comments about the effect of catalyst are given in §4.2.

4.1.4 Noncatalyzed DB Propellants

The results concerning noncatalyzed DB propellants #5 and #6 tested in the laser ignition apparatus are shown in Fig. 9. For both propellants at 21 atm of N₂, ignition data show no pressure dependence but the different slope of the two straight lines (-2 for propellant #5 and -1.54 for propellant #6) again indicates the influence of the radiation penetration below the propellant surface. However, differently from all other cases examined so far, the flame that develops fully and persists as long as the radiation continues (overdriving the burning rate) is extinguished by rapid removal of the laser radiant beam (deradiation time was approximately 0.001 sec for the experiments of Fig. 9). This new phenomenon is denoted as "dynamic extinction" and has been dealt with in detail in previous works.⁷⁷⁻⁷⁸ Here, the following facts are recalled:

1. evidence has been offered of the existence of a self-sustaining flame in the ignition corridor limited by the ignition boundary on one hand and by the dynamic extinction boundary on the other hand (see Fig. 9).
2. the dynamic extinction boundary shifts toward the right, i.e., the width of the ignition corridor increases if the pressure of N₂ in the combustion chamber is increased.
3. increasing the deradiation time, i.e., the actuation time of the closing shutter, makes the dynamic extinction boundary shift toward the right until it eventually disappears.

Further boundaries shown in Fig. 9 and attributed to 3-D effects will be discussed later. The results concerning noncatalyzed DB propellant #6 tested in the arc image ignition apparatus in the range 5 to 21 atm of N₂ are shown in a subsequent figure. Now, dynamic extinction is no longer observed and, again, no ignition is found at 5 atm of N₂. More detailed comments are given in §4.2.

4.1.5 HMX Propellants

The results obtained from tests on HMX/PU propellants (which are known to be resistant to ignition) in the arc image ignition apparatus are shown in Fig. 10. In an N₂ atmosphere, propellants #11 and #13 at 5 and 11 atm could not be ignited using exposure times up to 500 msec; even at 21 atm relatively long exposure times are required to achieve ignition. Ignition of propellant #12 which contains 10% oxamide (a burning rate suppressant which decomposes endothermically on the surface) was very difficult. For example, at 50 cal/cm²-sec of radiant flux and at 21 atm of N₂, exposure times on the order of several seconds were required. The ignitability of HMX composite propellants

in air was explored only for propellant #12. The propellant ignited easily in air but a pressure-dependent behavior was observed. When propellants #11, 12, and 13 were tested in the laser apparatus there was a marked decrease in the ignition time; this is probably a result of the 10.6μ radiation from the laser being absorbed at the surface, whereas the 0.5 to 1.5μ radiation from the arc image may be partially attenuated by reflection from the surface as well as transmitted below the propellant surface.

4.1.6 Visual Inspection of Flame Structure

The differences in the flame structure of the several propellant classes were revealed by high-speed shadowgraph movies (16 mm, 1000 frames/sec) taken during propellant ignition by the laser. For AP-based propellants (Fig. 11), the movies show that first appearance of the incipient flame corresponds to the crossing of the go/no-go ignition boundary and that soon afterward, a thin flame develops, strongly coupled to the surface. As clearly shown in Fig. 11, the incipient flame appears initially at discrete points on the surface without the gasification period observed during the ignition of DB propellant (see Fig. 13). Movies of noncatalyzed DB propellants ignited at 21 atm show that the visible flame develops well away from the surface (see Fig. 12). Catalyzed DB propellants ignited at 21 atm manifest a more compact type of flame that is more closely coupled to the surface. This might assure a more energetic heat feedback from the gas phase and also a more stable adjustment to the new equilibrium conditions after the removal of the laser beam.

A characteristic carbonaceous-appearing layer (Fig. 13) is observed when catalyzed DB propellants are ignited at low pressure (~ 4 atm). This is never observed for AP composite or noncatalyzed DB propellants; also, this is less pronounced when catalyzed DB propellants are ignited at high pressure (21 atm). Formation, growth, and shedding of carbonaceous-appearing filaments on the surface occurring prior to the time of self-sustaining combustion suggest some solid phase activity promoted by the catalysts.

4.2 Effect of Catalyst Addition in Double-Base Propellants

Experiments planned with the specific goal of ascertaining the effect of the addition of catalysts on the ignition properties of double-base propellants were performed both in the laser and in the arc image ignition apparatus. The results concerning catalyzed DB propellants are shown in Fig. 8 and in Fig. 14, and a comparison should be made with the results concerning noncatalyzed DB propellants shown in Figs. 9, 15 and 16. The pressure dependence of the ignition boundaries for catalyzed DB propellants #9 and #10 in the range 5 to 21 atm of N_2 is observed both in the arc and laser ignition apparatus. The qualitative aspects of this pressure dependence (more pronounced at pressure of 5 atm of N_2

and for radiant flux intensity of $100 \text{ cal/cm}^2\text{-sec}$) have already been mentioned in the previous section and are common to other propellants according to a well-established body of literature (Refs. 27 and 28, for example). Experimental evidence (movies and light detectors) proves that the region between the straight line and the curved ignition boundary is characterized by the presence of a non-self-sustaining flame. This is indicated in Fig. 8. The extra exposure times required at 11 atm, for example, compared to 21 atm for a fixed value of radiant flux intensity is necessary for establishing the proper thermal layer thickness below the propellant surface. Further comments on this point will be offered in the next chapter. Now, it is stressed that noncatalyzed DB propellants differ from this behavior in several respects:

1. no pressure dependence of ignition boundaries is observed in experiments performed in N_2 atmosphere in the laser ignition apparatus (when ignition is achieved).
2. ignition is not realized at 5 atm of N_2 for noncatalyzed DB propellant #6 tested both in the laser and arc image ignition apparatus. This indicates that lowering pressure toward 5 atm of N_2 makes ignition more and more difficult to realize.
3. a self-sustaining flame, even though well established, may be dynamically extinguished in the laser ignition apparatus in N_2 atmosphere.
4. a phenomenon indicated as "3-D reignition" directly connected with the dynamic extinction is observed in the laser ignition apparatus in N_2 atmosphere. This will be treated later.
5. pressure dependence, no dynamic extinction, no 3-D reignition, and no ignition in 5 atm of N_2 characterize ignition results in the arc image ignition apparatus (Fig. 16).

In summary, the presence of catalysts avoids the dynamic extinction and the consequent 3-D reignition observed in N_2 atmosphere for noncatalyzed DB propellants tested in the laser apparatus and, moreover, allows ignition also at 5 atm of N_2 , which is not possible for noncatalyzed DB propellants. The presence of catalysts is therefore highly beneficial from the point of view of a successful radiative ignition. Finally, a direct comparison between the DB propellants containing the same 0.2 percent of carbon addition, of which one is catalyzed (#10) while the other is not (#7) is shown in Fig. 5. The direct comparison is limited to heating at 21 atm of N_2 in the arc image ignition apparatus (the behavior at 11 atm of N_2 is shown respectively in Figs. 15 and 16).

The large difference in the ignition boundaries at 21 atm of N_2 for propellants #7 and #10 on Fig. 5 suggests that under arc image heating the burning rate catalysts promote surface reactions at lower temperatures and/or that the finely divided PbSa and CuSa particles act as opacifiers to concentrate the arc image radiation at the propellant surface. Evidence for the former action is lacking. Indeed, under laser radiation at 21 atm of N_2 , the ignition boundary for propellant #7 (Fig. 15) and propellant #10 (Fig. 14) almost coincide, which indicates that the catalysts do not accelerate (by simple heating) the surface decomposition processes. Thus, the opacifying action (with respect to the arc image radiation) of the finely divided PbSa and CuSa as the explanation of the differences in the ignition boundaries of propellants #7 and #10 (Fig. 5) appears to be reasonable. On the other hand, several hypotheses ranging from pure thermal effects to chemical and/or photochemical mechanisms (Refs. 100, 104 and 105, for example) have been made in order to rationalize the influence of lead and copper salts on the steady burning of DB propellants. In ignition experiments the explanations are further complicated because of the nonsteadiness of the phenomenon and the interfering presence of radiation. Since this study is dedicated to general radiative ignition trends and not to the definition of specific mechanisms, the problem of the catalyst action has not been further investigated.

4.3 Effect of Carbon Powder Addition

The importance of the optical properties of the propellants to be tested in radiative ignition apparatus is obvious. Experiments planned with the specific goal of evaluating quantitatively the effect of carbon powder addition to the basic propellants were performed both in the laser and arc image ignition apparatus. The results obtained testing two AP-based composite propellants (propellant #1 containing no carbon and propellant #2 containing 1% of carbon powder) in the laser and arc image ignition apparatus are presented in Figs. 5 and 6. The data were collected in the range 5 to 21 atm of N_2 and were already introduced in §4.1. Briefly recall that no effect was found when experiments were performed in the laser ignition apparatus, while a drastic change was found when experiments were performed in the arc image ignition apparatus.

The effect of carbon powder addition to noncatalyzed DB propellants was evaluated by testing three propellants (#6 containing no carbon, #7 containing 0.2% of carbon powder and #8 containing 1% of carbon powder) both in the laser and arc image ignition apparatus. The results obtained in the range 5 to 21 atm of N_2 are presented in Fig. 15. In general, an increase in carbon powder addition produces a progressive reduction of the minimum exposure time to radiation required for obtaining a self-sustaining flame over the whole range of radiant flux intensity. An exception to this, however, is the behavior of propellant #8 at

11 atm of N_2 for large values of radiant flux intensity. Note, also, that ignition at 5 atm of N_2 is never achieved in the investigated range of experimental parameters. The results obtained in the laser ignition apparatus will be discussed in §4.4 since they deal with the problem of dynamic extinction. For the time being, just note that no effect on the ignition boundary at 21 atm of N_2 is observed. This is similar to what has been observed in Figs. 5 and 6 for AP-based composite propellants.

Corresponding data concerning catalyzed DB propellants were not collected, since the presence of catalysts could interfere with the addition of carbon powder. Other data collected using air instead of N_2 as the pressurizing gas, are presented in Fig. 17 and will be discussed in §4.5.

Although it is not possible to offer conclusive evidence, from all indications the carbon powder seems to act like a very efficient opacifier. This beneficial effect is missing in the laser ignition apparatus since at 10.6μ all propellants are already dark.

4.4 Dynamic Extinction

The nature of this phenomenon, its interpretation, and some numerical results in the framework of the Zeldovich approach for q.s. transients have been the object of a previous paper⁷⁷ by the Princeton group. Some brief recapitulation was made in §4.1.4. The purpose of this section is to obtain a more complete understanding of the phenomenon by the analysis of new experimental facts. In particular, it is of relevance to know why such a remarkable behavior was never observed before.

Several directions were investigated. First of all, the data presented in Fig. 9 and in Fig. 15 show that dynamic extinction is observable for the general class of noncatalyzed DB propellants tested in the laser ignition apparatus in an N_2 atmosphere. Indeed, propellants #5, #6, #7, and #8 all show dynamic extinction boundaries when the laser beam is quickly removed (deradiation time 0.001 sec) at 21 atm of N_2 . However, the data presented in Fig. 16 show that propellants #6, #7, and #8 are not subject to dynamic extinction when tested in the same operating conditions in the arc image ignition apparatus. (Propellant #5 was not tested in the arc image ignition apparatus.) Likewise, the data presented in Fig. 17 show that propellants #6, #7, and #8, even in the laser ignition apparatus, are not subjected to dynamic extinction when tested in air. (Again, propellant #5 was not tested.) Furthermore, direct comparison between the noncatalyzed DB propellant #7 (Fig. 15) and the catalyzed DB propellant #2 (Fig. 14), containing the same 0.2% of carbon powder and both tested at 21 atm of N_2 in the laser ignition apparatus, confirms that the presence of catalysts precludes the occurrence of dynamic extinction. Also, from the results presented in Fig. 9

and in Fig. 15, it is inferred that carbon powder reduces the region of dynamic extinction of noncatalyzed DB propellants tested at 21 atm of N₂ in the laser ignition apparatus, but only if the addition is appreciable (1%). A negligible difference is found between the boundaries concerning propellant #6 (Fig. 9) containing no carbon powder and the boundaries concerning propellant #7 (Fig. 15) containing 0.2% of carbon powder.

For all of the situations showing the occurrence of dynamic extinction (Figs. 9 and 15), another boundary line consistently appears associated with the dynamic extinction boundary. This new line separated a region of no ignition (due to dynamic extinction) from a region in which ignition is again achieved. This reignition boundary is attributed to 3-D effects due to the spreading of the flame along the lateral surface of the strand. When the laser beam is shut off, no matter how fast, the dynamic effects are restricted to that portion of the burning propellant directly exposed to radiation. Consequently, the unperturbed deflagration wave surrounding the target area, in 3-D space, can reignite the entire surface. For this reason, the boundary is labelled as "3-D reignition" in the figures. Obviously, the 3-D reignition boundary is usually observed at relatively large heating times (about 0.1 sec) during which the radiation overdriven flame has time to spread beyond the directly irradiated spot. It follows that any mechanism accelerating the flame propagation will result in a reduction of the dynamic extinction region. This might be the role of the carbon powder in the case of the results concerning propellant #8, shown in Fig. 15.

It was not possible to obtain a self-sustaining flame at 5 atm of N₂ for any of the noncatalyzed DB propellants #5, #6, #7, and #8 tested in the laser ignition apparatus (Figs. 9 and 15). Likewise, it was not possible to obtain a self-sustaining flame at 5 atm of N₂ for the noncatalyzed DB propellants #6, #7, and #8 tested in the arc image ignition apparatus. Propellant #5 was not tested in the arc image ignition apparatus. From this, it is inferred that the non-achievement of a successful ignition at this relatively low pressure (5 atm) of N₂ is due to "static" reasons, i.e., the heat feedback from the gas phase to the condensed phase is not sufficient to sustain the flame. At 11 atm of N₂, the noncatalyzed DB propellants #6, #7, and #8 tested in the arc image ignition apparatus (Fig. 16) were all ignited. (Again, propellant #5 was not tested in the arc image ignition apparatus.) However, at 11 atm of N₂ in the laser ignition apparatus, a successful ignition was obtained for propellant #5⁷⁷ but not for propellants #6 and #7. For propellant #8 (Fig. 15) self-sustaining flame at 11 atm of N₂ was possible only above a boundary which was interpreted as a 3-D reignition limit. From this and from the fact that at 11 atm of N₂ the ignition corridor of propellant #5⁷⁷ appears clearly shrunken, it is inferred that the occasional non-achievement of a successful ignition at this intermediate pressure (11 atm) of N₂ in the laser ignition apparatus is due to "dynamic" reasons. In other words, the burning propellant

may not be able to stand the disturbance connected with the rapid removal of the laser beam (although it is statically stable) and, consequently, the ignition corridor is completely wiped out.

In summary, the data presented show that dynamic extinction and consequent 3-D reignition are only associated with the broad class of noncatalyzed DB propellants tested in the laser ignition apparatus in N₂ atmosphere. This is the reason why such remarkable behavior was never observed before in the vast body of experimental studies concerned with radiative ignition with sources other than the laser tube. Obviously, there is nothing magic about noncatalyzed DB propellants and it is expected that dynamic extinction and subsequent 3-D reignition will occur for any other propellant tested in the appropriate range of experimental parameters. This point will be better understood after reading Chapters 5 and 8. The question as to the unique effect of the laser radiative source is dealt with in §4.6.

4.5 Effect of Atmosphere in Chamber

Most of the results presented so far concern experiments performed in an N₂ atmosphere. Experiments planned with the specific goal of ascertaining the effect of the nature of the pressurizing gas on the ignition boundaries were performed in the laser ignition apparatus. The results concerning catalyzed and noncatalyzed DB propellants tested in the range of 5 to 21 atm of air are shown in Fig. 17. Within the range of parameters investigated, replacing N₂ with air in the combustion chamber gives the following effects:

1. pressure dependence of the ignition boundaries found for catalyzed DB propellants disappears;
2. dynamic extinction and associated 3-D reignition found for noncatalyzed DB propellants disappear;
3. ignition is achieved in the whole tested pressure range (5 to 21 atm) also for noncatalyzed DB propellants;
4. negligible dependence of the ignition boundaries on the chemical composition of the tested DB propellants is observed.

As already shown in Fig. 6, experiments performed with AP-based propellants in the laser ignition apparatus in the range 5 to 21 atm of air confirm the validity of the boundaries found for tests in N₂ (Fig. 6).

The results concerning IR signal detection from noncatalyzed DB propellant #6 tested in the laser ignition apparatus in the range of 5 to 21 atm of air and 11 to 21 atm of N₂ are presented in Fig. 18. Direct comparison of the data obtained in air and in N₂ show that:

1. the beginning of the IR emission from somewhere near the surface region is independent both of the nature of the pressurizing gas and on the pressure level;
2. the time required for obtaining an arbitrary but fixed intensity level of IR emission during the flame development sustained by laser radiation from the burning propellant increases if N_2 is used as the pressurizing gas instead of air or if the pressure is lowered.

The corresponding results concerning IR signal detection from catalyzed DB propellants were collected but are not presented here because of the lack of reasonable reproducibility of the data, mainly in the results associated with flame development history. This is due to scattering from the radiation background associated with the hot, carbonaceous-appearing residue that forms and sheds off the propellant surface. However, a negligible difference was found for the line associated with the beginning of IR emission from somewhere near the surface when compared to the corresponding (dashed) line for noncatalyzed DB propellant #6 shown in Fig. 18. This fact is in agreement with the previously mentioned negligible dependence of the ignition boundaries on the chemical composition when the DB propellants are tested in air (in the laser ignition apparatus).

In summary, the use of air instead of N_2 as the pressurizing gas avoids the dynamic extinction and the consequent 3-D reignition observed in N_2 atmosphere for noncatalyzed DB propellants tested in the laser ignition apparatus and makes successful radiative ignition generally easier to achieve. This is also confirmed by the results concerning HMX propellants presented in Fig. 10 and previously mentioned. From the IR signal detection data it is inferred that the beneficial effect of air (in the sense just specified) occurs during the flame development history rather than at the beginning of some not well-defined chemical activity in the region near the propellant surface. As to the implications of this fact, read Chapter 5. Simple visual inspection suggests that the presence of atmospheric oxygen creates a vigorous secondary diffusion flame surrounding and overlapping the primary (and possibly) weak self-flame of the propellant. The total flame is therefore sufficiently energetic to assure a successful ignition whenever the runaway exothermic processes at the propellant surface are triggered. Accordingly, self-sustaining ignition in these conditions is predictable by a simple thermal theory.

4.6 Effect of Radiation Source

The fundamental reasons beyond the choice of the laser tube rather than the arc image as a radiative source were briefly listed in Chapter 3. Obviously, it was considered of relevance to evaluate qualitatively and quantitatively what differences the use of the two radiative sources could imply in obtaining

data. Most of these differences have already been mentioned in the previous sections and they are only summarized here. From a direct comparison of the results obtained testing given propellants in the same operating conditions both in the laser and in the arc image ignition apparatus, the following facts emerge:

1. AP-based composite propellants (Figs. 5 and 6) show similar behavior in the laser and arc image ignition apparatus in that no pressure dependence is found, but the radiative heating of the solid phase is markedly different due to the different reflection at the surface and absorption possibly associated with scattering in depth of the radiant energy. Note that the ignition boundaries are all essentially parallel, except for the very fuel-rich composition.
2. Catalyzed DB propellants (Fig. 14) show totally similar behavior in the laser and arc image ignition apparatus. The data suggest that the $10.6\ \mu$ radiation from the laser source is more efficiently concentrated at the propellant surface.
3. Noncatalyzed DB propellants show totally different behavior in the laser (Figs. 9 and 15) and arc image (Fig. 16) ignition apparatus. Dynamic extinction and associated 3-D reignition typical of laser heating are not found for arc image heating, while pressure dependence typical of arc image heating is not found for laser heating.

The quantitative differences between arc and laser observed for AP-based composite propellants and catalyzed DB propellants are attributed exclusively to the dependence of the optical properties of the propellants on the radiation wavelength. Indeed, no evidence has been found so far of photochemical effects in either radiant sources. More detailed comments on these points are given in §4.7 and in Appendix B.

The qualitative differences observed for noncatalyzed DB propellants require more sophisticated explanations. Since all of the operating conditions (including the shutters) were the same in the experiments performed in the laser and in the arc image ignition apparatus, the difference lies in the radiant beam itself. The possibility that some dependence of the dynamic extinction on the radiation wavelength may occur is discussed in §9.4.3. Now, attention is confined to the spatial structure of the radiant beam. The qualitative difference between the spatial structure at the edge of the laser beam and of the arc beam as seen at the target surface are obvious if one compares the schematics of Figs. 2b and 3b. From this comparison, it is concluded that the dynamic extinction boundary is not observed in arc image tests for any of the noncatalyzed DB propellants, since

the weaker heat flux surrounding the target spot provides a region where the flame is less sensitive to the disruption in the energy balance necessary for deradiation extinction (and the disruption is less). It should be recognized, however, that this smoothing effect at the edge of the illuminated spot might also be due, to a minor extent, to the different configuration of the sample in the holder in the two ignition apparatus (see Chapter 3).

Further comments on the spatial structure of the radiant beam are given in the next section.

4.7 Pre-ignition Events and Qualitative Observations in the Laser Ignition Apparatus.

A considerable advantage of the CO₂ laser (IR light) as a radiative source is the possibility of examining the flame development on the surface of the propellant being ignited without interference from the external radiative source. This fact has been exploited to obtain qualitative and quantitative information about the events preceding the fast runaway processes during an ignition transient. The information collected also clarified some uniquenesses connected with the laser heating.

Although the laser beam is sharply focused, the spatial structure of the beam (Fig. 3b) implies a nonuniform succession of events on a microscopic scale over the irradiated spot. This is illustrated in the four microphotographs (about 50X magnification) presented in Fig. 19. The pictures have been taken of a series of samples of catalyzed DB propellant #10, each subjected to laser radiation for a different time at the fixed conditions of 37 cal/cm²-sec of radiant flux intensity and 11 atm of N₂. The width of the area in the picture (2 mm) is slightly less than the irradiated footprint (2.5 mm). The succession of the pictures in time shows abrupt evidence of gasification (Picture b) at the core and at the outer region of the beam footprint on the sample surface and successive spreading of the gasification from these regions (Picture c). High-speed movies (e.g., see Figs. 11 to 13) and simple visual inspection of the irradiated sample relics confirm that bubbling, chemical activity, and flame appearance first occur at those small regions ("hot spots") within the illuminated footprint where the radiant flux is more intense.

Comparison between data from IR signal detection and high-speed movies show that the beginning of IR emission corresponds to the first appearance of the flame. For example, for the sequence represented in Fig. 11, the first (localized) appearance of flame for AP composite propellant #1 is observed at 0.057 sec while IR signal detection for the same operating conditions shows the beginning of IR emission at 0.055 sec. On the other hand, data collected from go/no-go experiments in the laser ignition apparatus for propellant #1 (Fig. 6) show that for these same

operating conditions, the corresponding point on the ignition boundary very closely corresponds to the flame appearance as seen either by high-speed movies or by IR signal detection. Comparison of the results obtained testing noncatalyzed DB propellant #6 in the laser ignition apparatus also shows that the ignition boundary in air (Fig. 17) and at 21 atm of N_2 (Fig. 9) very closely correspond to the beginning of IR emission (dashed line in Fig. 18) from somewhere near the surface region. The same connection has been found for the catalyzed DB propellant #10 between the beginning of IR emission and the ignition boundary in air (Fig. 17) and at 21 atm of N_2 (Fig. 8) in the laser ignition apparatus.

The typical pressure dependence of catalyzed DB propellant ignition boundaries was exploited for a more detailed investigation of the events preceding the achievement of the self-sustaining flame. The microphotographic technique mentioned above was used in order to follow the gasification evolution in time of propellant #9. The results obtained at 5 and 11 atm of N_2 and with a radiant flux intensity of $37 \text{ cal/cm}^2\text{-sec}$ are presented in Fig. 20. The collection of data in the region where gasification starts (hot spots) was particularly difficult due to the spatial nonuniformity of the laser beam. The following facts emerge from the analysis of the data:

1. a stationary gasification process sustained by the radiant beam occurs in the region of non-self-sustaining flame. Similar data by Price²⁷ using an arc image ignition apparatus demonstrate that this behavior does not depend on the radiative source.
2. the gasification rate is well above the s.s. burning rate of the propellant measured in a strand burner without radiation assistance,¹⁰⁰ but is close to the s.s. burning rate of the propellant measured in the arc image apparatus under the same radiant flux intensity.¹⁰⁵
3. the occurrence of an overdriven q.s. deflagration wave implies a dynamic burning response will occur when the laser beam is removed.
4. the period of time between the beginning of gasification and the achievement of a self-sustaining flame is used for building up the appropriate thermal wave in the condensed phase. However, at the present state of knowledge, this is nothing more than a speculation requiring the further assumption of a surface temperature fixed by the boiling temperature of the liquefied propellant mixture. Other interpretations might very well be correct.

Similar results can be obtained for noncatalyzed DB propellants. The results concerning propellant #6 tested in the laser ignition apparatus at 11 atm of N_2 with a radiant flux intensity of $37 \text{ cal/cm}^2\text{-sec}$ shows scattering of the data for large exposure times, likely due to the 3-D spreading of the radiation-sustained flame. The comments made above for propellant #9 still hold, except that now a self-sustaining flame is never achieved due to dynamic extinction. The results obtained from the gasification experiments are summarized in Table 6.

In summary, in the laser ignition apparatus, the ignition boundary in air (5 to 21 atm) or at large pressure (21 atm) of N_2 for all propellants tested in this study corresponds to the beginning of some observable chemical activity (IR emission, gasification, flame appearance, etc.). These processes are triggered at hot spots within the illuminated area mainly due to the spatial nonuniformity of the laser beam. A steady state gasification exists until either the laser beam is shut off or a self-sustaining flame occurs. It is inferred that, under appropriate experimental conditions, this behavior may be observed for all propellants subjected to radiative heating.

CHAPTER 5

DISCUSSION OF EXPERIMENTAL RESULTS

A phenomenological description of the ignition processes as observed in the laser ignition apparatus is given. The difficulty of acquiring a detailed knowledge of processes in all cases is illustrated. As a conclusion to the experimental part of this work, a generalized ignition map is offered by which most of the phenomena usually occurring in an ignition transient are put in a rational framework. A list of major experimental observations is given in §10.1.

5.1 Phenomenological Description of Radiant Ignition Transients

Some of the basic processes can be distinguished in the complex interplay of physical and chemical phenomena occurring during ignition. The initially cold propellant sample is heated in depth by the radiant beam (and possibly a thin surface layer is heated by exothermic decomposition reactions occurring near the surface region) until a runaway process leads to an incipient gas phase flame; this early flame may be localized at hot spots on the propellant surface. At this point (i.e., incipient flame appearance) energy feedback from the gas phase augments the energy input into the condensed phase supplied by the external ignition source. Depending on the spatial structure of the radiant beam and on the nature of the propellant, more hot spots are generated from which other flamelets develop, spread, and eventually merge into one large flame covering the entire surface. The unsteady deflagration wave so established accelerates the gasification process at (and possibly below) the surface which, in turn, increases the gas phase energy release. Eventually a steady state, radiation-assisted burning is achieved.

The competition at the solid/gas interface (or, more generally, at the interface of the reacting/inert regions of the solid phase) between the energy required to sustain the deflagration wave in the solid phase and the energy input provided by the gas phase heat feedback is the mechanism which controls the establishment of a self-sustaining process. This critical energy balance depends on the pressure level, the nature of the propellant, the radiant flux intensity, the rate of termination of the external energy source, and the nature of the pressurizing gas. If the propellant is able to quickly provide a vigorous energy feedback to the surface, ignition will be assured by the mere appearance of the incipient flame which is a solid phase controlled process. This is the case when air or nitrogen at high pressure (> 21 atm) are used as the pressurizing gas. Conversely, failure to establish a self-sustaining burning process may be due to either a weak and slow-to-be-built-up energy feedback from the gas phase or to dynamic instability of the propellant. Obviously, in both cases smoothing down the radiant flux

intensity cut off (i.e., low radiant flux intensity, long deradiation time, etc.) and/or increasing gas phase energy feedback will make the self-sustainment easier.

The results obtained in this experimental investigation are therefore interpreted in the following way. In the case of AP composite propellants, a vigorous heat feedback is quickly supplied to the surface due to the strong coupling of a thin flame to the solid phase. In the case of a noncatalyzed DB propellant, a weakly coupled flame requires a relatively large value of pressure to achieve self-sustained burning. Moreover, such propellants are particularly sensitive to dynamic extinction. Platinizing catalysts make the energy feedback to DB propellants more vigorous; consequently, the pressure dependence of the self-sustainment condition is reduced while the dynamic extinguishment following deradiation totally disappears.

As already mentioned, AP composite propellants are expected to have the same type of pressure dependence as exhibited by DB propellants at pressures of the order of 1 atm. Conversely, catalyzed and noncatalyzed DB propellants do not show any pressure dependence when the pressure is increased, e.g., to 31 atm. Likewise, tests conducted in air minimize pressure dependence again due to the vigorous gas phase kinetics of the secondary diffusion flame.

5.2 A Generalized Radiant Ignition Map

The ignition process has been seen in the previous section to be the synthesis of many physical and chemical sub-processes acting in series and parallel. It starts with the initial application of a stimulus and ends with appearance of vigorous self-sustaining reactions. As a propellant is heated to (and possibly past) the conditions for self-sustaining ignition, well characterized successive events occur when various limits are passed. The vertical line in Fig. 21 shows a traverse of event limits (or signals) on an ignition map. The traverse is at a fixed value of pressure and radiant flux intensity. The events traversed on the ignition map are categorized in terms of limits that signal the onset of the following actions:

- L_{1a} the surface is heated to the point that it is being gasified and a carbonaceous layer may form on the surface, but vigorous exothermic reactions are not occurring.
- L_{1b} gas phase and/or surface reactions begin to accelerate rapidly (as indicated by the appearance of a detectable IR emission from the surface region of the sample).

- L_{1c} "incipient flame" appears (the definition in time of this event depends on the specific detection method, i.e., high-speed movies or a prescribed level of IR emission, etc.).
- L_{1d} self-sustaining ignition.
- L_2 rapid deradiation (of some propellants) between limits L_2 and L_3 results in dynamic extinguishment.
- L_3 sustained combustion following deradiation (assured by flame spreading away from the target area of radiant heating).

Limits L_{1d} , L_2 , and L_3 must be established by go/no-go testing.

The limits L_{1d} , L_2 , and L_3 are well-defined limits whose positions (and even existence) are strongly dependent on propellant type and test conditions (i.e., pressure, atmosphere, deradiation time, spatial distribution of radiant beam, etc.). Furthermore, as indicated in Fig. 21, the limits L_{1a} , L_{1b} , L_{1c} , and L_{1d} may not be detectable as four individual limits since two or more of the limits may occur nearly simultaneously, depending on pressure, heat flux, and atmosphere. When all four limits occur nearly simultaneously, the limits will be referred to simply as the L_1 limit.

In terms of limits shown in Fig. 21, there are two essential conditions for ignition. The first is the development of the initial exothermic reactions (i.e., limits L_{1a} , L_{1b} , and L_{1c}) partially within the propellant surface reaction layer and partially in the adjacent gas phase boundary layer. Corresponding quantitative theories, which have evolved to treat this condition, were mentioned in §1.2 and §1.3. The second condition is focused on the final stage of the surface reactions and flame development and emphasizes the requirements for flame retention after the heat source is removed, i.e., limit L_{1d} . This second condition is called a late-stage condition in contrast to the first condition which is called early-stage. In the late-stage, attention is focused on matching of the heat feedback from a quasi-steady (fully developed) flame to the heating rate required to prepare the condensed phase for burning. As already mentioned, there are many instances in which the appearance of visible flame does not insure self-sustaining combustion.

Previous experimental and theoretical work described the conditions under which a nitrocellulose double-base (DB) propellant can be brought successfully to ignition in terms of the late-stage definition (self-sustaining combustion following deradiation), but, if the heating time is increased beyond L_2 , the propellant will fail to retain the flame following rapid deradiation and the propellant stops burning. The upper limit, L_3 , above which dynamic extinction does not occur, corresponds

to the time required for flame to spread over the irradiated surface beyond the target area of direct exposure. Since the long exposure times cause the one-dimensionality of the ignition process to break down, as already mentioned, the subsequent disappearance of dynamic extinction is referred to on the ignition maps as "3-D reignition".

Measurement of the time to a prescribed level of IR emission from the propellant surface region reveals that the appearance of the (incipient) flame corresponds to be a well-defined boundary, L_{1c} . Significantly, the beginning (L_{1b}) of the rapidly accelerating IR signal from the propellant surface region is independent of pressure and O_2 concentration, but whether and how rapidly strong surface region reactions occur depend on both. Therefore, the appearance of initial surface reaction (L_{1b} limit) is controlled by condensed phase and surface processes and can be described by simple thermal theory. However, as previously pointed out, neither the appearance of an incipient flame (L_{1c} limit) nor condensed phase thermal theories (L_{1a} or L_{1b} limits) are in general adequate for declaring that sustained ignition (crossing of L_{1d} limit) will occur. In particular situations (e.g., high pressure and low heat flux), the condensed phase thermal profile is well established and the propellant is able to provide vigorous energy feedback to the surface and rapid flame development occurs; the requirements for a self-sustaining flame are immediately satisfied as soon as the L_{1a} limit is reached and gasification begins. In this case, no late-stage theory is needed.

In many situations, the "early stage" and the "late stage" events cannot be neatly separated. Thus, the challenge exists to find a rational line of analysis to join these two events. Indeed, theories of the early stage must depend on knowledge of the heat-up process in the solid that leads to surface activity. On the other hand, theories of the late stage depend on knowing the chemical kinetics or the equivalent thermal feedback functions of fully developed flames. Fortunately, fully developed flame feedback data can be approximated from steady-state experiments with little knowledge of the chemical rates. In view of the success of the Zeldovich approach⁷⁷ in predicting ignition transients, the theoretical problems dealt with next in this work are focused on the general problem of q.s. heterogeneous flames in the presence of radiation rather than on the specific question of radiative ignition.

As a summary, three types of radiative ignition maps, which reoccur on the log-log plots of time-to-ignition versus incident-heat-flux for tests conducted in N_2 at pressures between 5 and 21 atm, can be categorized by propellant class:

1. AP composite propellants (see Figs. 5 and 6) are characterized by a single L_1 limit between nonignition and sustained ignition regions, i.e., the L_{1a} , L_{1b} ,

L_{1c} , and L_{1d} limits merge into one. The boundary is a straight line whose location and slope are independent of pressure, but depend to some extent on radiation penetration below the surface. (Below 5 atm, pressure dependence becomes pronounced, particularly in the high intensity range.) See Refs. 28, 63 and 73, for example.

2. Catalyzed DB propellants (see Figs. 8 and 14) are characterized by the existence of clearly defined L_{1a} and L_{1d} limits. As pressure increases, the L_{1d} limit becomes a single straight line and the non-self-sustaining flame region between the L_{1a} and L_{1d} limits decreases until it is eliminated.
3. Noncatalyzed propellants tested in the laser ignition apparatus (Figs. 9 and 15) have a single L_{1d} limit between nonignition and sustained ignition regions. Moreover, noncatalyzed DB propellants can be extinguished by rapid removal of the laser radiant beam. (Defined by the L_2 limit.)

CHAPTER 6

THEORETICAL BACKGROUND ON UNSTEADY COMBUSTION OF SOLID PROPELLANTS

This chapter provides the basis for understanding the analytical and numerical developments of the next three chapters. As such, it is essentially tutorial in nature. The contribution made here is limited to specific questions concerning the presence of radiation. The problem of radiation-assisted burning has been already treated by several investigators both in this country^{59,105-110} and in the Soviet Union.^{33,111-113} In this chapter a detailed formulation of the general quasi-steady transient problem in terms of a flame model is given. Also, a qualitative comparison with Zeldovich's approach is offered. For further information on the quasi-steady assumption, the reader is referred to Appendix A.

6.1 The Quasi-Steady State Gas Phase Assumption

The physical system of Fig. 22a representing a strand of solid propellant subjected to a radiant flux impinging with instantaneous intensity $(1 - r) \cdot I_0(t)$ at its surface, burning with instantaneous rate $R(t)$ in a closed vessel at instantaneous pressure $P(t)$ and ambient temperature $T_a(t)$ is considered. The overall problem of transient solid propellant combustion consists of determining quantitatively the parameters of the deflagration wave and, in particular, to predict the evolution of burning rate in time.

In general, this is a formidable problem and a solution can be found only within the framework of convenient approximations. A very constructive approach is based on the quasi-steady state assumption for the gas phase. This implies that the gas phase is in equilibrium not only with the external parameters (e.g., pressure) but also with the instantaneous conditions existing in the condensed phase (e.g., burning rate). The meaning of this assumption is discussed in Appendix A and is based on the fact that the ratio of the characteristic times in gas and solid phases

$$\frac{\tau_g}{\tau_c} = O(0.01)$$

In this section recall that the requirements expressed above are frequently satisfied and, therefore, the quasi-steady state approximation is often used. It is worthwhile to remark that this separation into steady and unsteady portions of the deflagration wave is made simultaneously with the separation of the condensed phase in reacting and inert portions. From a mathematical point of view, the overall unsteady nonlinear problem is split into an unsteady nonlinear part (inert condensed phase) and a steady nonlinear part (reacting gas phase). This distinction is the essence of the quasi-steady assumption.

The description of the quasi-steady gas phase may be made either analytically by means of a flame model or mechanistically by means of the Zeldovich approach. In either case, the quasi-steady gas phase behavior is uniquely defined by two parameters (e.g., burning rate and pressure), whereas one parameter is enough to define the steady-state gas phase behavior. In this study, the flame model approach will be implemented according to the scheme illustrated in the next sections.

Finally, it is stressed that the possible presence of an external radiant beam (see Fig. 23) does not jeopardize the validity of the quasi-steady gas phase assumption to the extent that no interaction occurs between the radiant beam and the gas phase (this hypothesis is discussed in §A.3).

6.2 The MTS Flame Model

The model known as the MTS flame model is the most general workable approach for dealing with the quasi-steady (q.s.) gas phase behavior. This approach will be used for most of our problems, but only qualitative comments will be offered here. For a detailed knowledge of how the model is derived, the reader is referred to the original development of Ref. 90 and also to Refs. 101, 114, and 115 treating the GDF theory from which the MTS flame model has evolved.

Any pattern of chemical reactions, no matter how complicated, involves the two physically distinct phenomena of mass diffusion and chemical kinetics. It is known from homogeneous combustion theory that quite often diffusion processes dominate the kinetic processes in the sense that

$$\tau_{di}/\tau_{ch} \gg 1$$

or, conversely, the opposite extreme may be true. These two limiting configurations are respectively known as diffusion and premixed flames. For heterogeneous combustion, in particular of solid propellants, there are instances in which the gas phase portions of the deflagration wave may be treated according to one of the above limiting configurations. But, in principle, especially for transients connected to large excursions of the controlling parameters, the gas phase treatment of a heterogeneous combustion wave has to account for both processes. This was originally done by Summerfield in his GDF theory for the AP steady-flame model. Later, an extension was made for the AP q.s. flame model accounting for variable flame and surface temperatures. Although derived for the specific case of the AP class of propellants, the formulation of the MTS flame model is quite general and may be adapted to other cases. The most important parameter characterizing the gas phase during a q.s. transient is the heat feedback to the burning surface. Obviously, any flame model is able to define all the details of the q.s. deflagration wave in

the gas phase, but for determining the burning rate evolution in time of a solid propellant, it is sufficient to obtain from the flame model only the heat feedback law. Then, the general problem of unsteady combustion of a solid propellant is reduced to analyzing the unsteady thermal profile of the condensed phase when it is subjected to time-varying boundary conditions.

According to the MTS flame model, the nondimensional heat feedback is

$$(6.2.1) \quad \frac{\lambda_g}{\lambda_c} \left(\frac{\partial \theta}{\partial X} \right)_{g,s} = Q \cdot RR \cdot \left[\frac{\sqrt{\tau'_{ch}}}{\sqrt{\tau'_{re}}} e^{-RR^2 \tau'_{re}} + \frac{\sqrt{\tau'_{di}}}{\sqrt{\tau'_{re}}} \frac{1 - e^{-RR^2 \tau'_{re}}}{RR^2 \tau'_{re}} \right]$$

where τ'_{ch} is a nondimensional kinetic time parameter;
 τ'_{di} is a nondimensional diffusion time parameter;
 τ'_{re} is a nondimensional reaction time parameter;
 $Q \equiv Q_f/Q_{ref}$ is the heat release in the gas phase.

Following the MTS flame model development, we put

$$(6.2.2) \quad \sqrt{\tau'_{ch}} = A_M \frac{TT_f}{PP} e^{\frac{E_f}{2RT_{f,ref}}} \left[\frac{1}{TT_f} - 1 \right]$$

where a second order gas phase reaction has been postulated to occur wholly at the highest temperature TT_f (p. 29 of Ref. 101) and

$$(6.2.3) \quad \sqrt{\tau'_{di}} = B_M \frac{(TT_f)^{5/6}}{(TT_s)^{7/8} (PP)^{1/3}}$$

where the diffusional mixing rate of fuel pockets with the surrounding atmosphere of oxygen-rich gases is assumed to depend on the surface temperature TT_s (p. 31 of Ref. 101).

The two constants A_M and B_M are determined for each specific propellant by "the best fit of the steady state burning rate theory to the measured burning rate data" (p. 38 of Ref. 90b). An application is shown in Fig. 24 for an AP propellant whose properties are listed in Table 7. It is further assumed (e.g., see p. 33 of Ref. 90b) that the overall solid propellant reaction time parameter can be expressed as the following simple combination of the two above limiting cases:

$$(6.2.4) \quad \sqrt{\tau'_{re}} = \sqrt{\tau'_{di}} + \sqrt{\tau'_{ch}}$$

This relation has been shown to represent the pressure dependence of the burning rate quite accurately for a wide range of composite solid propellants¹⁰¹ and also to describe the depressurization extinction correctly for both composite and double-base solid propellants.⁹⁰

Notice that the Krier-T'ien-Sirignano-Summerfield (KTSS) heat feedback law, derived for a diffusionally controlled AP flame, is a particular case of Eq. (6.2.1) when

$$(6.2.5) \quad \sqrt{\tau'_{re}} \approx \sqrt{\tau'_{di}} \gg \sqrt{\tau'_{ch}}$$

$$(6.2.6) \quad e^{-RR^2 \tau'_{re}} \ll 1$$

$$(6.2.7) \quad \tau'_{di} = \frac{B_M^2}{(PP)^{2/3}} \frac{(TT_f)^{5/3}}{(TT_s)^{7/4}} \approx \frac{\text{const}}{(PP)^{2/3}}$$

That is, when the diffusion time parameter is much larger than the kinetic time parameter (Eq. 6.2.5), the product $RR^2 \cdot \tau'_{re}$ is large enough to satisfy the condition of Eq. (6.2.6), and the diffusion time parameter is temperature independent. Extensive experimental investigation¹⁰¹ shows that for AP propellant flames the diffusional mixing is, indeed, sensibly slower than the chemical kinetics as long as the pressure is larger than 1 atm. It is also expected^{90b} that flame temperature undershoots during decelerated transients slow down the chemical kinetics much more effectively than the diffusional mixing (compare Eq. 6.2.2 vs Eq. 6.2.3). The constraint of Eq. (6.2.6) is not acceptable in extinction transients,⁹⁰ since under this circumstance $RR \rightarrow 0$ while τ'_{re} remains finite and, therefore,

$$e^{-RR^2 \cdot \tau'_{re}} \rightarrow 1.0$$

In summary, at low pressure and/or low burning rate, AP flame is kinetically controlled and therefore cannot be described by the KTSS model. Furthermore, Merkle⁹⁰ observes that the KTSS model can never predict extinction because the heat feedback law is found to be inversely proportional to the burning rate. However, stationary or small perturbation solutions (see Chapter 7) of the MTS and KTSS flame models are similar at high pressure, since in these instances only small changes in temperature and burning rate are considered.

6.3 Matching of the Deflagration Wave at the Interface of the Condensed and Gas Phases

The two portions of the generally unsteady deflagration wave in the condensed and gas phase have to match at the interface in terms of temperature, energy, and mass.

With the hypothesis of an infinitesimally thin planar burning surface, the temperature matching condition at the surface for generally unsteady conditions is, in dimensional terms

$$(6.3.1) \quad T(x+0^-) = T(x+0^+) \equiv T_s$$

With the hypotheses of 1-D laminar flow and thermally perfect fluid in the gas phase, the continuity equation for generally unsteady conditions in dimensional terms, is

$$(6.3.2) \quad \frac{\partial m}{\partial x} + \frac{\partial \rho_g}{\partial t} = 0$$

With the assumption of q.s. gas phase, the time derivatives are small and can be neglected as compared to other terms in the gas phase equations. Therefore, the mass matching condition in dimensional terms is

$$(6.3.3) \quad R(t) = \frac{\rho_g}{\rho_c} U(t)$$

from which the gas velocity $U(t)$ is always in phase with the burning rate.

As to the pyrolysis law, the following Arrhenius-type expression is usually assumed also for an unsteady state in dimensional terms

$$(6.3.4) \quad R(t) = A_s e^{-\frac{E_s}{RT_s(t)}}$$

The true $R(T_s)$ relationship is still unknown, even for steady states. However, experimental results (e.g., Figs. 41 and 51 of Ref. 100 and Fig. 24 of Ref. 101), although scattered, suggest that large changes of the burning rate are required in order to affect appreciably the surface temperature.

This evidence and the fact that the solid phase decomposition is very likely a one-way (far from equilibrium) process support the use of an Arrhenius expression. However, since this is nothing more than a phenomenological relationship expressing a strong dependence of the burning rate on the surface temperature, the alternative KTSS formulation¹¹⁵ will often be used, in dimensional terms

$$(6.3.5) \quad R(t) = b(T_s - T_a)^S$$

This is more easily handled than the previous Eq. (6.3.4) in analytical developments. Notice that all the constants such as

A_s , E_s , b , s , etc., are essentially empirical factors and usually are determined by the best fitting of experimental q.s. data of R vs T_s . For example, see Table 7 for the propellant AP/PBAA #941.

The energy matching condition is somewhat more delicate to deal with under general conditions. With reference to the schematic drawing of Fig. 22b, in dimensional terms:

$$(6.3.6) \quad \dot{q}_c = \dot{q}_f - \dot{q}_s + (1 - N_t)(1 - r)\dot{q}_r$$

where \dot{q} , cal/cm²-sec generally stands for energy flux;

\dot{q}_s is conventionally supposed positive if endothermic;

$N_t = 0$ for opaque condensed phase; and

$N_t = 1$ for transparent condensed phase.

The last point deserves some comment. The hypothesis of a collapsed reacting layer might imply in some cases that a certain thickness of condensed phase is shrunk to an infinitesimally small value. For consistency, then, the (external) radiant flux should be separated in a portion deposited directly at the surface (as if the propellant were opaque) and in a (remaining) portion distributed volumetrically in the condensed phase according to the proper extinction coefficient. The factor N_t , therefore, should be set equal to the fraction of radiant flux absorbed in the reacting layer when it is thought of as extended. But a new difficulty arises: the extent and the very existence of a condensed phase reacting layer is an extremely controversial question. On the other hand, for the large class of AP propellants, it is currently accepted that the surface reactions account for a reacting layer in the gas phase (premixed $NH_3 + HClO_4$ flame) whose structure is important only at $P = O(1)$ atm. For details, consult pp. 49-53 of Ref. 90b. Since the mathematical developments of this work concern composite AP propellants at $P = O(10)$ atm, N_t is taken here either as 0 or 1, although this is not a necessity.

Finally, notice that Eq. (6.3.6) is valid both for steady and unsteady states. In the latter case, the unsteady thermal profile in the condensed phase is related to the quasi-steady thermal profile in the gas phase: mathematically, this hybrid situation reflects the physical "contradiction" of two systems connected at the burning surface and of which only one is varying explicitly its configuration in time.

6.4 Further Relationships Required by the Presence of an External Radiant Flux

The s.s. burning rate of a propellant is assumed to be experimentally known. Indeed, it is a current practice to use a strand burner for constructing the plot of R vs P , often at different

ambient temperature. Unfortunately, such data are not currently available as functions of the external radiant flux intensity, too. Some experiments were performed by Ohlemiller¹⁰⁵ with an arc image furnace apparatus for platonized and unplatonized DB propellants. Two conclusions were reached: (1) the s.s. burning rate dependence on the external radiant flux intensity R vs I_0 at a given pressure $P = 13.6$ atm is linear up to a value of about $30 \text{ cal/cm}^2\text{-sec}$ and then is less pronounced; (2) no non-thermal wavelength dependence is noticeable in the range of 0.3 to 1.5μ . We can account for Ohlemiller's results by a phenomenological expression in nondimensional terms of the type:

$$(6.4.1) \quad RR(PP, F) = RR(PP, F=0) \cdot [1 + \beta(PP, F) \cdot (1 - r) \cdot F]$$

where the positive coefficient $\beta(PP, F)$ has been determined for each deradiation transient.

A similar problem arises for the flame temperature. By thermochemical computation, the s.s. $T_f(P)$ may be evaluated with good accuracy, together with final (equilibrium) products of decomposition. For the propellant AP/PBAA #941, T_f has been found^{90b} to have a slight dependence on the pressure. In this work the following relationship has been used for $P < 100$ atm

$$(6.4.2) \quad T_f(P) = T_{f, \text{ref}} - \frac{50}{68} (P_{\text{ref}} - P)$$

where $T_{f, \text{ref}} \equiv T_f(P_{\text{ref}}) = 2430 \text{ K}$ and $P_{\text{ref}} = 68 \text{ atm}$.

When an external radiant flux impinges on the surface of the condensed phase, without interacting with the gas phase, an energy balance over the whole combustion wave gives, in nondimensional terms:

$$RR \cdot \theta_s + RR \cdot (C_g/C_c) \cdot \theta_f + RR \cdot H = RR \cdot Q + (1-r) \cdot F$$

from which one obtains

$$(6.4.3) \quad \theta_f(PP, F) = \theta_f(PP, F=0) + (1 - C_c/C_g) [\theta_s(PP, F) -$$

$$\theta_s(PP, F=0)] + (1 - r) \frac{C_c}{C_g} \frac{F}{RR(PP, F)}$$

where $\theta_f(PP, F=0)$ is furnished by thermochemical computation (e.g., Eq. 6.4.2). It should be noticed that only when $C_c/C_g = 1$ the above relationship may be simplified to

$$(6.4.4) \quad \theta_f(PP, F) = \theta_f(PP, F=0) + (1 - r) \frac{F}{RR(PP, F)}$$

In deriving the balance of Eq. (6.4.3), two more assumptions were tacitly made. The first is

$$(6.4.5) \quad Q = Q(\text{PP}) = H + \theta_s(\text{PP}) + \frac{C_g}{C_c}[\theta_f(\text{PP}) - \theta_s(\text{PP})]$$

in which the heat release in the gas phase is considered to be uniquely defined by the pressure. This implies that the gas energetic parameter is independent not only of the radiant flux intensity (no photochemical effects) but also of the instantaneous value of burning rate (no dynamic effects). The dependence on the pressure is again found through an energy balance in the gas phase.

The second assumption is:

$$(6.4.6) \quad H = \text{constant}$$

by which the heat release at the surface is considered strictly dependent on the original condensed phase composition only. This hypothesis has been used in Eqs. (6.4.3) and (6.4.5).

6.5 Formulation of the General Quasi-Steady Transient Problem

We conclude the previous discussions by the following summary. Except where explicitly excluded, the following set of assumptions is valid throughout this development:

a. Condensed Phase

1. 1-D, semi-infinite slab.
2. Uniform and isotropic composition.
3. Constant properties.
4. Energy exchange through the burning surface only.
5. Chemically inert.
6. No radiation scattering.
7. No photochemical effects.

b. Interface

1. Infinitesimally thin plane surface.
2. Arrhenius or KTSS pyrolysis law.
3. Constant properties.

c. Gas Phase

1. Quasi-steady MTS flame model.
2. No interaction with external radiation.
3. 1-D, laminar, nonviscous flow and thermally perfect fluid (from which $P(x) = \text{constant}$ follows).
4. Constant properties.

d. Entire Strand

1. Adiabatic and (at cold boundary) in thermal equilibrium with ambient.
2. Subjected to no external forces.
3. No emission of radiation.

Except where explicitly excluded, the following set of reference parameters is used for nondimensionalizing (with specific reference to AP/PBAA #941):

$P_{\text{ref}} = 68$	atm
$R_{\text{ref}} = R(P_{\text{ref}})$	cm/sec
$T_{s,\text{ref}} = T_s(P_{\text{ref}})$	K
$T_{f,\text{ref}} = T_f(P_{\text{ref}})$	K
$x_{\text{ref}} = \alpha_c / R_{\text{ref}}$	cm
$t_{\text{ref}} = \alpha_c / R_{\text{ref}}^2$	sec
$Q_{\text{ref}} = C_c (T_{s,\text{ref}} - T_{\text{ref}})$	cal/gr
$I_{\text{ref}} = \rho_c C_c R_{\text{ref}} (T_{s,\text{ref}} - T_{\text{ref}})$	cal/cm ² -sec

from which one gets:

$PP = P/P_{\text{ref}}$	nondimensional pressure
$RR = R/R_{\text{ref}}$	nondimensional burning rate
$X = x/x_{\text{ref}}$	nondimensional distance
$\tau = t/t_{\text{ref}}$	nondimensional time
$H = Q_s/Q_{\text{ref}}$	nondimensional surface heat release
$Q = Q_f/Q_{\text{ref}}$	nondimensional gas heat release
$F = I_0/I_{\text{ref}}$	nondimensional radiant flux intensity

Notice that for the temperature, both of the following definitions are used according to need.

$$(6.5.1a) \quad \theta = \frac{T - T_a}{T_{s,ref} - T_{ref}} \quad \text{nondimensional temperature}$$

$$(e.g.,) \quad \theta_s = (T_s - T_a) / (T_{s,ref} - T_{ref}) \quad \text{nondimensional surface temperature}$$

$$\theta_f = (T_f - T_a) / (T_{s,ref} - T_{ref}) \quad \text{nondimensional flame temperature}$$

$$(6.5.1b) \quad TT = T / T_{ref} \quad \text{nondimensional temperature}$$

$$(e.g.,) \quad TT_s = T_s / T_{s,ref} \quad \text{nondimensional surface temperature}$$

$$TT_f = T_f / T_{f,ref} \quad \text{nondimensional flame temperature}$$

The choice of the particular definition depends on the specific physical phenomenon considered.

The general nondimensional q.s. transient formulation includes the unsteady condensed phase problem, the q.s. gas phase problem, relationships accounting for the surface mass production (gasification) and for changes in time of the controlling parameters, and, finally, several auxiliary conditions required if a radiative flux is present.

$$(6.5.2) \quad \left\{ \begin{array}{ll} \frac{\partial \theta}{\partial \tau} + RR \cdot \frac{\partial \theta}{\partial X} = \frac{\partial^2 \theta}{\partial X^2} + N_t \cdot \frac{1-r}{\ell_{rad}} \cdot F \cdot e^{X/\ell_{rad}} & \text{II PDE} \\ \theta(X, \tau=0) = \text{given} & \text{IC} \\ \theta(X \rightarrow -\infty, \tau) = 0 & \text{BC2} \\ \left(\frac{\partial \theta}{\partial X} \right)_{c,s} = \frac{\lambda_g}{\lambda_c} \left(\frac{\partial \theta}{\partial X} \right)_{g,s} - H \cdot RR + (1 - N_t)(1 - r) \cdot F & \text{BC1} \end{array} \right.$$

$$(6.5.3a) \quad RR = e^{-\frac{E_s}{RT_{s,ref}}} \left(\frac{1}{TT_s} - 1 \right)$$

$$(6.5.3b) \quad RR = \theta_s^S$$

$$(6.5.4) \quad \frac{\lambda_g}{\lambda_c} \left(\frac{\partial \theta}{\partial X} \right)_{g,s} = Q \cdot RR \left[\frac{\sqrt{\tau'_{ch}}}{\sqrt{\tau'_{re}}} e^{-RR^2 \tau'_{re}} + \frac{\sqrt{\tau'_{di}}}{\sqrt{\tau'_{re}}} \frac{1 - e^{-RR^2 \tau'_{re}}}{RR^2 \tau'_{re}} \right]$$

$$(6.5.5) \quad \sqrt{\tau'_{ch}} = A_M \frac{TT_f}{PP} e^{+\frac{E_f}{2AT_{f,ref}} \left(\frac{1}{TT_f} - 1 \right)}$$

$$(6.5.6) \quad \sqrt{\tau'_{di}} = B_M \frac{(TT_f)^{5/6}}{(TT_s)^{7/8} (PP)^{1/3}}$$

$$(6.5.7) \quad \sqrt{\tau'_{re}} = \sqrt{\tau'_{ch}} + \sqrt{\tau'_{di}}$$

$$(6.5.8) \quad \theta_f = \theta_s + Q \frac{C_g}{C_c} - \frac{1}{RR} \frac{\lambda_g}{\lambda_c} \left(\frac{\partial \theta}{\partial X} \right)_{g,s} \frac{C_g}{C_c}$$

$$(6.5.9) \quad PP = PP(\tau)$$

$$(6.5.10) \quad F = F(\tau)$$

$$(6.5.11) \quad \theta_a = \theta_a(\tau)$$

$$(6.5.12) \quad RR(PP, F) = RR(PP, F=0) \cdot [1 + \beta(PP, F) \cdot (1 - r) \cdot F]$$

$$(6.5.13) \quad \theta_f(PP, F) = \theta_f(PP, F=0) + (1 - r) \cdot F / RR(PP, F)$$

$$(6.5.14) \quad Q(PP, F) = Q(PP)$$

The further relationship of Eq. (6.5.8) is derived from the integral energy balance in the gas phase and is used for determining the q.s. flame temperature required for the evaluation of the chemical time parameter (Eq. 6.5.5) and the diffusion time parameter (Eq. 6.5.6) in the heat feedback law (Eq. 6.5.4). Obviously, the computation requires, in general, an iterative loop in the flame temperature as far as the condensed phase is concerned. As an illustration, the q.s. heat feedback of the propellant AP/PBAA #941 is shown graphically in Fig. 25 and has been obtained by solving Eqs. (6.5.3a) and (6.5.4 - 6.5.8). It should be noticed that the heat feedback is not directly affected by the radiant flux intensity.

Equation (6.5.2) for the unsteady thermal profile in the condensed phase is a strongly nonlinear second order partial differential equation of parabolic type. There is today no rigorous analytical method of dealing with such a problem. Numerical methods have, therefore, been implemented; this is treated in Chapter 9.

However, before solving the general problem, several other questions, solvable by or requiring analytical methods, are treated in Chapters 7 and 8. The theoretical background for any future development has been presented in detail in this chapter; later there will be only brief reminders.

6.6 An Alternative Approach for the Gas Phase: The Mechanistic Approach of Ya. B. Zeldovich

The general q.s. transient behavior of a solid propellant may be analyzed by two basic types of approaches as to describing the gas phase. The line of attack described in the previous sections, consisting of a detailed flame model, is able to define the structure of the deflagration wave in the gas phase and in particular provides, from a rational basis, the q.s. heat feedback function, \dot{q}_f , on the gas side of the burning surface. An alternative approach has been proposed by Ya. B. Zeldovich^{23,116} and extensively used in the Soviet literature¹¹⁷⁻¹²⁰ and recently in the U.S., too.^{92,121,122} The method bypasses any detailed knowledge of the gas phase and through two sets of experimental s.s. data, $R = R(P, T_a)$ and $T_s = T_s(P, R)$, is able to construct the q.s. heat feedback function, \dot{q}_c , directly on the condensed side of the burning surface. The method is developed in Fig. 26; for details consult Ref. 92. The heat feedback plot of Fig. 25 explains graphically how this is possible. In a q.s. transient, e.g., a decrease of radiant flux at $P = P^*$, the heat feedback depends only on two variables, e.g.,

$$\dot{q}_f = \dot{q}_f(P^*, R)$$

where $R(t)$ is changing in time. But the plot of Fig. 25 shows that the same functional dependence at $P = P^*$ may be obtained in a s.s. method by allowing a proper variation in time of $T_a(t)$.

For solving the general q.s. problem of §6.5, the flame model type of approach furnishes analytically the BC1 for the unsteady thermal profile in the condensed phase, whereas the mechanistic type of approach furnishes the BC1 experimentally. Consequently, following the mechanistic approach, Eqs. (6.5.4) - (6.5.8) are eliminated and BC2 for Eq. (6.5.2) is replaced by a tabulated experimental function. All assumptions about the gas phase are removed. The q.s. assumption has to be extended to the burning surface, though. This is a delicate point, since an

infinitesimally thin surface in principle has no inertia. Actually, Zeldovich and his co-workers consider the burning surface as a collapsed reacting layer whose structure they neglect, but not the proper characteristic time.

As to the features of this method, the advantage of eliminating the need of a detailed flame model is obvious, but the difficulties of obtaining reliable s.s. $R = R(P, T_a)$ and $T_s = T_s(P, R)$ data over a sufficiently wide range of T_a (even at negative absolute temperature) should not be overlooked. However, two observations from Ref. 92 are in order. First, in the absence of surface temperature data, "a partial Zeldovich method can be devised that relies on an estimated pyrolysis law" (p. 258 of Ref. 92). This is also justified from the fact that $T_s(P, R)$ has little influence on the q.s. heat feedback law. Second, the effective range of T_a (even equivalent negative absolute temperature) over which s.s. $R(P, T_a)$ data can be obtained is largely extended by the use of a heat sink for low temperatures and by a radiant flux for high temperatures. The logical equivalence of the flame model type of approach (in particular, the MTS flame model) and mechanistic type of approach is shown in Ref. 92. However, until the present work only the mechanistic method, with the notable exception of Ref. 123, was capable (see Ref. 92, for example) of predicting dynamic extinction by means of a stability analysis, in principle, limited to a linearized criterion for small pressure fluctuations. Most of the stability analyses carried out in the framework of flame models are addressed to determining the frequency response function (see Refs. 115, 124-126, for example). Complete details concerning these questions are presented in Chapter 7.

CHAPTER 7

LINEARIZED BURNING STABILITY ANALYSIS

In this and the following chapter, we will discuss the conditions of stability of a strand of propellant burning in different situations from various points of view. Although some of the methods introduced later can also be used to evaluate q.s. transients, our main interest is to discuss qualitative considerations and quantitative criteria about the stability of a burning propellant.

7.1 Background and Nomenclature

The physical system dealt with is represented in its most general form in the schematic drawing of Fig. 22a. The pressure of the vessel, the radiant flux impinging on the surface of the strand (originating exclusively from some external energy source), the ambient temperature measured at the cold boundary of the propellant sample which is supposed to be infinitely long, and any other parameter which can be controlled in a known way from the outside of the vessel are designated as controlling parameters. A change of one or more of these controlling parameters will affect, in some way, the state of the physical system and, consequently, they are also called external perturbations.

On the other hand, all those "small" (in a sense to be specified) irregularities and imperfections always present in the real world but which are nevertheless neglected in the idealized picture of Fig. 22a are designated as intrinsic perturbation sources. For example, nonuniform composition of the propellant impurities variously scattered in the condensed phase, complicated geometry of the burning surface, etc., all contribute to hopefully small but persistent differences of the actual phenomena from those described by the mathematical models developed in the previous chapter.

Whether the perturbation sources are external or intrinsic, the prior, supposedly unperturbed s.s. profile of temperature in the combustion wave will be modified to some new perturbed unsteady profile. Let us define the disturbance temperature profile as the profile of the point-by-point difference between the perturbed profile and the original, unperturbed profile. The general problem of stability may be stated as follows: given a stationary state of the physical system, the system is forced to a close but non-stationary state and it is asked whether the system, after a long period of time, will go back to its initial state or will move away from it. In the specific physical configuration considered in this study, it is asked whether the disturbance temperature profile will die out in time or not. Mathematically, the problem is an initial value problem and is usually described by a parabolic type of partial differential equation.

It is of concern to make a conventional distinction between static and dynamic stability. The stability of a system where intrinsic perturbation sources exclusively are considered to be acting is called static. Conversely, the stability of a system in which the external controlling parameters are changing in time is called dynamic. It will be shown that in the latter case, the rate of change in time of the pressure, for example, is of fundamental importance and this explains the expression "dynamic stability".

In this and the following chapter, the ultimate objective is to establish boundaries separating regions of stability from those of instability on some convenient graphical plot. It will be shown that static and dynamic stability boundaries are completely different in nature.

Since the mathematical problem is formidable, no general method has been found so far for solving the stability problem in its various aspects. Historically, a large amount of work has been devoted to stability problems in fluid dynamics. A standard treatment in this and related fields is the linearized approach, which is based on two essential assumptions: disturbance quantities infinitesimally small and a mathematical model (differential equations, boundary conditions, and any other relationship) containing only disturbance quantities of first order. Under these hypotheses, and others which will be specified in the next section, the problem reduces to an eigenvalue formulation whose mathematical theory is very well developed. Besides this standard approach, several other approximate and often ad hoc methods have been set up in various fields of applied sciences. The reason for such a confusing state of affairs is essentially one: the behavior of most physical systems is described by nonlinear equations and nowadays, not only a mathematical theory encompassing all types of nonlinearities, but even analytical methods capable of dealing with specific types of nonlinearities, are not yet available.

The question, then, arises of how good are the results obtained from the linearized theory. The assumption of infinitesimally small disturbances is a first serious drawback. Following Ref. 127 we can affirm: "infinitesimal disturbances are certainly unavoidable, but not all unavoidable disturbances may be considered infinitesimal. . . . Instability to finite size perturbations . . . may be considered one of the most typical phenomena associated with nonlinear stability problems." The assumption of linearity is also a serious drawback. Should any disturbance quantity grow in time much above the level which was set as small at the beginning, the linearity assumption fails. In this event, the validity of the approach is still valid but only for some limited period of time starting from the initial instant in which by hypothesis the disturbance quantities are all infinitesimally small. On the other hand, at least for intrinsic perturbation

sources, a general stability criterion has to consider arbitrary perturbations (infinitesimally small) and also the possibility of a succession in arbitrary order of arbitrary perturbations. In this respect, a linearized theory profits from the superposition principle by which "it makes no difference how many times and in what order of succession different perturbations have been introduced.¹²⁷ In conclusion, "the linearized analysis may be considered as the first step in any stability theory; moreover, it is a natural starting point for the description and definition of nonlinear problems.¹²⁷

In §7.2 a linearized analysis is offered of the stability of a strand of propellant burning at constant pressure (or radiant flux intensity) subjected to small externally controlled sinusoidal perturbations of radiant flux intensity (or pressure). Following the trend of the current literature, the behavior of the propellant in these specific configurations will be characterized by the fluctuations of the mass burning rate consequent to the fluctuations of the controlling parameters. The analytical relationship describing this coupling is called a response function or, more exactly, frequency response function, since interest is particularly in the dependence of the fluctuating mass burning rate on the frequency of the sinusoidally fluctuating controlling parameters.

In §8.2 a nonlinear static stability analysis by means of an approximate ad hoc approach is offered. Basically, the initial value problem will be transformed from a PDE into an ODE formulation to which the Lyapunov first criterion of stability will be applied. This will allow a definition of static stability boundary to be made.

In §8.3 the linearized analysis of sinusoidally fluctuating controlling parameters of §7.2 is generalized to a nonlinear analysis of finite size disturbances consequent to timewise monotonic changes of the controlling parameters. Following again the method of reducing the problem to an ODE, the analysis will be made in very general conditions. A dynamic stability boundary will be defined for some specific but relevant cases.

7.2 Response Function of a Burning Propellant Surface

Within the framework of a linearized analysis, the frequency response of a propellant will be considered. The forcing term is a sinusoidal fluctuation with frequency ω either of pressure or radiant flux intensity. In the past decade large efforts have been made, both theoretically^{115,124-126,128-143} and experimentally,¹⁴⁴⁻¹⁴⁶ in studying the solid propellant combustion instability by means of a response function describing the mass burning rate fluctuations subsequent to pressure fluctuations. The difficulties in obtaining such a function (see the excellent review by Price¹⁴⁴ in 1967) on a purely theoretical ground led Muhlfeith¹²⁶

in 1972 to suggest that the pressure-driven response function could be determined experimentally from a radiation-driven response function. The purpose of this section is to offer a critical review of the work by Mihlfeith and, therefore, the novelty here is limited to some hopefully constructive comments. For a good background on this material, the interested reader might wish to consult the works by Culick,¹³⁷ by Mihlfeith,¹²⁸ and by T'ien.¹³⁹ In order to make easier the comparison of the results, Mihlfeith's nomenclature will be used as much as possible.

The mass burning rate response function \mathcal{R}_b is defined, in the case of pressure driven oscillations, as

$$(7.2.1) \quad \mathcal{R}_{b,p} \equiv \frac{\dot{m}'/\bar{m}}{p'/\bar{p}}$$

This is, in general, a complex quantity. The real part of the response function gives that portion of the mass burning rate which fluctuates in phase with the pressure and therefore allows energy to be exchanged between the pressure waves in the gas phase and the burning surface. A positive real part of the response function implies an amplification of the pressure waves. It follows that the response function can be seen as an index which measures the tendency of the combustion processes to drive waves and, ultimately, to trigger instability.

The coupling of the combustion processes to the fluid dynamic field in the region of the burning surface is sensitive to fluctuations not only of pressure but also of the gas velocity component parallel to the burning surface. However, except a recent work by Lengelle,¹⁴⁰ most of the theoretical investigations are concerned only with the pressure coupling. Also, a complete study of stability, even if linearized, should take into account all the possible mechanisms of energy losses and gains associated with the presence of a combustion chamber. In this work, no velocity coupling is considered and no reference is made to the combustion chamber (see §1.1). Following Mihlfeith's suggestion, a radiation-driven response function for the mass burning rate is defined as

$$(7.2.2) \quad \mathcal{R}_{b,I} = \frac{\dot{m}'/\bar{m}}{I_0'/\bar{I}_0}$$

This is a straightforward generalization of the previous pressure-driven response function and all the comments previously made still hold true.

With this in mind, let us consider the situation represented in Fig. 22c. We wish to predict the fluctuation of burning rate, or any related parameters, subsequent to an externally controlled fluctuation of the forcing term (pressure or radiant flux intensity).

The following assumptions are made:

1. Gas phase is q.s. (with all the related assumptions of §6.5).
2. Solid phase temperature can be expressed as

$$T(x,t) = \bar{T}(x) + T'(x)e^{i\omega t}$$

where $\bar{T}(x)$ is the unperturbed q.s. profile and $T'(x)$ is a small disturbance profile to be determined. Following Culick's suggestion for the reference system, the condensed phase c translates toward right with speed \bar{R} and, therefore, the surface position fluctuates between two unknown locations ($x = s^-$ and $x = s^+$) across the equilibrium location $x = 0$. A brief summary of how to obtain the response function will be given.

As a first step, the fluctuating thermal gradient on the condensed phase side will be evaluated.

The condensed phase thermal profile is fully described by

$$(7.2.3) \left\{ \begin{array}{ll} \frac{\partial T}{\partial t} + \bar{R} \frac{\partial T}{\partial x} = \alpha_c \frac{\partial^2 T}{\partial x^2} + N_t \frac{a}{\rho_c C_c} (1-r) \bar{I}_0 e^{ax} & \text{PDE} \\ T(x \rightarrow -\infty, \tau) = T_a & \text{BC2} \\ T(x = 0, \tau) = T_s & \text{BC1} \end{array} \right.$$

For small amplitude fluctuations, assumption 2 of a separated dependence of temperature on space and time variables holds. The problem of Eq. (7.2.3) is then split into two parts:

the steady portion

$$(7.2.4) \left\{ \begin{array}{ll} \bar{R} \frac{d\bar{T}}{dx} = \alpha_c \frac{d^2 \bar{T}}{dx^2} + N_t \frac{a}{\rho_c C_c} (1-r) \bar{I}_0 e^{ax} & \text{ODE} \\ \bar{T}(x \rightarrow -\infty, \tau) = T_a & \text{BC2} \\ \bar{T}(x = 0, \tau) = T_s & \text{BC1} \end{array} \right.$$

admitting the solution

$$(7.2.5) \quad \bar{T}(x) = T_a + \left[\bar{T}_s - T_a \right] e^{\bar{R}x/\alpha_c} + \frac{(1-r)\bar{I}_0 N_t}{\rho_c C_c [\alpha_c a - \bar{R}]} \left[a \frac{\alpha_c}{\bar{R}} e^{\bar{R}x/\alpha_c} - e^{ax} \right]$$

and the nonsteady portion

$$(7.2.6) \left\{ \begin{array}{l} \frac{\partial T'}{\partial t} + \bar{R} \frac{\partial T'}{\partial x} = \alpha_c \frac{\partial^2 T'}{\partial x^2} + N_t \frac{a}{\rho_c C_c} (1 - r) I'_0 e^{i\omega t} e^{ax} \\ T'(x \rightarrow -\infty, \tau) = 0 \\ T'(x = 0, \tau) = T'_s \end{array} \right.$$

admitting the solution

$$(7.2.7) \quad T'(x) = T'_{co} e^{\lambda \bar{R} x / \alpha_c} + \frac{(1 - r) I'_0 \cdot N_t}{\rho_c C_c (\alpha_c a - \bar{R} \lambda - i\omega/a)} \left[\frac{a}{\lambda} \frac{\alpha_c}{\bar{R}} e^{\lambda \bar{R} x / \alpha_c} - e^{ax} \right]$$

where T'_{co} is the contribution to the disturbance surface temperature due to conduction.

The complex characteristic root associated with Eq. (7.2.6) is $\lambda = \left[1 + \sqrt{1 + i4\omega\alpha_c/\bar{R}^2} \right] / 2$. The fluctuating portion of the thermal gradient is $\dot{q}'_c \equiv \lambda_c \frac{dT'}{dx}$. Since the surface is itself fluctuating around the mean position $x = 0$, a Taylor expansion is useful.

$$(\dot{q}'_c)_{s-} \equiv \lambda_c \left(\frac{dT'}{dx} \right)_{s-} = \lambda_c \left(\frac{dT'}{dx} \right)_{0-} + x_s \lambda_c \left(\frac{d^2 T'}{dx^2} \right)_{0-} + \dots$$

Culick¹³⁷ shows how to derive from this the following

$$(7.2.8) \quad (\dot{q}'_c)_{s-} = \bar{m} C_c \left[\lambda T'_s + \frac{\bar{T}_s - T_a}{\lambda} \frac{m'_s}{\bar{m}} \right]$$

The next step is to determine the gas phase counterpart of the fluctuating thermal gradient.

Since in this study the specific interest in the gas phase is the heat feedback law rather than the temperature profile, two lines of attack are possible. The first consists of writing an energy balance across the boundaries indicated in Fig. 22c; the second consists of integrating once the temperature distribution in differential form and it therefore requires a detailed flame model. The energy balance for the q.s. gas phase gives

$$(7.2.9) \quad \dot{q}_f = m[Q_f - C_g(T_f - T_s)]$$

where $m = \rho_g U = \rho_c R$ is the mass flux. The differential expression for the temperature distribution in the q.s. gas phase is

$$(7.2.10) \quad m C_g \frac{dT}{dx} = \lambda_g \frac{d^2 T}{dx^2} + Q_f \rho_g \dot{\epsilon}$$

where $\dot{\epsilon}$ is the chemical reaction rate. If $\dot{q}(x) \equiv dT/dx$ is the thermal gradient, the heat feedback law will be determined by integrating the following ODE:

$$(7.2.11) \quad \begin{cases} \frac{d\dot{q}}{dx} - m \frac{C_g}{\lambda_g} \dot{q} = Q_f \rho_g \dot{\epsilon} & \text{I ODE} \\ \dot{q}(x \rightarrow +\infty) = 0 & \text{BC} \end{cases}$$

from which one obtains formally

$$(7.2.12) \quad \dot{q}_f \equiv \dot{q}(x=0) = -Q_f \int_0^{+\infty} e^{-m \frac{C_g}{\lambda_g} x} (\rho_g \dot{\epsilon}) dx$$

The function $\dot{q}_f(P, R)$ is strongly dependent on the choice of the flame model. In general, the mass reaction rate $W \equiv \rho_g \dot{\epsilon}$ is a local function of temperature, composition, etc., and $W = W(x)$ should be considered. However, in order to avoid unnecessary complications in an already approximate treatment, only two limiting, although typical, situations are here examined. For a complete discussion on this point, Ref. 137 is very appropriate.

For a diffusion flame anchored at the surface (distributed flame model), there is only a weak dependence $W = W[T(x)]$ through the dependence of gas temperature on the space variable. The limiting model for this situation is a step function

$$(7.2.13) \quad \begin{cases} W(x) = W_d & 0 < x < x_f \\ = 0 & x > x_f \end{cases}$$

where $W_d = \text{constant}$ to be evaluated and $x_f = \text{thickness of the flame}$ (to be evaluated, if necessary). From Eq. (7.2.12) one gets

$$(7.2.14) \quad \dot{q}_f = Q_f \frac{\lambda_g}{C_g} \frac{W_d}{m} \left[1 - e^{-m \frac{C_g}{\lambda_g} x_f} \right]$$

which is further approximated in the KTSS treatment as

$$(7.2.15) \quad \dot{q}_f \approx Q_f \frac{\lambda_g}{C_g} \frac{W_d}{m}$$

since $m \frac{C_g}{\lambda} x_f \gg 1$ for AP propellants.¹¹⁵ Physically, the last approximation is true whenever the heat feedback to the surface is small compared to the heat release in the gas phase.

For a premixed flame, there is a strong dependence $W = W(T)$ on the temperature so that the reaction is concentrated in a thin space region (sharp flame model); this is a consequence of the Arrhenius temperature dependence of the rate constant. The limiting model for this situation is a Dirac δ function located some distance x_f from the surface

$$(7.2.16) \quad W(x) = W_c \delta(x - x_f) = B P^v T_f^\alpha e^{-E_f/RT_f} \delta(x - x_f)$$

where v = reaction order,

B = pre-exponential factor,

α = flame temperature coefficient, and

E_f = activation energy of the chemical reaction.

Here some further difficulties arise: the flame sheet location x_f needs to be known and E_f needs to be theoretically infinite to shrink the reaction thickness to an infinitesimally small value. In any event, Culick obtains in this case

$$(7.2.17) \quad \dot{q}_f = Q_f \frac{\lambda_g}{C_g} \frac{W_c}{m} \left[\frac{Q_f - C_g(T_f - T_s)}{Q_f} \right]^2$$

The fluctuating portion of the thermal gradient in the gas phase at the surface is, for a diffusion flame

$$(7.2.18) \quad (\dot{q}_f')_{s+} = \lambda_g \left(\frac{dT'}{dx} \right)_{s+} = \bar{m} C_c \bar{T}_s \left[\left(1 - \frac{T_a}{\bar{T}_s} \right) \frac{W P'}{\bar{P}} - \frac{Q_f}{C_c \bar{T}_s} \frac{W_d}{\bar{m}^2} \frac{\lambda_g}{C_g} \frac{m'}{\bar{m}} \right]$$

where $W \equiv n \left[2(1 - H) + \frac{C_g}{C_c} \frac{1 - n_s/n}{s} \right]$ is a constant property of

the propellant. For a premixed flame, one gets

$$(7.2.19) \quad (\dot{q}_f')_{s+} = \frac{3m'q}{\bar{m}} - v \frac{P'}{\bar{P}} - \left(\alpha + \frac{E_f}{RT_f} \right) \frac{T_f'}{\bar{T}_f}$$

where the flame temperature fluctuation can be derived from the integral energy balance Eq. (7.2.9).

As a third step, the matching conditions at the surface are determined. This concerns both mass and energy. At the surface, the mass flux by pyrolysis may be generally written in an Arrhenius form as

$$(7.2.20) \quad m_s = B_s P^{n_s} T_s^{\alpha_s} e^{-E_s/RT_s}$$

where n_s = pressure coefficient
 α_s = surface temperature coefficient
 B_s = pre-exponential factor
 E_s = activation energy of surface pyrolysis.

From the pyrolysis law, the surface temperature fluctuation can be derived

$$(7.2.21) \quad T'_s/\bar{T}_s = (m'_s/\bar{m}_s - n'_s P'/\bar{P})/(\alpha_s + E_s/RT_s)$$

The heat release at the surface is

$$\dot{q}_s = m_s Q_s$$

where Q_s is positive when endothermic.

The mass matching condition is simply

$$(7.2.22) \quad m'_s = m'_g = m'$$

The energy matching condition is more involved; generalizing Culick's approach to include radiation one

$$(7.2.23) \quad (\dot{q}'_f)_{s+} = (\dot{q}'_c)_{s-} + m'_s Q_s + \bar{m} \dot{Q}'_s - (1 - r) I'_0 (1 - N_t)$$

The last two relationships contain all our information about the problem. Upon substitution of Eqs. (7.2.8), (7.2.18) [or (7.2.19)], (7.2.21) and (7.2.22) in (7.2.23), the response function will be defined. For the case of pressure fluctuations only ($I'_0 = 0$) and for a diffusion flame one

$$(7.2.24) \quad \frac{m'/\bar{m}}{P'/\bar{P}} = \frac{(AW + n_s C_g/C_c) + n_s (\lambda - 1)}{\lambda + A/\lambda + EA^2 C_g/C_c + AH + C_g/C_c - 1}$$

where

$$\Lambda^2 \equiv (Q_f W_d \lambda) / (\bar{T}_s \bar{m}^2 C_g^2)$$

$$E \equiv \alpha_s + E_s / (2\bar{T}_s)$$

$$A \equiv (1 - T_a / \bar{T}_s) E$$

$$H \equiv Q_s / [C_c (\bar{T}_s - T_a)] \text{ nondimensional heat release at surface}$$

For the case of radiant flux fluctuations, one can neglect the pressure contribution in Eqs. (7.2.18) [or (7.2.19)] and (7.2.21). For a diffusion flame and a transparent condensed phase one gets

$$(7.2.25) \quad \frac{m'}{\bar{I}_0} = \frac{\frac{E}{C_c \bar{T}_s} \frac{l_{\text{rad}} (l_{\text{rad}} - \lambda)}{l_{\text{rad}}^2 - l_{\text{rad}} - \lambda(\lambda - 1)}}{\lambda + A/\lambda + E\Lambda^2 C_g / C_c + AH + C_g / C_c - 1}$$

where $l_{\text{rad}} \equiv \alpha_c \bar{R}$ in this chapter only stands for the inverse of the nondimensional radiant layer thickness. For a diffusion flame and an opaque condensed phase, one sets $N_t = 0$ in Eqs. (7.2.7) and (7.2.23) or directly $l_{\text{rad}} = \infty$ in the above expression.

For a premixed flame, Eq. (7.2.19) substitutes for Eq. (7.2.18). For radiant flux fluctuations Muhlfeith obtains

$$(7.2.26) \quad \frac{m'}{\bar{I}_0} = \frac{C_3 \frac{l_{\text{rad}} (l_{\text{rad}} - \lambda)}{l_{\text{rad}}^2 - l_{\text{rad}} - \lambda(\lambda - 1)}}{\lambda + A/\lambda + AH + C_5}$$

where

$$C_5 = \left[\frac{C_g}{C_c} \frac{E_s}{2\bar{T}_s} - C_2 - C_1 \right] / C_2 - C_3 C_4 \quad \text{being}$$

$$C_1 = C_g \bar{T}_s / 2C_4$$

$$C_2 = \frac{E_f \bar{T}_s}{2\alpha \bar{T}_f^2} - C_1$$

$$C_3 = \frac{E_s}{2\alpha \bar{T}_s^2 C_c}$$

$$C_4 = Q_f - C_g (\bar{T}_f - \bar{T}_s)$$

For convenience, the mass burning rate fluctuation driven by pressure for a premixed flame is also given, using Muhlfeith's nomenclature:

$$(7.2.27) \quad \frac{m'/\bar{m}}{p'/\bar{p}} = \frac{EW_c + n_s(C_5 + \lambda)}{\lambda + A/\lambda + AH + C_5}$$

The correctness of using a diffusion or a premixed flame model has to be decided case by case. However, for two general classes of propellants considered here, experience and previous studies⁹⁰ suggest the proper choice. A diffusion flame is considered a good approximation for AP type of propellants, while a premixed flame is particularly apt to represent the gas phase of double-base type of propellants. For the case of AP-based composite propellant considered in Ref. 126 and having the specific properties listed in Table 8, a plot of the real part of the radiation-driven response function normalized to the zero frequency limit vs the nondimensional frequency $\Omega \equiv \omega \alpha_c / \bar{R}^2$ is given in Fig. 27. This plot is different from that obtained in Ref. 126, where a premixed flame model has been surprisingly adopted, and which is represented with dashed lines in Fig. 27. Moreover, in the above reference the value of $Q_s = 25$ cal/g has been used: this is numerically small compared to current values in the literature and, in any event, does not satisfy the integral energy balance across the combustion wave. As a consequence, although the qualitative behavior of the plottings in Fig. 27 is correct for both gas phase models, the curves for the distributed flame model hardly show any frequency dependence. This is due to the fact that a wrong set of data has been used. Before making the required correction, let us stress a further point of discussion.

Independently of the choice of the flame model, for radiation-driven fluctuations

$$(7.2.28) \quad \frac{(m'/I_0')_{\text{transp}}}{(m'/I_0')_{\text{opaque}}} = \frac{\ell_{\text{rad}}(\ell_{\text{rad}} - \lambda)}{\ell_{\text{rad}}^2 - \ell_{\text{rad}} - \lambda(\lambda - 1)}$$

whose limit for $\ell_{\text{rad}} \rightarrow 0$ is 0. For a given frequency, then, a larger value of ℓ_{rad} makes the condensed phase more and more insensitive to the fluctuating radiant flux intensity. This effect is obviously lacking in pressure-driven fluctuations. An important implication then is that the only hope of getting a response function for pressure fluctuations from experiments with radiant flux fluctuations is to consider an opaque condensed phase. In this regard, the choice of the flame model is very relevant. Culick observed that any pressure-driven admittance function, if correct, has to respect the static limit defined by the experimental s.s. ballistic law

$$m = ap^n$$

from which $\frac{m'/\bar{m}}{p'/\bar{p}} = n$ for $\omega = 0$. It is therefore required that

$$(7.2.29) \quad \lim_{\omega \rightarrow 0} \mathcal{R}_{b,p}(\omega) = n$$

both for the diffusion (Eq. 7.2.24) and the premixed (Eq. 7.2.27) flame model. It is easily verified that the constraint of Eq. (7.2.29) is always satisfied for a diffusion flame model, whereas for a premixed flame model this is true only for a specific value of the pressure exponent n_s appearing in the surface pyrolysis law (Eq. 7.2.20). For some typical cases it has been found that $n_s = 2$ is required for a pressure-driven admittance function with a premixed flame model to verify the static limit. This strong dependence of the surface pyrolysis law on the pressure might be suspect if one considers that most models of heterogeneous flames work successfully with the simple assumption of $n_s = 0$.

The experimental determination of the pressure-driven response function through radiation-driven tests is possible for all propellants whose gas phase can be modeled by a diffusion flame and for which $n_s = 0$. (This is a common assumption in the literature.) From Eq. (7.2.24) and Eq. (7.2.25), it is then immediately possible to find for an opaque condensed phase that

$$(7.2.30) \quad \frac{(m'/P')_{op}}{(m'/I'_0)_{op}} = \frac{(\bar{m}/\bar{P})AW}{E/(C_c \bar{T}_s)}$$

from which one gets:

$$\frac{\mathcal{R}_{b,p}(\omega)}{\mathcal{R}_{b,I_{op}}(\omega)} = \frac{(m'/P')/(\bar{m}/\bar{P})}{(m'/I'_0)_{op}/(\bar{m}/\bar{I}_0)} = \frac{C_c \bar{T}_s}{E} \frac{AW}{(\bar{m}/\bar{I}_0)}$$

$$\text{Since } \lim_{\omega \rightarrow 0} \frac{m'/P'}{\bar{m}/\bar{P}} = \frac{AW}{[\lambda + A/\lambda + EA^2 C_g/C_c + AH + C_g/C_c - 1]} = n$$

$$\text{and } \lim_{\omega \rightarrow 0} \frac{(m'/I'_0)_{op}}{(\bar{m}/\bar{I}_0)} = \frac{E/(C_c \bar{T}_s)}{[\lambda + A/\lambda + EA^2 C_g/C_c + AH + C_g/C_c - 1](\bar{m}/\bar{I}_0)}$$

one gets

$$(7.2.31) \quad \frac{\mathcal{R}_{b,p}(\omega)/\mathcal{R}_{b,p}(\omega=0)}{\mathcal{R}_{b,I_{op}}(\omega)/\mathcal{R}_{b,I_{op}}(\omega=0)} = 1$$

This shows that there is only a scale factor between the two normalized admittance functions and, indeed, Muhlfeith's suggestion of obtaining the pressure-driven response function from the experimental determination of the radiation-driven response function is very promising. The result, however, is restricted to opaque condensed phases: this restrictive requirement may be somewhat relaxed by careful use of opacifiers (see Refs. 68 and 70, for example) at the surface of the strand and/or by the choice of appropriate wavelength or range of wavelengths of the incident radiation. In general, the above result holds whenever the radiant layer thickness is much smaller than the thermal layer thickness at the operating pressure so that infinite opacity is not required. If interfering effects are minimal one could also think of performing several series of tests (one series for each value of transparency) and then extrapolating the results to zero transparency.

The effects of the parameters discussed on the pressure-driven response function for a sharp flame model are graphically shown in Fig. 28. Except when explicitly denied, the curves have been plotted using, again, the values listed in Table 8. The curve given in Ref. 126 corresponds to $n_s \neq 0$. A comparison with the curve $a \rightarrow \infty$ of the radiation-driven admittance function with a sharp flame model (Fig. 27) shows immediately that the two behaviors are different, mainly in the region of high frequency following the resonance value. Note that if one arbitrarily puts $n_s = 0$, the pressure-driven response function (Fig. 28) exactly corresponds (in the sense specified above) to the radiation-driven response function for $a \rightarrow \infty$ (Fig. 27) even for a sharp flame model. However, in this case, the value of n_s is fixed by the other input parameters and one has to use the value satisfying the requirements of Eq. (7.2.29). As previously mentioned, the s.s. input data used in Ref. 126 and listed in Table 8 are not correct, in that too many parameters have been assigned and, by consequence, the integral balance of energy across the overall combustion wave cannot be satisfied. Indeed,

$$(7.2.32) \quad \bar{m}C_c(\bar{T}_s - T_0) + \bar{m}C_g(\bar{T}_f - \bar{T}_s) = \bar{m}(Q_f - Q_s)$$

$$\text{but} \quad C_c(\bar{T}_s - T_0) + C_g(\bar{T}_f - \bar{T}_s) = 726 \text{ cal/g}$$

$$\text{while} \quad Q_f - Q_s = 825 \text{ cal/g}$$

Obviously, this can be corrected in several ways. For example, the balance of Eq. (7.2.32) can be used to evaluate $Q_f = 701$ cal/g, which is about 12% less than the value used in Ref. 126. In Fig. 28, the curve for $n_s \neq 0$ and the evaluated value of $Q_f = 701$ cal/g shows how drastically the pressure-driven admittance function is changed. The radiation and pressure-driven response functions for the distributed (diffusive) flame model are plotted in Fig. 29. Here the value $Q_s = -125$ cal/g has

been used for the surface heat release; this corresponds to a nondimensional value $H = -0.69$ which is much closer to the currently accepted values in literature.¹¹⁵ The curves in Fig. 29 have been plotted for several values of the volumetric absorption coefficient a ; the curve for $a \rightarrow \infty$ (opaque condensed phase) gives, at the same time, the nondimensional pressure and radiation-driven admittance function in the assumption of $n_s = 0$. The effect of the surface heat release on the admittance function (pressure-driven or radiation-driven for opaque condensed phase) for a distributed flame model is shown in Fig. 30. An increase of the energy release at the surface is destabilizing, in that the maximum amplitude of the admittance function is increased; also, a more marked frequency dependence is observed.

Notice that, independently of the gas phase model, the peak of the admittance function is always located in the region of nondimensional frequency $\Omega \approx 6$, i.e., the range of frequency, at which the burning propellant responds more intensively corresponds roughly to the proper frequency of the system. This can be seen as a resonance phenomenon. Lengellé¹⁴⁷ shows a shift of the resonance region toward larger values of the nondimensional frequencies when the dynamics of the reacting surface layer is also considered. Indeed, this is due to the introduction of a second characteristic frequency of the system higher than the one corresponding to the conductive inert layer in the condensed phase. Conversely, the transparency, in case of radiation-driven admittance function, decreases the characteristic frequency of the condensed phase to an extent proportional to the amount of radiation penetration. Consequently, in this case, the resonance frequency shifts toward smaller values of Ω . Notice, also, that for $\Omega \rightarrow \infty$ all curves trend toward zero, since the inertia of the system becomes more and more important for faster and faster sinusoidal change in time of the external controlling parameters (pressure or radiant flux intensity). The transparency, in the case of radiation-driven admittance function, has a smoothing effect on the response of the system over the whole frequency range; again, this is due to the volumetric heating associated with the radiation penetration.

As a final comment, whether this whole line of research is worth a great effort is debatable. The basic assumption of linearity is usually too drastic in the overall field of combustion. Indeed, only two clear results have been obtained so far:

1. The pressure-driven response function shows a maximum (resonance) when the period of the forcing term approaches the characteristic time of the condensed phase;
2. The radiation-driven response function shows also such resonance phenomenon besides the damping effect of the transparency on the amplitude of the function.

Both results are predictable a priori on simple physical grounds. To extract less immediate results is a cumbersome task and, moreover, is strongly limited by the requirement of linearity.

The excellent work by T'ien,¹³⁹ however, has to be noted. T'ien was able to define a boundary for all possible static solutions and also to determine a more restrictive "dynamic" limit by means of a small perturbation analysis with a combustion model including heat loss by radiation from the burning surface. The response function concept was used by T'ien for predicting the (linearized) stability boundaries rather than for rating the instability trends of solid propellants. In conclusion, the idea of predicting the pressure-driven behavior by means of radiation-driven tests is appealing, but one must first ask how much practical value the pressure-driven response function has.

CHAPTER 8

NONLINEAR BURNING STABILITY ANALYSIS

No general method exists for studying the stability properties of a strongly nonlinear partial differential equation (PDE) subjected to finite disturbances. On the other hand, rigorous methods of investigation have been established by Lyapunov for the case of ordinary differential equations (ODE). In this chapter, therefore, we are going to re-formulate our problem in terms of an ODE. This will be accomplished by means of an approximate approach known as an "integral method". The problem will be then analyzed in this new formulation from the point of view of intrinsic or static stability. The results of this analysis will prove to be of basic importance in the theory of dynamic burning for the case when the external parameters change monotonically in time. It will be found that, in principle, burning solid propellants are subjected to static and dynamic instabilities in both low (fractions of cm/s) and high (some cm/s) ranges of burning rate. A method of determining the static and dynamic stability boundaries will be described and their dependence on several parameters will be discussed. Finally, a method of specifying the range of parameters for which self-sustained oscillations are the only allowed stationary reacting solutions (limit cycle phenomena) will be described.

8.1 Current Status of the Theory of Nonlinear Dynamic Stability of Solid Propellant Combustion

The question of the dynamic extinction by depressurization and, in general, of the burning stability has been well debated in the technical literature,¹⁴⁸⁻¹⁵⁶ but few works have been really constructive. The erroneous application of the quasi-steady gas phase assumption,⁹¹ the strong limitations due to the use of linearized theories, and the empirical nature of several of the proposed criteria^{149,150} are the most serious drawbacks in this area. For a critical review, the interested reader might wish to consult the work by Merkle.^{90a} A paper by T'ien¹²³ is the only one aimed directly at establishing an extinction criterion for fast depressurization. Merkle did not formulate any criterion; indeed, in his work in order "to facilitate the actual detection of extinction by the computer, an 'extinction' temperature (analogous to an ignition temperature) of 600 K [$\theta_g = 0.43$] was specified" (p. 64 of Ref. 90b), below which all chemical reactions were considered unimportant. Likewise, no criterion has been formulated so far for the case of dynamic extinction by fast deradiation reported by the Princeton group (see §4.4 of this work and Ref. 77).

T'ien¹²³ argues that heat losses are the mechanism for both static and dynamic extinctions of solid propellants; this view is not fully shared in this instance (see §8.8).

In any event, T'ien concludes that for depressurization transients, if the instantaneous burning rate drops below the unstable burning rate solution at the final pressure, extinction will occur. T'ien¹³⁹ derives his quantitative criterion from another study by him of flammability limits of premixed flames under the influence of environmental disturbances. A somewhat similar result will be obtained here by following a completely different approach.

The line of research evolved within the framework of the mechanistic (Zeldovich) approach has been unable to reach truly meaningful conclusions so far about the dynamic stability boundary. Istratov, et al¹⁵⁷ in 1964 used an integral method in order to determine an approximate solution to the unsteady nonlinear energy equation in the condensed phase of a propellant burning with constant surface temperature. Extinction was assumed to occur when the surface thermal gradient on the condensed side exceeded a critical value corresponding to the static stability line. This is a serious mistake, since nothing can really be said a priori about the possibility of a dynamic burning regime in a range of burning rate that is statically unstable. Here a similar mathematical formulation has been used, but completely different results have been found. Novozhilov,¹¹⁸ in 1967, improved the previous model by considering a variable surface temperature and recognizing that dynamic burning is allowed also in the range of parameters where statically stable solutions are not found. Extinction is then assumed to occur when the burning rate at the final pressure drops below a limiting value established experimentally in nonstationary burning conditions. This criterion heavily relies on very delicate experimental results and, moreover, fails to assign any premonitory signal, if any, about the approaching of the limit.

This question of a possible early warning of extinction during a depressurization transient evaluated via the Zeldovich method was examined in a paper by the Princeton group⁹² in 1972. The possibility was checked that the crossing of the static stability boundary is sufficient to subsequently produce dynamic extinction. No clear answer to this question was given. The position taken here is that the static stability boundary has only secondary relevance in a dynamic situation. Indeed, according to the same Princeton reference, "the dynamic conditions of extinguishment tend to shift the stability line" (p. 257 of Ref. 92). More extensive work¹²¹ in this area also failed to reach any significant conclusion. In any event, Novozhilov, in 1973, observes that this "question requires certain information about the properties of the system outside the area of smooth burning. Such information cannot be obtained from experiments on steady state combustion. For the calculation of unsteady conditions in the unstable region it is necessary to draw on certain schemes of combustion, which make it possible to predict the properties of propellants beyond the [static]

stability limit." (p. 216 of Ref. 158). In other words, the author admits the failure of the mechanistic approach in this respect and recognizes that burning in the statically unstable region can be treated only with a flame model. However, the need for more advanced treatments in the framework of flame models is advocated in Ref. 159.

In this work, quantitative criteria for dynamic extinction are defined by means of the MTS flame model. An integral approach is used in order to apply known mathematical methods to the resulting approximate ODE formulation. The integral approach has been applied to several burning problems by Soviet investigators.^{24,157,160,161} Somewhat simpler use has been made also at Princeton.^{3,162} Within the framework of this approximation, the static stability analysis associated with intrinsic random disturbances is given in §8.2, while the dynamic stability analysis associated with finite size disturbances following a monotonic decay of externally controlled parameters is given in §8.3. A restrictive comment about quantitative criteria for dynamic extinction is made in §8.4. A general discussion (§8.5) on the possible equilibrium configurations of heterogeneous combustion waves, unreacting or steady reacting or self-sustained oscillating, and more specific considerations (§8.6) on limit cycle phenomena related to burning solid propellants are offered in the next two sections. Further comments on the dynamic burning regime in §8.7 and a summary of the findings in §8.8 conclude the chapter. The reader should note that the dynamic stability analysis heavily relies on the static stability analysis.

8.2 Nonlinear Static Stability Analysis

In this section the integral approach used for reducing the PDE problem to an approximate ODE problem is briefly described. Comments on the validity of the approach are given where appropriate. The reader should pay more attention to the physical interpretation of the results than to the mathematical formulation. This section gives the basis for understanding the subsequent developments.

Basically, the mathematical method is the one set up for the first time by Von Karman and Polhausen in the study of boundary layers and later generalized by Goodman, among others, to a large number of thermal problems. The method can be extended to any other problem described by nonlinear PDE of parabolic type. In the present case, the approach consists of defining a parameter $\delta(\tau)$, called the penetration distance of the thermal wave in the condensed phase, "such that for $|x| > \delta(\tau)$ the [propellant] slab, for all practical purposes, is at an equilibrium temperature and there is no heat transferred beyond this point" (p. 53 of Ref. 163). The evolution in time of the thermal profile in the condensed phase is obtained by following the time history of the penetration distance propagating into an initially

uniform temperature field. Within this penetration layer, progressing in time, the qualitative space distribution of temperature is assumed known a priori; but note that, in so doing, the integral balance of thermal energy in the condensed phase is preserved. In other words, the limitation imposed by making the transformation from PDE to ODE formulation is an approximate solution of the local space distribution of temperature; this is not such a serious drawback because the interest is in the time evolution of the surface temperature. In any event, several investigations found an error of only some percents for various cases in which both the exact and the integral solutions were evaluated. For example, see Fig. 5 on p. 89 of Ref. 163 showing the temperature time history at the surface of a semi-infinite slab with triangular surface heat flux.

In order to get a deeper understanding of questions related to the integral method as applied to thermal problems, the interested reader might wish to consult the excellent review by Goodman¹⁶³ and the references given there. Reading of Refs. 164 and 165 might help the reader to put the method in the right perspective. In any event, before getting involved in mathematical details, the reader should be warned about the limits of the integral method. It is obvious that any solution obtained by the integral method contains, hopefully, small but irrevocable errors in the final numerical results. The question of how to improve the accuracy then arises. It has been argued that "there is no a priori guarantee that increasing the order of the polynomial [used to represent the space distribution of the unsteady temperature profile] will improve the accuracy. Although the accuracy is frequently improved with this technique, it can be demonstrated, nonetheless, that there are cases for which it actually worsens" (p. 96 of Ref. 163). In this same reference it is suggested that the method of weighted residuals provides a very efficient method for improving the accuracy of the results obtained by using the integral method. As a hint for future work, the method of weighted residuals is now briefly described. Suppose an approximate solution $\theta_n(X, \tau)$ of a given nonlinear operator L [e.g., the condensed phase energy equation of Eq. (6.5.2)] is somehow known. The solution θ_n is such that all boundary conditions are satisfied and n unknown parameters are contained. For an exact solution $\theta(X, \tau)$ one would find

$$L(\theta) \equiv 0$$

For the approximate solution $\theta_n(X, \tau)$, instead, one finds

$$L(\theta_n) = \epsilon_n$$

where ϵ_n is a residual. A solution θ_n which makes ϵ_n conveniently small in some sense is sought. In order to do this, we set equal to zero the average (over all space) of product of

the residual ϵ_n by a weighting function w_j

$$\int_X w_j L(\theta_n) dx = 0 \quad j = 1, 2, \dots, n.$$

The solution has to satisfy the above equation. Since the solution θ_n contains n unknown parameters C_{nj} , n different weighting functions are required to defining θ_n . The weighting functions w_j may be the independent variables X_j , for example, or the dependent variable θ_n or any other reasonable function.

For the remainder of this work, a simple integral method will be implemented. This can be considered a special case of the method of weighted residuals when just one parameter (the penetration distance δ) and one weighting function ($w_1 = 1$) are considered. Under these circumstances, the above equation reduces to the heat balance integral (see below). The solution will be assumed to be a cubic profile (see Eq. 8.2.5) in space. Since, as stated above, the integral method assumes a uniform initial distribution of temperature, a new nondimensional variable is defined:

$$(8.2.1) \quad u(X, \tau) \equiv \bar{\theta}_i(X) - \theta(X, \tau)$$

where $\bar{\theta}_i(X)$ is the initial s.s. distribution of temperature and $\theta(X, \tau)$ is the temperature distribution following some perturbation. The new variable $u(X, \tau)$ may therefore be conveniently interpreted as the finite temperature disturbance propagating inside the condensed phase and superimposed on the initial temperature distribution after the action of perturbation. At the initial instant $\tau = 0$, by definition $\theta(X, \tau) = \bar{\theta}_i(X)$ and $u(X, \tau) = 0$. Suppose now that, in the following instant, a perturbation starts acting on the system and makes $u(X, \tau) \neq 0$: the goal of the analysis is to determine the ultimate effect of such a temperature disturbance after waiting a period of time sufficiently long for the perturbation to disappear. In contrast with the previous linearized analysis, no assumption is made as to the size of the temperature disturbance.

The analysis will be restricted to the case of an opaque propellant (in the sense discussed in §A.2). The basic set of nondimensional equations for an opaque propellant burning at constant (initial) pressure PP_i , while subjected to a radiant flux of constant (initial) intensity F_i is:

$$\left\{ \begin{array}{l} \frac{\partial \theta}{\partial \tau} + RR \frac{\partial \theta}{\partial X} = \frac{\partial^2 \theta}{\partial X^2} \\ \theta(X, \tau = 0) = \bar{\theta}_i(X) \\ \theta(X = -\infty, \tau) = 0 \\ \left(\frac{\partial \theta}{\partial X} \right)_{c,s} = \frac{\lambda_g}{\lambda_c} \left(\frac{\partial \theta}{\partial X} \right)_{g,s} - RR \cdot H + (1 - r) F_i \end{array} \right.$$

where $RR(\tau)$ is the burning rate defined by the Arrhenius or KTSS or any appropriate pyrolysis law and $(\lambda_c/\lambda_g)(\partial\theta/\partial X)_{g,s}$ is the nondimensional heat feedback law defined by the MTS (or any appropriate) flame model. In terms of the disturbance temperature $u(X, \tau)$, the set of equations is:

$$(8.2.2) \left\{ \begin{array}{ll} \frac{\partial u}{\partial \tau} = RR \left(\frac{d\bar{\theta}_i}{dX} - \frac{\partial u}{\partial X} \right) + \frac{\partial^2 u}{\partial X^2} - \frac{d^2 \bar{\theta}_i}{dX^2} & \text{II PDE} \\ u(X, \tau = 0) = 0 & \text{X} = (0, -\infty) \\ & \tau \geq 0 \\ u(X \rightarrow -\infty, \tau) = 0 & \text{IC} \\ \left(\frac{\partial u}{\partial X} \right)_{c,s} = \frac{\lambda_g}{\lambda_c} \left(\frac{\partial u}{\partial X} \right)_{g,s} - \frac{\lambda_g}{\lambda_c} \left(\frac{d\bar{\theta}_i}{dX} \right)_{g,s} + RR \cdot H + & \text{BC2} \\ \left(\frac{d\bar{\theta}_i}{dX} \right)_{c,s} - (1 - r) \cdot F_i & \text{BC1} \end{array} \right.$$

$$\text{where } RR(\tau) = e^{-\frac{E_s}{RT_{s,ref}}} \left[\frac{1}{\left(\bar{\theta}_{i,s} - u_s \right) \left(1 - \frac{T_{ref}}{T_{s,ref}} \right) + \frac{T_{ref}}{T_{s,ref}}} - 1 \right]$$

$$\text{or } RR(\tau) = \left[\bar{\theta}_{i,s} - u_s(\tau) \right]$$

and $(\lambda_g/\lambda_c)(\partial u/\partial X)_{g,s}$ is defined, e.g., by the MTS flame model.

Notice that at $\tau = 0$, the surface energy balance is

$$(8.2.3) \quad \left(\frac{d\bar{\theta}_i}{dX} \right)_{c,s} - \frac{\lambda_g}{\lambda_c} \left(\frac{d\bar{\theta}_i}{dX} \right)_{g,s} - (1-r) \cdot F_i = -\overline{RR}_i \cdot H$$

$$- \frac{E_s}{\bar{\alpha} T_{s,ref}} \left[\frac{1}{\bar{\theta}_{i,s} \left(1 - \frac{T_{ref}}{T_{s,ref}} \right) + \frac{T_{ref}}{T_{s,ref}}} - 1 \right]$$

where $\overline{RR}_i = e$ Arrhenius
pyrolysis

or $\overline{RR}_i = \bar{\theta}_{i,s}^s$ KTSS
pyrolysis

Therefore, BCl of Eq. (8.2.2) can be written as

$$(8.2.4) \quad \left(\frac{\partial u}{\partial X} \right)_{c,s} \equiv (u_X)_{c,s} = \frac{\lambda_g}{\lambda_c} \left(\frac{\partial u}{\partial X} \right)_{g,s} - H \cdot (\overline{RR}_i - RR)$$

In what follows, the integral method will be applied without further explanations other than what has been said at the beginning of this section; for applications similar to the one made here, see Kuo¹⁶² or Peretz.³ We first assume a cubic dependence of the disturbance temperature on the space variable:

$$(8.2.5) \quad u(X, \tau) = K_0(\tau) + K_1(\tau) \cdot (X) + K_2(\tau) \cdot (X)^2 + K_3(\tau) \cdot (X)^3$$

Comments about the implications of this particular thermal profile are given below. The above four coefficients $K_i(\tau)$ are to be determined from the boundary conditions which express no disturbance (up to the second derivative) at the cold end of the penetration depth and the energy balance at the hot boundary of the penetration depth. With our formulation this implies:

$$(8.2.6) \quad \left\{ \begin{array}{l} 1. \quad \frac{\partial u}{\partial X}(X = 0, \tau) = (u_X)_{c,s} \\ 2. \quad u(X = X_\delta, \tau) = 0 \\ 3. \quad \frac{\partial u}{\partial X}(X = X_\delta, \tau) = 0 \\ 4. \quad \frac{\partial^2 u}{\partial X^2}(X = X_\delta, \tau) = 0 \end{array} \right.$$

where $X_\delta = -\delta$ is the penetration distance to be obtained below. After algebraic manipulations, one obtains for the unknown profile of the disturbance temperature

$$u(X, \tau) = (u_X)_{c,s} \cdot \frac{\delta}{3} \cdot \left(1 + \frac{X}{\delta}\right)^3$$

For $X = 0$ we get at the surface

$$u(X = 0, \tau) \equiv u_s = (u_X)_{c,s} \cdot \frac{\delta}{3}$$

from which we can express the unknown penetration depth as

$$(8.2.7) \quad \delta(\tau) = \frac{3u_s}{(u_X)_{c,s}}$$

The disturbance temperature profile is then given by:

$$(8.2.8) \quad u(X, \tau) = u_s \left(1 + \frac{X}{\delta}\right)^3$$

where $u_s(\tau)$ is the unknown surface temperature disturbance to be determined. It is obvious from the above relationship that the time history of the disturbance temperature is restricted to disturbance thermal profiles monotonically decaying in space. Indeed, there is no way for a cubic profile to accommodate an inflection point. This difficulty may be overcome by "allowing a new penetration depth to begin propagating at each maximum or minimum" (p. 96 of Ref. 163) of the heat input into the condensed phase. However, this procedure will not prove necessary here, since testing both the static and dynamic stability does not require a detailed knowledge of the structure of the thermal profile.

As a second step, a space integration is performed over X from 0 to $(-\delta)$ of the PDE:

$$\int_0^{X_\delta = -\delta} \frac{\partial u}{\partial \tau} dX = \int_0^{X_\delta = -\delta} \left[RR \cdot \frac{d\theta_i}{dX} - RR \cdot \frac{\partial u}{\partial X} + \frac{\partial^2 u}{\partial X^2} - \frac{d^2 \theta_i}{dX^2} \right] dX$$

$$\frac{d}{d\tau} \int_0^{-\delta} u(X, \tau) dX = -RR \cdot \Delta \left[\bar{\theta}_i \right] + RR \cdot u_s - (u_X)_{c,s} + \Delta \left[\frac{d\bar{\theta}_i}{dX} \right]$$

where

$$(8.2.9) \quad \begin{cases} \Delta(\bar{\theta}_i) \equiv \bar{\theta}_i(X=0) - \bar{\theta}_i(X=-\delta) \\ \Delta\left(\frac{d\bar{\theta}_i}{dX}\right) \equiv \frac{d\bar{\theta}_i}{dX}(X=0) - \frac{d\bar{\theta}_i}{dX}(X=-\delta) \end{cases}$$

Upon substituting the approximate profile found above, one obtains

$$(8.2.10) \quad -\frac{3}{4} \frac{d}{d\tau} \left[\frac{u_s^2}{(u_X)_{c,s}} \right] = -RR \cdot \Delta(\bar{\theta}_i) + RR \cdot u_s - (u_X)_{c,s} + \Delta\left(\frac{d\bar{\theta}_i}{dX}\right)$$

Since $(u_X)_{c,s} = f(u_s(\tau); PP, F)$ one can write for the burning rate relaxation (at constant pressure and radiant flux)

$$(8.2.11) \quad \frac{d(u_X)_{c,s}}{d\tau} = \frac{du_s}{d\tau} \left(\frac{\partial (u_X)_{c,s}}{\partial u_s} \right)_{PP, F = \text{const}}$$

which can be evaluated once a flame model (in this case, the MTS one) has been established. After manipulations, the following ODE for the time dependent surface temperature disturbance is obtained

$$(8.2.12) \quad \begin{cases} \frac{du_s}{d\tau} = -\frac{2}{3} \frac{(u_X)_{c,s}}{u_s} \frac{RR \cdot u_s - (u_X)_{c,s} + \Delta\left(\frac{d\bar{\theta}_i}{dX}\right) - RR \cdot \Delta(\bar{\theta}_i)}{1 - \frac{1}{2} \frac{u_s}{(u_X)_{c,s}} \left[\frac{\partial (u_X)_{c,s}}{\partial u_s} \right]_{PP, F}} \\ u_s(\tau=0) \approx 0 \end{cases}$$

which is approximately equivalent to the initial PDE + boundary conditions formulation. Notice that in the above equation $\bar{\theta}_i(X)$ is known (see Eq. A.2.5), that only the surface temperature appears, and that the denominator (evaluated according to the MTS flame model) is found to be always positive in the range of values of interest.

The above nonlinear ODE in $u_s(\tau)$ also describes the response of the system when a finite departure (from the stationary value) of the surface temperature $u_s(\tau=0) \neq 0$ occurs for intrinsic reasons, in a propellant initially burning steadily at a given ambient temperature, pressure, and external radiant flux

intensity. If one wishes to know the whole temperature profile, he has only to substitute $u_s(\tau)$ in Eq. (8.2.8), evaluate $\delta(\tau)$ from Eq. (8.2.7) with the help of Eq. (8.2.4), and then use the $u_s(\tau)$ definition (Eq. 8.2.1) in order to determine the resultant temperature profile.

Considerations of a general character on the stability of the system described by Eq. (8.2.12) can now be made. According to the theory based on the Lyapunov theorems, a given equilibrium configuration of the system is asymptotically stable if

$$\text{or} \quad \left. \begin{aligned} u_s(\tau) &\rightarrow 0 \\ \theta(X, \tau) &\rightarrow \bar{\theta}_i(X) \end{aligned} \right\} \text{for } \tau \rightarrow \infty$$

In other words, the system is (asymptotically) stable if the disturbance disappears at large time and the system returns to its initial configuration. Following Lyapunov (p. 216 of Ref. 166), Eq. (8.2.12) can be written as

$$\frac{du_s}{d\tau} = -f(u_s)$$

or, considering the $u_s(\tau)$ definition (Eq. 8.2.1), as

$$(8.2.13) \quad \frac{d\theta_s}{d\tau} = +f(\bar{\theta}_{i,s} - \theta_s)$$

One can then think of the chemically reacting system comprised of the burning propellant as analogous to a mass-spring type mechanical system with the nonlinear characteristic $f(\bar{\theta}_{i,s} - \theta_s)$. In what follows, the function $f(\bar{\theta}_{i,s} - \theta_s)$ will be called the nonlinear static restoring function.

Consider the qualitative plot of Fig. 31a and Fig. 31b before examining the quantitative plots of Figs. 32-35. Quantitative plots of the function $f(\bar{\theta}_{i,s} - \theta_s)$ vs θ_s are given in Figs. 32 to 35 for the propellant AP/PBAA #941 having the properties listed in Table 7. They have been obtained by assuming a modified (see below) Arrhenius-type pyrolysis law at the surface and an MTS type of flame model. According to Eq. (8.2.13), all the points (algebraic roots) for which $f(\bar{\theta}_{i,s} - \theta_s) = 0$ define possible equilibrium configurations for the burning propellant, since they correspond to $d\theta_s/d\tau = 0$. It is seen in Fig. 31a that, in addition to the trivial $\theta_s = 0$ (unburning propellant, root C), two more equilibrium solutions (roots A and B) are allowed, in general, for a given set of parameters. Let us consider the equilibrium configuration corresponding to root A. Suppose that, for some unspecified reason, the burning rate RR or the surface temperature θ_s increases a finite amount; then

the burning propellant is no longer in a stationary configuration, $d\theta_s/d\tau = f(\theta_{i,s} - \theta_s)$ is negative, and the system reacts by decreasing its surface temperature. Conversely, if for an unspecified reason, the surface temperature of a propellant burning according to the configuration of root A decreases, the system reacts by increasing its surface temperature. These movements, around point A, are indicated by arrows in Fig. 31a. It is concluded that the equilibrium configuration corresponding to root A is stable because, when disturbed, the system always moves back toward A. By the same arguments, it is concluded that the equilibrium configuration corresponding to root B is unstable; any disturbance yields movement away from the point. Therefore, in steady state experiments, only solution A is observed.

If the set of parameters is changed, for example the pressure is increased from P to P_1 , the initial condition of the ODE (see Eq. A.2.5) is changed so that a new pair of roots, A_1 and B_1 , is found in addition to the trivial $\theta_s = 0$ of root C. Again, root A_1 defines a stable equilibrium configuration, while root B_1 defines an unstable equilibrium configuration corresponding to the new set of parameters. Likewise, a new pair of roots, A_2 and B_2 , in addition to the trivial $\theta_s = 0$ of root C, is found if the pressure is decreased from P to P_2 . It follows that the θ_s axis in Fig. 31a includes, in addition to the trivial solution of nonburning propellant at the root C, a segment of stable solution A_i and a segment of associated unstable solution B_i (each pair of roots corresponds to a given set of parameters).

It should be explicitly observed that the trivial $\theta_s = 0$ solution may be obtained only if the exponential Arrhenius-type pyrolysis law for mass production at the surface is dropped. For purposes of this study, it is convenient to assume the exponential form as standard pyrolysis law for most of the surface temperature range, while the KTSS power form is considered valid at low surface temperature values. The two pyrolysis laws are arbitrarily matched at $\theta_s = 0.15$. Obviously, the trivial $\theta_s = 0$ solution implies that no external energy source (e.g., radiation) is acting on the solid propellant.

The qualitative picture of Fig. 31a illustrates the general behavior of the static restoring function when the pressure is varied parametrically at fixed ambient temperature and surface heat release. The behavior of the static restoring function when the surface heat release is varied parametrically, at fixed ambient temperature and pressure, is illustrated by the qualitative picture of Fig. 31b. Of course, all previous considerations hold true. For example, when the surface heat release is low enough (in a sense which will be better understood below), the system described by Eq. (8.2.13) behaves again according to the static restoring function represented by curve CBA (Fig. 31b). However, for increasing values of the surface heat release, it

is found that the static restoring function is represented by curve $CB_1A_1D_1E_1$. This is rather surprising; in principle, there are now five equilibrium configurations for this system.

Based on the previous analysis, however, it is immediately recognized that C is the stable equilibrium solution for the unreacting state (trivial solution). But further discussion is required to understand the nature of the remaining four roots. This is most easily accomplished by considering the steady state energy balance of the overall combustion wave. For example, the graphic plot of Fig. 25 suggests that for each set of parameters only one solution exists for the reacting state. Conventionally, let us call A that particular root of Figs. 31a and 31b corresponding to the energy balance solution of Fig. 25. It follows that root E_1 , although stable according to Lyapunov, is eliminated as being a reacting equilibrium solution. The remaining roots B_1 and D_1 are, then, both unstable equilibrium solutions for the reacting state.

For further increase of the surface heat release, it is observed that A- and D-type roots respectively increase (moving to right) and decrease (moving to left) in the plot of Fig. 31b, until coalescence and then crossing over occur with exchange of stability character. This important point will be discussed in detail later (see §8.5). For further increasing of the surface heat release, B- and D-type roots disappear after coalescence, while both A_2 and E_2 roots, for different reasons, are eliminated as being stable reacting solutions (curve CA_2E_2 in Fig. 31b). Under these circumstances, it follows that the only allowed solution is the trivial unreacting configuration represented by root C. Any attempt to produce a stationary combustion wave with a static restoring function of type CA_2E_2 will inevitably result in extinction. This type of extinction, however, cannot be qualified as "dynamic" (see §8.3 and §8.5).

The implications of the different shapes of the static restoring functions will be discussed throughout this chapter. Now, a most important feature common to all static restoring functions is emphasized. The specific surface temperature value, θ_s^S , at which the pair of solutions A_1^S stable and B_1^S unstable coalesces, at a given pressure (Fig. 31a) and for a given set of parameters,

$$A_1^S = B_1^S \equiv \theta_s^S$$

defines the branching or metastable point at that pressure (and for that set of parameters). Corresponding to this special value of the surface temperature a change of the character of stability occurs at the given pressure, in that for $\theta_s < \theta_s^S$ all the equilibrium solutions at that pressure are statically unstable (roots B_i) while for $\theta_s > \theta_s^S$ all the equilibrium solutions at

that pressure are statically stable (roots A_i). Therefore, the branching point at a given pressure isolates the critical static stability value, θ_s^* , of the surface temperature at that pressure. Construction of the static stability boundary on the MTS plane RR vs q_g , in a range of pressure, consists of connecting the critical static stability points defined for each pressure of interest in the wanted range. This implies the search of the branching point at any fixed pressure. A method of implementing the search is discussed below.

The above stability arguments can be put on a quantitative basis by means of the "first" Lyapunov criterion. According to this, the solution of the nonlinear autonomous ODE of Eq. (8.2.13) is stable in the neighborhood of a point θ_s^* if

$$\left[\frac{df(\bar{\theta}_{i,s} - \theta_s)}{d\theta_s} \right]_{\theta_s = \theta_s^*} < 0$$

at the point of interest θ_s^* . The physical meaning of this criterion has been explained above. In keeping with the spirit of this physical interpretation, the strength of the stability of the solution at a point θ_s^* may be measured by the magnitude of the derivative $df/d\theta_s$ evaluated at $\theta_s = \theta_s^*$. How this value is affected by typical parameters is discussed below. In the exceptional case of a branching, or metastable, point in which the unstable and the stable solutions coalesce, the above first criterion is not valid. In the present situation, however, it is enough to say that the point θ_s^* is stable from one side ($\theta_s > \theta_s^* + \epsilon$) while it is unstable on the other side ($\theta_s < \theta_s^* - \epsilon$), so that, overall, the point θ_s^* is said to be unstable. It should be clear that the first Lyapunov criterion (used for measuring the strength of the stability) is essentially a linearization criterion of the originally nonlinear ODE. However, it is plausible that both roots C and A are stable to finite disturbances of an unknown size, also. The extent of the stability region around the stable roots could be estimated by the Lyapunov "direct" method; but this is not one of the purposes of this analysis. Physically, it is expected that the range of stability of C root (always stable) is limited upward by B while the range of stability of A root (if stable) is limited downward by B. But dynamic effects may increase the range of stability of C root against the range of stability of A root.

The effect of the ambient pressure on the static restoring function $f(\bar{\theta}_{i,s} - \theta_s)$ plotted vs the nondimensional surface temperature θ_s is illustrated in Fig. 32 for the indicated set of parameters. An increase of pressure implies an increase of the stable equilibrium surface temperature, but a less pronounced increase of the unstable equilibrium surface temperature. The strength of the stability is enhanced by an increase of

pressure; numerical values are listed in Table 9. Curves are of the type CBA (see Fig. 31a), except at $P = 10$ atm; this will be discussed in detail in §8.5. Similar comments hold true as to the effect of an external radiant flux on the restoring function (Fig. 33). It is important, however, to note that an increase of the external radiant flux decreases the unstable equilibrium surface temperature and above a certain value of radiant flux intensity (e.g., $40 \text{ cal/cm}^2\text{-s}$ for the set of parameters in Fig. 33) no more unstable solutions are found. This implies that, in principle (see §8.3), at each pressure a minimum value of external radiant flux intensity exists above which the dynamic boundary can no longer be defined. The effects of surface heat release (Figs. 34a and 34b) are more involved and will be discussed in detail in §8.5 and §8.6. Note, however, that for increasing values of the surface heat release, the behavior of the static restoring function shifts from a CBA-type (see Fig. 31a) curve for $Q_s = 150$ and -158.2 cal/g , to CBADE (see Fig. 31b) for $Q_s = -170$ and -180 cal/g , and to CBDAE for $Q_s = -200 \text{ cal/g}$ with A-D roots coalescence occurring at $Q_s = -190 \text{ cal/g}$. This implies that at 30 atm the system will show dynamic stability effects not only in the low range of surface temperature (root B in Fig. 31a) but also in the large range (root D in Fig. 31b). The effects of ambient temperature (Fig. 35) are of little interest in the range investigated. Values of the stability strength in various conditions are summarized in Table 9.

The attention of the reader has already been called to the fact that the most important piece of information in this non-linear static stability analysis is the value of the surface temperature corresponding to the branching point at any given pressure. A general method (based on nonadiabaticity of the propellant) for solving this problem is mentioned in §8.8. However, for the specific case of a solid composite propellant in the range 2 - 40 atm, the search for the branching point may be performed immediately, although not rigorously, based on observation of the physical processes. Consider the qualitative picture superimposed in Fig. 36 on a standard MTS flame model plot. Recall that burning rate and surface temperature are univocally related by an appropriate pyrolysis law. Therefore, it is irrelevant to define the branching point in terms of burning rate or surface temperature. Now, as schematically indicated in Fig. 36, the branching point is determined at each pressure by the geometrical condition of vertical tangent, i.e., infinite slope or maximum heat feedback. Indeed, for $\theta_s > \theta_s^*$ a change of burning rate or surface temperature produces opposing effects on the thermal gradients at the surface from the condensed and the gas phase sides; for example, the former increases but the latter decreases when the burning rate is disturbed upward. This competition is the stabilizing mechanism. For $\theta_s < \theta_s^*$ a change of burning rate affects, in the same direction, both thermal gradients; this is destabilizing. Just at the point with

vertical tangent, the two unstable and stable static roots $A_s = B_s$ coalesce and an exchange of the stability character of the solutions occurs; therefore, we may identify this point as the wanted branching or metastable point θ_s^S . For $\theta_s = \theta_s^S$ the behavior of the system depends on the direction of the perturbation. Now, in order to construct a static stability boundary in the plane \dot{R}_R vs \dot{q}_g , it is enough to connect the branching points θ_s^S, \dot{q}_g^S associated with each pressure. This boundary separates the region where static solutions are allowed from the region where no static solution can be found.

The following observations are of concern at this point. This analysis gives more general and more reliable results than the previous linearized analysis (Chapter 7). There are two reasons for this: (1) we dropped the strongly restrictive assumptions of linearized equations and infinitesimal disturbances, and (2) we adopted a more general flame model. In principal, this type of analysis may be applied to any heterogeneous deflagration wave, provided a proper flame model is furnished. For the specific system (a composite solid propellant) presently dealt with, a reasonably complete picture of the static stability properties was obtained with little effort as compared to other types of stability analysis.

In conclusion, let us summarize the findings of this section. Within the accuracy of an unsophisticated integral method approach, it has been shown that for a fixed set of parameters (if the surface heat release is low enough):

1. two equilibrium solutions exist for the surface temperature of a burning propellant, in addition to the trivial $\theta_s = 0$ corresponding to a nonreacting configuration.
2. of the two equilibrium states, one is stable ($df/d\theta_s < 0$), while the other is unstable ($df/d\theta_s > 0$).
3. the exceptional case of a branching (or metastable) point, in which the stable and the unstable solutions coalesce, corresponds to the nonlinear static boundary point.
4. the branching point may be determined by the intuitive approach illustrated in Fig. 36.

Within the accuracy of the integral method approach, it has also been shown that increasing the surface heat release (for an otherwise fixed set of parameters) the following facts are observed:

5. a new pair of roots, D_1 unstable and E_1 stable, appear in the high burning rate region (see Fig. 31b).

6. roots A and D approach until coalescence (with stability character exchange) occurs. The steady state reacting solution (root A), stable before coalescence, is unstable after.
7. roots B and D approach until they merge and disappear, so that only C, A_2 , and E_2 roots are left (see Fig. 31b).

For all cases, the steady state energy balance is verified only at roots C (unreacting mode) and A (reacting mode). Therefore, these are, in general, the only allowed stationary solutions and can be observed either experimentally or theoretically as long as they are stable. But increasing surface heat release displaces the reacting parameters toward faster regimes with loss of stability of root A: this also, then, becomes unobservable.

With this background, one is now ready to approach the more difficult but fruitful area of nonlinear dynamic burning.

8.3 Nonlinear Dynamic Stability Analysis (Dynamic Extinction)

In the next four sections (§8.3 - 8.6) we examine the general problem of the behavior of a propellant initially burning steadily under a given set of external parameters, then subjected to arbitrary but known changes in time of radiant flux intensity and/or pressure. In this section, inquiry is made, in particular, about the possibility of dynamic extinction of the propellant even though it may be capable of statically stable burning for the given final set of external parameters. It is expected that this will be a function of the rate of decrease of the external parameters from the initial set of values. Specific reference to this question will be made, but the overall line of attack is of a general nature.

Two broad hypotheses are made as to the burning propellant: quasi-steady behavior of the gas phase (with all the related assumptions of §6.5) and, in order to apply the integral method without excessive difficulties, optical opacity of the condensed phase. This second hypothesis is relevant in the case of radiant flux change, but it is not expected to affect the conclusions in a significant way, as will be discussed at the end of this section.

The approach followed in the previous section will now be generalized: let $u(X, \tau)$ again be the disturbance temperature in the sense already specified. The basic set of equations is easily derived from §8.2.

$$(8.3.1) \quad u(X, \tau) = \bar{\theta}_i(X) - \theta(X, \tau)$$

definition

$$(8.3.2) \quad \bar{\theta}_i(X) = f(X; PP_i, F_i \dots)$$

known from the
initial s.s.
configuration

$$(8.3.3) \quad \left\{ \begin{array}{l} \frac{\partial u}{\partial \tau} = -RR \cdot \frac{\partial u}{\partial X} + \frac{\partial^2 u}{\partial X^2} + RR \cdot \frac{d\bar{\theta}_i}{dX} - \frac{d^2 \bar{\theta}_i}{dX^2} \\ u(X, \tau = 0) = 0 \\ u(X \rightarrow \infty, \tau) = 0 \\ \left(\frac{\partial u}{\partial X} \right)_{c,s} = \frac{\lambda_g}{\lambda_c} \left(\frac{\partial u}{\partial X} \right)_{g,s} - \frac{\lambda_g}{\lambda_c} \left(\frac{d\bar{\theta}_i}{dX} \right)_{g,s} + RR \cdot H + \\ \left(\frac{d\bar{\theta}_i}{dX} \right)_{c,s} - (1 - r) \cdot F(\tau) \end{array} \right.$$

II PDE
 $X = (0 - \infty), \tau \geq 0$

IC

BC2

BC1

$$(8.3.4) \quad RR(\tau)$$

a pyrolysis law

$$(8.3.5) \quad \frac{\lambda_g}{\lambda_c} \left(\frac{\partial u}{\partial X} \right)_{g,s}$$

MTS flame model

$$(8.3.6) \quad P(\tau) \text{ and } F(\tau)$$

externally assigned

Using Eq. (8.2.3), BC1 of Eq. (8.3.3) is written as

$$(8.3.7) \quad (u_X)_{c,s} = \frac{\lambda_g}{\lambda_c} (u_X)_{g,s} - H \cdot (\overline{RR}_i - RR) + (1 - r) \cdot (F_i - F)$$

Since $(u_X)_{c,s} = f[u_s(\tau); PP(\tau), F(\tau)]$ Eq. (8.2.11) for the time derivative of the thermal gradient at the condensed phase side is then generalized to

$$(8.3.8) \quad \frac{d(u_X)_{c,s}}{d\tau} = \frac{du_s}{d\tau} \left[\frac{\partial (u_X)_{c,s}}{\partial u_s} \right]_{PP,F} + \frac{dPP}{d\tau} \left[\frac{\partial (u_X)_{c,s}}{\partial PP} \right]_{F,u_s} + \\ -(1 - r) \frac{dF}{d\tau}$$

This can be explicitly written as

$$\frac{d(u_X)_{c,s}}{d\tau} = \frac{du_s}{d\tau} \left[\frac{\partial}{\partial u_s} \left(\frac{\lambda}{c} g(u_X)_{g,s} + H \cdot RR \right) \right]_{PP} +$$

$$\frac{\lambda}{c} g \frac{dPP}{d\tau} \left[\frac{\partial (u_X)_{g,s}}{\partial PP} \right]_{u_s} - (1-r) \frac{dF}{d\tau}$$

which can be evaluated once a flame model has been chosen and the laws $PP(\tau)$ and $F(\tau)$ have been externally assigned.

The above formulation of Eq. (8.3.3) of the problem in terms of the PDE + boundary conditions is now transformed to an approximate equivalent ODE formulation by means of the integral method. The first step is to define the disturbance temperature profile in the condensed phase. The same cubic law as in Eq. (8.2.5) is assumed. Since the four boundary conditions are formally the same as in Eq. (8.2.6) again the following approximate disturbance temperature profile is obtained:

$$(8.3.9) \quad u(X, \tau) = u_s (1 + X/\delta)^3$$

where, again, the penetration depth is given by

$$(8.3.10) \quad \delta(\tau) = \frac{3u_s}{(u_X)_{c,s}}$$

In other words, this first step is formally a copy of the corresponding portion of the previous section except for the substitution of Eq. (8.3.7) for Eq. (8.2.4) as far as $(u_X)_{c,s}$ is concerned. The second step is to integrate the PDE of Eq. (8.3.3) over the space variable from $X = 0$ to $X = -\delta$, taking into account BC1 and BC2. This also is formally a copy of the corresponding portion of the previous section, except for the appropriate evaluation of $(u_X)_{c,s}$. Therefore, one obtains again the following differential expression:

$$(8.3.11) \quad \frac{d}{d\tau} \frac{u_s}{(u_X)_{c,s}} = - \frac{4}{3} \left[RR \cdot u_s - (u_X)_{c,s} - RR \cdot \Delta(\bar{\epsilon}_i) + \Delta \left(\frac{d\bar{\theta}_i}{dX} \right) \right]$$

where the symbol Δ has been defined in Eq. (8.2.9). The final step is to substitute Eq. (8.3.8) defining the time derivative of $(u_X)_{c,s}$ into the above differential expression. One obtains, after manipulations, the following ODE formulation of the problem:

$$(8.3.12) \left\{ \begin{aligned} \frac{du_s}{d\tau} &= -\frac{2}{3} \frac{(u_X)_{c,s}}{u_s} \frac{RR \cdot u_s - (u_X)_{c,s} - RR \cdot \Delta(\bar{\theta}_i) + \Delta\left(\frac{d\bar{\theta}_i}{dX}\right)}{1 - \frac{1}{2} \frac{u_s}{(u_X)_{c,s}} \left[\frac{\partial (u_X)_{c,s}}{\partial u_s} \right]_{PP,F}} + \\ &\frac{\frac{dPP}{d\tau} \left[\frac{\partial (u_X)_{c,s}}{\partial PP} \right]_{F,u_s} - (1-r) \frac{dF}{d\tau}}{\frac{2(u_X)_{c,s}}{u_s} - \left[\frac{\partial (u_X)_{c,s}}{\partial u_s} \right]_{PP,F}} \\ u_s(\tau = 0) &= 0 \end{aligned} \right.$$

which generalizes the previous Eq. (8.2.12). The above ODE describes not only the response of the system to finite size departure of the surface temperature, $u_s(\tau = 0) \neq 0$ but given, from the stationary value due to intrinsic perturbation sources acting on the system (static stability), but also it describes the full history of the disturbed surface temperature subsequent to any arbitrary but externally assigned change in time of controlling parameters such as pressure and radiant flux intensity. The dependence of the fate of the disturbed surface temperature on the rate of change in time of the controlling parameters is the focus of the dynamic stability analysis. Also in this respect, the formulation of the problem is not complete without assigning

$$PP = PP(\tau) \quad \text{being} \quad PP(\tau = 0) = PP_i$$

$$F = F(\tau) \quad \text{being} \quad F(\tau = 0) = F_i$$

Typical, but by no means necessary, laws are:

$$(8.3.13) \quad PP(\tau) = PP_i - (PP_i - PP_f)(1 - e^{-B_p \cdot \tau}) \quad \tau \geq 0$$

$$(8.3.14) \quad F(\tau) = F_i - (F_i - F_f)(1 - e^{-B_r \cdot \tau}) \quad \tau \geq 0$$

describing the forced transition of the system from an initial s.s. configuration corresponding to point I (see Fig. 37) toward a final allowed s.s. configuration corresponding to point F (note that the system may extinguish instead of reaching the final s.s.

configuration). The coefficients B_p and B_r are two nondimensional assigned constants upon which the rate of decrease of $PP(\tau)$ and $F(\tau)$, respectively, depend. These specific laws are considered as representative of the experimental depressurization tests performed among others by Merkle⁹⁰ and of the deradiation tests performed at Princeton University.⁷⁶⁻⁷⁹

The objective here is to predict when an allowed static transition (realized through a succession of exclusively s.s. configurations) becomes forbidden if one attempts to realize it in a q.s. fashion. In order to illustrate the physical situation, let us consider a pure deradiation transient performed according to Eq. (8.3.14) on an opaque propellant with fixed pressure $PP = PP_i$. Such a transition is represented by a dashed line in Fig. 37a. It is assumed that I and F are both statically stable points. If an undershoot occurs, the transition will be dynamically stable only if a recovery point (defined in Fig. 37a as the point where $dRR/d\tau = 0$) occurs. Dynamic stability means than an inquiry is made about the possibility of the occurrence of a recovery point.

In order to determine the location of a dynamic stability boundary (if it exists) on the standard RR vs q_g plane used for the MTS flame model, we heuristically follow the same approach as for the static stability boundary. First, a definition is sought for a critical dynamic stability point at a given pressure and, second, a connection is made of all the dynamically critical points in the desired range of pressure. The critical dynamic stability point may now be identified with that special value θ_g^D of the surface temperature, if any, such that extinction necessarily follows when the surface temperature is even momentarily less than this special value. All points $\theta_s < \theta_g^D$ (Fig. 38) are "no-return" points since they do not allow recovery, while all points $\theta_s > \theta_g^D$ are possible "return" points since they do allow recovery. The critical dynamic stability point, if any, is isolated by the coalescence of the return with the no-return points.

In the case of deradiation only according to Eq. (8.3.14), the general expression of Eq. (8.3.12) may be specialized to

$$(8.3.15) \quad \frac{d\theta_s}{d\tau} = f(\bar{\theta}_{i,s} - \theta_s; PP_i, F_i \dots) - g(\tau, \bar{\theta}_{i,s} - \theta_s; B_r, F_i, F_f)$$

where

$$(8.3.16) \quad \begin{cases} g(\tau \geq 0^+, \bar{\theta}_{i,s} - \theta_s) = \frac{(1-r) \cdot B_r (F_i - F_f) \cdot e^{-B_r \cdot \tau}}{\frac{2(u_X)_{c,s}}{u_s} - \left[\frac{\partial(u_X)_{c,s}}{\partial u_s} \right]_{PP,F}} \\ g(\tau \leq 0^-, \bar{\theta}_{i,s} - \theta_s) = 0 \end{cases}$$

The dynamic stability analysis requires consideration of the nonlinear ODE of Eq. (8.3.15). The basic difference from the static stability analysis is that the rate of return of the surface temperature toward the equilibrium value now depends explicitly on time, so that no a priori analysis is possible. However, Eq. (8.3.15) shows that the rate of the response of the system can be separated in two terms: of these, $f(\bar{\theta}_{i,s} - \theta_s)$ is the "autonomous" contribution discussed in the previous section while $g(\tau, \bar{\theta}_{i,s} - \theta_s)$ is the "nonautonomous" contribution due to the finite disturbance subsequent to a given deradiation law.

The main interest is the asymptotic behavior of the system for $\tau \rightarrow \infty$ (i.e., times much longer than an external characteristic time scale): to predict whether the final stable equilibrium point F or the trivial solution $\theta_s = 0$ will be reached (Figs. 37a - 37b). For the wide range of controlling parameters varying in time according to monotonically decreasing functions, the qualitative behavior of the nonautonomous term $g(\tau, \bar{\theta}_{i,s} - \theta_s)$ may be portrayed. Indeed, Eq. (8.3.16) shows (see Fig. 37c - 37d) that:

$$(8.3.17) \left\{ \begin{array}{l} 1. \quad g(\tau \geq 0^+, \bar{\theta}_{i,s} - \theta_s) \geq 0 \text{ at any instant following} \\ \quad \text{the beginning of the transition, since the denom-} \\ \quad \text{inator is found to be a positive quantity in the} \\ \quad \text{range of interest.} \\ 2. \quad g(\tau \rightarrow \infty, \bar{\theta}_{i,s} - \theta_s) = 0 \text{ asymptotically in time.} \end{array} \right.$$

It follows that before and after (for $\tau \rightarrow \infty$) the externally controlled transition, the rate of return of surface temperature toward the equilibrium value is governed by the (autonomous) nonlinear static restoring function $f(\bar{\theta}_{i,s} - \theta_s)$, i.e., Eq. (8.3.15) reduces to Eq. (8.2.13) whose properties have been already illustrated in §8.2.

A qualitative picture of the behavior of the system governed by Eq. (8.3.15), under the conditions specified by Eq. (8.3.17) and for given initial conditions, can be portrayed in the plane $d\theta_s/d\tau$ vs θ_s (Fig. 38). The points I and F (cf. Figs. 37a - 37b and 38) are respectively the statically stable initial and final equilibrium configurations. All trajectories (representing the history of the system) in Fig. 38 start from the point I and terminate either at the point F or at the origin of the axes (dynamic extinction). In the qualitative portrait of Fig. 38 the nonlinear characteristics $f(\bar{\theta}_{i,s} - \theta_s)$ at $\tau=0$ and $f(\bar{\theta}_{f,s} - \theta_s)$ at $\tau \rightarrow \infty$ have been represented. On the horizontal axis, the nondimensional surface temperature corresponding to the branching point θ_s^* at the operating pressure has been marked. This value (statically critical point) separates the statically stable points (I, F...) from the statically unstable points (L, M...). Notice that in Fig. 31a, points I, F... correspond to stable roots of type A, while points L, M... correspond to unstable roots of type B. For a q.s. transition, the trajectory

starting from point I progresses into the negative half-plane $d\theta_s/d\tau < 0$, since the term $g(\tau, \bar{\theta}_{i,s} - \theta_s)$ initially dominates the term $f(\bar{\theta}_{i,s} - \theta_s)$ in the ODE of Eq. (8.3.15). But the sketch of Fig. 37d shows that $g(\tau, \bar{\theta}_{i,s} - \theta_s)$ decreases monotonically toward zero. When $g(\tau, \bar{\theta}_{i,s} - \theta_s)$ becomes negligible compared to $f(\bar{\theta}_{i,s} - \theta_s)$, the latter term might drive the trajectory toward the final point F.

The rate of return of the surface temperature toward equilibrium for $\tau \rightarrow \infty$ is controlled only by the autonomous term. This means that, in the disturbance history, it is the intrinsic stability of the final state that tends to govern the behavior of the system. Therefore, at a given value of pressure, the critical "no-return" point is defined by the statically unstable root θ_s^D (point M) associated with the final statically stable root $\bar{\theta}_{f,s}$ (point F) through the function $f(\bar{\theta}_{f,s} - \theta_s)$. It will be noticed that the whole segment between θ_s^S and θ_s^D is statically unstable but allows a dynamic burning regime. The unstable root θ_s^D in Fig. 38 represents a limiting condition which is a unique property of the system at the operating (final) pressure. This analysis can be repeated for different values of pressure, so that a dynamic stability boundary may be constructed as shown in Fig. 39 for standard ambient temperature (300 K) and no residual radiant flux.

Note that in the general ODE formulation of Eq. (8.3.12) the influence of time-varying external parameters is felt only through their time derivatives. This implies that, if no change of pressure and/or radiant flux occurs, the system is only subjected to random intrinsic fluctuations and the results from the static stability analysis apply. It is also implied that, in the case that $g(\tau, \bar{\theta}_{i,s} - \theta_s) \ll f(\bar{\theta}_{i,s} - \theta_s)$ in Eq. (8.3.12), the dynamic stability boundary is a no-return boundary for any τ (even finite) and for any external law (even non monotonic or increasing). Note at last that, for clarity sake (cf. §8.5), the dynamic stability boundary just determined will be called, for the remainder of this work, lower dynamic stability boundary.

The unstable root θ_s^D in Fig. 38 represents a limiting condition which is a unique property of the propellant at the operating pressure (for a given set of parameters it depends only on the properties of the intended final state.) It follows that the line connecting all the points θ_s^D is the lower dynamic stability boundary not only for deradiation transients, monotonically decaying toward zero, but also for depressurization transients monotonically decaying. Moreover, the unstable root θ_s^D is determined for $\tau \rightarrow \infty$, that is, when the radiant flux is no longer acting and, therefore, whether the propellant is or is not transparent is irrelevant. Then, for deradiation transients monotonically decaying toward zero, the transparency of the condensed phase has no influence on the dynamic stability. No problem arises if one wishes to consider the effect of other

parameters, for example the ambient temperature, on the lower dynamic stability boundary: it is enough to determine the statically unstable root (B-type in Fig. 31a) for each ambient temperature of interest (e.g., see Fig. 35).

In conclusion, the following facts emerge from the dynamic stability analysis of adiabatic solid propellants, in the low (fractions of cm/s) burning rate regime, for a given monotonic law of timewise change of the controlling parameters:

1. extinction may occur even though the final point of the transition is statically stable,
2. the lower dynamic stability boundary is the locus of the statically unstable roots associated with the final statically stable root through the static restoring function $f(\bar{\theta}_{f,s} - \theta_s)$, and
3. a dynamic stability analysis requires a flame model approach (see §8.1).

8.4 The Question of the Critical Conditions for Dynamic Extinction

In the previous section the existence of a lower dynamic stability boundary different from the static stability boundary has been shown. It has been said that crossing of this boundary is enough to assure dynamic extinction for the wide range of controlling parameters varying in time according to monotonically decreasing functions. A major problem in the theory of heterogeneous flame dynamics is the prediction of the maximum rate of change of a controlling parameter allowed without suffering dynamic extinction. It should be clear that no general answer can be given to this question, not even for the class of monotonically decreasing functions, since, in general, the full dynamic history of the system has to be considered. The best one can hope to do is to assign a criterion for a specific type of monotonically decreasing law, for example the exponential law of Eq. (8.3.14) for a deradiation transient. In this case, the trajectories of Fig. 38 show that a critical value $|d\theta_s/d\tau|*$ exists such that for $|d\theta_s/d\tau| < |d\theta_s/d\tau|*$ a recovery point subsequently occurs, whereas for $|d\theta_s/d\tau| > |d\theta_s/d\tau|*$ no recovery point is possible. Likewise, one could have an even earlier warning about the occurrence of dynamic extinction by considering a critical value $|d^2\theta_s/d\tau^2|*$ associated with the paths leaving point I. However, no great importance is attached to this idea of obtaining an "early warning" being this strictly dependent on the specific external law being considered.

All criteria assigning critical conditions for predicting extinction are necessarily approximate, often to an unknown extent. Indeed, the lower dynamic stability boundary is uniquely defined as a property of the system and does not depend on the

specific decay law externally assigned as long as this law is monotonic. Conversely, any prediction is necessarily associated to a specific monotonic decay law. Furthermore, it will be shown in §8.5 that dynamic extinction may occur in other, unexpected circumstances. Therefore, approximate criteria are not only of very limited use but might also be badly mistaken.

8.5 Lower and Upper Dynamic Stability Analysis

So far, only dynamic effects associated with a B-type root (see Figs. 31a and 31b) have been discussed. In fact, similar dynamic effects are also associated with a D-type root (see Fig. 31b). The former is called lower dynamic stability and the latter is called upper dynamic stability. Although the last has been essentially neglected in the literature, both types of instabilities are very important in practice. Lower dynamic stability relates to extinction. Upper dynamic stability relates to vigorous accelerations of the combustion wave and, therefore, pressure build-up due to large mass production; eventually mechanical failure of the enclosing vessel or dynamic extinction might follow.

With reference to Fig. 34a, it is seen that a burning rate increase, occurring for $Q_s = 158.2$ cal/g (no D-type root), is immediately and effectively balanced by the strong stability character associated with the reacting equilibrium configuration of root A (see Table 9). Obviously, this is true only up to a finite size of the initial disturbance. With reference to Fig. 34b, it can be seen that for $Q_s = -170$ cal/g the static restoring function features two dynamically unstable roots, B ($\theta_s = 0.68$) and D ($\theta_s = 1.15$), sitting at the sides of the stable steady state configuration A ($\theta_s = 0.95$). Under these circumstances, if the surface temperature during a transient goes past B or D, the combustion wave will accelerate respectively toward C ($\theta_s = 0$; lower dynamic instability) or E ($\theta_s = 1.29$; upper dynamic instability). In the case of lower dynamic instability, the fate of the combustion wave is extinction; this has been studied in detail in §8.3. In the case of upper dynamic instability, the fate of the combustion wave is more involved. As soon as root D is passed, a vigorous acceleration occurs. The increase of burning rate may be of orders of magnitude. Root E, although strongly stable, is not allowed as stationary solution. Therefore, after reaching E the wave is violently recalled toward a stable steady state configuration. Depending on the dynamics of the whole process, this can be either the reacting mode A or the unreacting mode C (dynamic extinction due to overstability). In other words, a dynamic extinction may be the unexpected result of a "too fast" pressurization (for example) transient.

Even more striking is the behavior of the system for $Q_s = 200$ cal/g (Fig. 34b). In this case, the static restoring function features two stable roots, D ($\theta_s = 0.93$) and E ($\theta_s = 1.61$),

neither of which is allowed as a stationary solution, sitting at the sides of the unstable stationary solution A ($\theta_s = 0.99$). Under these circumstances, even in a static environment, the burning propellant is not capable of finding an equilibrium reacting configuration and bounces back and forth around A under the competing influences of D and E. It is confirmed (see §9.5) by numerical integration that, after a transient, the combustion wave undergoes sharp self-sustained oscillations around A with peaks near D and E. This suggests, under the specified conditions, the existence of a limit cycle. If so, being a limit cycle an overall property of the governing differential equation, once triggered this oscillatory behavior would not depend on the initial conditions of the system (see §8.6). With this notable difference, i.e., self-sustained oscillations substituting for the stationary solution as a regime reacting state, all previous considerations on transients are valid. If the surface temperature momentarily goes past B ($\theta_s = 0.72$), the combustion wave will irresistibly accelerate toward C (dynamic extinction). This may happen if we try to slow down the combustion wave (e.g., by depressurization) and also if, in trying to accelerate the combustion wave (e.g., by pressurization), the system goes too much past E during the initial transient. Therefore, depending on the dynamics of the whole process, the final result of a transient toward a state controlled by a static restoring function of the type CBDAE is either a self-sustained oscillating combustion wave or dynamic extinction.

For $Q_s = -230$ cal/g (for clarity not represented in Fig. 34b), the static restoring function is found to be of the type CAE. As noted in §8.2, under these circumstances the only possible solution, even in a static environment, is the trivial unreacting state. Since there is no alternative solution, this should be considered a static extinction. In other words, too much surface energy release excludes any reacting solution in the high burning rate regime just as well as too low gas phase energy release (or sufficiently large heat losses) excludes any reacting solution in the low burning rate regime.

The values of the nondimensional surface temperature, associated with the various types of roots discussed, are listed in Table 10 in function of the nondimensional surface heat release at $P = 30$ atm. At this pressure, upper dynamic stability (i.e., existence of a D-type root) shows up for $|Q_s| > 170$ cal/g. For decreasing pressure, the minimum value of $|Q_s|$ at which upper dynamic instability shows up also decreases (Table 11). In particular, at $P = 10$ atm there is upper dynamic instability already at $Q_s = -158.2$ cal/g. This implies that in the MTS plot of Fig. 39, the region of dynamic stability is not only bounded downward by a lower dynamic limit (see §8.3) but also upward by an upper dynamic limit (not drawn) which, for the specific set of parameters of Fig. 39, would lie somewhere in the upper left corner of the plot.

8.6 Self-Sustained Oscillations of Burning Solid Propellants

In this section more results concerning the self-sustained oscillations of heterogeneous combustion waves mentioned in §8.5 are given. First, a simple procedure for detecting the existence of a limit cycle should be straightforward from the previous discussion. The simultaneous presence of two ingredients in the static restoring function is required: (1) A root unstable, and (2) D and E roots stable. The critical condition for satisfying the first requirement is the coalescence of A-D roots (cf. Fig. 34b); the second condition is satisfied as long as coalescence of B-D roots has not yet occurred (cf. Fig. 34b). Therefore, in order to detect the existence of a limit cycle at a given pressure, it is enough to plot the values of the relevant roots in function of the surface heat release at the given pressure. For example, in the case considered in Table 10 (adiabatic opaque AP/PBAA #941 burning at $P = 30$ atm and $T_a = 300$ K), the existence of a limit cycle is expected between $Q_s = 190$ cal/g (A-D coalescence) and $Q_s \sim 225$ cal/g (B-D coalescence). Similar plots can be made for any other set of operating conditions. The results found in the range 10 - 30 atm are summarized in Table 12. It is seen that the minimum value of surface heat release, at which self-sustained oscillations are expected, increases with pressure; the range of surface heat release, at which self-sustained oscillations are expected at a given pressure, seems also to increase with pressure.

A physical explanation of the above results might be the following. Any self-sustained reactive system is capable of exothermic reactions. These partly occur in the gas phase (Q_f) and partly in the condensed phase (Q_s). The total energy release $Q_f(P) + Q_s$ is determined by the energy balance on the overall steadily burning propellant at the given set of operating conditions. Moreover, for a fixed set of operating conditions (pressure, radiant flux, and ambient temperature), q_s increases while q_f decreases for increasing burning rate. For low values of Q_s , an increase of burning rate and thereby of $\dot{q}_s \equiv \rho_c R Q_s$ is counterbalanced through a simultaneous decrease of $\dot{q}_f \sim 1/R$ and increase of the heat flux $q_c \sim RT_s$ absorbed into the condensed phase. However, for large values of Q_s , an increase of burning rate might be destabilizing if q_s increases more than $(q_c - q_f)$. This implies an acceleration of the combustion wave, that is the appearance of a D-type root in the nonlinear static restoring function (see Fig. 31b). On the other hand, for the same set of operating conditions, a large increase of burning rate (up to two orders of magnitude, as shown in §9.5) is strongly stabilizing. Indeed, under these circumstances, the increase of \dot{q}_c is much larger than the increase of $(\dot{q}_c + \dot{q}_f)$ due to the Arrhenius-type dependence of the surface temperature on the burning rate. This corresponds to the appearance of an E-type root in the nonlinear static restoring function (see Fig. 31b). Therefore, at each pressure

(see Table 10) a critical (A-D coalescence) value of surface heat release exists above which the energy coupling between condensed and gas phases becomes locally unstable, i.e., a burning rate disturbance due to the change of heat flux absorbed into the condensed phase is counterbalanced only "in the large" (through a limit cycle process) by an appropriate change of heat feedback from the flame and the surface reacting layer. Furthermore, at each pressure (see Table 10) a second larger critical (B-D coalescence) value of surface heat release exists above which the energy coupling between condensed and gas phases becomes totally unstable (except at the trivial root C), due to the excessively large thermal gradients occurring in the condensed phase near the burning surface.

As to the pressure effect, recall that increasing pressure implies increasing Q_f , which subsequently requires a larger value of Q_s for destabilizing the combustion wave. Therefore, larger pressures require larger values of Q_s for triggering both the upper instability (see Table 11) and the self-sustained oscillation mechanism (see Table 12).

The reader has probably already realized that an estimate of the amplitude of the limit cycle oscillations can be immediately derived by a plot of the appropriate static restoring function (e.g., Fig. 34b or Table 10). Indeed, the extent of the oscillations are basically limited by roots D (minimum value) and E (maximum value). Instead, the frequency of the oscillations depend on the thermal wave relaxation in the condensed phase. Comments on these points are given in §9.5.

In conclusion, it is emphasized that this remarkable mechanism of self-sustained oscillations, once triggered, is absolutely independent of the previous history of the system. Although detection of the existence of a limit cycle and prediction of its basic properties are made, much work remains to be done, in particular as to the excitation of the oscillations.

8.7 Further Considerations Regarding the Dynamic Burning Regime

The plot of the static or autonomous nonlinear restoring function $f(\bar{\theta}_{f,s} - \theta_s)$ in Fig. 38 shows that the trajectories, in the case of both static and dynamic extinction, approach the trivial stable solution $\theta_s = RR = 0$ asymptotically and tend to coalesce more and more near the final point O. Indeed, in the region $\theta_s < \theta_s^D$ below the dynamic limit, the initial information is being lost and it becomes very difficult to distinguish trajectories which had different previous dynamic histories. All this is obvious from the physical point of view.

Notice that, within the accuracy of the method, the transient paths leading to extinction may be fully evaluated by means of the integral approach. Notice also that, differently from all previous works, the existence of a boundary in the present theory

implies that the crossing of the critical line may occur at any stage of the transition, not only at the final conditions. For very fast transients this crucial condition may occur at the beginning of the dynamic burning history (in a sense this could be considered as a warning signal).

As to the other stable solution $\theta_s = \bar{\theta}_{f,s}$ (the intended end point of the transient), the prediction of the behavior of the trajectories, in approaching it, is much more involved. First, the final portion of the path may be evaluated only by numerical integration or by an integral approach considering multiple penetration depths in order to account for the inflection point in the thermal profiles. Therefore, in this section, it is necessary to resort to qualitative comments. The magnified view of the restoring function $f(\bar{\theta}_{f,s} - \theta_s)$ in the region surrounding the final point F in Fig. 38 suggests that either an asymptotic or a damped oscillatory behavior may be expected. Intuitively, one expects that the damped oscillatory type of approach toward the final equilibrium is favored when a strong restoring force has been acting on the system, so that an excessive momentum has built up. In the actual burning propellant, this implies that an excessive (compared to the final equilibrium state) thickness of the thermal layer in the condensed phase is still present in the system. This persistent memory arises with either a transparent propellant subjected to fast q.s. deradiation or with any propellant that has experienced a deep undershoot in burning rate during a fast q.s. transient near the dynamic limit. In any event, the excess of energy, stored either in the radiant layer at the beginning of the transition or momentarily in the thermal layer in the dynamic burning regime, has to be dissipated. The damped oscillations around the point F in Fig. 38 provide this dissipating mechanism. Since the phenomenon is controlled by the inertia of the condensed phase, the period of these oscillations is expected to be of the order of the relaxation time of the condensed phase thermal wave.

The nonlinear nature of the restoring function opposing the excursion of the propellant during a given transient is featured by the occurrence of a sharp maximum (see Figs. 32-35) near the static limit θ_s^* . If, in a dynamic burning regime, the surface temperature falls below this value ($\theta_s < \theta_s^*$), the resistance of the propellant to extinction quickly decreases although dynamic stability is still assured. This region, therefore, is expected to be particularly sensitive to any change of initial conditions. Experimental tests in this marginal zone of dynamic stability would have to be very accurate; it is very likely that inevitable data scattering could mask this extension of the stability zone. Computer simulated runs might also require a precision of initial data larger than in any real situation, as is indeed shown in the results to be discussed in §9.3.

A check on the validity and on the accuracy of the analysis offered can be made only by computer simulation using the full unsteady equation and by experimental tests. Computer runs were performed with this specific goal and the results are reported in Chapter 9. It should be emphasized that the computer checks were made by solving numerically the PDE formulation of the general q.s. transient problem, whereas the stability boundaries have been found by analytical means from considerations of the approximately equivalent ODE formulation. As to experimental tests, any q.s. transient induced by a monotonic change in time of any of the controlling parameters is adequate for checking the validity of the proposed method. Simple go/no-go results are sufficient to locate, at least approximately, the lower (for example) dynamic stability line as a border between a region of burning continuing after the transition and a region of extinction induced by the transition. Typical experiments of this nature are the depressurization tests of Ref. 90 and the deradiation tests of Refs. 76 - 79, for example. A method of performing more meaningful experimental tests is suggested in §10.3.

8.8 Summary and Conclusions

In this chapter the problem of the q.s. burning of a solid propellant in its more general form has been dealt with. In order to retain the nonlinearity of the problem, an approximate formulation in terms of an ODE has been written. This has been done by means of a rather simple integral approach limited, for sake of simplicity, to situations in which no inflection point in the history of the condensed phase thermal profiles would occur. Nevertheless, it has been shown that the important facts (see below) of heterogeneous combustion may be ascertained. The two fundamental regimes of the static (intrinsic random perturbations) and of the dynamic (finite size disturbances following externally assigned change of the controlling parameters) stability of heterogeneous flames have been examined.

The following facts emerge from the nonlinear static stability analysis. For a given set of parameters:

1. a stable stationary nonreacting equilibrium configuration (trivial solution) is always found;
2. a stable, stationary or self-sustained oscillating, reacting equilibrium configuration may be found;
3. with reference to Fig. 3lb, the static stability boundary is the locus of the branching points (A-B roots coalescence) in the RR, \dot{q}_g plane;
4. self-sustained oscillations are found between A-D roots coalescence and B-D roots coalescence;

5. after B-D roots coalescence, no stable reacting equilibrium solution is found.
6. The effect of the relevant parameters can be easily evaluated (see Figs. 32-35).

The following facts emerge from nonlinear dynamic stability analysis. For a given monotonic law of timewise decrease of the controlling parameters:

1. extinction may occur even though the final point of the transition is statically stable;
2. the lower dynamic stability boundary is the locus of the statically unstable roots (B-type) associated with the final statically stable root through the static restoring function (see Fig. 31a);
3. upper dynamic stability is related to D and E roots (see Fig. 31b) and may cause vigorous acceleration of the combustion wave with final failure of the vessel or dynamic extinction.

It is important to recall that the use of a flame model is essential in these theoretical developments (see §8.1). It is also stressed that, although heat loss from the system is an important aspect of the problem as rightly pointed out by T'ien,¹²³ the basic reason for the dynamic extinction is the thermal inertia of the condensed phase which is a most important heat sink. Indeed, in this work nonadiabaticity is not considered an essential ingredient of stability theories (cf. §8.1), since the sheer existence of unstable solutions is not necessarily related to nonadiabatic propellants (see Figs. 32-35 for example). However, in qualitative agreement with this work, T'ien found that the critical condition for dynamic extinction by depressurization is fixed by the (statically) unstable root at the final pressure. On the other hand, the present work is of a more general nature since it allows the prediction of dynamic extinction under various conditions, the definition of both static and dynamic stability boundaries, and the possibility of ascertaining self-sustained oscillations of burning propellants. In any event, it seems suitable to incorporate the heat loss mechanisms considered by T'ien into the present model in order to obtain more accurate results. Indeed, this analysis has been restricted since the beginning to adiabatic propellants only for simplicity and no major problem arises if one wishes to consider the more realistic model of a nonadiabatic propellant. Preliminary work in this direction shows that all boundaries are shifted so as to make burning more difficult, until combustion is no longer allowed even in static conditions (pressure deflagration limit). In particular, it is found that for a given pressure, increasing the heat loss from the propellant, a limiting reacting

solution is determined for the surface temperature or burning rate. This limit exactly coincides with the critical static point as defined in §8.2. Nonadiabaticity allows, then, an alternative and physically more sound approach to the determination of the static stability boundary.

It is also important to point out explicitly that, in order to obtain meaningful results, a better model of the condensed phase at low burning rates is required. Indeed, the critical values of surface temperature corresponding to the static and dynamic boundaries fall in a range of values so low that physico-chemical properties different from those used in the usual range of burning rates may be found. The proper pieces of information, provided at least by an intelligent experimentation if not theoretically, should be taken into account when considering very special phenomena such as the disappearance of the dynamic limit shown in Fig. 33.

Notice that numerical values have been given only for a particular composite propellant (AP/PBAA #941). This was done simply because the properties of that particular propellant and a good flame model were readily available. It is felt, however, that all analyses were conducted from a broad point of view, and in no way were they dependent on the particular type of propellant chosen as the datum case. Therefore, the conceptual results are expected to hold, although in different ranges of the relevant parameters, for any kind of solid propellant.

It has already been mentioned that the above theory may be checked by numerical integration (see Chapter 9) or by experiments (see suggestions in §10.3). Finally, it is recalled (see §8.2) that the accuracy of the theoretical predictions might be sensibly improved by the use of more sophisticated methods (for example, method of weighted residuals) for constructing the nonlinear static restoring function from the original partial differential equation.

CHAPTER 9

NUMERICAL RESULTS

In this chapter the results obtained by numerical solution of the basic set of Eqs. (6.5.2)-(6.5.14) are presented. Fast quasi-steady transients are simulated, with exponential laws for the history of the controlling parameters. The assumptions are those listed in §6.5. Computations have been performed for the propellant AP/PBAA #941 whose properties are listed in Table 7. Comments about the numerical approach are given in §9.1 - 9.3.

9.1 Numerical Schemes

The nonlinear parabolic PDE of Eq. (6.5.2) has been integrated according to a numerical scheme taken from Ref. 167 (scheme #13, p. 191) and shown in Fig. 40a. Consider the simple problem

$$\begin{cases} \frac{\partial \theta}{\partial \tau} - \sigma \frac{\partial^2 \theta}{\partial x^2} = 0 \\ \theta(X, \tau=0) = \text{given initial condition} \\ \text{boundary conditions} \end{cases}$$

where $\theta = \theta(X, \tau)$ and

σ is a constant assumed positive.

The time derivative is numerically approximated by a weighted average of the values in the neighborhood of the point we are solving for θ_{j+1}^{n+1} :

$$\begin{aligned} \frac{\partial \theta}{\partial \tau} = & \frac{1}{2} \frac{3/2 \theta_{j+1}^{n+1} - 2\theta_{j+1}^n + 1/2 \theta_{j+1}^{n-1}}{\Delta \tau} + \\ & \frac{5}{6} \frac{3/2 \theta_j^{n+1} - 2\theta_j^n + 1/2 \theta_j^{n-1}}{\Delta \tau} + \\ & \frac{1}{2} \frac{3/2 \theta_{j-1}^{n+1} - 2\theta_{j-1}^n + 1/2 \theta_{j-1}^{n-1}}{\Delta \tau} \end{aligned}$$

The second space derivative is numerically approximated by a standard central difference:

$$\frac{\partial^2 \theta}{\partial x^2} = \frac{\theta_{j+1}^{n+1} - 2\theta_j^{n+1} + \theta_{j-1}^{n+1}}{(\Delta x)^2}$$

This scheme is particularly convenient for rapidly varying functions and is known to be always stable. An estimate of the truncation error is given in Fig. 40a.

However, our problem includes other lower order terms, such as the first space derivative in the convective term, which can jeopardize the utility of the above numerical scheme. It is shown in Ref. 167 (p. 195) that stability is unaffected by the presence of lower order terms with constant coefficients. In our case, the strong nonlinear dependence of the convective term not only affects the choice of the time step size but also might influence the stability of the overall approach. Unfortunately, no general safe method exists for dealing with a complicated problem such as the one in Eqs. (6.5.2) - (6.5.14) and the obvious method of using the above numerical scheme with sufficiently small (to be defined) discretization steps has been adopted.

Both the boundary conditions of Eq. (6.5.2) have a direct influence on the space net dimension, but their requirements are in opposing directions: BC2 requires an extended space net which goes deep inside the solid phase, while BC1 requires a fine space net. In order to avoid unnecessary expenditure of computer core and time, the temperature at the cold boundary is considered to be approximately zero when it is of several orders of magnitude less than the surface temperature. Computer runs performed for different sets of input data indicate that cold boundary temperatures $\theta(X \rightarrow -\infty, \tau) = O(10^{-5})$ or less have no appreciable influence on the structure of the thermal profile near the surface of the condensed phase. For each run the total number, JF , of space integration steps is then chosen by requiring that $\theta(X \rightarrow -\infty, \tau) = O(10^{-6})$ at least.

The numerical treatment of BC1 of Eq. (6.5.2) has proved to be most delicate. This is obvious if one considers that the coupling of the gas with the solid phase is expressed precisely through the energy balance of BC1. An error is introduced whenever the temperature gradient at the surface is evaluated using a too large space step. Physically, this is due to the fact that volumetric terms (radiation penetration, convective and unsteady effects) become important compared to the surface terms (collapsed reacting layer, condensed and gas phase side thermal gradients) and cannot be neglected in the energy balance across the finite thickness ΔX required by the numerical approach. For each run the space mesh size ΔX is then chosen by requiring that across ΔX

$$\text{BC1 error} \equiv \frac{\text{temperature change due to volumetric terms}}{\text{temperature change due to surface terms}} \ll 1$$

The above check is made at each time integration step. Computer runs performed for different sets of input data indicate that a BCl error up to a few percent, at most, has no appreciable influence on the overall numerical solution.

The numerical molecule shown in Fig. 40a is associated with a single mesh of dimensions $\Delta X \cdot \Delta \tau$ and implies the solutions of JF simultaneous algebraic equations on 3 time levels. The parameter JF is an integer assigning the total number of nodes in the space net. As mentioned above, JF and ΔX are fixed by a convenient compromise between cost and accuracy of the numerical results in the spacewise dimension. The time step size $\Delta \tau$ is chosen by requiring that the change in time of the surface temperature be limited to a few percent, at most, at each integration step. Typical values used for the time and space step sizes are given in §9.2.

The algebraic system derived from the discretization of the PDE is then cast in a very special form called a tridiagonal matrix. An efficient method of solution suitable for automatic computation is indicated in Ref. 167 (p. 199). It should be noticed that an initialization procedure is required, since the scheme of Fig. 40a implies the knowledge of the two previous time vectors $\theta^{n-1}(X)$ and $\theta^n(X)$ when solving for the current $\theta^{n+1}(X)$. This is accomplished by using a simple Crank-Nicholson scheme (shown in Fig. 40b) for the first few time integration steps. This classical Crank-Nicholson scheme uses two time levels and is always initiabile, since in our transients the first vector in time is just the solution of the s.s. thermal profile.

Both the schemes shown in Fig. 40 are implicit and unconditionally stable (when applied to the simple diffusion problem discussed at the beginning of this section). However, scheme (a) is superior to scheme (b) in that, containing more "memory of the past", it better represents rapidly varying functions. Moreover, the truncation error for scheme (a) is of order $(\Delta X)^4$ rather than $(\Delta X)^2$ as it is for scheme (b).

9.2 Organization of the Numerical Program

A flow chart of the overall program is shown in Fig. 41. The program allows the user to perform 4 different types of calculations: steady state or quasi-steady state transients due to external radiant flux and/or ambient pressure changing in time according to any arbitrary but fixed law. The type of calculation is optional, but has to be specified at the beginning by the user by assigning a certain code value to the parameter IOP (see Fig. 41).

As a first step, the s.s. configuration corresponding to the arbitrary but fixed initial condition is evaluated. This is done numerically by the subroutine RTMI (taken from an IBM scientific package) solving the nonlinear algebraic energy conservation equation by a bisection method¹⁶⁸. The transient is, then,

evaluated by implementing the numerical scheme of Fig. 40b (for the first time integration step at least) and Fig. 40a (for all successive time integration steps).

As already mentioned in §6.5, the coupling of the condensed phase energy equation to the surface pyrolysis law through the convective term of Eq. (6.5.2) requires an iterative procedure for the surface temperature θ_s . Moreover, the coupling of the condensed phase energy equation to the gas phase heat feedback law through BC2 of Eq. (6.5.2), requires another iterative procedure for the flame temperature θ_f . The flow chart given in Fig. 41 shows that the θ_f loop is internal to the θ_s loop, so that the overall approach consists in evaluating θ_f (subroutine MEAP74) for an assumed value of θ_s and then in checking θ_s . This is done with a simple trial and error procedure for the first few integration steps. Successively, for computational efficiency, a less primitive predictor-corrector type of approach is implemented through a parabolic extrapolation.¹⁶⁸ This is accomplished separately for both loops and for each of them a convergence test is applied at every integration step according to the following definition:

$$\text{loop error} = \left| \frac{\text{corrected value} - \text{predicted value}}{\text{corrected value}} \right|$$

For most runs an error of less than 1% has been specified. The numerical evaluation of the transient proceeds until negligible values of burning rate (extinction) or negligible oscillations of burning rate around the final intended s.s. value are observed.

Typical values used for the time and space step sizes are:

$$\Delta\tau = 0.01 \text{ and } \Delta X = 0.01$$

The reasons behind this choice were given in §9.1. Such values are by no means mandatory and have been adapted to specific situations with the overall goal of the best compromise of cost vs accuracy. A minimum number of about one hundred steps in time is usually performed. Since the surface temperature gradient in most of the cases dealt with decreases in time, a variable time step size is used during the same computer run. Usually a transient starts with an (initial) $\Delta\tau = 0.01$ and then proceeds with larger value up to $\Delta\tau = 0.10$. A minimum number of about one thousand steps in space is usually adopted. However, particular situations (e.g., self-sustained oscillations of burning rate or oscillatory change in time of external radiant flux intensity impinging on a sensibly transparent propellant) may require much more tedious computations.

The program has been written in the FORTRAN IV language and has been run both on IBM 360/91 and UNIVAC 1108 computers. A typical run resulting in dynamic extinction requires a core

of about 250 K and 30 seconds of machine time with an H level compiler in the IBM system.

9.3 Checks on the Numerical Approach

A series of checks were made, and some were incorporated permanently in the program, in order to make sure that the overall numerical approach was performing as intended. Actually, the difficulties inherent in the numerical solutions of Eqs. (6.5.2 - 6.5.14) deserve a full study by themselves; therefore, only semi-empirical tests are reported.

The first obvious check is to compare the results obtained in this study with those found in previous investigations. In this respect the work by Merkle⁹⁰ has been found particularly useful as to the depressurization tests. Likewise, very helpful is the comparison of the steady state solutions found numerically with the corresponding analytical solutions. These checks were used to localize all possible trivial errors upstream of the overall numerical approach.

The appropriate choice of the time and space size was verified according to the standard procedure of varying the time and space mesh size in a programmed manner, while keeping the input data fixed. For the values of Δt and ΔX given in §9.2 no appreciable difference in the results could be detected by halving or doubling the mesh size.

The stability of the overall numerical approach was checked by letting the computer run free on hypothetical transients with no change in time of the controlling parameters. Oscillations of negligibly small amplitude around the initial s.s. configuration (known to be physically stable) were observed.

All these checks, although successful, not only are not conclusive but also are, in principle, restricted to those specific situations in which they were performed. It was felt convenient to have some form of internal check in the program itself, so that each run could at least be considered self-consistent. Therefore, at each integration step, not only the cold boundary temperature and the BCl error (discussed in §9.1), but also the integral balances of energy in the solid phase and across the whole deflagration wave are checked. Again, these also are not conclusive tests but must rather be viewed as effective warning signals whenever the integral balance is not satisfied at any stage of the transient.

9.4 Numerical Results from Quasi-Steady Fast Transients

In this section the results obtained by computer simulated experiments of quasi-steady (in the sense explained in §6.1) transients driven by fast change in time of ambient pressure or external radiant flux are described.

9.4.1 Background and Qualitative Considerations

The general set of assumptions underlying the results presented in this and following sections has been summarized in §6.5. It should be recalled that because of the q.s. assumption, all of the results of this work are not valid if the characteristic time in a gas phase is not small compared with the characteristic time associated with the external change. In particular, this implies that stepwise change of the controlling parameters should not be considered. Notice that the non-dimensional temperature defined according to (Eq. 6.5.1a) has been used. Likewise, the surface pyrolysis law defined according to the mixed Arrhenius -KTSS type law discussed in §8.2 has been used.

The results have been obtained by numerical solution of the basic set of Eqs. (6.5.2) - (6.5.14) following the approach described in §9.1 - 9.3. Due to their relevance to practical situations, only results concerning fast change of ambient pressure or external radiant flux following the exponential laws of Eqs. (8.3.13) and (8.3.14) are reported. Most of the results are presented in terms of surface temperature θ_s evolution during the time τ (θ_s vs τ plane) measured from the instant $\tau=0$ in which the assigned change of some controlling parameter is started. As previously done, the computing has been specialized to the case of an AP based composite propellant (AP/PBAA #941) whose properties have been already listed in Table 7. However, no specific importance is attached to this and the results are expected to show general trends.

In the plane θ_s vs τ the general behavior of a propellant subjected to a fast (exponential) decrease of pressure or external radiant flux intensity is similar. This is evident if one compares, for example, Figs. 42-44 with Fig. 45. In both cases the undershoot of burning rate or surface temperature is followed by asymptotic or damped oscillatory recovery toward the final s.s. value.

As previously mentioned, extinction will occur whenever the trajectory goes past the no-return point in the RR or θ_s vs \dot{q}_w plane. There is no way, in general, to predict whether this will happen for a given set of initial conditions. Due to the complex nature of the problem, all criteria predicting extinction or recovery without fully solving the proper set of equations are necessarily approximate to an unknown extent and, therefore, should be considered with caution. This is an intrinsic difficulty with any nonlinear system. On the other hand, physical intuition allows only a very qualitative statement: the more "intense" the disturbance due to the controlling parameter change is, the more likely it is that extinction will occur. Within the framework of the q.s. assumption, the intensity of the disturbance is somehow measured by the adjustments required in the condensed phase thermal profile. This implies that extinction is favored by an external change which is fast

compared to the characteristic time in the condensed phase or by a large gap between the initial and final s.s. values and so on. Another intrinsic property with any nonlinear system is that a very small change of initial conditions may yield a completely different response of the system to the given disturbance. This strong dependence of the fate of the transient on the initial conditions is shown, for example, in Fig. 44: here a recovery process changes into a dynamic extinction when the initial radiant flux intensity suffers an extremely small increase of about 0.01% from $I_{0,i} = 156.85 \text{ cal/cm}^2\text{-sec}$ to $I_{0,i} = 156.87 \text{ cal/cm}^2\text{-sec}$. The point we wish to make is that, in general, numerical integration is the only "exact" method available for studying all of the intriguing aspects of a nonlinear system.

9.4.2 Comparison Between Deradiation and Depressurization Runs

In Fig. 42 the surface temperature (or, with a nonlinear change of scale, the burning rate) evolution in time is shown for a deradiation transient from an initial value $I_{0,i}$ (parametrically changed) of the external radiant flux intensity to a final value $I_{0,f} = 0$, according to the exponential law of Eq. (8.3.14) with $\dot{B}_r = 10$. The point at $\tau = 0$ gives the s.s. value corresponding to $I_{0,i}$, while the dashed line indicates the final s.s. value corresponding to $I_{0,f} = 0$. The runs in Fig. 42 have been performed for an opaque propellant burning at a pressure $P = 30 \text{ atm}$. Several values of $I_{0,i}$ have been tested: for $I_{0,i}$ increasing, the initial s.s. value of surface temperature increases too while the undershoot becomes greater. However, the qualitative aspect of the system response is the same: an asymptotic recovery follows the end of the deradiation. It will be noticed that the duration of the undershoot is approximately 2 units of nondimensional time, that is, it is of the order of the characteristic time (indicated as $\tau_p \approx 2.13$ in the figures) associated with the condensed phase conductive thermal wave at the operating pressure.

In Fig. 43 the evolution of the surface temperature for still larger values of $I_{0,i}$ is shown. It is seen that the undershoot region becomes wider and wider until recovery no longer occurs and the surface temperature decreases monotonically down to zero (ambient temperature in dimensional terms). This phenomenon is called dynamic extinction, since we know that a static solution actually exists. This fact confirms the dynamic nature of the extinctions observed in ignition experiments for fast actuation of the shutters. It will be noticed that the change of the system response occurs abruptly for $I_{0,i} \approx 157 \text{ cal/cm}^2\text{-sec}$. As already mentioned, if one takes a closer look at the transition from recovery to extinction (see Fig. 44) the effect of the nonlinearity of the system will be fully evident. The propellant tested is able to go through a prolonged undershoot period at $I_{0,i} = 156.85 \text{ cal/cm}^2\text{-sec}$, but will extinguish for $I_{0,i} = 156.87 \text{ cal/cm}^2\text{-sec}$. Notice that there is practically no difference between the two curves for about 50% of the transient. Comparison of Figs. 42, 43 and 44

also makes it evident that the recovery is more abrupt when the undershoot is more pronounced. This was indeed expected after the qualitative comments about the nature of the restoring function made in §8.7. Further discussions on Fig. 44 are given in §9.5.

In Fig. 45 the evolution of the surface temperature for deradiation runs at the pressure $P = 10$ atm is shown. The same comments previously made hold true, except that the recovery process is now oscillatory in nature. In agreement with the qualitative expectations from §8.7, the oscillations are damped and have a period of the order of relaxation time of the conductive thermal wave in the condensed phase.

A similar behavior may be observed for depressurization runs. In Fig. 46, for example, exponential depressurizations from the initial pressure $P_i = 30$ atm to the final pressure $P_f = 10$ atm are shown. For increasing values of the coefficient B_p from 0.15 to 1.0, the undershoot is more and more pronounced and consequently the oscillatory nature of the recovery process more and more evident. The damping shrinks the amplitude of the waves to a few percent of the final s.s. value within two or three oscillations (having a period of the order of magnitude of the relaxation time in the condensed phase at the final pressure). Further increasing of the initial rate of depressurization up to $B_p = 10$ makes the recovery process more abrupt. This is shown in Fig. 47.

In a RR vs \dot{q}_w plane the trajectory of a deradiation transient (being isobaric) is drastically different from the trajectory of a depressurization transient. This is illustrated in Fig. 48. The deradiation path depicted corresponds to an exponential decrease of radiant flux intensity from $I_{0,i} = 156$ cal/cm²-sec to $I_{0,f} = 0$ with $B_r = 10$ at the pressure $P = 30$ atm. The related surface temperature evolution in time is shown in Fig. 43. Notice that the recovery point occurs well below the static stability line. The two depressurization paths depicted correspond to an exponential decrease of ambient pressure from $P_i = 30$ atm to $P_f = 2$ atm with $B_p = 0.10$ (recovery) and $B_p = 0.15$ (extinction). A comparison with Fig. 47 shows that, by lowering the final pressure to $P_f = 2$ atm, dynamic extinction occurs for $B_p = 0.15$ (Fig. 48), whereas for $P_f = 10$ atm (all the other parameters being kept constant) extinction is avoided even for $B_p = 10$ (Fig. 47).

9.4.3 Effect of Radiation Penetration

The effect of radiation penetration inside the condensed phase is shown in Fig. 49. Here a simple Beer's law has been used for the distribution of the radiant flux intensity in the interior of the slab. This can be a gross mistake for situations in which scattering of radiation may occur. How to cope with this difficulty is discussed in Appendix B.

In any event, the volumetric heating of the condensed phase implies a less steep temperature gradient at the surface and therefore has a smoothing effect on the dynamics of the system. Two limiting cases are evident: when the absorption coefficient $a \rightarrow \infty$ or, more generally, whenever $\ell_{th}/\ell_{rad} \gg 1$ (see App. A.2) the results found for opaque samples should be valid; conversely, for $a \rightarrow 0$ the sample is totally transparent and therefore totally insensitive to deradiation disturbances. This is verified in Fig. 49, in which the minimum initial radiant flux intensity $I_{0,i}$ for obtaining dynamic extinction is plotted vs the absorption coefficient a . The horizontal asymptotic corresponds to the critical value of $I_{0,i}$ as already determined in Fig. 45. All the other values have been determined by go/no-go tests at the computer. For $a = 200 \text{ cm}^{-1}$ the critical value of $I_{0,i}$ is much above $200 \text{ cal/cm}^2\text{-sec}$ and further computer simulated testing has been considered unrealistic. The plot has been made for a given set of values (indicated in figure) of the operating conditions. An increase of pressure or a decrease of deradiation rate would make the burning region wider.

It will be noticed that the transparency of the condensed phase strongly affects the results for a less than approximately 700 cm^{-1} . In particular, for $a = 250 \text{ cm}^{-1}$ (which is approximately expected to be the value of the absorption coefficient for AP propellants at 10.6μ) a value of $I_{0,i}$ (of the order of several $100 \text{ cal/cm}^2\text{-sec}$) much above the experimental range investigated in this report is required for causing dynamic extinction at $P = 10 \text{ atm}$. Although the plot is not intended to represent any specific actual situation, there is an indication that in order to verify experimentally the occurrence of dynamic extinction for AP propellants the proper attention should be given also to the optical properties of the sample. On the other hand, it is known (see Table 5, for example) that AP propellants exhibit considerably lower absorption coefficient in the arc image wavelength. This might be another reason why AP propellant dynamic extinction has not been reported even in those laboratories where large power output arc image furnaces with fast shutters are currently operated.

Specific histories of the surface temperature during a deradiation transient are shown in Figs. 50 and 51 for the indicated sets of operating conditions. The smoothing effect of the transparency on the undershoot is self-evident for the absorption coefficient decreasing to 500 cm^{-1} . For even lower values of the absorption coefficient (Fig. 51), the undershoot is less and less pronounced but a stronger oscillatory behavior is observed. Again, the oscillations are damped and have a period of the order of the relaxation time (τ_p) of the conductive thermal wave in the condensed phase at the ambient pressure. Notice, however, that in general at the beginning of the deradiation transient the characteristic time τ_p is reduced (as compared to the final value taken when the external radiant flux no longer acting) to the extent in which the burning rate is increased by the presence of radiation.

Further comments about the effects of transparency on dynamic burning are given in the next section.

9.5 Check of the Dynamic Stability Analysis by Computer Simulated Tests.

The basic conclusion of the nonlinear stability analysis presented in Ch. 8 is the existence of two well distinguished lines as static and lower dynamic stability boundaries in the RR vs θ plane. The meaning of these boundaries has been explained in detail in §8.2 and §8.3. We wish now to check the validity of these developments by running computer simulated tests.

Focusing again our attention to Fig. 44 (already introduced in §9.4.2), we can tentatively infer from the nature of the depicted trajectories that a no-return point, if it exists, is located at about $\theta_s \approx 0.67$ at the operating pressure of $P = 30$ atm. This is in very good agreement with the prediction of $\theta_s = 0.66$ of Fig. 32 (see the unstable root at $P = 30$ atm). Moreover, it was shown in Fig. 48 that the recovery point for a fast deradiation from $I_{0,i} = 156$ cal/cm²-sec occurs well below the static boundary point $\theta_s^S = 0.81$ at the operating pressure of $P = 30$ atm. This confirms that static boundaries have no direct pertinence to dynamic burning regimes.

In order to get more substantial evidence for the validity of the ideas underlying the dynamic stability analysis, other runs have been made with the specific purpose of defining the no-return point, if it exists, for different situations by a go/no-go procedure at the computer. The results are summarized in Fig. 52. At 10, 20 and 30 atm the no-return point for exponential deradiation is just above the lower dynamic stability boundary as determined in Ch. 8 and much below the static stability boundary. The strong dependence of the results on the initial conditions may be appreciated by considering the figures reported in Table 13 for the "bracketing" values of initial radiant flux intensities $I_{0,i}$ defining the no-return point in terms of surface temperature θ_s . The above results have been interpreted as suggesting the existence of a lower dynamic boundary line in the sense specified in §8.3.

As a further check the no-return point has also been determined at $P = 10$ atm for several values of the absorption coefficient a . For reasons of economy the go/no-go procedure has not been pushed too far and the results summarized in Fig. 53 have been judged to be satisfactory. Again the bracketing values of $I_{0,i}$ and the observed limiting values of θ_s are reported in Table 13. The comparison with the predicted limiting values of θ_s (see Fig. 32) is excellent.

The generality of the approach suggested in Ch. 8 has been tested by considering a deradiation transient with a variable coefficient B_r in Eq. (8.3.14). It was found that increasing or decreasing the rate of the exponential decay at any moment of the transition would result in dynamic extinction.

only if the lower dynamic stability boundary is crossed. Incidentally, it was observed that changes in the decay rate are most effective in affecting the overall fate of the dynamic history if realized in the early portion of the transition.

Similar considerations can be made for monotonic, typically exponential, go/no-go depressurization tests. See, for example, Fig. 54 and the last two lines of Table 13. Again, a very good agreement is found between the observed and the predicted limiting values of θ_s .

It should be clearly understood that the above result of detecting recovery points down to $\theta_s = 0.6$ is important only to the extent to which it illustrates the validity of the analytical developments of this report. Indeed, it is very questionable whether chemical processes are still active at such low surface temperatures. Moreover, heat loss mechanisms are very likely not negligible in that surface temperature range. All this implies that more sophisticated flame models have to be considered, if one wishes accurate results in the marginal domains of burning.

The point we wish to make here is that the numerical integration of the basic set of equations in terms of the PDE suggests the existence of a no-return point for fast transients and defines its value by a trial and error procedure. The values obtained in several different configurations are in excellent agreement with the predictions made from an analysis of the approximate ODE describing the system. This also confirms that the static stability boundary, as determined for example in the Zel'dovich approach, has no relevance in dynamic disturbances of finite size.

Results concerning the upper dynamic stability limits are illustrated in Figs. 55-57. Runs with exponential increase of pressure from $P_i = 10$ atm to $P_f = 30$ atm are plotted for several values of the surface heat release Q_s (cf. Table 10). For Q_s sufficiently low (Fig. 55), one observes a smooth transition from the initial to the final steady state equilibrium configuration (see, for example, $Q_s = -150$ cal/g). For larger values of Q_s , a vigorous acceleration of the wave occurs (Fig. 56). Following this, the heterogeneous deflagration wave will relax toward a regime solution (Fig. 57). This is the stable steady state reacting configuration for Q_s less than the A-D roots coalescence value (for example, $Q_s = -180$ cal/g), self-sustained oscillations for Q_s larger than the A-D roots coalescence value (for example, $Q_s = -200$ cal/g), and the stable steady state unreacting configuration for Q_s larger than the B-D roots coalescence value (for example, $Q_s = -230$ cal/g, not drawn) or whenever the dynamics of the transient are too fast (for example, $Q_s = -210$ cal/g) compared to the propellant response capability.

Self-sustained oscillations have been observed in several different situations. The nature of oscillations depends only on the static restoring function associated to the final burning conditions. For example, the same regime oscillations have been found with $B_p = 1.0$ and $B_p = 200$ for the pressurization transient shown in Fig. 57. Notice that the peaks of the oscillations, $\theta_s \approx 1.65$ maximum and $\theta_s \approx 0.83$ minimum, are comparable respectively with the value of the E root ($\theta_s = 1.61$) and D root ($\theta_s = 0.94$) listed in Table 10 for $Q_s = -200$ cal/g. Moreover, the period of the oscillations is about 1.5 nondimensional units of time, which is of the order of the relaxation time of the conductive thermal wave in the condensed phase.

Upper instability phenomena of one-dimensional AP deflagrations were discussed by Strable¹⁶⁹ in 1971. However, only very recently ¹⁷⁰ numerical results showing self-sustained oscillations of solid propellants were reported. Experimentally, oscillatory behavior in a pressurization test was observed in Ref. 171, but burning rate oscillations there were attributed to the experimental apparatus.

CHAPTER 10

CONCLUSIONS

Before unifying in §10.2 the conclusions from the broad variety of findings and concepts which have been presented, a schematic list of major observations and results is given in §10.1. Suggestions for future work, both theoretical and experimental, are offered in §10.3.

10.1 Major Observations and Results

In the experimental portion (Chapters 3 to 5) of this investigation, the following points have been made within the limits of the experimental range investigated:

1. AP composite propellants at low pressure (e.g., 5 atm) ignite as soon as a critical surface temperature is reached (Figs. 6 and 7).
2. The flame structure (Fig. 11) of the AP propellants (i.e., a thin flame strongly coupled to the burning surface) provides a strong energy feedback to the propellant surface (compare with #7 below).
3. The effect of large metal content in AP propellants greatly reduces radiation penetration below the surface (Table 4).
4. Noncatalyzed DB propellants exhibit dynamic extinction when exposed to rapid deradiation in the laser ignition apparatus (Figs. 9 and 15).
5. Noncatalyzed DB propellants are difficult to ignite at low pressure (e.g., 5 atm).
6. Catalyzed DB propellants do not exhibit dynamic extinction and are ignitable also at low pressure (e.g., 5 atm).
7. The flame structure of the noncatalyzed DB propellants (i.e., a thick gas phase weakly coupled to the burning surface) provides a relatively weak energy feedback to the propellant surface when compared to the energy feedback from AP propellants (Fig. 12).
8. A characteristic carbonaceous-appearing layer (Fig. 13) is observed at the surface of catalyzed DB propellants burning at low pressure (e.g., 4 atm).
9. The difficulty in igniting HMX propellants with the arc image furnace is possibly due to the high surface reflectivity and endothermic surface decomposition processes.

10. The effect of carbon addition to AP or DB propellants is essentially physical, i.e., concentrates radiation at the surface.
11. The presence of O_2 (Fig. 17) in the environmental gas:
 - eliminates the dynamic extinction of noncatalyzed DB propellants.
 - eliminates the pressure dependence of ignition of catalyzed DB propellants in the low pressure domain (e.g., 5 to 10 atm).
 - does not affect the high pressure (e.g., > 21 atm) ignition boundary of the propellants tested in N_2 .
12. The appearance of the flame (experimentally) and the simple thermal theory (theoretically) are acceptable ignition criteria within the limits of this experimental investigation:
 - in presence of oxygen: for any experimental condition and for any of the tested propellants.
 - for AP composite propellants: for any experimental condition.
 - for catalyzed DB propellants in inert gas: only at high pressure (e.g., 21 atm) and low radiant flux (e.g., $10 \text{ cal/cm}^2\text{-s}$).
 - for noncatalyzed DB propellants in inert gas: for no experimental condition.
13. A steady pre-ignition gasification has been observed for both noncatalyzed and catalyzed DB propellants (§4.7, Fig. 20 and Table 6).
14. The same qualitative behavior is found when propellants are tested in the laser and arc image ignition apparatus, except the dynamic extinction phenomenon (§4.6).
15. The large differential within the illumination profile (Fig. 2) and, possibly, a considerable radiation penetration (§9.4) prevent dynamic extinction using the arc image apparatus.
16. Long exposure times destroy the dynamic extinction due to 3D re-ignition effects and flame spreading beyond impingement area (§4.4).

17. Laser ignition tests are more easily interpretable than arc image ignition tests, in that only one wavelength is involved.
18. The structure of the laser beam implies a nonuniform succession of events on a microscopic scale over the irradiated spot (§4.7).~

A unifying interpretation of the above facts has been made by means of the generalized radiative ignition map shown in Fig. 21. Overall conclusions are offered in the next section.

As to the analytical developments (Chapters 6 to 8), it has been shown that:

1. Mihlfeith's analysis of radiation-driven response function can be improved (§7.2) by a better choice of the flame model (Fig. 27) and by assigning a consistent set of input data.
2. a large surface energy release is destabilizing in the framework of a linearized theory (Fig. 30).
3. A nonlinear (lower) static stability boundary has been defined in the low (fractions of cm/s) burning rate region (§8.2).
4. a nonlinear lower dynamic stability boundary has been defined in the low (fractions of cm/s) burning rate region (§8.3).
5. nonlinear static and dynamic stability boundaries may be defined also in the large (several cm/s) burning rate region (§8.5).
6. dynamic extinction may occur both for too fast deceleration (e.g., by depressurization) and acceleration (e.g., by pressurization) of the heterogeneous combustion wave (Figs. 54 and 56).
7. for a range of parameters, self-sustained oscillations of the burning rate are the only allowed regime solution (§8.6).
8. a large surface energy release is destabilizing also in the framework of nonlinear theory (Figs. 34a and 34b).
9. stability properties of burning solid propellants are contained in the algebraic nonlinear static restoring function, which is strictly dependent on the nature of the solid propellant (Figs. 31 to 35).

A more detailed summary of the findings from the nonlinear stability analysis has already been given in §8.8. Overall conclusions are offered in the next section.

In the last portion of this investigation (Chapter 9) numerical results have been collected which indicate that:

1. depressurization and deradiation transients are similar in a burning rate vs time plane, in that dynamic extinction or asymptotic recovery or damped oscillation may follow the transient (cf. Figs. 42-45 with Figs. 46-47).
2. depressurization and deradiation trajectories are different in a burning rate or surface temperature vs heat feedback plane (Fig. 48).
3. optical transparency of the propellants moderates the dynamic burning effects (Figs. 49-51).
4. computer simulated tests confirm the validity of the nonlinear stability analysis (Figs. 52-57 and Table 13).

10.2 Conclusions

The first part of this research consists of a systematic experimental investigation of several classes of solid rocket propellants. The ignition trends of different propellant types have been rationalized in terms of basic differences in the structure of the deflagration wave in the solid and gas phases. For example, double-base propellants, in which a large portion of the heat feedback is from the surface reactions, show ignition characteristics with more pronounced dependence on pressure and dynamic burning conditions than ammonium perchlorate-based composite propellants, in which lesser portion of the heat feedback is from the surface reactions.

In agreement with other studies, the data clearly isolate the domains (high pressure, low radiant flux intensity, presence of oxygen, etc.) where simple thermal ignition theories apply and those domains (low pressure, high radiant flux intensity, inert pressurizing gas) where ignition theories taking into account the interaction of the incipient gas phase flame with the solid phase are required.

With respect to the measurement technique, it has been found that the use of a laser ignition apparatus is an improvement over the previous radiant ignition furnaces in that dependence of the results on wavelength and angular distribution of the impinging radiant flux is eliminated. It has been shown that the basic phenomena are the same in the arc image and laser ignition apparatus but differing quantitative results may be found due to the differing physical configurations. A major source of the

quantitative difference is the wavelength dependence of the radiation penetration. An exception to the general agreement of ignition behavior is found with the simultaneous occurrence of fast actuation of shutters and a uniform illumination profile. Under these circumstances, dynamic extinction of noncatalyzed DB propellants is observed in the laser ignition apparatus.

This study offers evidence that radiative ignition tests are a powerful diagnostic technique for the understanding of heterogeneous flames but are not suitable for propellant ignitability rating. Reasons for this are: (1) difficult-to-interpret effects of the solid propellant optical transparency, (2) the slow chemical kinetics in the cool gas phase near the surface (already stressed in previous studies), (3) the problems posed by the dynamic response of the propellant, and (4) the spatial distribution of the impinging radiation (these are studied in detail here for the first time).

The dynamic extinction phenomenon prompted a theoretical study of the solid propellant burning stability. This was performed both for linear (small disturbances) and nonlinear (large disturbances) situations. First, a review has been made of the study of Mihlfeith dealing with a linearized frequency response analysis of both pressure- and radiation-induced disturbances. After correcting Mihlfeith's work, the normalized nondimensional admittance function for opaque propellants is shown to be the same for variable pressure or radiation intensity driven mechanisms for the wide class of AP-based composite propellants. This confirms the validity of Mihlfeith's suggestion of testing the stability of a propellant by its response to a radiative stimulus. For example, the admittance function shows the destabilizing effect of a large amount of energy release at the surface of a burning propellant. The potential of this approach, however, is limited by the assumption of small disturbances.

A nonlinear stability analysis of solid propellant burning was carried out. This required an integral method in reducing the partial differential equation for the condensed phase heat conduction to an approximate ordinary differential equation. It is shown that, within the limits of this approximation, an algebraic function can be defined that contains all basic properties of equilibrium and stability of burning solid propellants. This is called nonlinear static restoring function; it does not depend on time, but strictly on the nature of the solid propellant. Analysis of the restoring function reveals that two well-defined burning regimes exist, each limited by a stability boundary: the static regime, which can be observed experimentally and therefore can be studied also in the framework of Zeldovich approach; and the dynamic regime, which cannot be observed experimentally in a stationary mode and (in principle) can only be studied in the framework of a flame model. The fundamental importance of this distinction is stressed by the fact that under dynamic conditions the propellant may pass through a region which is statically unstable.

The static stability boundary (defined as the line of separation between a region where stable steady-state solutions are allowed and a region where only unstable or no steady solutions are found) has been determined theoretically in the burning rate vs heat feedback plane in the framework of the MTS flame model. This static stability boundary corresponds to the intrinsic stability boundaries found by other investigators with linearized analyses. Moreover, in this work, for the first time, a lower dynamic stability boundary has been defined that is applicable under broad conditions. The lower dynamic stability boundary is defined as that ultimate burning condition beyond which extinction necessarily follows during a burning transient.

Analysis of the dependence of the restoring function on the surface heat release reveals other, unexpected phenomena. For increasing values of the surface heat release at constant pressure, it is found that static and dynamic instabilities may appear both in the low and in the high burning rate regions. Upper dynamic instability implies vigorous oscillations of the combustion wave, possibly followed by dynamic extinction. Upper static instability implies that the stationary reacting equilibrium solution is no longer allowed. Under these circumstances, it is found that either self-sustained oscillations or the non-burning state are the only stable solutions, depending on the surface heat release value. A technique to determine these upper boundaries and the domains of self-sustained oscillations is demonstrated. Estimates of the oscillation amplitude and frequency are also made on a very simple basis.

An entirely new spectrum of phenomena arises in this examination of heterogeneous flame dynamics. It is shown, for example, that no dynamic limit exists if a minimum value (depending on the ambient pressure) of residual radiant flux impinges on the burning propellant following a fast quasi-steady transient. It is shown that a large ratio of gas/surface heat release is strongly stabilizing. It is shown that stability properties are not necessarily related to heat losses from propellants. It is shown that dynamic extinction may occur due to fast deceleration of the combustion wave (e.g., by depressurization) as well as due to fast acceleration (e.g., by pressurization), if an excessively large burning rate overshoot is attained.

Numerical results based on the Merkle-Turk-Summerfield (MTS) flame model show that transients following both fast depressurization or fast deradiation are similar in that dynamic extinction, exponential recovery, and damped oscillations may occur in both cases. The thermal wave relaxation time in the condensed phase is the controlling time parameter for the dynamic response of the system. However, as expected from previous studies, the optical transparency of the solid phase decreases the sensitivity of the propellant to dynamic disturbances of burning when radiation

is the forcing function. Likewise, scattering of the radiation (considered here for the first time) at the interior of the solid phase also has a damping effect (see Appendix B).

The validity of the approximate analytical approach has been verified by computer-simulated transients. Excellent agreement has been found between the analytical predictions and the numerical results obtained by integration of the governing partial differential equation. In particular, the lower dynamic stability boundary has been verified by go/no-go deradiation and depressurization runs under several different operating conditions; the existence of an upper instability region has been verified by pressurization runs; self-sustained oscillations have been found in the expected range of parameters.

Numerical values are given only for a particular ammonium perchlorate composite propellant. Nevertheless, it is expected that the conceptual findings of the theoretical part of this work may be extended not only to other types of solid rocket propellants, but more generally to deflagration waves associated with any condensed reactive substance, provided a proper flame model is employed.

Finally, notice that the transformation from a partial into an ordinary nonlinear differential equation has been performed by a standard, but approximate, integral method. This can be strongly improved by a more sophisticated approach, for example, the weighted residuals method. Nevertheless, it is again expected that the conceptual findings will not be affected although the accuracy of the predictions should be further improved.

10.3 Suggestions for Future Work

Several questions are still open as to the use of radiant energy sources in heterogeneous combustion problems. First, a detailed knowledge of the optical properties of the propellants is still lacking; progress in this direction is being made (see Ref. 103). The interaction of the impinging radiant beam with the gas phase plume extending above the propellant surface also needs to be investigated; this could affect, in particular, the occurrence of dynamic extinction following fast deradiation. Experimental results in this area have been given by Muhlfeith (Section F.1 of Ref. 126b), but as yet no data for the laser ignition apparatus used here are available.

With specific reference to the radiative ignition experiments performed in this investigation, the occurrence of dynamic extinction for AP composite and DB catalyzed propellants has yet to be proved. The effects of catalyst addition to DB propellants and, partially, of carbon powder addition still are largely unexplored. The presence of a stationary gasification process prior to ignition also needs to be put in some comprehensive context.

A major experimental objective would be to define the dynamic stability line. As already mentioned in §8.7, go/no-go testing by fast depressurization or deradiation is sufficient to locate the lower dynamic stability boundary in the same way as done by computer-simulated tests (see Fig. 41, for example). In order to perform more meaningful experiments, it is suggested as future work to run deradiation tests in a stepwise fashion from an initial radiant flux intensity $I_{0,i}$ to a residual or final radiant flux intensity $I_{0,f}$. To the extent in which the condensed phase reacting layer is negligible as compared to the radiantly heated layer (§A.2), the final radiant flux intensity $I_{0,f}$ may be converted to an equivalent ambient temperature (Fig. 25). In this case, the meaning of Zeldovich's stability boundary (expressed in terms of ambient temperature) and the existence of the lower dynamic stability boundary as defined in §8.3 may be tested simultaneously. Indeed, for a given $I_{0,f}$, $I_{0,i}$ could be increased until a recovery point occurs in the statically unstable region; according to Zeldovich this always implies dynamic extinction, whereas according to the theory developed in this study, dynamic extinction occurs only when the limiting no-return point is passed. This check can be done for different sets of values of $I_{0,i}$ and $I_{0,f}$. It is also expected from the analysis presented in Chapter 8 that above a certain minimum value (depending on the ambient pressure) of $I_{0,f}$ the dynamically stable burning region is extended (see Fig. 33); on the contrary, the Zeldovich criterion is unable to predict any change in the stability properties of the system. This procedure can be repeated for different pressures. The degree of freedom associated with a variable $I_{0,f}$ is then used both for testing the reproducibility of the resulting stability boundary (whatever it is, if it exists) and for discriminating between the predictions of the Zeldovich approach from those of the approach proposed in this work.

It is suggested to perform the above experimental check in the laser apparatus by testing opaque propellants in a inert gas atmosphere. Attention should be paid to the fact that a steady deflagration wave has to be established before starting the deradiation.

As to the theoretical aspects, some improvements on the model (see §6.5) used throughout this investigation are in order. Following T'ien's¹²³ suggestion, heat loss mechanisms should be accounted for in order to obtain more accurate results. Likewise, it is believed that the inertia of the condensed phase reacting layer might be very important in the marginal region of dynamic burning stability. The necessity of an optical model explicitly accounting for possible radiation scattering in condensed phase has been often mentioned; a background in this area is offered in Appendix B. However, it has already been mentioned that a basic improvement of the theoretical model will be the use of more sophisticated methods (e.g., weighted residual method) for obtaining the nonlinear static restoring function.

REFERENCES

1. Most, W. J. and Summerfield M., "Starting Thrust Transients of Solid Rocket Engines", AMS Report No. 873, July 1969, Princeton University, Princeton, N.J.
2. Larue, P. and Nadaud, L., "Processus d'Allumage des Propergols Solides," ONERA T.P. No. 1182, 1972. See also: Rech. Aér., No. 6, 1972, pp. 297-311.
3. Peretz, A., Caveny, L.H., Kuo, K. K. and Summerfield, M., "The Starting Transient of Solid Propellant Rocket Motors With High Internal Gas Velocities", AMS Report No. 1100, April 1973, Princeton University, Princeton, N.J.
4. Summerfield, M., Shinnar, R., Hermance, C.E., and Wenograd, J., "A Critical Review of Recent Research on the Mechanism of Ignition of Solid Propellants," Aeronautical Engineering Laboratory Report No. 661, AF-AFOSR- 92-63, August 1963, Princeton University, Princeton, N.J.
5. Price, E. W., Bradley, H.H., Jr., Dehority, G. L., and Ibiricu, M. M., "Theory of Ignition of Solid Propellants", AIAA Journal, Vol. 4, No. 7, July 1966, pp. 1153-1181.
6. Barrère, M., "Solid Propellant Ignition: General Considerations", Rech. Aér., No. 123, 1968, pp. 15-28.
7. Merzhanov, A. G. and Averson, A. E., "The Present State of the Thermal Ignition Theory: An Invited Review," Combustion and Flame, Vol. 16, No. 1, February 1971, pp. 89-124.
- 8a. Ohlemiller, T. J. and Summerfield, M., "Radiative Ignition of Polymeric Fuels in an Oxidizing Gas", AMS Report No. 876, AFOSR Contract AF-69-1651, August 1969, Princeton University, Princeton, N.J.
- 8b. Ohlemiller, T. J. and Summerfield, M., "Radiative Ignition of Polymeric Materials in Oxygen/Nitrogen Mixtures", Thirteenth Symposium (International) on Combustion, The Combustion Institute, 1971, pp. 1087-1094.
9. Frank-Kamenetskiy, D. A., "Distribution of Temperatures in a Reaction Vessel and the Steady State Theory of Thermal Explosion," J. Phys. Chem., Vol. 13, No. 6, 1939.
10. Frank-Kamenetskiy, D. A., "A Nonsteady Theory of Thermal Explosion", J. Phys. Chem., Vol. 20, No. 2, 1946.
11. Barzykin, V. V., Gontkovskaya, V. T., Merzhanov, A. G. and Khudyayev, "A Theory of Thermal Explosion in Unsteady State", PMTF. Translation AFSC #FTD-MT-64-319, pp. 196-209.

12. Merzhanov, A. G. and Strunina, A. G., "Laws of Thermal Explosion with Constant Heating Rate", Combustion, Explosion, and Shock Waves, Vol. 1, No. 1, 1965, pp. 59-69.
13. Strunina, A. G., Gontkovskaya, V. T., and Merzhanov, A. G., "Laws of Thermal Explosion. III. Temperature Field and Transition from Autoignition to Ignition", Combustion, Explosion, and Shock Waves, Vol. 1, No. 3, 1965, pp. 36-40.
14. Vilyunov, V. N., "On the Thermal Theory of Ignition", Combustion, Explosion, and Shock Waves, Vol. 2, No. 2, 1966, pp. 77-82.
15. Rozenband, V. I., Barzykin, V. U., and Merzhanov, A. G., "Ignition of Condensed Substances by Convective Heat Fluxes of Medium Intensity under Dynamic Conditions", Combustion, Explosion, and Shock Waves, Vol. 4, No. 2, 1968, pp. 171-175.
16. Lisitskii, V. I. and Pribytkova, K. V., "Ignition of Condensed Substances in the Presence of a Phase Transition in the Heated Layer", Combustion, Explosion, and Shock Waves, Vol. 4, No. 4, 1968, pp. 501-512.
17. Averson, A. E. and Rozenbad, V. I., "Approximate Methods of Calculating Critical Ignition Conditions", Combustion, Explosion, and Shock Waves, Vol. 4, No. 4, 1968, pp. 519-525.
18. Zelikman, E. G., "Degenerate Thermal Explosion Regimes of Autocatalytic Reactions", Combustion, Explosion, and Shock Waves, Vol. 4, No. 4, 1968, pp. 563-567.
19. Frazer, J. H. and Hicks, B. L., "Thermal Theory of Ignition of Solid Propellants", J. Phys. Coll. Chem., Vol. 54, No. 6, 1950, pp. 872-876.
20. Hicks, B. L., "Theory of Ignition Considered as a Thermal Reaction", J. Chem. Phys., Vol. 22, No. 3, 1954, pp. 414-429.
- 21a. Bradley, H. H., Jr., "Theory of Ignition of a Reactive Solid by Constant Energy Flux", NWC TP 4618, November 1968, Naval Weapons Center, China Lake, Calif.
- 21b. Bradley, H. H., Jr., "Theory of Ignition of a Reactive Solid by Constant Energy Flux", Combustion Science and Technology, Vol. 2, No. 1, August 1970, pp. 11-20.
22. Altman, D. and Grant, A. F., Jr., "Thermal Theory of Solid Propellant Ignition by Hot Wires", Fourth Symposium (International) on Combustion, 1953, pp. 158-161.
23. Zeldovich, Ya. B., "On the Theory of Combustion of Powder and Explosives", Zh. Eksperim i Teor. Fiz., Vol. 12, No. 11-12, 1942, pp. 498-524.

24. Librovich, V. B., "Ignition of Powders and Explosives", PMTF, No. 6, November-December 1963, pp. 74-80.
25. Vilyunov, V. N., and Sidonskii, O. B., "Ignition of Condensed Systems by Radiant Energy", Combustion, Explosion, and Shock Waves, Vol. 1, No. 4, 1965, pp. 39-43.
26. Baer, A. D., and Ryan, N. W., "Ignition of Composite Propellants By Low Radiant Fluxes", AIAA Journal, Vol. 3, No. 5, May 1965, pp. 884-889.
27. Price, E. W., Bradley, H. H., Jr., and Fleming, R. O., Jr., "Ignition of Solid Propellants", Western States Section of the Combustion Institute, WSS/CI Paper 63-6, April 1963.
28. Price, E. W., Bradley, H. H., Jr., Hightower, J. D., and Fleming, R. O., Jr., "Ignition of Solid Propellants", AIAA Preprint #64-120, January 1964.
29. Rosser, W. A., Fishman, N., and Wise, H., "Ignition of Simulated Propellants Based on Amonium Perchlorate", AIAA Journal, Vol. 4, No. 9, September 1966, pp. 1615-1622.
30. Gray, P. and Harper, M. J., "The Thermal Theory of Induction Periods and Ignition Delays", Seventh Symposium (International) on Combustion, Butterworths Publ., 1959, pp. 425-430.
31. Gray P. and Harper, M. J., "Thermal Explosions. Part I. Induction Periods and Temperature Changes Before Spontaneous Ignition", Trans. Far. Soc., Vol. 55, Part 4, April 1959, pp. 581-590.
32. Gray, P. and Harper, M. J., "Contribution of Self-Heating to the Reactivity of Solids", Fourth International Symposium on the Reactivity of Solids, edited by J. H. DeBoer, Elsevier Publ., 1961.
33. Koval'skii, A. A., Khlevnoi, S. S., and Mikheev, V. F., "The Ignition of Ballistite Powders", Combustion, Explosion, and Shock Waves, Vol. 3, No. 4, 1967, pp. 527-541.
34. Averson, A. E., Barzynin, V. V., and Merzhanov, A. G., "Dynamic Ignition Regimes", Combustion, Explosion, and Shock Waves, Vol. 4, No. 1, 1968, pp. 20-32.
35. Zarko, V. E. and Khlevnoi, S. S., "Hot Wire Ignition of Ballistite Propellants", Combustion, Explosion, and Shock Waves, Vol. 4, No. 2, 1968 pp. 158-170.
- 36a. Baer, A. D. and Ryan, N. W., "Ignition and Combustion of Solid Propellants", Final Report AFOSR 68-1858, September 1967, Utah University.
- 36b. Baer, A. D., and Ryan, N. W., "An Approximate but Complete Model for the Ignition Response of Solid Propellants", AIAA Journal, Vol. 6, No. 5, May 1968, pp. 872-877.

37. Von Elbe, G., "Theory of Solid Propellant Ignition and Response to Pressure Transients", Bulletin of the 18th Interagency Solid Propulsion Meeting, CPIA No. 18, Vol. III, June 1963, pp. 95-127.
38. Pantoflicek, J., and Lebr, F., "Ignition of Propellants", Combustion and Flame, Vol. 11, No. 6, December 1967, pp. 464-470.
39. McAlevy, R. F. III, Cowan, P. L., and Summerfield, M., "The Mechanism of Ignition of Composite Solid Propellants by Hot Gases", ARS Progress in Astronautics and Rocketry: Solid Propellant Rocket Research, Vol. 1, edited by M. Summerfield, Academic Press, New York, 1960, pp. 623-652.
40. Kling, R., Maman, A., and Brulard, J., "La Cinétique de l'Allumage des Poudres Composites sous l'Influence de Flux de Chaleur Élevés", Rech. Aér., No. 103, 1964, pp. 3-10.
41. Hermance, C. E., Shinnar, R., and Summerfield, M., "Ignition of an Evaporating Fuel in a Hot Oxidizing Gas Including the Effect of Heat Feedback", Astronautica Acta, Vol. 12, No. 2, 1966, pp. 95-112.
42. Hermance, C. E. and Kumar, R. K., "Gas Phase Ignition Theory for Homogeneous Propellants under Shock Tube Conditions", AIAA Journal, Vol. 8, No. 9, September 1970, pp. 1551-1558.
43. Kashiwagi, T., MacDonald, B. W., Isoda, H., and Summerfield, M., "Ignition of a Solid Polymeric Fuel in a Hot Oxidizing Gas Stream", Thirteenth Symposium (International) on Combustion, The Combustion Institute, 1971, pp. 1073-1085.
44. Anderson, R., Brown, R. S. and Shannon, J., "Ignition Theory of Solid Propellants", AIAA Preprint No. 64-156, Solid Propellant Rocket Conference, January 1964.
45. Brown, R. S., Wirrick, T. K., and Anderson, R., "Theory of Ignition and Ignition Propagation of Solid Propellants in a Flow Environment", AIAA Preprint 64-157, January 1964.
46. Williams, F. A., "Theory of Propellant Ignition by Heterogeneous Reaction", AIAA Journal, Vol. 4, No. 8, August 1966, pp. 1354-1357.
47. Waldman, C. H. and Summerfield, M., "Theory of Propellant Ignition by Heterogeneous Reaction", AIAA Journal, Vol. 7, No. 7, pp. 1359-1361, July 1969.
48. Bradley, H. H., Jr., "Heterogeneous Ignition Theory", NWC TP 4864, February 1970, Naval Weapons Center, China Lake, Calif.

49. Bradley, H. H., Jr. and Williams, F. A., "Theory of Radiant and Hypergolic Ignition of Solid Propellants", Combustion Science and Technology, Vol. 2, No. 1, August 1970, pp. 41-52.
50. Waldman, C. H., "Theory of Heterogeneous Ignition", Combustion, Science and Technology, Vol. 2, No. 2-3, November 1970, pp. 81-93.
51. Bowden, F. P. and Yoffe, A. D., Initiation and Growth of Explosions in Liquids and Solids, Cambridge at the University Press, 1952.
52. Bowden, F. P. and Yoffe, A. D., Fast Reactions in Solids, Butterworths Scientific Publications, London, 1958.
53. Johansson, C. H. and Persson, P. A., Detonics of High Explosives, Academic Press, London, 1970.
54. Jost, W., Explosion and Combustion Processes in Gases, McGraw Hill Book Co., Inc., New York 1946, translated by H. O. Croft.
55. Lewis, B. and Von Elbe, G., Combustion, Flames and Explosions of Gases, Academic Press, New York, III Edition, 1970.
56. Gaydon, A. G. and Wolfhard, H. G., Flames, Their Structure, Radiation and Temperature, Chapman and Hall Ltd., London III Edition, 1971.
57. Williams, F. A., Combustion Theory, Addison -Wesley Co., Mass., 1965.
58. Anderson, L. O. and Shook, G. B., "Experimental Study of Factors Affecting the Mechanics of Ignition", Bulletin of the Fifth Mtg of the Army-Navy Solid Propellant Group, SPIA, 1949, Applied Physics Laboratory, J. Hopkins University, Silver Spring, Md.
59. Avery, W. H., "Radiation Effects in Propellant Burning", J. Phys. Chem., Vol. 54. No. 6, June 1950, pp. 917-928.
60. Baer, A. D., "Ignition of Composite Rocket Propellants", Ph. D. Thesis, University of Utah, 1959.
61. Baer, A. D., Ryan, N. W. and Salt, D. L., "Ignition of Composite Propellants", Report AFOSR TN59-516, March 1959, University of Utah.
62. Mitchell, R. C., Keller, J. A., Baer, A. D. and Ryan, N. W., "Ignition and Combustion of Solid Propellants", Final Technical Report AFOSR 2225, September 1961, University of Utah.

- 63a. Beyer, R. B., and Fishman, N., "Solid Propellant Ignition Studies with High Flux Radiant Energy as a Thermal Source", ARS Progress in Astronautics and Rocketry: Solid Propellant Rocket Research, Vol. 1, edited by M. Summerfield, Academic Press, New York, 1960, pp. 673-692.
- 63b. Beyer, R. B., Ferguson, F. A., and Fishman, N., "Arc Image Furnace Ignition Studies", Final Report No. PRU-3614, June 1961, Hercules Powder Co., Stanford Research Institute.
- 64a. Hightower, J. D., NOTS letter to participants, Inter-laboratory Solid Propellant Ignition Exchange Program, October 1964.
- 64b. Hightower, J. D., NOTS Memorandum, "Comparative Calibration of Calorimeters", April 1965.
- 65. Arc Image Ignition Brochure, CPIA Publication 238, June 1973.
- 66. Bastress, E. K., Allan, D. S., and Richardson D. L., "Solid Propellant Ignition Studies", Technical Documentary Report No. RPL-TDR-64-65, Contract AF04(611)-9065, October 1964.
- 67. Bastress, E. K., "Test Methods For Solid Propellant Rocket Igniter Development", Proceedings of the 2nd ICRPG Combustion Conference, 1966, pp. 551-561.
- 68. Sutton, D., and Wellings, P. C., "The Ignition of Solid Propellants by Radiant Energy", Report #RDE-TR-66/4, April 1966, Rocket Propulsion Establishment, Essex, England.
- 69. Evans, M. W., Beyer, R. B., and McCulley, L. "Initiation of Deflagration Waves at Surfaces of Ammonium Perchlorate-Copper Chromite-Carbon Pellets", J. Chem Phys., Vol. 40, May 1964, pp. 2431-2438.
- 70. Fleming, R. W. and Derr, R. L., "The Use of Nonreactive Coatings in Solid Propellant Arc-Image Ignition Studies", Proceedings of the Seventh JANNAF Combustion Meeting, CPIA Publication 204, Vol. 1, Feb. 1971, pp. 379-389.
- 71. Shannon, L. J., "Composite Solid Propellant Ignition Mechanism", Technical Report # UTC 2138-ASR1, May 1966, United Technology Center, Sunnyvale, Calif.
- 72a. Shannon, L. J., "Composite Solid Propellant Ignition Mechanisms", Final Report AFOSR 67-1765, September 1967, United Technology Center, Sunnyvale, Calif.
- 72b. Shannon, L. J., and Deverall, L. I., "Composite Solid Propellant Ignition Characteristics", Bulletin of the Fourth ICRPG Combustion Conference, Vol. 1, October 1967, p. 409, Stanford Research Institute, Menlo Park, Calif.

73. Beyer, R. B., Anderson, R., McLaren, R. D., and Corcoran, W. J., "Ignition of Solid Propellant Motors Under Vacuum", Final Report UTC 2079-FR, April 1965, United Technology Center, Sunnyvale, Calif.
74. Fishman, N., "Solid Propellant Ignition Studies", Report #AFRPL-TR-65-213, November 1965, Stanford Research Institute, Menlo Park, Calif.
75. Summerfield, M., and Ohlemiller, T. J., "A Critical Analysis of Arc Image Ignition of Solid Propellants", AIAA Journal, Vol. 6, No. 5, May 1968, pp. 878-886.
- 76a. Kondrikov, B. N., Ohlemiller, T. J. and Summerfield, M., "Kinetics and Gasification of a DB Propellant Induced by CO₂ Laser Radiation", presentation at the Thirteenth Symposium (International) on Combustion, Utah, A-Part, 1970.
- 76b. Kondrikov, B. N., Ohlemiller, T. J., Caveny, L. H. and Summerfield, M., "Ignition Criteria and Self-Heating of Propellants Subjected to Radiative Heating", presentation at the Eastern Section of Combustion Institute, Ga., November 1970.
77. Ohlemiller, T. J., Caveny, L. H., DeLuca, L. and Summerfield, M., "Dynamic Effects on Ignitability Limits of Solid Propellants Subjected to Radiative Heating", Fourteenth Symposium (International) on Combustion, 1973, pp. 1297-1307.
78. Summerfield, M., Caveny, L. H., and DeLuca, L., "Radiative Ignition Characteristics of Several Propellant Classes", presented at the Second Review of AMC-Fundamentals Of Ignition Task, Aberdeen, Md., November 1972.
- 79a. DeLuca, L., Ohlemiller, T. J., Caveny, L. H. and Summerfield, M., "Radiative Ignition of Double Base Propellants: I. Some Formulation Effects", AIAA Journal, Vol. 14, No. 7, July 1976, pp. 940-946.
- 79b. DeLuca, L., Ohlemiller, T. J., Caveny, L. H. and Summerfield, M., "Radiative Ignition of Double Base Propellants: II. Pre-Ignition Events and Source Effects", AIAA Journal, Vol. 14, No. 8., August 1976, pp. 1111-1117.
80. Altman, D. and Nichols, P. L., Jr., "Ignition of Solid Propellants," Report No. 20-85, September 1954, Jet Propulsion Laboratory, Calif. Inst. of Tech.
81. Hottel, H. C. and Williams, C. C. III, "Transient Heat Flow In Organic Materials Exposed to High Intensity Thermal Radiation," Industrial and Engineering Chemistry, Vol. 47, No. 6, June 1955, pp. 1136-1143.

82. Roth, J. F., and Wachtell, G. P., "Heat Transfer and Chemical Kinetics in the Ignition of Solid Propellants", Industrial and Engineering Chemistry Fundamentals, Vol. 1, No. 1, February 1962, pp. 62-67.
83. Hightower, J. D., "An Investigation of the Effect of Environmental Gases and Pressure on the Ignition of Solid Rocket Propellants", Technical Report #NWC-TP-4431, October 1967, Naval Weapons Center, China Lake, Calif.
84. Baer, A. D., and Ryan, N. W., "Ignition and Combustion of Solid Propellants", Final Report AFOSR TR-69-0349, September 1968, University of Utah.
85. Inami, S. H., McCulley, L., and Wise, H., "Ignition Response of Solid Propellants to Radiation and Conduction", Report Contract NONR-3415(00), October 1968, Stanford Research Institute.
86. Atallah, S., Allan, D. S., Comstock, D. F., Jr. and Bakerjian, B. H., "The Ignition of Solid Propellants by Radiative, Convective and Chemical Heating", Final Report November 1969, A.D. Little Inc.
87. Lenchitz, C., Hayes, E., Velicky, R. W., and Silvestro G., "The Ignition Characteristics of Nitrocellulose", First Review of AMC-Fundamentals of Ignition Task-BRL, 1971, Aberdeen Proving Ground, Md.
88. Evans, M. W., Moore, D. B. and McCarty R. C., "Error Analysis of Data From Arc Image Furnace Ignition Experiments", AIAA Paper No. 66-669.
89. Shannon, L. T., "Composite Solid Propellant Ignition Mechanisms", UTC, Final Report AFOSR 69-1250 TR, April 1969.
- 90a. Merkle, C. L., Turk, S. L., and Summerfield, M., "Extinguishment of Solid Propellants by Depressurization: Effects of Propellant Parameters", AIAA Paper No. 69-176, 1969.
- 90b. Merkle, C. L., Turk, S. L. and Summerfield M., "Extinguishment of Solid Propellants by Rapid Depressurization", AMS Report No. 880, July 1969, Princeton University, Princeton, N.J.
91. Summerfield, M., and Krier, H., "Errors in Non Steady Combustion Theory in the Past Decade (A Review)", AIAA Paper No. 69-178, 1969.
92. Summerfield, M., Caveny, L. H., Battista, R. A., Kubota, N., Gostintsev, Yu. A., and Isoda, H., "Theory of Dynamic Extinguishment of Solid Propellant with Special Reference to Non-steady Heat Feedback Law", JSR, Vol. 8, No. 3, March 1971, pp. 251-258.

93. Mikheev, V. F., Koval'skii, S. S., and Khlevnoi, S. S., "Ignition of a Ballistite Propellant by Light Radiation", Combustion, Explosion, and Shock Waves, Vol. 4, No. 1, 1968, pp. 3-9.
94. Khlevnoi, S. S., and Kalmykova, A. P., "Ignition of Nitro-glycerine Powder by Light Radiation in a Cold Stream of Gas", Combustion, Explosion, and Shock Waves, Vol. 4, No. 1, 1968, pp. 122-124.
95. Khlevnoi, S. S., and Mikheev, V. F., "Effect of Initial Temperature and Transparency of Nitroglycerine Powder on its Ignition by a Light Pulse", Combustion, Explosion and Shock Waves, Vol. 4, No. 4, 1968, pp. 579-583.
96. Webb, G. E., Stokes, B. B. and Graves, A. E., "Development of a Standard Comparison Test Procedure for Initiators", Report No. U-65-23A, May 1965, Thiokol Chemical Corp.
97. Dinsdale, V. T., "Study of Arc Ignition Techniques for Solid Rocket Propellants", Report No. RPT-TDR-64-116, August 1964, Thiokol Chemical Corp.
98. Beyer, R. B., McCulley, L., and Evans, R. W., "Measurement of Energy Flux Density Distribution in the Focus of an Arc Image Furnace", Applied Optics, Vol. 3, 1964, pp. 131-135.
99. Thomas, P. H., "Some Conduction Problems in Heating Small Areas on Large Solids", Quart. Journal of Mech. and Appl. Math., Vol. 10, 1957, pp. 482-493.
100. Kubota, N., Ohlemiller, T. J., Caveny, L. H. and Summerfield, M., "The Mechanism of Super-rate Burning of Catalyzed Double Base Propellants", AMS Report No. 1087, March 1973, (AD 763 786), Princeton University, Princeton, N.J.
101. Steinz, J. A., Stang, P. L. and Summerfield, M., "The Burning Mechanism of Ammonium Perchlorate Based Composite Propellants", AMS Report No. 830, February 1969, (AD 688 944), Princeton University, Princeton, N.J.
102. Derr, R. L., Beckstead, M. W. and Cohen, N. S., "Combustion Tailoring Criteria for Solid Propellant", Lockheed Propulsion Company Report No. 235-F, Technical Report AFRPL-TR-69-190, May 1969.
103. Caveny, L. H., Summerfield, M. and May, I. W., "Propellant Optical Properties and Transient Burning Characteristics as Modified by Particulate Carbon", Abstract of paper submitted to the AIAA 13th Aerospace Sciences Meeting, January 1975, Pasadena, Calif.

104. Camp, A. T., et al, "A Decade of Progress in the Understanding of Certain Ballistic Properties in Double Base Propellants", Navord Rept. 5824, 1958.
105. Ohlemiller, T. J. and Summerfield, M., "Radiation Augmented Burning of a Solid Propellant", AMS Report No. 799, July 1967, Princeton University, Princeton, N.J.
106. Thompson, C. L., Jr. and Suh, N. P., "The Interaction of Thermal Radiation and M-2 Double-Base Solid Propellant", Combustion Science and Technology, Vol. 2, No. 2-3, November 1970, pp. 59-66.
107. Horton, M. D. and Youngberg, L. Z., "Effect of Radiant Energy on the Burning Rate of a Composite Solid Propellant", AIAA Journal, Vol. 8, No. 10, October 1970, pp.1738-1741.
108. Coates, R. L. and Kwak S., "Effect of External Radiation on the Burning Rates of Solid Propellants", JSR, Vol. 9, No. 10, October 1972, pp. 742-745.
109. Linan A. and Williams, F. A., "Radiant Ignition of a Reactive Solid with In-Depth Absorption", Combustion and Flame, Vol. 18, No. 1, February 1972, pp. 85-97.
110. Caveny, L. H., Ohlemiller, T. J. and Summerfield, M., "Influence of Thermal Radiation on Solid Propellant Burning Rate", AIAA Journal, Vol. 13, No. 2, February 1975, pp. 202-205.
111. Konev, E. V. and Khlevnoi, S. S., "Influence of Light on the Rate of Burning of Nitroglycerine Powder", PMTF, No. 2, March-April 1963. Translation AFSC #FTD-MT-64-87, February 1966, pp. 294-300.
112. Konev, E. B., "Influence of Light Radiation on the Burning Rate of N-Powder", Combustion, Explosion, and Shock Waves, Vol. 1, No. 2, 1965, pp. 76-82.
113. Konev, E. V. and Khlevnoi, S. S., "Burning of a Powder in the Presence of Luminous Radiation", Combustion, Explosion, and Shock Waves, Vol. 2, No. 4, 1966, pp. 33-41.
114. Summerfield, M., Sutherland, G. S., Webb, M. J., Taback, H. J., and Hall, U. P., "Burning Mechanism of Ammonium Perchlorate Propellants", ARS Progress in Astronautics and Rocketry: Solid Propellant Rocket Research, Vol. 1, edited by M. Summerfield, Academic Press, New York, 1960, pp. 141-182.

115. Krier, H., T'ien, J. S., Sirignano, W. A., and Summerfield, M., "Nonsteady Burning Phenomena of Solid Propellants: Theory and Experiments", AIAA Journal, Vol. 6, No. 2, February 1968, pp. 278-285.
116. Zeldovich, Ya. B., "The Burning Velocity of Powder Under Variable Pressure", PMTF, No. 3, January-February 1964, pp. 126-130. Translation AFSC #FTD-MT-64-319, pp. 210-232.
117. Gostintsev, Ya. A. and Margolin, A. D., "On Nonstationary Burning of Powder", PMTF, No. 5, 1964.
118. Novozhilov, B. V., "Nonstationary Burning of Powders Having a Variable Surface Temperature", PMTF, No. 1, pp. 54-63, January-February 1967. Translation AFSC #FTD-MT-24-376-68.
119. Novozhilov, B. V., "Theory of Non Stationary Combustion of Homogeneous Propellants", Combustion, Explosion and Shock Waves, Vol. 4, No. 4, 1968, pp. 482-493.
120. Libroich, V. B., "Theory of Propellant Combsution: A Review of Russian Works", Manuscript based on the lectures presented at Princeton University, Revised draft May 1970.
121. Battista, R. A., Caveny, L. H. and Summerfield, M., "Nonsteady Combustion of Solid Propellants", AMS Report #1049, October 1972, Princeton University, Princeton, N.J.
122. Turk, S. L., Battista, R. A., Kuo, K. K., Caveny, L. H. and Summerfield, M., "Dynamic Responses of Solid Rockets During Rapid Pressure Change", JSR, Vol. 10, No. 2, February 1973, pp. 137-142.
123. T'ien, J. S., "A Theoretical Criterion for Dynamic Extinction of Solid Propellants by Fast Depressurization", Combustion Science and Technology, Vol. 9, No. 1-2, March-April 1974, pp. 37-39.
124. Denison, M. P., and Baum E., "A Simplified Model of Unstable Burning in Solid Propellants", ARS Journal, Vol. 31, 1961, pp. 1112-1122.
125. Sehgal, R., "Low Pressure Combustion and Ignition of Solid Rocket Propellants", Astronautica Acta, Vol. 13, 1967, pp. 167-181.
- 126a. Mihlfeith, C. M., Baer, A. D. and Ryan, N.W., "The Response of a Burning Solid Propellant Surface to Thermal Radiation", AIAA Journal, Vol. 10, No. 10, October 1972, pp. 1280-1285.

- 126b. Mihefeith, C. M. "Some Experiments on the Effect of Thermal Radiation on Composite Rocket Propellants", Ph.D. Thesis, University of Utah, June 1971.
- 127. Eckhaus, W., "Studies in Nonlinear Stability Theory", Springer Tracts in Natural Philosophy, No. 6, Springer, N.Y., 1965.
- 128. Hart, R. W. and McClure, F. T., "Combustion Instability: Acoustic Interaction with a Burning Propellant Surface", J. Chem. Phys., Vol. 30, No. 6, June 1959, pp. 1501-1514.
- 129. Bird, J. F., Hart, R. W. and McClure F. T., "Effect of Solid Propellant Compressibility on Combustion Instability", J. Chem. Phys. Vol. 32, No. 5, May 1960, pp. 1423-1429.
- 130. Hart, R. W. and Cantrell, R. H., "Amplification and Attenuation of Sound by Burning Propellants", AIAA Journal, Vol. 1, No. 2, 1963, pp. 98-404.
- 131. Williams, F. A., "Response of a Burning Solid to Small-Amplitude Pressure Oscillations", Journal Appl. Phys., Vol. 33, No. 11, November 1962, pp. 3153-3166.
- 132. Ryan, N. W., Coates R. L. and Baer, A. D., "Participation of the Solid Phase in the Oscillatory Burning of Solid Rocket Propellants", Fourteenth Symposium (International) on Combustion, 1963, pp. 328-334.
- 133. Friedly, J. C. and Petersen, E. E., "Influence of Combustion Parameters on Instability in Solid Propellant Motors: Part I. Development of Model and Linear Analysis", AIAA Journal, Vol. 4, No. 9, September 1966, pp. 1604-1610.
- 134. Marxman, G. A. and Wooldridge, C. E., "Effect of Surface Reactions on the Solid Propellant Response Function", AIAA Journal, Vol. 6, No. 3, March 1968, pp. 471-478.
- 135. Culick, F. E. C., "Calculation of the Admittance Function for a Burning Surface", Astronautica Acta, Vol. 13, 1962, pp. 221-237.
- 136. Culick, F. E. C., "A Review of Calculations for Unsteady Burning of a Solid Propellant," AIAA Journal, Vol. 6, No. 12, December 1968, pp. 2241-2225.
- 137. Culick, F. E. C., "Some Problems in the Unsteady Burning of Solid Propellants," NWC TP 4668 February 1969, Naval Weapons Center, China Lake, Calif.
- 138. Barrère, M., and Nadaud, L., "Prevision des Domaines de Fonctionnement Instable d'un Propulseur à Propergol Solide", ONERA T.P. No. 1016, 1971.

139. T'ien, J. S., "The Effects of Perturbations on the Flammability Limits", Combustion Science and Technology, Vol. 7, No. 4, June 1973, pp. 185-188.
140. Lengellé, G., "A Model Describing the Velocity Response of Composite Propellants", ONERA T.P. 1285, 1973. See also: AIAA Paper No. 73-1224.
141. Novikov, S. S., and Riazantzev, Y. S., "Acoustic Admittance of the Burning Surface of the Condensed System", PMTF, No. 6, 1961.
142. Novikov, S. S., and Riazantzev, Y. S., "On the Acoustic Admittance of the Burning Surface of the Condensed Systems", PMTF, No. 6, 1964.
143. Novikov, S. S., and Riazantzev, Y. S., "On the Interaction of Acoustic Waves and the Burning Surface of the Condensed Systems", PMTF, No. 2, 1966.
144. Price, E. W., "Status of Solid Rocket Combustion Instability Research", NOTS, China Lake, Calif., February 1967.
145. Beckstead, M. W. and Culick, F. E. C., "A Comparison of Analysis and Experiment for Solid Propellant Combustion Instability", NWC, May 1968, China Lake, Calif.
- 146a. Brown, R. S., Muzzy, R. J. and Steinle, M. E., "Research on Combustion of Solid Propellants", UTC, Final Report No. 2136FR, September 1968.
- 146b. Brown, R. S., Muzzy, R. J. and Steinle, M. E., "Surface Reaction Effects on the Acoustic Response of Composite Solid Propellants", AIAA Journal, Vol. 6, No. 3, March 1968, pp. 479-488.
147. Lengellé, G., Kuentzmann, P., and Rendolet, C., "Response of A solid Propellant to Pressure Oscillations", ONERA T. P. 1410, 1974.
148. Friedley, J. C. and Petersen E. E., "Influence of Combustion Parameters on Instability in Solid Propellant Motors: Part II. Nonlinear Analysis", AIAA Journal, Vol. 11, No. 4, April 1966, pp. 1932-1937.
149. Horton, M. D., Bruno, P. S. and Graesser, E. C., "Depressurization Induced Extinction of Burning Solid Propellant", AIAA Journal, Vol. 6, No. 2, February 1968, pp. 292-297.

150. Von Elbe, G. and McHale, E. T., "Extinguishment of Solid Propellants by Rapid Depressurization", AIAA Journal, Vol. 6, No. 7, July 1968, pp. 1417-1419.
151. Marxman, G. A. and Wooldridge, C. E., "Nonlinear Solid Propellant Burning Rate Behavior During Abrupt Pressure Excursion", AIAA Paper, No. 68-172, 1969.
152. Brown, R. S. and Muzzy, R. J., "Linear and Nonlinear Pressure Coupled Combustion Instability of Solid Propellants", AIAA Journal, Vol. 8, No. 8, August 1970, pp. 1492-1500.
153. Coates, R. L. and Horton, M. D., "Predicted Effects of Motor Parameters on Solid Propellant Extinguishment", JSR, Vol. 7, No. 12, December 1970, pp. 1468-1470.
154. Park, C. P., Ryan, N. W. and Baer, A. A., "Extinguishment of Composite Propellants at Low Pressures", AIAA Preprint No. 73-175.
155. Istratov, A. G. and Librovich, V. B., "Burning Stability of Powder", PMTF. Translation AFSC #FTD-MT-65-161.
156. Barrère, M., "Response à un Regime Transitoire de la Surface de Combustion d'un Propergol Solide Hétérogène", ONERA T. P. No. 748, 1969.
157. Istratov, A. G., Librovich, V. B. and Novozhilov, B. V., "An Approximate Method in the Theory of Unsteady Burning Velocity of Powder", PMTF, No. 3, 1964. Translation AFSC #FTD-MT-64-319, pp. 233-242.
158. Novozhilov, B. V., Nonstationary Combustion of Solid Rocket Fuels, 1973. Translation FTD-MT24-317-74.
159. Boggs, T. L. and Beckstead, N. W., "Failure of Existing Theories to Correlate Experimental Nonacoustic Combustion Instability Data", AIAA Journal, Vol. 8, No. 4, April 1970, pp. 626-631.
160. Gostintsev, Ya. A. and Margolin, A. D., "Nonstationary Combustion of a Powder Under the Action of a Pressure Pulse", Combustion, Explosion, and Shock Waves, Vol. 1, No. 2, March-April 1965, pp. 69-75.
161. Rozenbad, V. I., Averson, A. E., Barzykin, V. V., and Merzhanov, A. G., "Some Characteristics of Dynamic Ignition Regimes", Combustion, Explosion and Shock Waves, Vol. 4, No. 4, 1968, pp. 494-500.
162. Kuo, K. K., "Theory of Flame Front Propagation in Porous Propellant Charges under Confinement", Ph.D. Thesis, August 1971, AMS Department, Princeton University, Princeton, N.J.

163. Goodman, T. R., "Application of Integral Methods to Transient Nonlinear Heat Transfer", Advances in Heat Transfer, Vol. 1, 1964, Academic Press, New York, pp. 51-122.
164. Anisimov, S. I. and Perel'man, "On One Nonlinear Problem of Thermal Conduction", PMTF, No. 5, 1963. Translation AFSC #FTD-MT-64-61, pp. 223-228.
165. Gostintsev, Ya. A., "Method of Reduction to Ordinary Differential Equations in Problems of the Nonstationary Burning of Solid Propellants", Combustion, Explosion, and Shock Waves, Vol. 3, No. 3, 1967, pp. 355-361.
166. Andronov, A. A., Vitt, A. A. and Khaikin, S. E., Theory of Oscillators, English edition by Pergamon Press Ltd., London; U.S.A. edition distributed by Addison-Wesley, Mass., 1966.
167. Richtmyer, R. D. and Morton, K. W., Difference Methods for Initial-Value Problems, Interscience Publishers, New York, 1967.
168. Salvadori, M. G. and Baron, M. L., Numerical Methods in Engineering, Prentice Hall, Inc., Englewood Cliffs, N.J., 1961.
169. Strahle, W. C., "One-Dimensional Stability of AP Deflagrations", AIAA Journal, Vol. 9, No. 4, April 1971, pp. 565-569.
170. Barrows, A. W., Kooker, D. E., and Nelson, W., "Solid Propellant Unsteady Combustion", Second International Symposium on Dynamics of Chemical Reactions, University of Padova, December 15-17, 1975.
171. Brulard, J., Kuentzmann, P., and Kling, R., "Réponse d'un Propergol Solide à un Echelon de Pression", Rech. Aér., No. 169, 1975, pp. 267-277.

Table 1

Propellants used in ignition experiments*

Ammonium perchlorate (AP)/hydrocarbon binder composite propellants:

Nonmetallized -

1. 75% unimodal AP (45 μ) without C. Batch 1086.
2. Same as propellant #1 but with 1% C. Batch 1087.
3. 60% bimodal AP (30% 15 μ and 70% 180 μ). Batch 1020.

Metallized -

4. 24% AP and 51% boron.

Nitrocellulose (NC) double base (DB) propellants:

5. Standard U.S. Army M-9 (39.6% NC, 49.4% NG, 11.0% plasticizer and stabilizer).
6. Nitrocellulose (NC) Plastisol [53.7% NC, 39.2% trimethylolethane trinitrate (MTN), 7.1% triethylene glycol dinitrate (TEGDN)]. Batches 1069 and 1070.
7. Opacified NC plastisol, propellant #6 with 0.2% C. Batch 1059.
8. Opacified NC plastisol, propellant #6 with 1.0% C. Batch 1088.
9. Standard U.S. Navy N-5 (50.0% NC, 34.9% NG, 12.5% plasticizer and stabilizer, 2.6% Pb salts). (A JANNAF reference propellant.)
10. Catalyzed NC plastisol, propellant #6 with 2.0% lead salicylate (PbSa) and copper salicylate (CuSa) and 0.2% C. Batch 1050.

Nitramine (HMX)/polyurethane (PU) propellants:

11. High energy propellant (85% HMX, 15% PU).
12. Cool propellant (75% HMX, 15% PU, 10% oxamide).
13. Propellant #11 containing 0.4% elemental phosphorus in the form of ammonium polyphosphate.

*Propellants #1, 2, and 3 were processed at Princeton using the standard techniques described in Ref. 101. Propellant #4 was supplied by the Huntsville Division of the Thiokol Chemical Corporation. Propellants #6, 7, 8, and 10 were processed at Princeton using the techniques described in Ref. 102. Propellants #11, 12, and 13 were supplied by the Wasatch Division of the Thiokol Chemical Corporation. Propellants #9 and 10 were catalyzed to produce increased burning rates and plateaus between 10 and 80 atm. Carbon was added to propellants #2, 7, 8, and 10 in the form of a powder (Neo Spectra TA, manufactured by Columbian Carbon Co.) with a mean diameter on the order of 0.01 μ .

Table 2

Scope of tests described in Chapter 4*

Pro- pel- lant #	Pressures used in Arc Image Tests, atm				Pressures used in Laser Tests, atm				Dynamic Extinction Boundary Established	Movie Sequences Shown taken at Pressure and Radiant Flux Intensity of
	5	11	21	N ₂	5	11	21	Air		
1	7	7	5,7		6	6	6	6	No	11 atm N ₂ 30 cal/cm ² -sec
2	7	7	7		6	6	6	6	No	
3					6	6	6	6	No	
4					6	6	6	6	No	
5					T	T	9		Yes	21 atm N ₂ 51 cal/cm ² -sec
6	T	16	5,16		T	18,T	9,18	17,18	Yes	
7	T	16	5,16		T	T	15	17	Yes	
8	T	16	5,16		T	15	15	17	Yes	
9	11	11	11		8	8	8		No	4 atm N ₂ 42 cal/cm ² -sec
10	14	14	5,14		8,14	8,14	8,14	17	No	
11	T	T	10				T	T	-	
12			T	10	10	10	T	T	-	
13	T	T	5,10				T	T	-	

*Numbers refer to figure in which data appears. The entry T means that data are discussed only in the text.

TABLE 3 (cont.)
SUMMARY OF EXPERIMENTAL RADIATIVE IGNITION WORK

14	Leane, et al SRI June 1966	88	Arc image, carbon $I_0 \times 208 \text{ cal/cm}^2\text{-sec}$	Go/no go	Transcoid pulse 3 coaxial slotted discs AP/PAM/OC/C Mixture	31 - 38 atm H_2, O_2 mixture	Radiant flux intensity, Ambient gas Propellant va.	Carbon reduce: ignition delay, solid and liquid propellant applied to experimental data.
15	Reamer, et al SRI Sept 1966	29	Arc image, carbon $I_0 \times 208 \text{ cal/cm}^2\text{-sec}$	Go/no go	Transcoid pulse 3 coaxial slotted discs AP/PAM/OC/C Mixture	31 - 38 atm H_2, O_2 mixture	Radiant flux intensity, Ambient gas Propellant va.	Carbon reduce: ignition delay, solid and liquid propellant applied to experimental data.
16	Shannon UTC May 1966	71	Arc image, carbon $I_0 \times 1,366 \text{ cal/cm}^2\text{-sec}$	Go/no go	Transcoid pulse 3 coaxial slotted discs AP/PAM/OC/C Mixture	31 - 38 atm H_2, O_2 mixture	Radiant flux intensity, Ambient gas Propellant va.	Carbon reduce: ignition delay, solid and liquid propellant applied to experimental data.
17	Shannon UTC Sept 1967	72A	Arc image, carbon $I_0 \times 1,306 \text{ cal/cm}^2\text{-sec}$	Go/no go	Transcoid pulse 3 coaxial slotted discs AP/PAM/OC/C Mixture	31 - 38 atm H_2, O_2 mixture	Radiant flux intensity, Ambient gas Propellant va.	Carbon reduce: ignition delay, solid and liquid propellant applied to experimental data.
18	Hightower UTC Oct 1967	83	Arc image, carbon $I_0 \times 126 \text{ cal/cm}^2\text{-sec}$	First light emission (photoconductive sensitivity $0.6 - 1.0\mu$)	Transcoid pulse 3 coaxial slotted discs AP/PAM/OC/C Mixture	31 - 38 atm H_2, O_2 mixture	Radiant flux intensity, Ambient gas Propellant va.	Carbon reduce: ignition delay, solid and liquid propellant applied to experimental data.
19	Isaacs, et al SRI Oct 1968	85	Arc image, carbon $I_0 \times 208 \text{ cal/cm}^2\text{-sec}$	Arc image, carbon current characteristic of the igniting ribbon for conductive elements Go/no go for radiative expo.	Transcoid pulse 3 coaxial slotted discs AP/PAM/OC/C Mixture	31 - 38 atm H_2, O_2 mixture	Radiant flux intensity, Ambient gas Propellant va.	Carbon reduce: ignition delay, solid and liquid propellant applied to experimental data.
20	Shannon UTC April 1969	80	Arc image, carbon $I_0 \times 1,306 \text{ cal/cm}^2\text{-sec}$	Go/no go	Transcoid pulse 3 coaxial slotted discs AP/PAM/OC/C Mixture	31 - 38 atm H_2, O_2 mixture	Radiant flux intensity, Ambient gas Propellant va.	Carbon reduce: ignition delay, solid and liquid propellant applied to experimental data.
21	Atkinson, et al A. D. Little Jan 1970	86	Arc image, carbon $I_0 \times 208 \text{ cal/cm}^2\text{-sec}$	First visible light at 0.43 μ (typ) first in light at 3.7% (typ)	Transcoid pulse 3 coaxial slotted discs AP/PAM/OC/C Mixture	31 - 38 atm H_2, O_2 mixture	Radiant flux intensity, Ambient gas Propellant va.	Carbon reduce: ignition delay, solid and liquid propellant applied to experimental data.
22	Fleming, Gurr Lockheed Prop. Co. Aug 1971	70	Arc image, carbon $I_0 \times 126 \text{ cal/cm}^2\text{-sec}$	Ignition delay by first light emission observed by Go/no go testing	Transcoid pulse 3 coaxial slotted discs AP/PAM/OC/C Mixture	31 - 38 atm H_2, O_2 mixture	Radiant flux intensity, Ambient gas Propellant va.	Carbon reduce: ignition delay, solid and liquid propellant applied to experimental data.
23	Lachner, et al Nov 1971	87	Arc image, carbon $I_0 \times 126 \text{ cal/cm}^2\text{-sec}$	Go/no go	Transcoid pulse 3 coaxial slotted discs AP/PAM/OC/C Mixture	31 - 38 atm H_2, O_2 mixture	Radiant flux intensity, Ambient gas Propellant va.	Carbon reduce: ignition delay, solid and liquid propellant applied to experimental data.
24	Chamiller, et al Princeton Univ. August 1969	8	Laser, 10.6 μ $I_0 \times 108 \text{ cal/cm}^2\text{-sec}$	First visible light	Transcoid pulse 3 coaxial slotted discs AP/PAM/OC/C Mixture	31 - 38 atm H_2, O_2 mixture	Radiant flux intensity, Ambient gas Propellant va.	Carbon reduce: ignition delay, solid and liquid propellant applied to experimental data.
25	Randolph, et al Nov 1970	76	Laser, 10.6 μ $I_0 \times 108 \text{ cal/cm}^2\text{-sec}$	Go/no go	Transcoid pulse 3 coaxial slotted discs AP/PAM/OC/C Mixture	31 - 38 atm H_2, O_2 mixture	Radiant flux intensity, Ambient gas Propellant va.	Carbon reduce: ignition delay, solid and liquid propellant applied to experimental data.
26	Chamiller, et al Princeton Univ. August 1971	77	Laser, 10.6 μ $I_0 \times 108 \text{ cal/cm}^2\text{-sec}$	Go/no go	Transcoid pulse 3 coaxial slotted discs AP/PAM/OC/C Mixture	31 - 38 atm H_2, O_2 mixture	Radiant flux intensity, Ambient gas Propellant va.	Carbon reduce: ignition delay, solid and liquid propellant applied to experimental data.
27	Glaser, et al Princeton Univ. Jan 1973	70	Laser, 10.6 μ $I_0 \times 108 \text{ cal/cm}^2\text{-sec}$ (laser) (laser)	Go/no go	Transcoid pulse 3 coaxial slotted discs AP/PAM/OC/C Mixture	31 - 38 atm H_2, O_2 mixture	Radiant flux intensity, Ambient gas Propellant va.	Carbon reduce: ignition delay, solid and liquid propellant applied to experimental data.

Table 4

Measured slopes of ignition boundaries at 21 atm N₂
showing dependence of results on radiative energy source
and optical properties of propellants

Propellant #	Laser Heating	Arc Heating
1	-1.3	-1.4
2	-1.6	-1.5
3	-1.3	Not determined
4	-2.0	-2.0
5	-2.0	Not determined
6	-1.54	-1.55
7	-1.65	-1.55
8	-1.65	-2.00
9	-1.7	Not determined
10	-1.60	-1.77
11	Not determined	-1.8
12	Not determined	-2.0 (air)
13	Not determined	-1.1

Table 5

Surface reflectivity and volumetric absorption of some of the tested propellants showing strong dependence on wavelength. (Values taken from Ref.103).

Propellant type and number	r		r_{av}^*	a, cm^{-1}	a, cm^{-1}
	10.6 μ	0.9 μ	0.2 - 2.0 μ	1 μ	10.6 μ
AP/PBAA binder composite propellants:					
1. 75% unimodal AP (45 μ) without 1% C	0.013	0.35	0.29	2.5	---
2. Same as #1 but with 1% C	0.038	0.036	0.05	175	---
Double Base Propellants					
6. Noncatalyzed NC Plastisol	0.001	0.7	0.59	5	941
7. Opacified non-catalyzed NC plastisol #6 with 0.2% C	0.026	0.041	0.06	50	1472
8. Opacified non-catalyzed NC plastisol #6 with 1.0% C	0.016	0.055	0.05	120	1872
10. Catalyzed NC plastisol #6 with 2.0% Pb and Cu Salts and 0.2% C	0.025	0.062	0.06	82	1871

*Reflectivity averaged after weighting in accord with the spectral distribution of the xenon arc.

Table 6

Measured rates of pre-ignition gasification showing the occurrence of a stationary radiation sustained deflagration wave*

Propellant & Ambient Pressure	Gasification rate as measured in this study at $I_0 = 37 \text{ cal/cm}^2\text{-sec}$ (laser apparatus)	Burning rate as measured in a conven- tional burner (no external radiation assistance)	Burning rate as measured in arc image apparatus (Ref.105) at $I_0 = 37 \text{ cal/cm}^2\text{-sec}$
Catalyzed NC plastisol (propellant #10) at $P = 5 \text{ atm N}_2$	5.13 mm/sec	1.7 mm/sec	4.8 mm/sec (extrapolated value)
Catalyzed NC plastisol (propellant #10) at $P = 11 \text{ atm N}_2$	6.66 mm/sec	3.3 mm/sec	6.4 mm/sec
Noncatalyzed NC plastisol (propellant #6) at $P = 11 \text{ atm N}_2$	5.83 mm/sec	1.8 mm/sec	Not available

*Price, et al (Ref.27) measured a pre-ignition gasification rate of 4.57 mm/sec for a JPN propellant subjected to $I_0 = 100 \text{ cal/cm}^2\text{-sec}$ at $P = 1.09 \text{ atm N}_2$.

Table 7

Properties of composite propellant AP/PBAA #941
used as datum case for nonlinear analysis

ASSUMED PROPERTIES

REFERENCE PRESSURE, P_{ref}	6.800E 01 atm
REFERENCE BURNING RATE, R_{ref}	8.370E-01 cm/s
REFER. SURF. TEMPERATURE, $T_{s,ref}$	1.000E 03 K
REFER. FLAME TEMPERATURE, $T_{f,ref}$	2.430E 03 K
REFER. LENGTH, α_c/R_{ref}	1.673E-03 cm
REFER. TIME, α_c/R_{ref}^2	1.998E-03 s
REFER. HEAT, Q_{ref}	2.310E 02 cal/g
REFER. THERMAL FLUX, I_{ref}	2.978E 02 cal/cm ² -s
EXOTH. AP DECOMP. HEAT, Q_c	2.540E 02 cal/g of AP
ENDOTH. BINDER VAP. HEAT, Q_v	2.250E 02 cal/g of binder
AP CONTENT	8.000E 01 %
BALLISTIC EXPONENT, n	4.600E-01
SURFACE ACTIVATION ENERGY, E_s	1.600E 04 cal/mole
FLAME ACTIVATION ENERGY, E_f	2.000E 04 cal/mole
CONDENSED PHASE DENSITY, ρ_c	1.540E 00 g /cm ³
CONDENSED PHASE SPECIFIC HEAT, C_c	3.300E-01 cal/g-K
CONDENSED PHASE THERMAL DIFFUSIVITY, α_c	1.400E-03 cm ² /s
GAS PHASE SPECIFIC HEAT, C_g	3.300E-01 cal/g-K
GAS PHASE THERMAL CONDUCTIVITY, λ_g	1.000E-04 cal/cm-K-s
REFLECTIVITY OF PROPELLANT SURFACE, r	4.000E-02
AMBIENT TEMPERATURE, T_a	3.000E 02 K

EVALUATED PROPERTIES

COND. PHASE THERMAL CONDUCTIVITY, λ_c	7.115E-04 cal/cm-K-s
REFER. FREQUENCY FACTOR, A_s	2.705E 03 cm/s
SURFACE GASIFICATION HEAT, Q_s	-1.582E 02 cal/g(+endoth.)
REFER. GAS HEAT RELEASE, $Q_{f,ref}$	5.447E 02 cal/g
CHEMICAL TIME CONSTANT, A_M	3.380E-01
DIFFUSION TIME CONSTANT, B_M	2.350E 00

Table 8

Properties of the datum case used for linearized frequency response function analysis. (Values taken from Ref.126).

AMBIENT PRESSURE, P	1 atm
BURNING RATE, \bar{r}_{ss}	0.2 cm/s
SURFACE TEMPERATURE, \bar{T}_s	850 K
FLAME TEMPERATURE, \bar{T}_f	2500 K
SURFACE ENERGY RELEASE, Q_s	25 cal/g
BALLISTIC EXPONENT, n	0.5
SURFACE ACTIVATION ENERGY, E_s	20,000 cal/mole
GAS PHASE ACTIVATION ENERGY, E_f	50,000 cal/mole
CONDENSED PHASE SPECIFIC HEAT, C_c	0.33 cal/g-K
GAS PHASE SPECIFIC HEAT, C_g	0.33 cal/g-K
CONDENSED PHASE THERMAL DIFFUSIVITY, α_c	0.017 cm ² /s
GAS PHASE ENERGY RELEASE, Q_f	800 cal/g

Table 9

Stability "measurements", according to Lyapunov, of steady state burning opaque strands of AP/PBAA #941. Results show beneficial effect of large ambient pressure and radiant flux but destabilizing effect of large surface heat release and heat loss.

Pressure, P, atm	Radiant Flux(*) Intensity, I_0 , $\text{cal/cm}^2\text{-s}$	Ambient Temperature, T_a, K	Surface Energy Release, Q_s , cal/g (+ endothermic)	Stability Strength of Steady State Solution According to Lyapunov, $(df/d\theta_s)_{\bar{\theta}_i, s}$
10	0	300	-158.2	-0.55
20	0	300	-158.2	-2.13
30	0	300	-158.2	-3.65
40	0	300	-158.2	-5.03
30	+20	300	-158.2	-4.03
30	+40	300	-158.2	-4.50
30	+60	300	-158.2	-5.18
30	+80	300	-158.2	-6.01
30	0	250	-158.2	-3.84
30	0	350	-158.2	-3.38
30	0	400	-158.2	-2.73
30	+20	300	-158.2	-3.15
30	+40	300	-158.2	-2.18
30	+60	300	-158.2	-1.29
30	0	300	-150.0	-3.82
30	0	300	-170.0	-2.92
30	0	300	-180.0	-1.80
30	0	300	-190.0	0

(*) negative values represent heat loss from the burning surface.

Table 10

Roots associated with the nonlinear static restoring function for an adiabatic opaque strand of AP/PBAA #941 deflagrating at $P = 30$ atm and $T_a = 300$ K. For all cases root C, corresponding to the trivial solution $\theta = 0$, is also found. The stationary unreacting configuration (root C) is always stable, while the stationary reacting configuration (root A) becomes unstable after coalescence with root D ($Q_g = -190$ cal/g).

	surface heat release, Q_g , cal/g	Nondimensional surface temperature, θ_s			
		root B (lower dynamic stability)	root A	root D (upper dynamic stability)	root E
steady burning	-150	0.66	0.929	=	=
	-155	0.66	0.934	=	=
	-158.2	0.67	0.937	=	=
	-165	0.67	0.944	=	=
	-170	0.68	0.949	1.14	1.29
	-175	0.68	0.955	1.08	1.38
	-180	0.69	0.962	1.04	1.43
	-185	0.69	0.968	1.00	1.48
self-sustained oscillations	-190	0.70	0.976	0.976	1.53
	-195	0.71	0.984	0.96	1.57
	-200	0.72	0.992	0.94	1.61
	-205	0.73	1.001	0.92	1.64
	-210	0.75	1.011	0.90	1.68
	-215	0.76	1.021	0.88	1.71
	-220	0.78	1.032	0.86	1.75
extinction	-225	=	1.044	=	1.78
	-230	=	1.057	=	1.81

Table 11

Critical values of surface heat release, at which upper dynamic instability shows up (appearance of D-E roots in Fig. 31b), in function of pressure for an adiabatic opaque strand of AP/PBAA #941 deflagrating at $T_a = 300$ K. For larger $|Q_s|$, upper dynamic instability effects are manifested as vigorous accelerations of the combustion wave possibly followed by dynamic extinction. Cf. Fig. 56.

pressure, P, atm	surface heat release, Q_s , cal/g
10	~145
20	160
30	167
40	174
50	178
60	182

Table 12

Range of values of surface heat release, for which self-sustained oscillating combustion waves are expected, in function of pressure for an adiabatic opaque strand of AP/PBAA #941 deflagrating at $T_a = 300$ K. Cf. Fig. 57.

Pressure, P, atm	Surface Heat Release, Q_s , cal/g	
	A-D coalescence	B-D coalescence
10	-168	-197
20	-182	-212
30	-190	-225

Table 13

Computer simulated go/no-go tests showing strong dependence of dynamic extinction on the initial conditions and very good agreement with the lower dynamic but not the static stability boundary. Compare with Figs. 52 and 53.

Pressure P, atm	Absorption Coefficient a, cm^{-1}	Controlling Parameter		Nondim. Burning Rate		
		Maximum initial value with no occur- ence of dynamic ex- tinction.	Minimum initial value with occurrence of dynamic extinction	Observed Dynamic Limit	Predicted Dynamic Limit	Static Limit
10	∞	$I_{O,i} = 44.52 \text{ cal/cm}^2\text{-s}$ (*)	$I_{O,i} = 44.55 \text{ cal/cm}^2\text{-s}$	0.057	0.053	0.15
20	∞	96.26 (*)	96.27	0.083	0.070	0.23
30	∞	156.85 (*)	156.87	0.093	0.083	0.29
10	1000	61.00 (*)	61.01	0.060	0.053	0.15
10	500	88.39 (*)	88.40	0.051	0.053	0.15
Radiant Flux, I_o , $\text{cal/cm}^2\text{-s}$						
0		$P_i = 34.42 \text{ atm}$ (**)	$P_i = 34.43 \text{ atm}$	0.051	0.053	0.15
0		$B_p = 3.336$ (***)	$B_p = 3.337$	0.054	0.053	0.15

* Exponential deradiation down to $I_{O,f} = 0 \text{ cal/cm}^2\text{-s}$ with rate coefficient $B_r = 10$.

** Exponential depressurization down to $P_f = 10 \text{ atm}$ with rate coefficient $B_p = 10$.

*** Exponential depressurization from $P_i = 40 \text{ atm}$ down to $P_f = 10 \text{ atm}$.

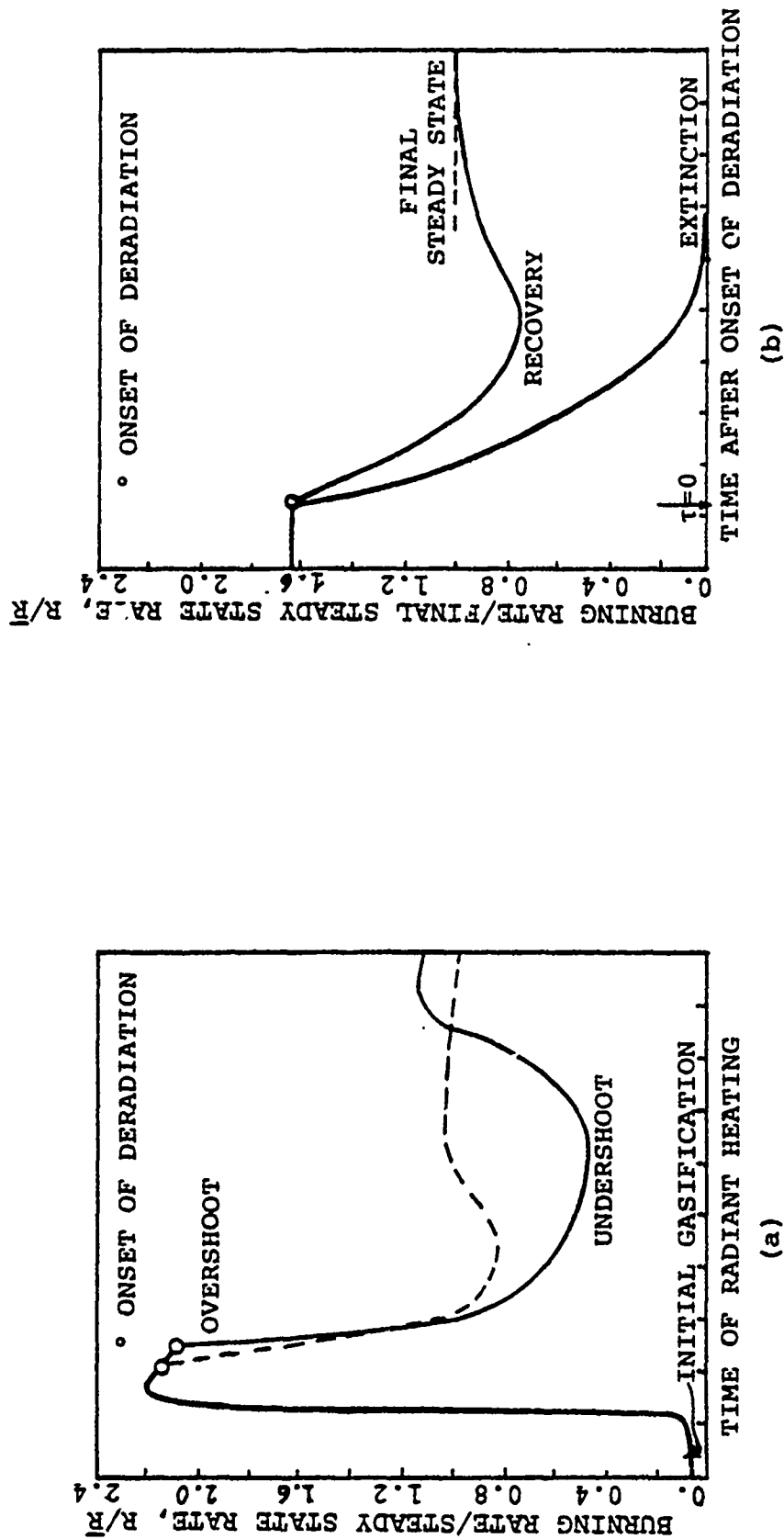


FIG. 1 a) Typical radiative ignition transient of a solid propellant showing importance of dynamic burning. Note initial burning rate overshoot and consequent undershoot.
b) Representative burning rate transient due to deradiation showing possible occurrence of dynamic extinction.

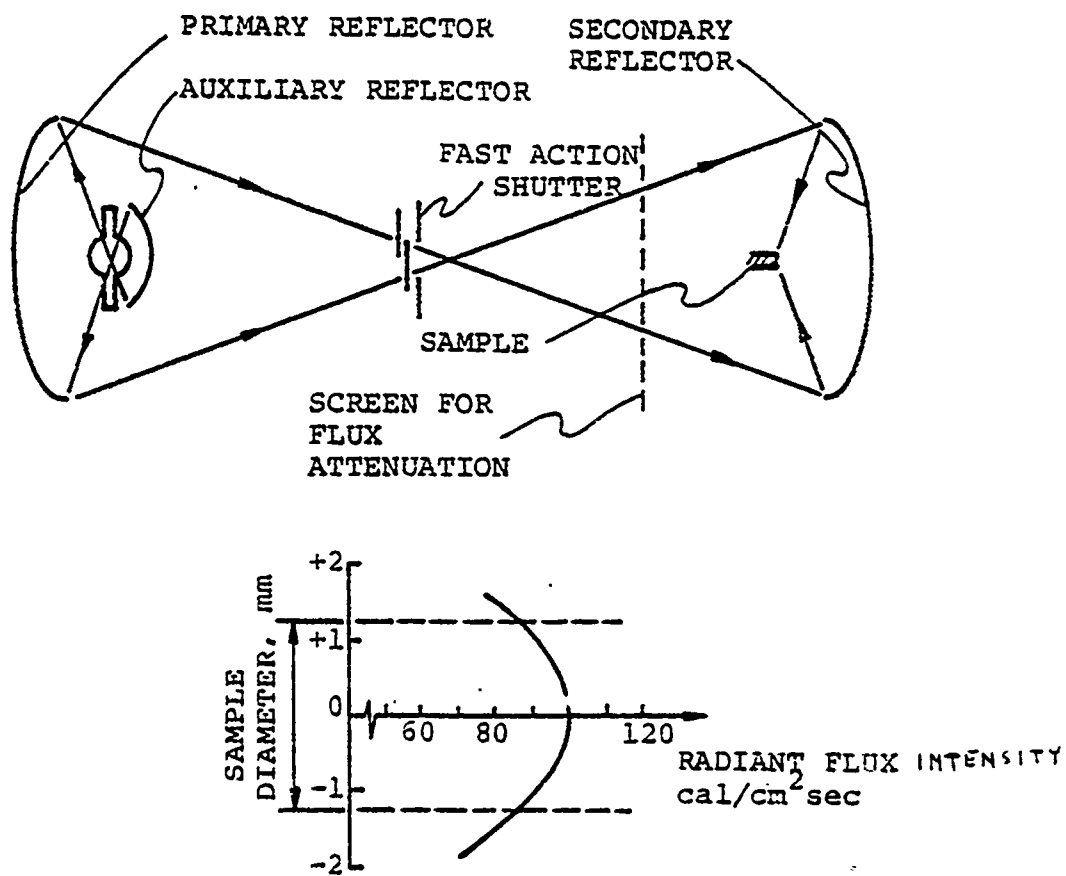


Fig. 2 a) Schematic diagram of arc image ignition apparatus.
 b) Typical illumination profile on sample showing radiant flux intensity decreasing of about 15% from the peak value at the center of the sample toward the boundary.

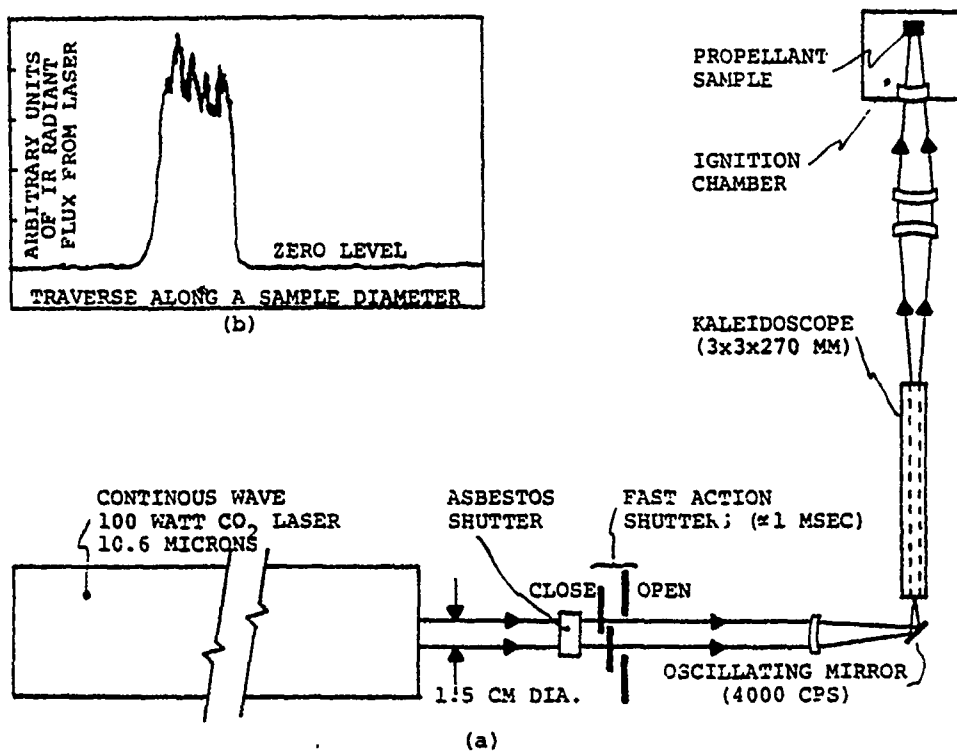


FIG.3 a) Schematic diagram of laser ignition apparatus.
 b) Typical illumination profile on sample showing
 +20% fluctuation of radiant flux intensity
 on either side of the average value.

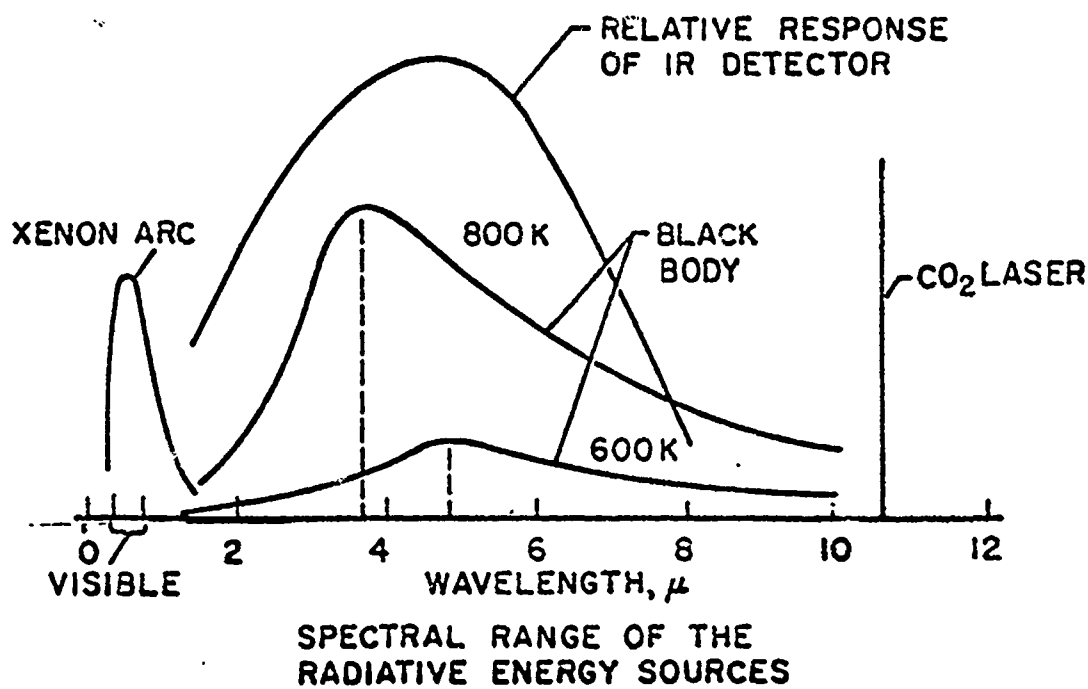
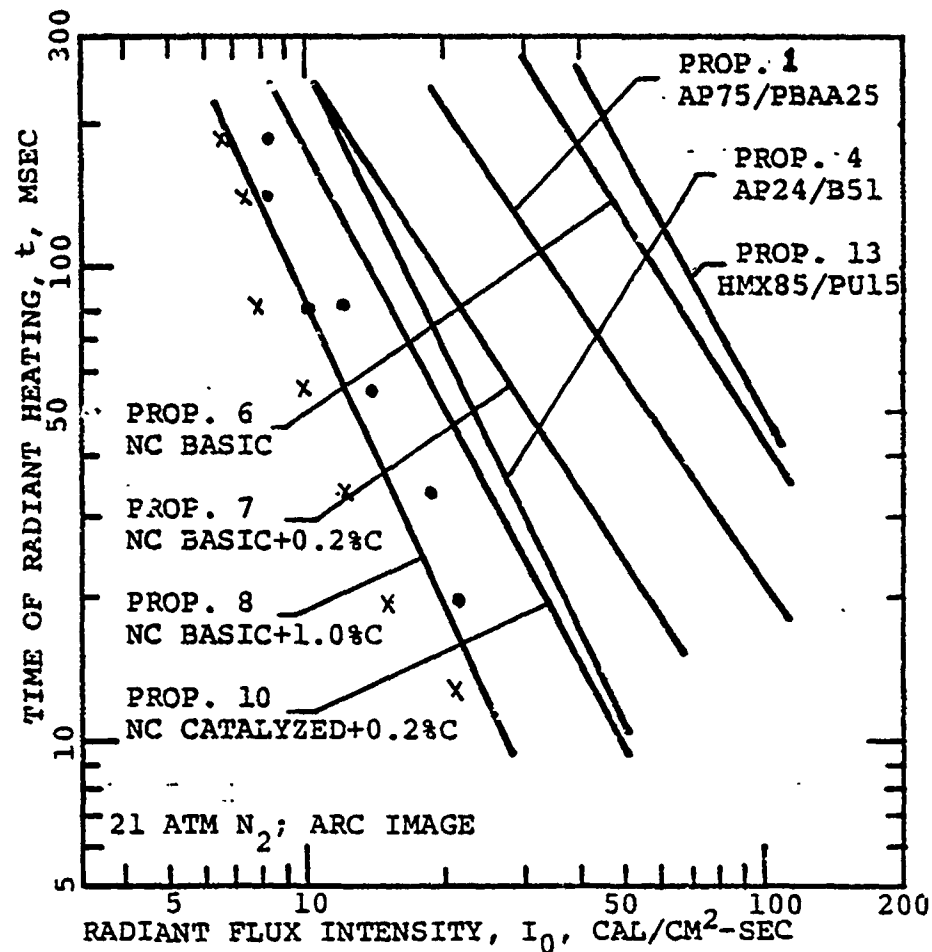


Fig. 4 Spectral range (not to scale) of energy sources showing complicate wavelength dependence of the arc beam structure and strong relative response of the IR detection system in the 2 - 7 μ range.



EXAMPLES OF GO/NO-GO DATA FOR PROP. 8 :

x NO IGNITION

• IGNITION

Fig. 5 Arc image ignition limits at 21 atm N₂ of several propellant classes showing correlation with the optical data given in Table 5.

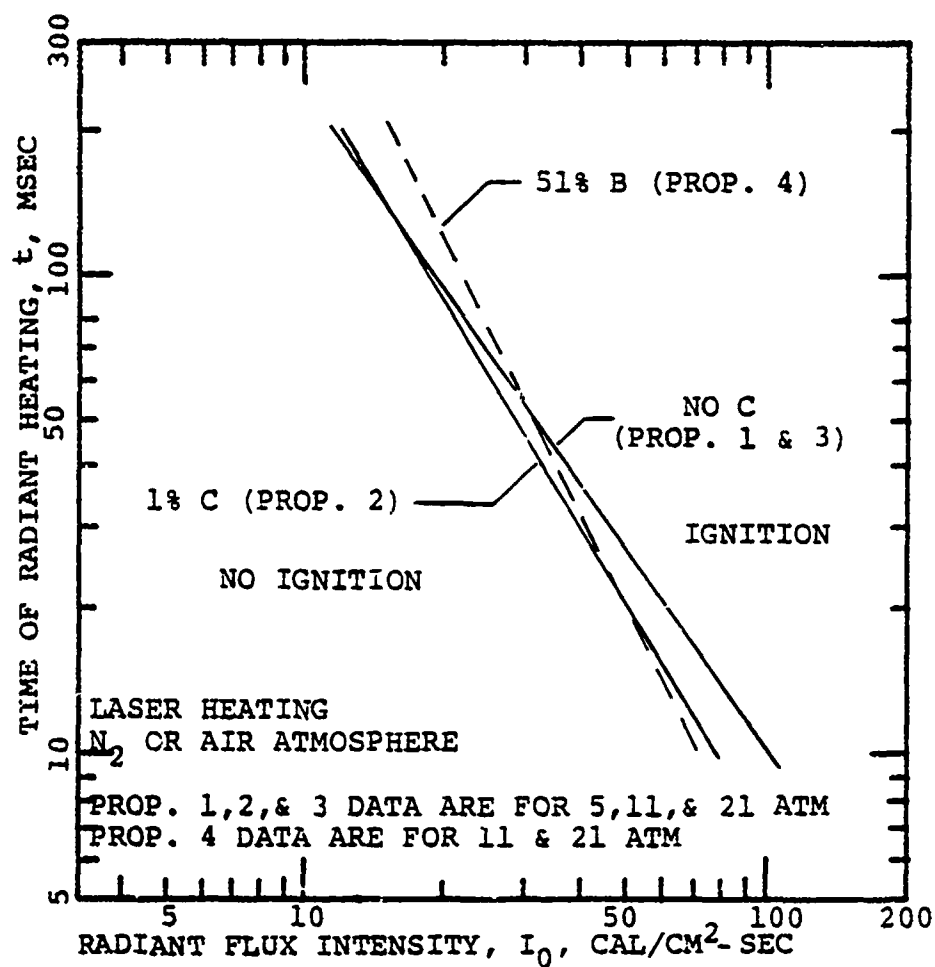


Fig. 6 Ignition of AP composite propellants #1, 2, 3, and 4 in the laser ignition apparatus demonstrating independence of pressure in the range 5-21 atm of N_2 or air.

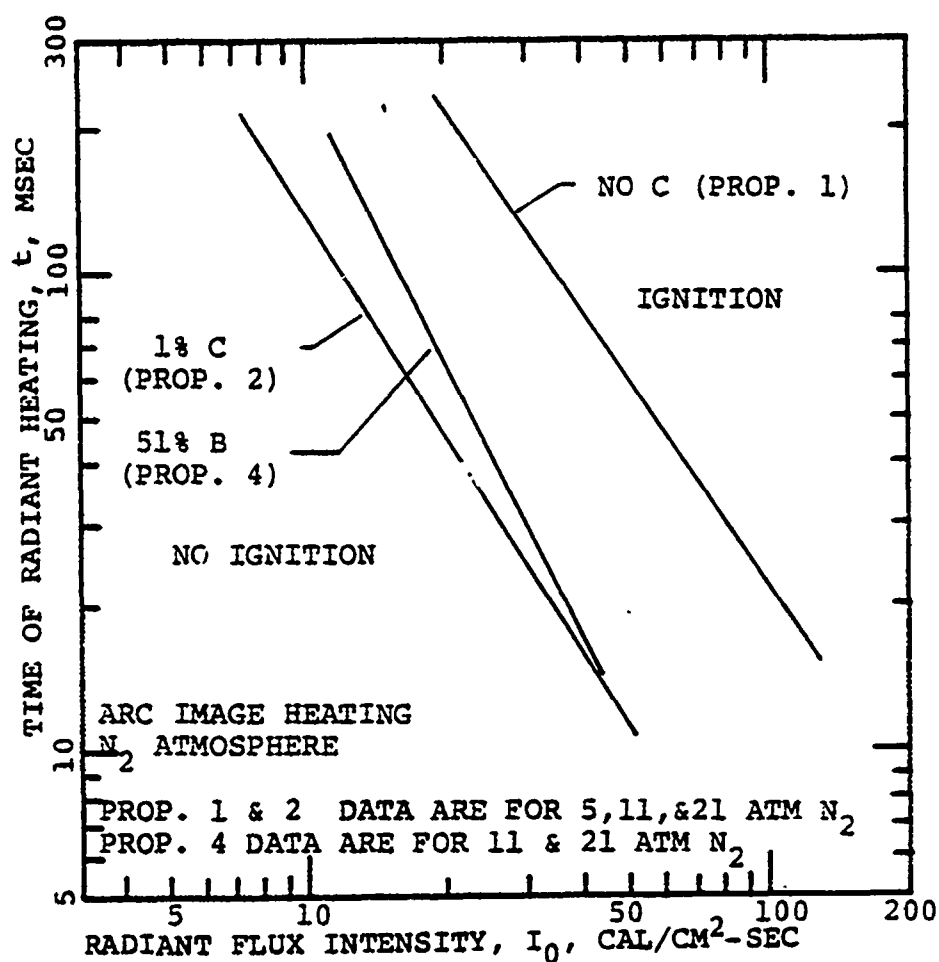


Fig. 7 Ignition of AP composite propellants #1, 2, and 4 in the arc image ignition apparatus demonstrating independence of pressure in the range 11 - 21 atm of N_2 and marked effect of radiation penetration.

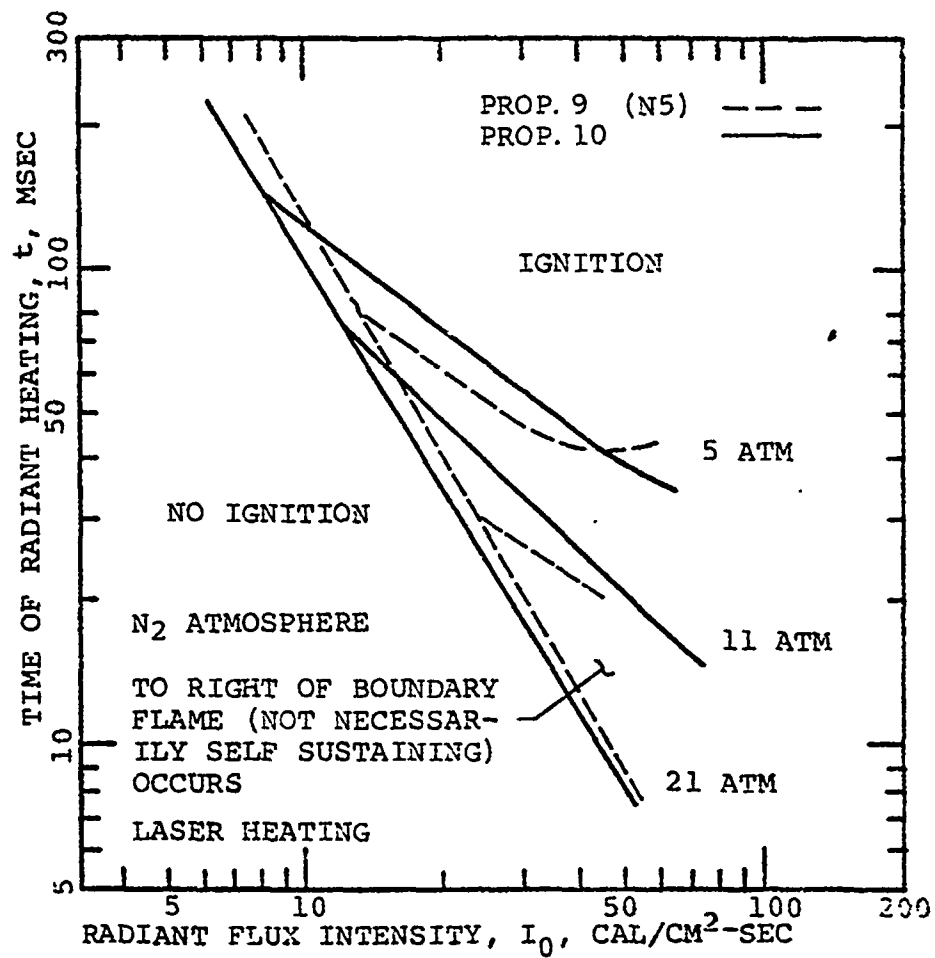


Fig. 8 Catalyzed DB propellants #9 and 10 tested in the laser ignition apparatus showing pressure dependence of ignition boundaries in the range 5-21 atm N₂.

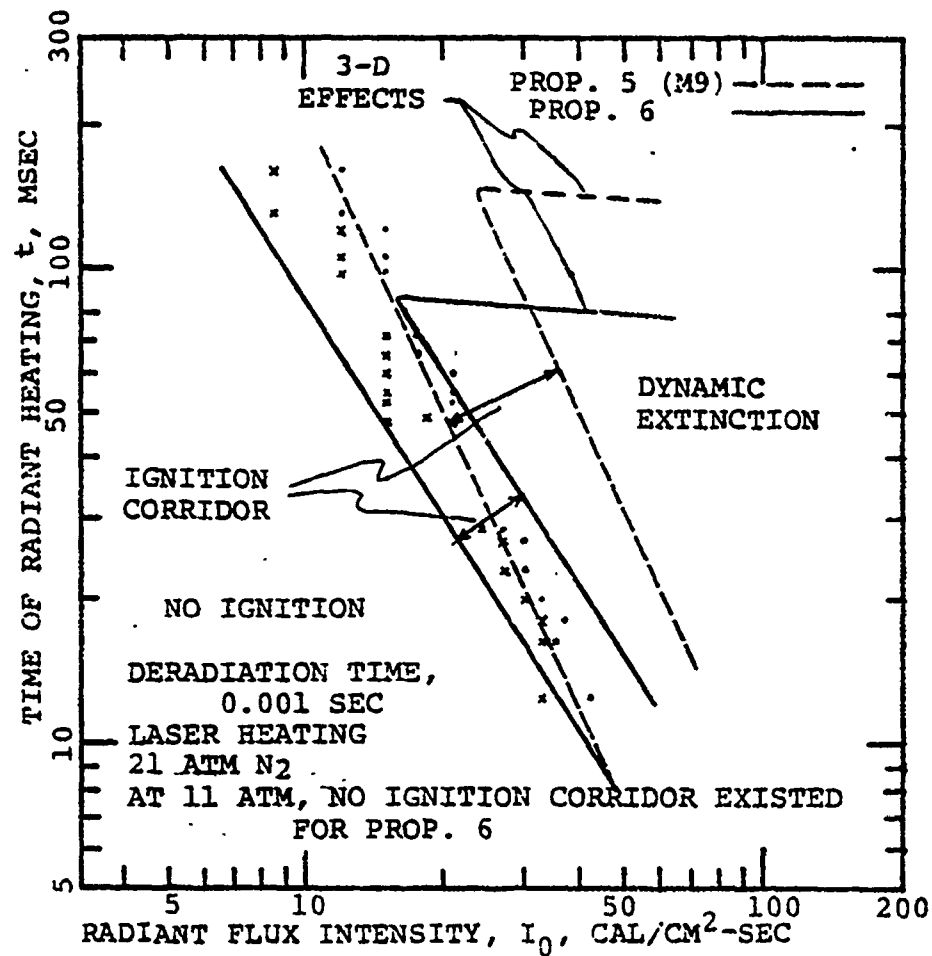


Fig. 9 Dynamic extinction of noncatalyzed DB propellants #5 and 6 tested in the laser ignition apparatus. (No such boundaries noted in arc image tests).

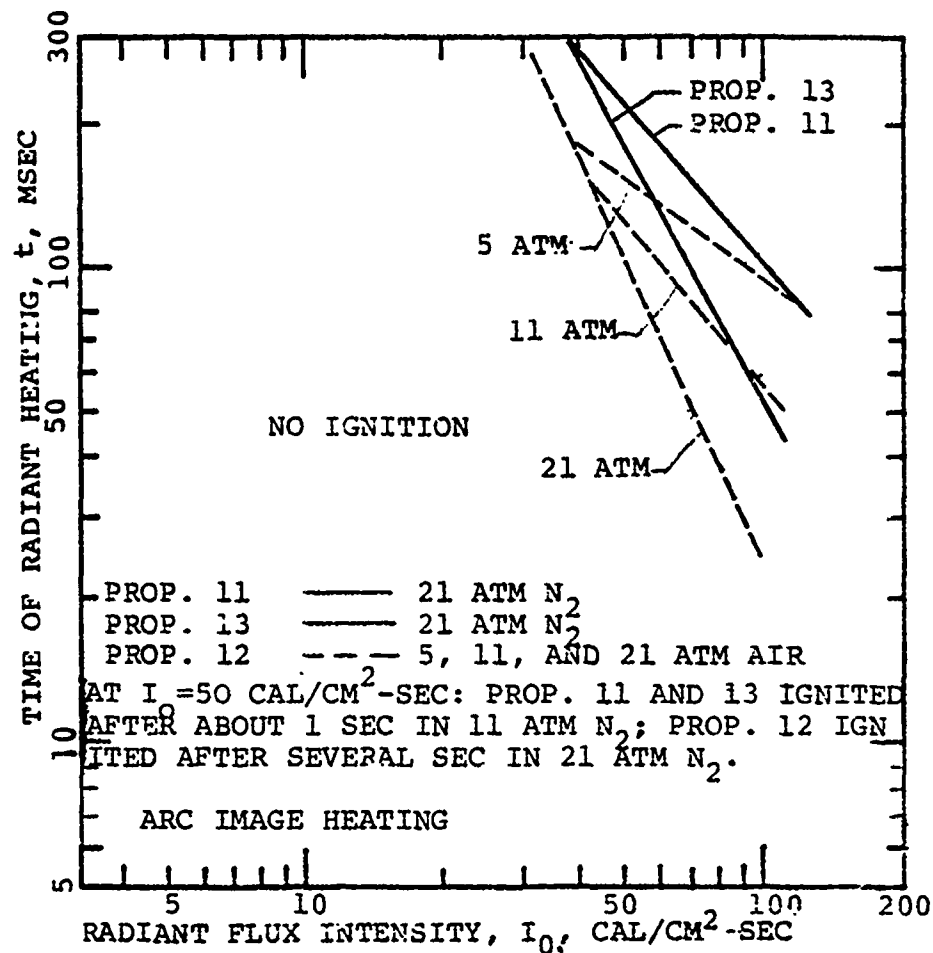
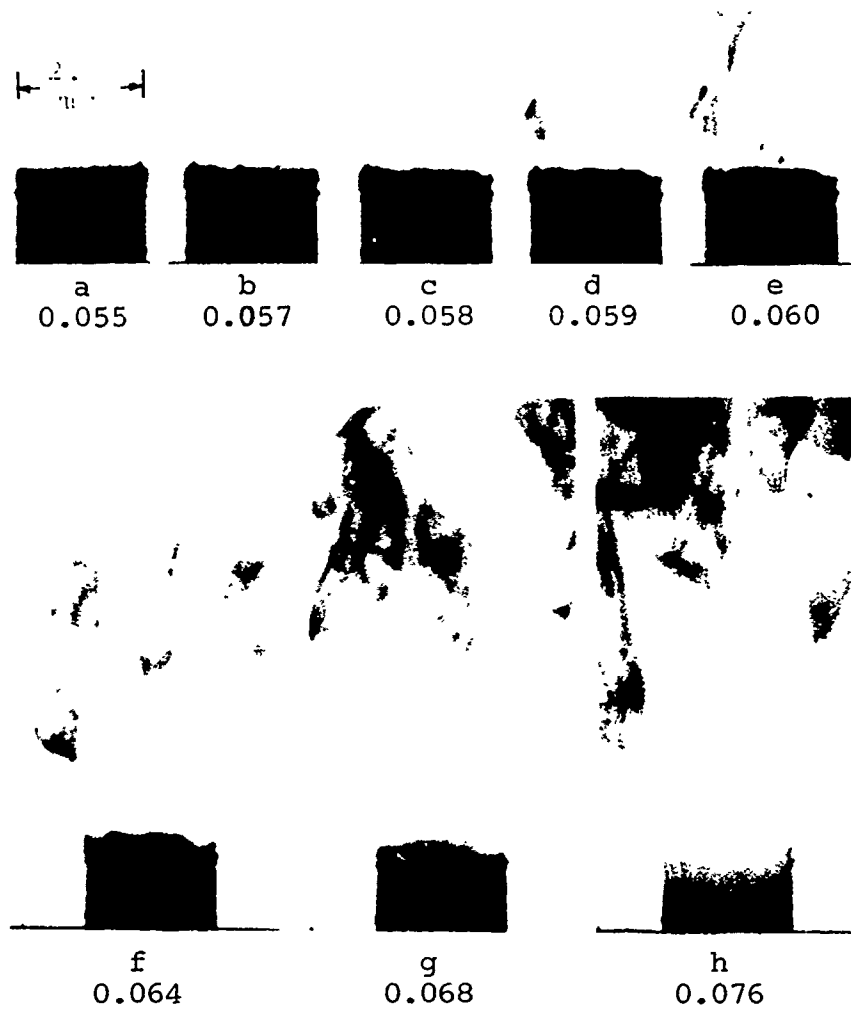
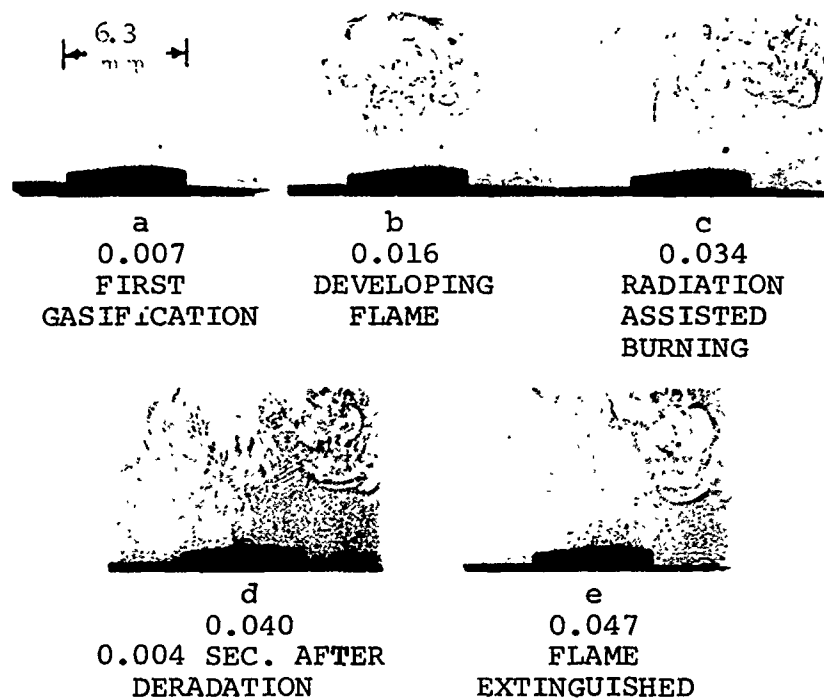


Fig. 10 Arc image ignition data for HMX composite propellants #11, 12, and 13 in nitrogen and in air showing resistance to ignition.



TIMES ARE SECONDS AFTER ONSET OF RADIANT HEATING.
PROPELLANT 1; PRESSURE, 11 ATM N_2 ;
HEAT FLUX, 30 CAL/CM²-SEC

Fig. 11 High speed shadowgraph movie illustrating flame development of an AP composite propellant and closely coupled flame.



TIMES ARE SECONDS AFTER ONSET OF
RADIANT HEATING.
PROPELLANT 5; PRESSURE, 21 ATM N_2
HEAT FLUX, 51 CAL/CM²-SEC

Fig. 12 High speed shadowgraph movie illustrating flame development of a noncatalyzed DB propellant and large stand-off distance of the luminous zone.

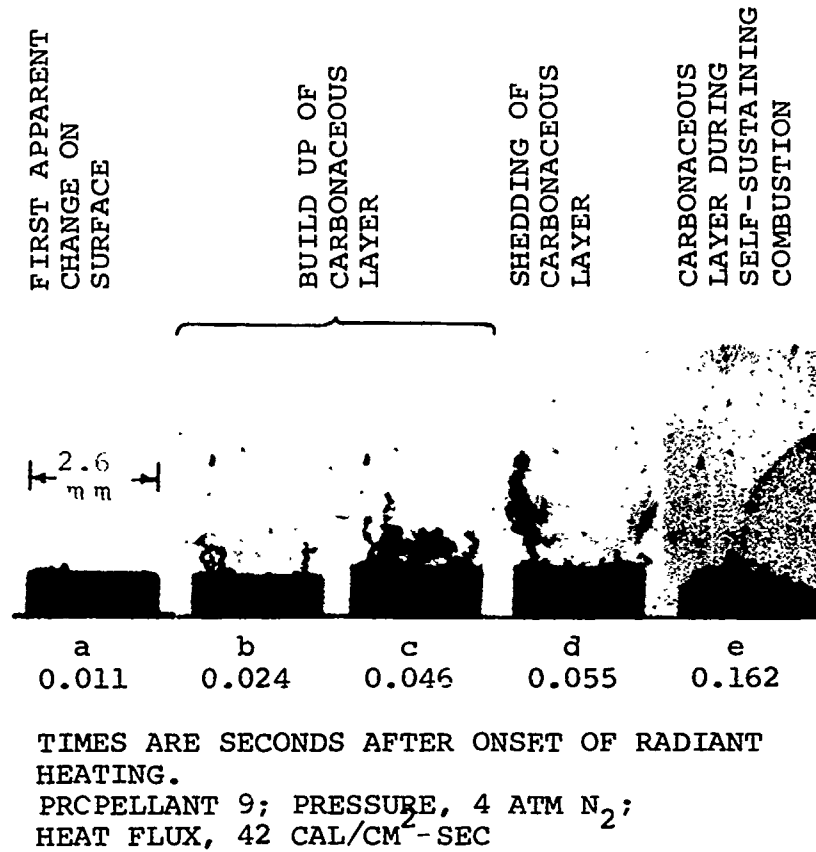


Fig. 13 High speed shadowgraph movie showing carbonaceous-appearing layer formation on the surface of a catalyzed DB propellant.

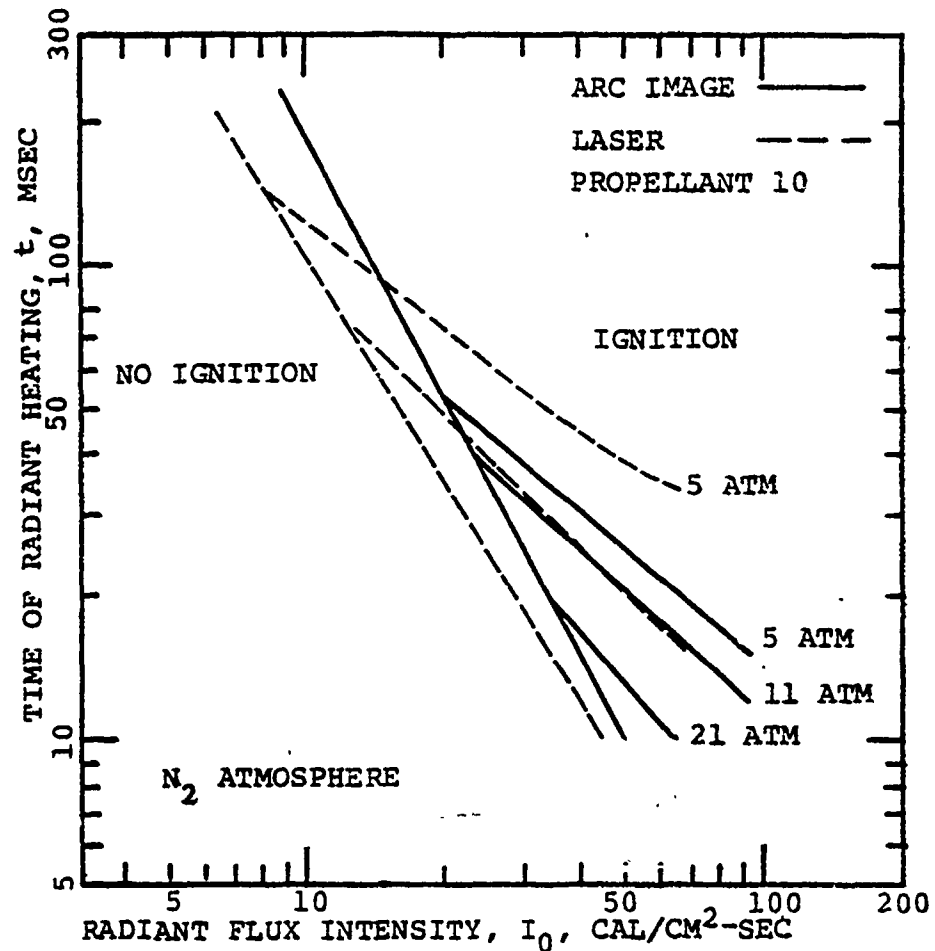


Fig. 14 Testing of catalyzed DB propellant #10 in the arc image and laser ignition apparatus showing similarity of the two ignition maps and that pressure dependence is characteristic of the propellant not the ignition apparatus.

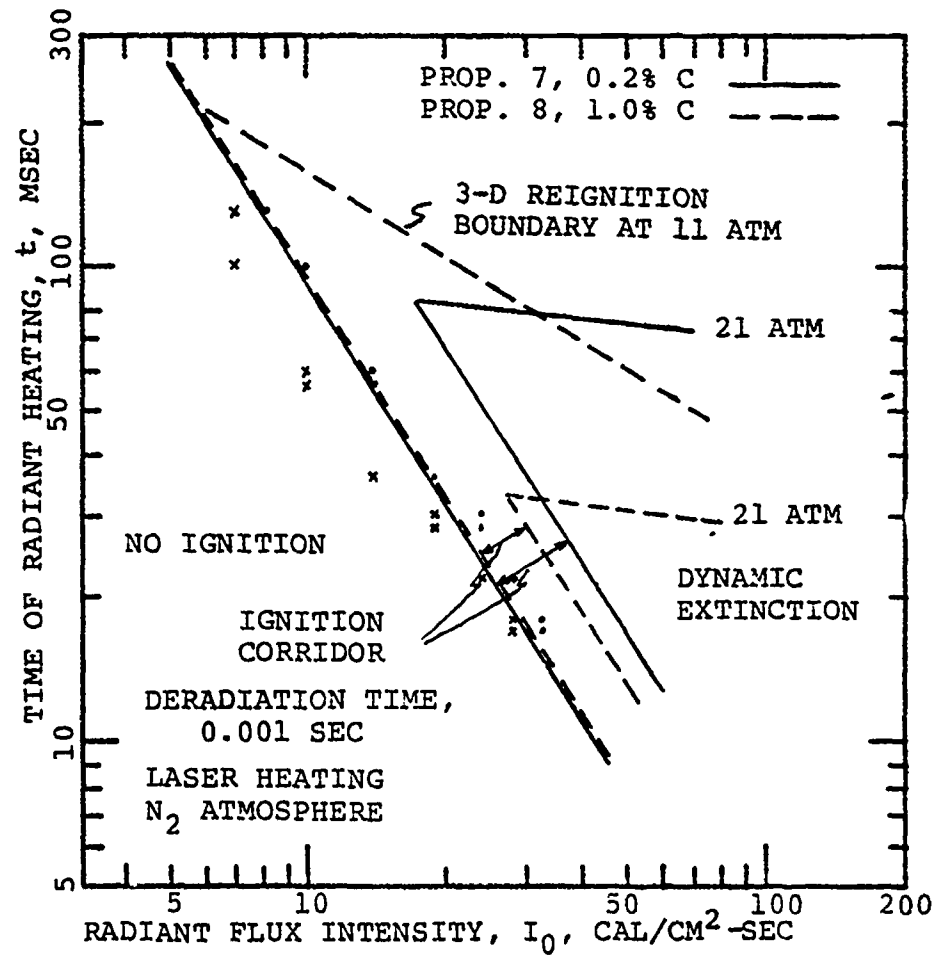


Fig. 15 Addition of carbon reducing dynamic extinction domain of noncatalyzed DB propellants #7 and #8.

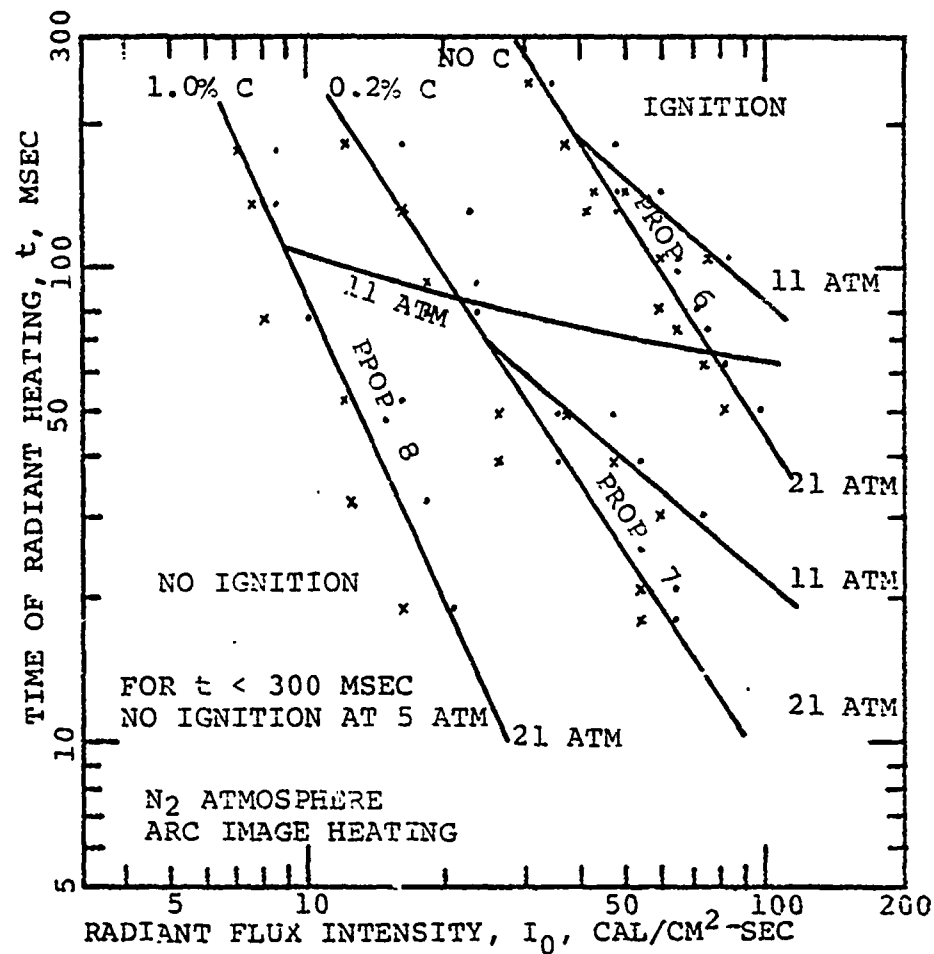


Fig. 16 Arc image ignition data showing decrease of ignition delay with increase of carbon content and absence of dynamic extinction for noncatalyzed DB propellants #6, 7, and 8. (Contrast with Figs. 8 and 14).

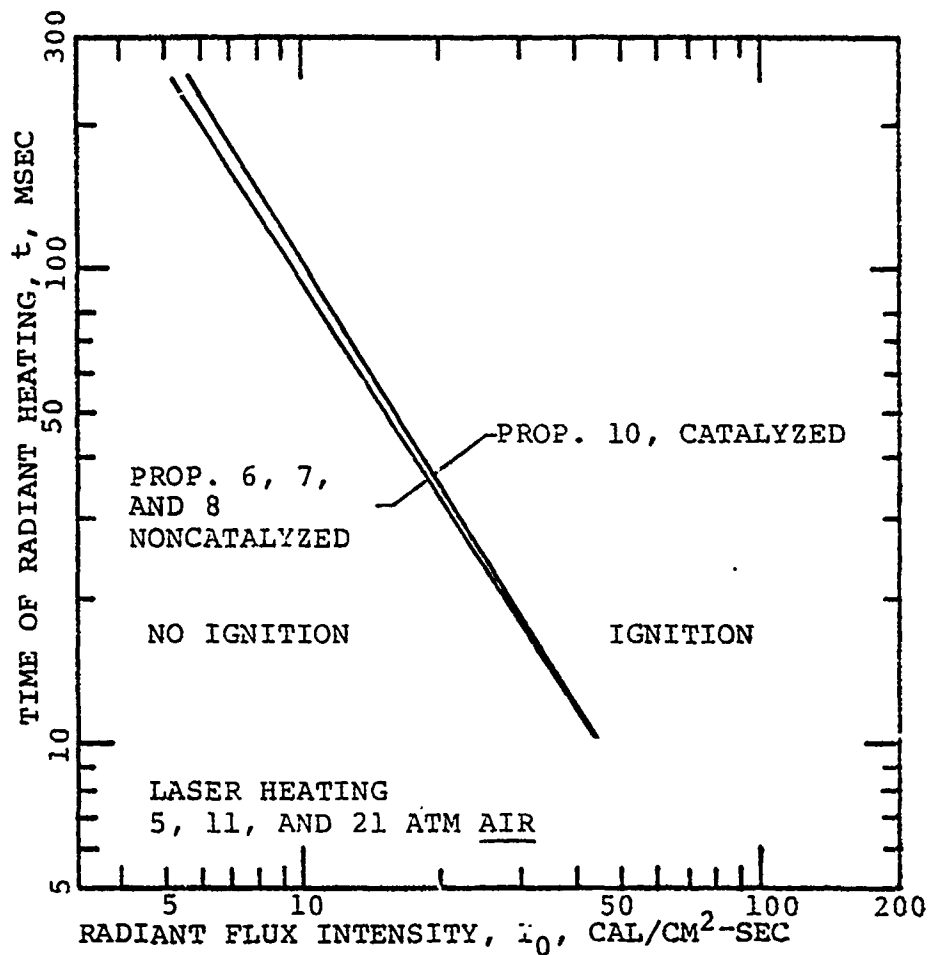


Fig. 17 Noncatalyzed DB propellants #6, 7, and 8, and catalyzed DB propellant #10, ignited in air, showing elimination of pressure dependence in the range 5 - 21 atm when air is the ambient gas.

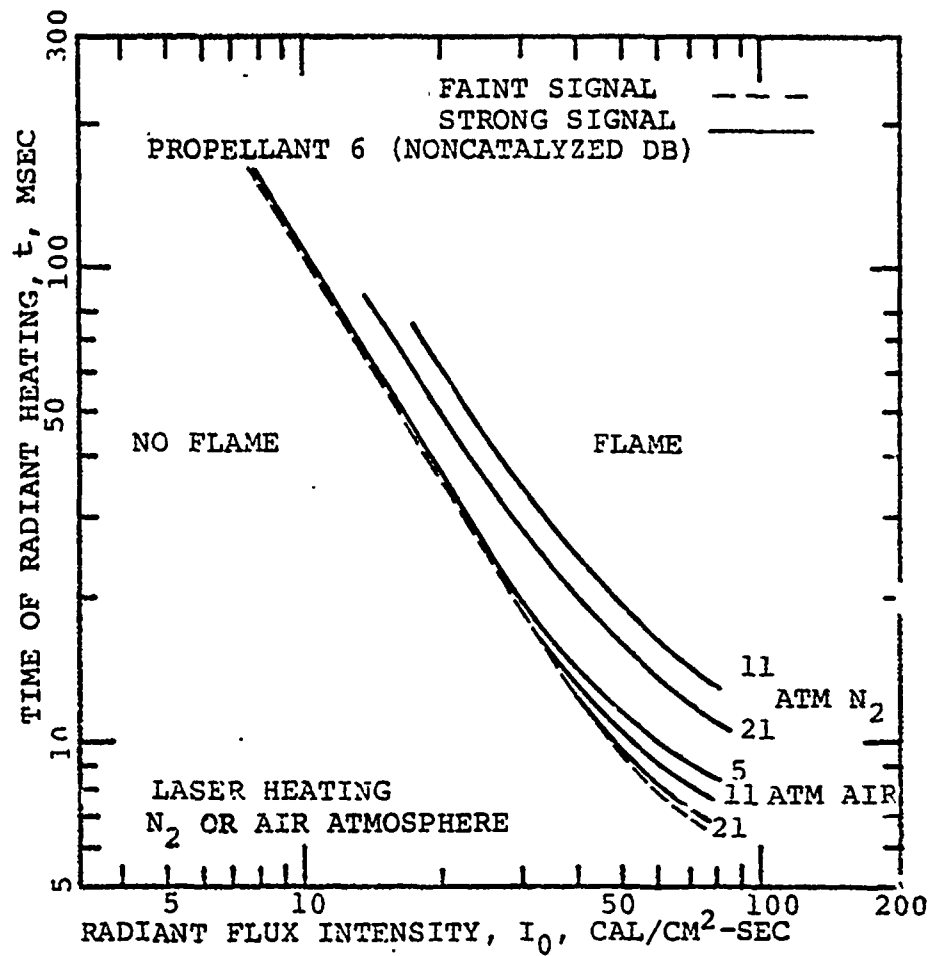


Fig. 18 Pressure dependence of strong IR signal for non-catalyzed DB propellant #6. (Weak signal is independent of pressure and ambient atmosphere).



a) 0.012 sec NO VISIBLE EVIDENCE OF SURFACE GASIFICATION



b) 0.014 sec EVIDENCE OF SURFACE GASIFICATION (IN OUTLINED REGIONS)



c) 0.018 sec SURFACE GASIFICATION MORE EXTENSIVE



d) 0.021 sec GASIFICATION OVER ENTIRE SPOT HEATED BY LASER

TIMES ARE SECONDS AFTER ONSET OF RADIANT HEATING.
PROPELLANT # 10 @ 11 ATM N_2 and $I_0 = 37 \text{ CAL/CM}^2\text{-SEC}$

Fig. 19 Spreading of gasification process over the surface of a catalyzed DB propellant subjected to laser heating showing presence of hot spots. Compare with Figs. 13 and 21.

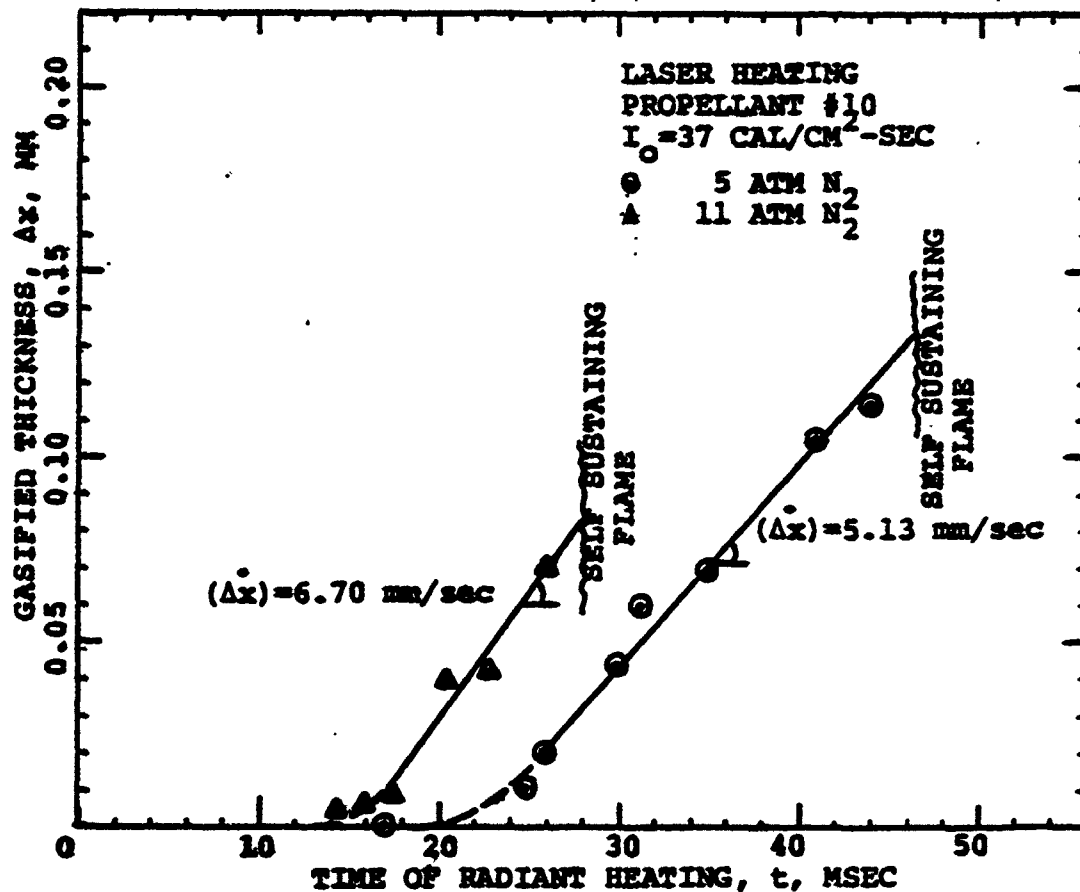


Fig. 20 Pre-ignition ablation of a catalyzed DB propellant subjected to laser radiation showing occurrence of stationary gasification process prior to the self-sustained flame. See also Table 6.

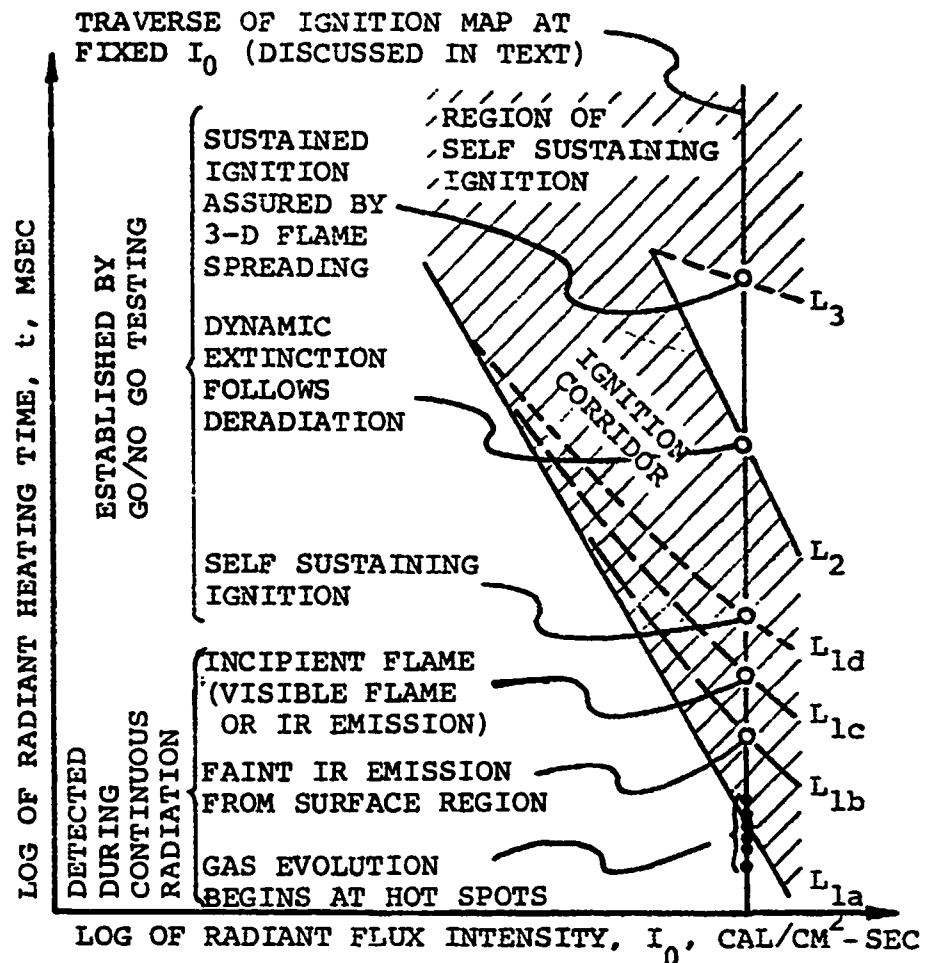


Fig. 21. Generalized ignition map showing event limits or signals that occur during radiant heating of solid propellants.

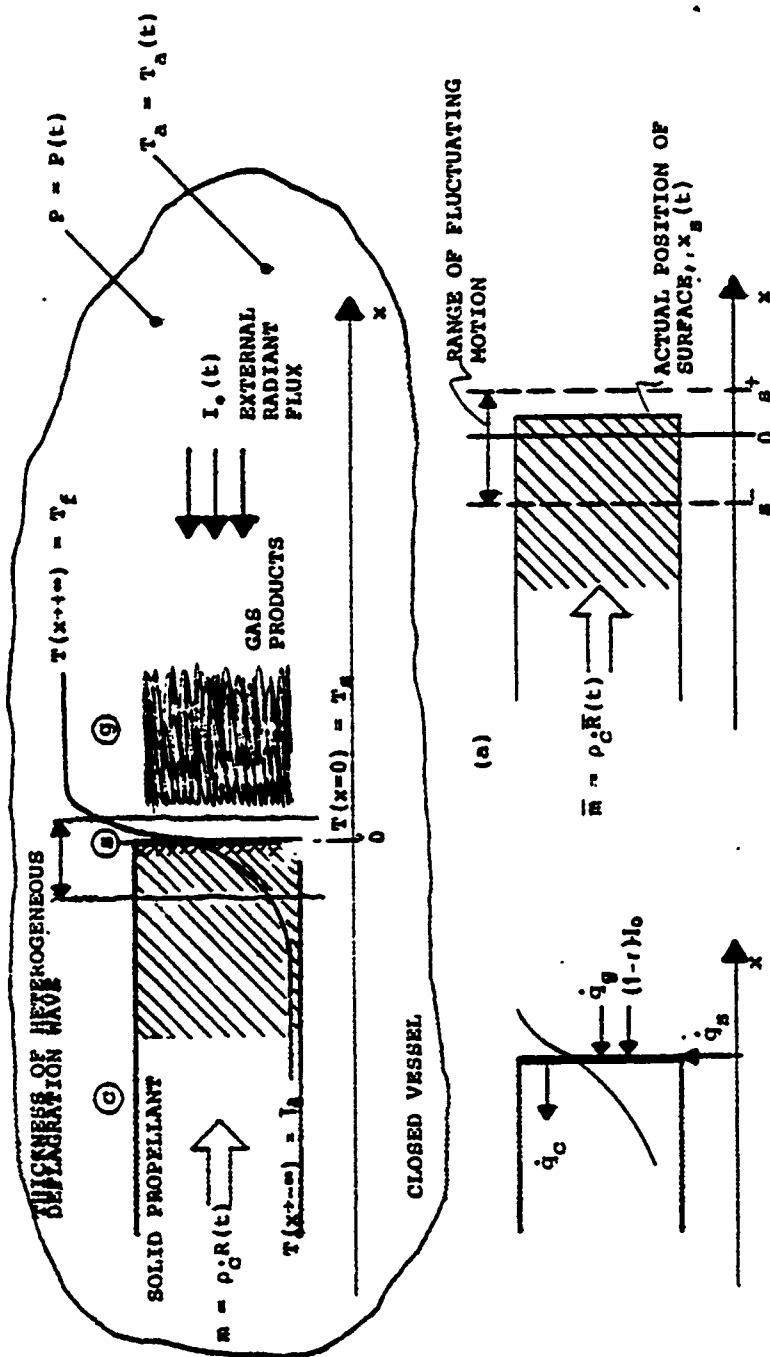


Fig. 22 (a) Schematic diagram of the physical problem.
 (b) Schematic diagram of energy balance at the surface
 (c) Schematic diagram of Culick's nomenclature for the acoustic admittance function determination.

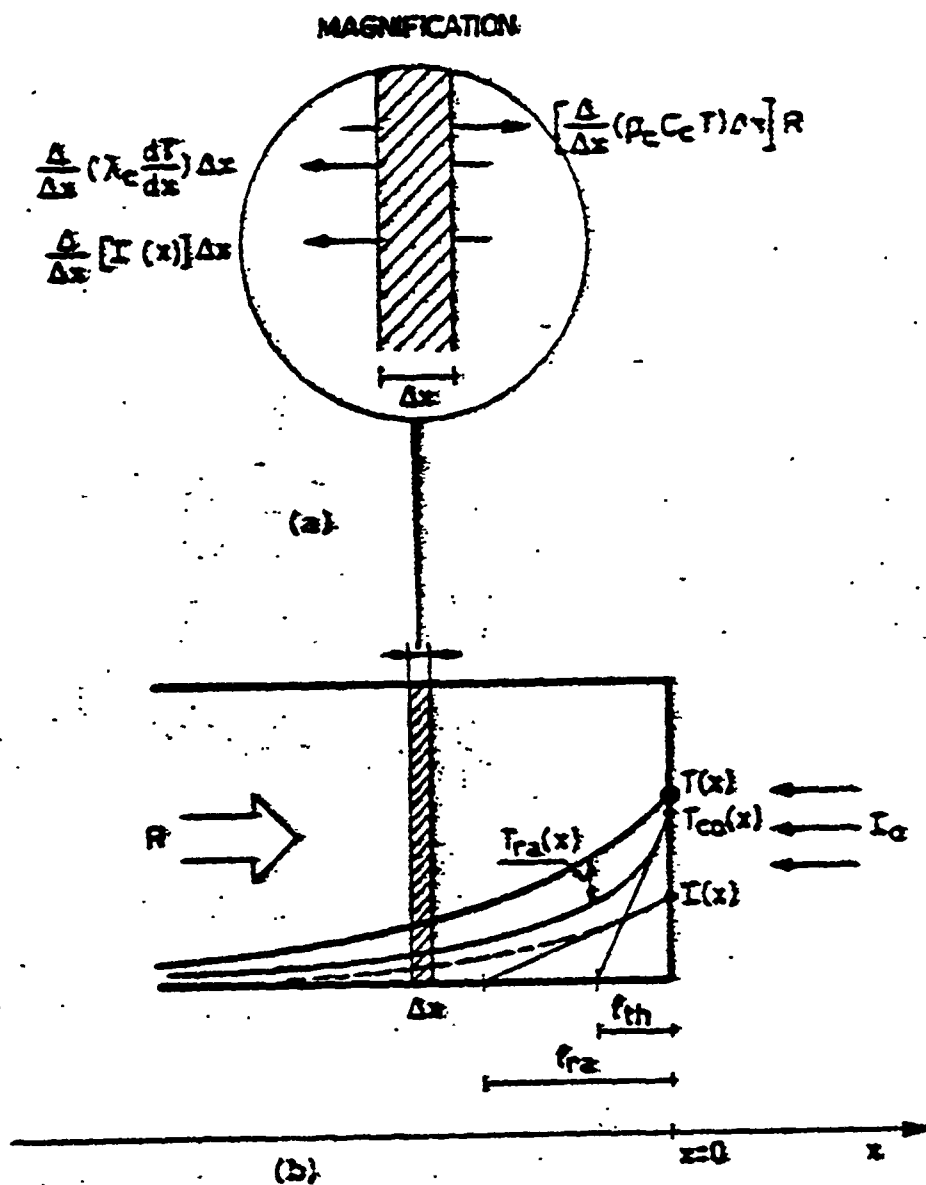


Fig. 23a Energy balance in differential form at the interior of a slab subjected to conductive and radiative heating.

Fig. 23b Steady state thermal profile in a slab subjected to conductive and radiative heating.

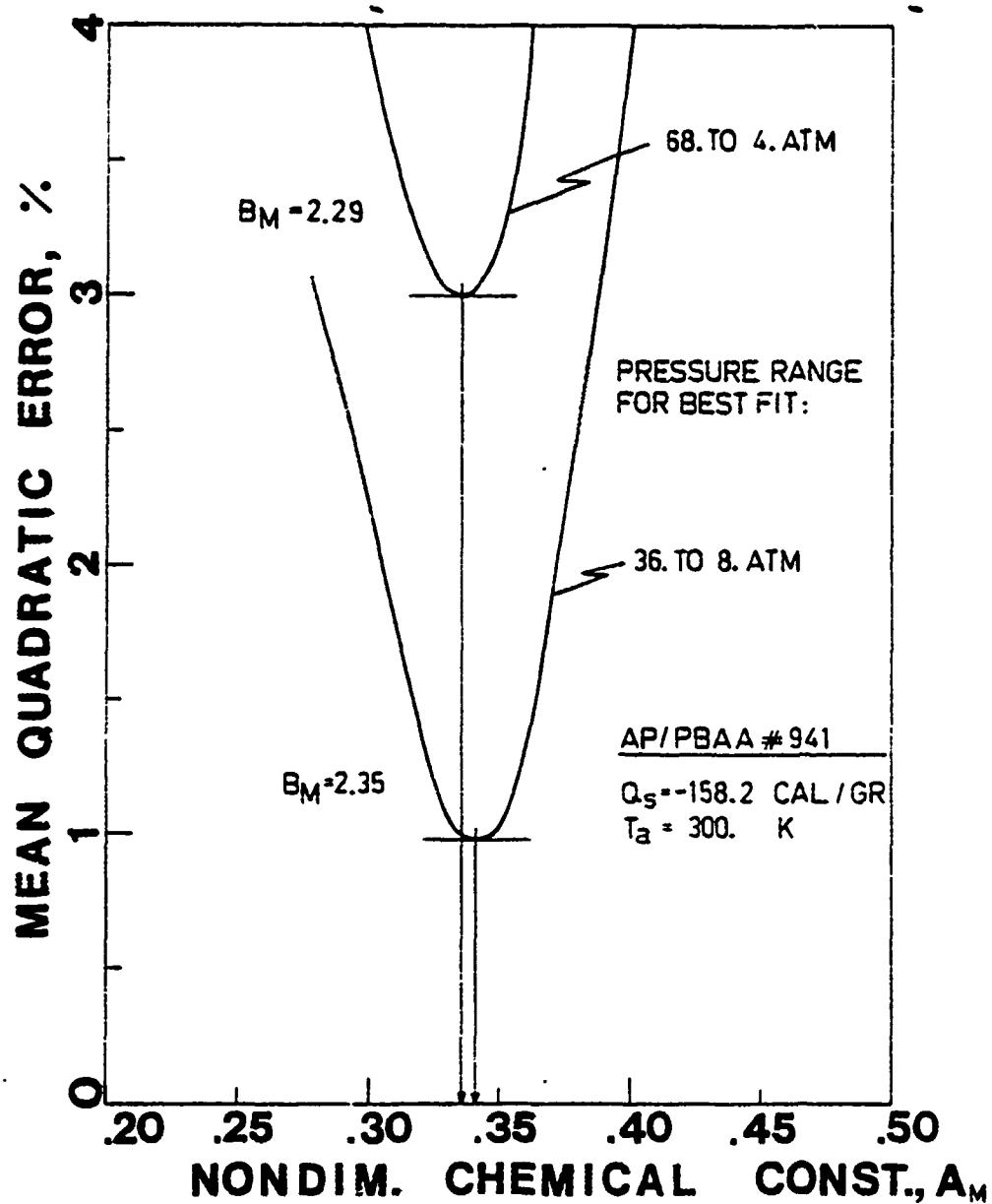


Fig. 24 Determination of gas phase constants required in the MTS flame model.

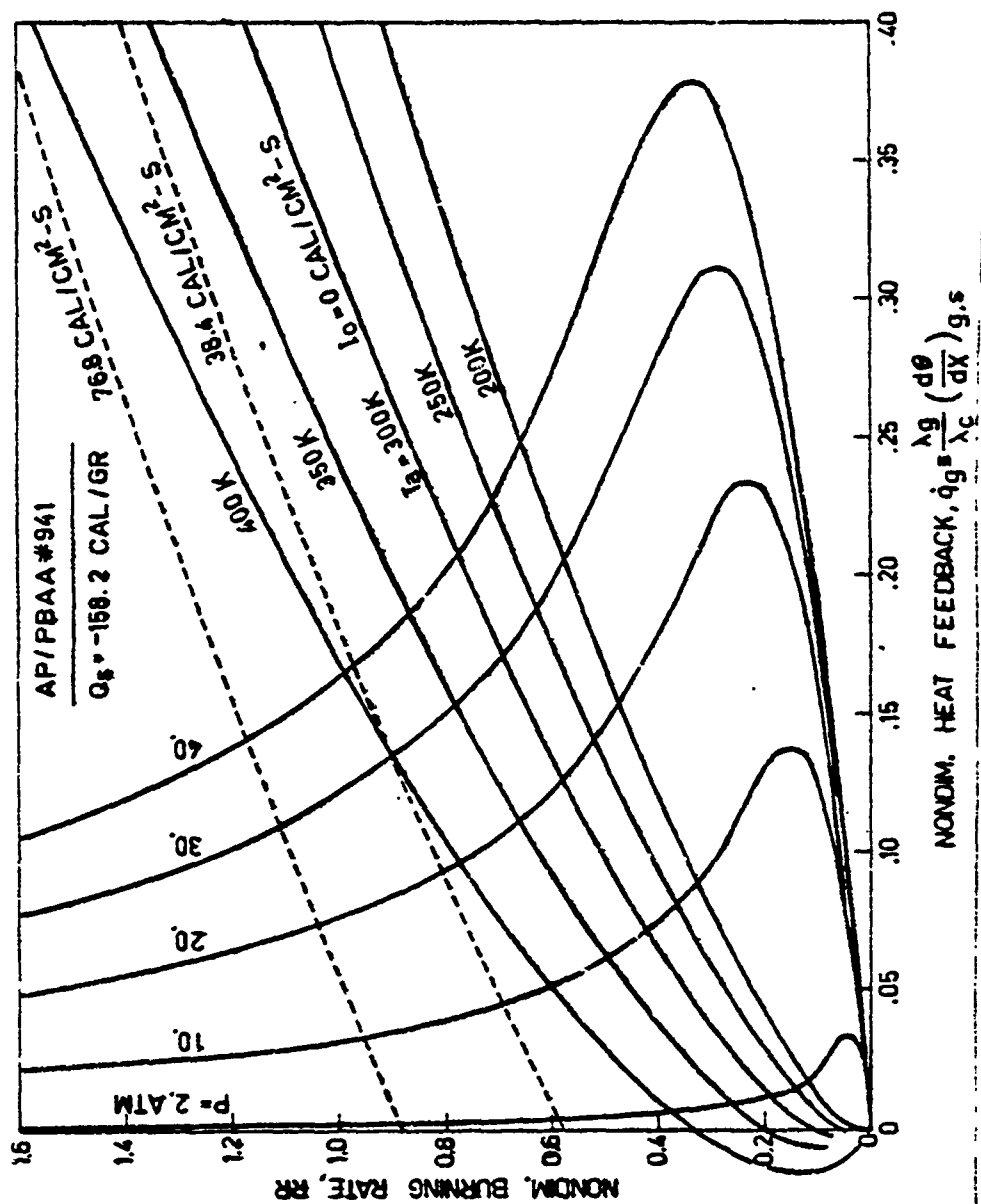


Fig. 25 Quasi-steady burning rate vs heat feedback plot according to MTS flame model.

CONSTRUCTION OF THE REQUIRED $R(q_c, P)$ CHART

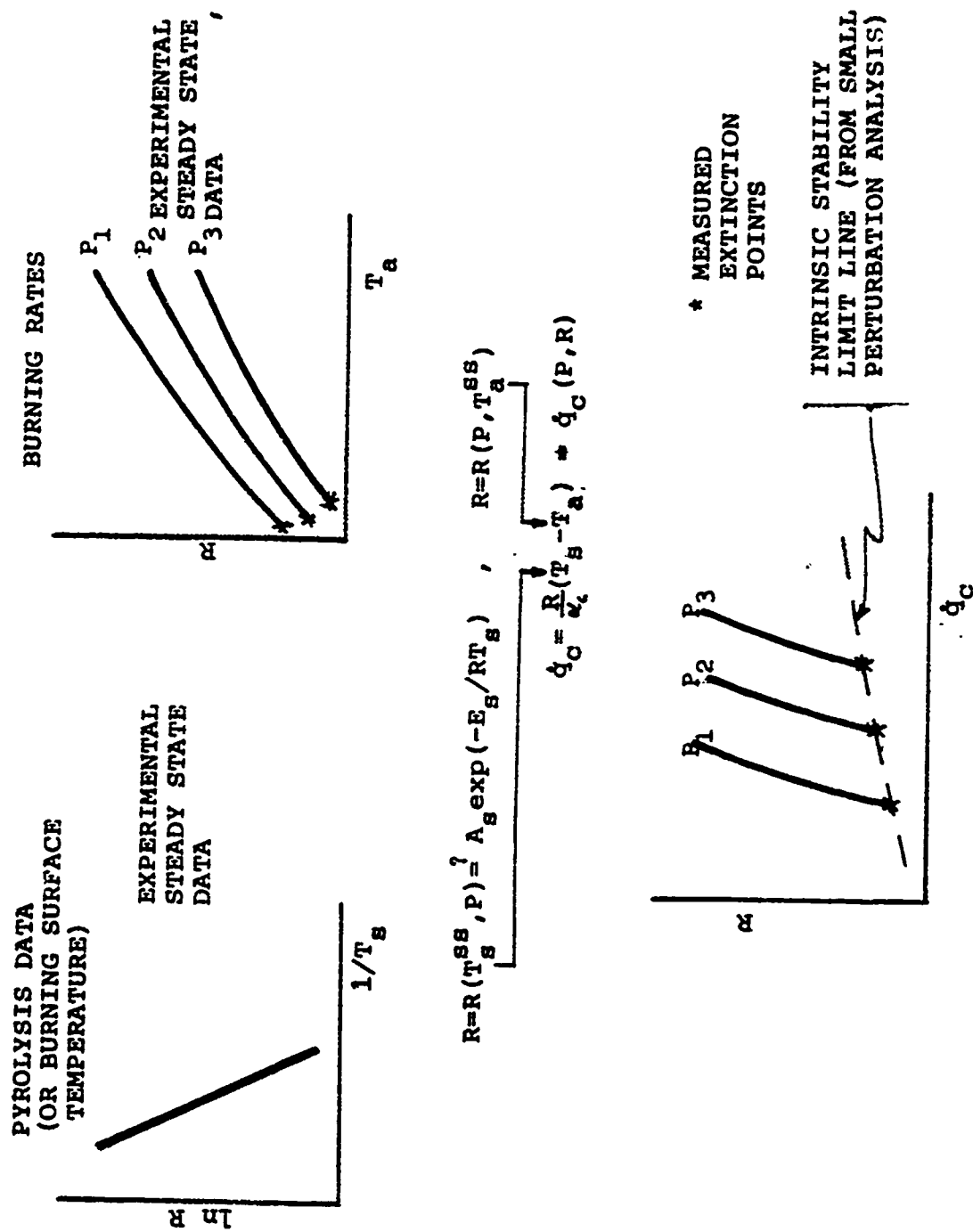


Fig. 26 Construction of the quasi-steady thermal gradient at the condensed/surface boundary according to Ya. B. Zeldovich.

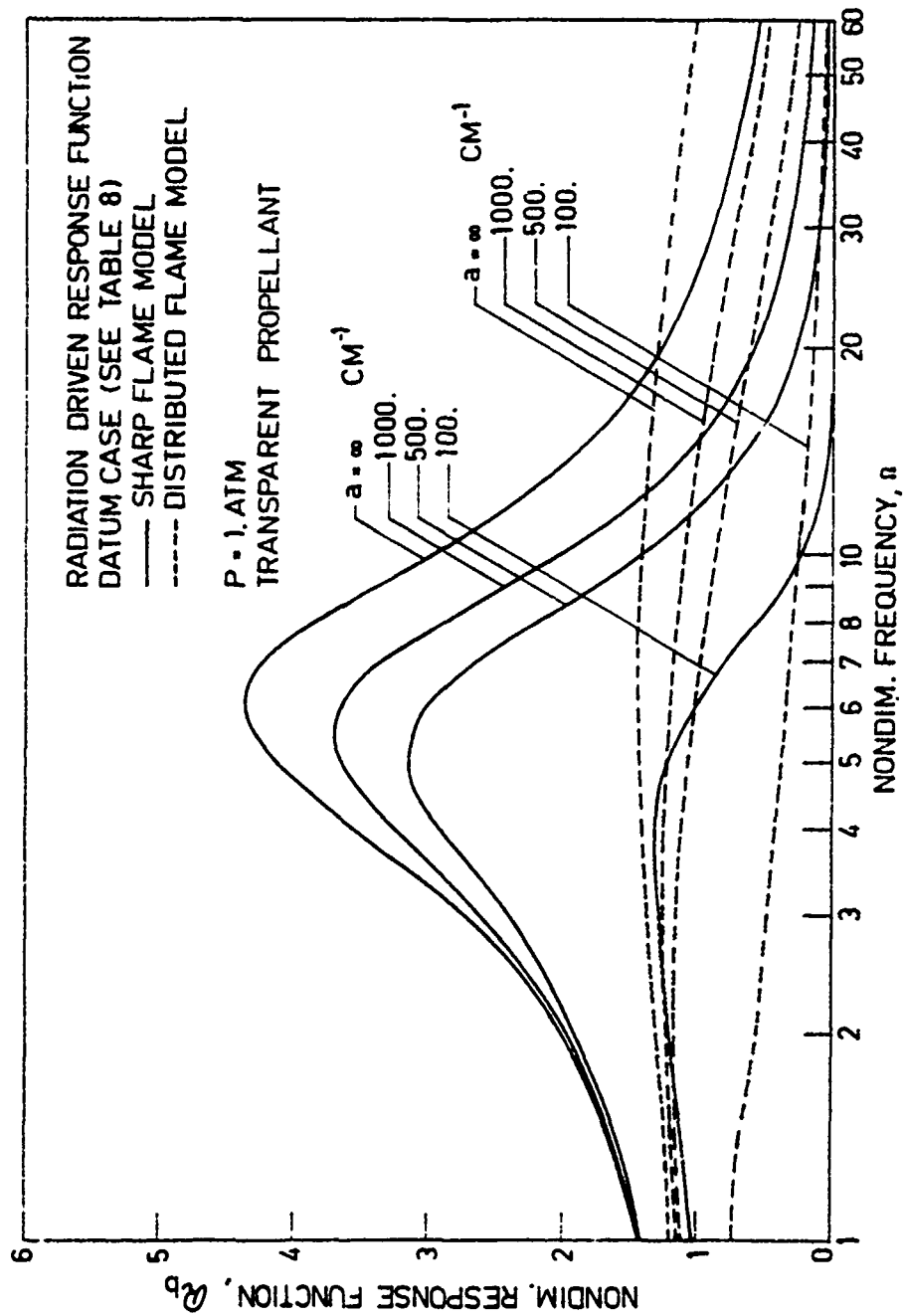


Fig. 27 Response function of a propellant strongly affected by the assumed flame model.

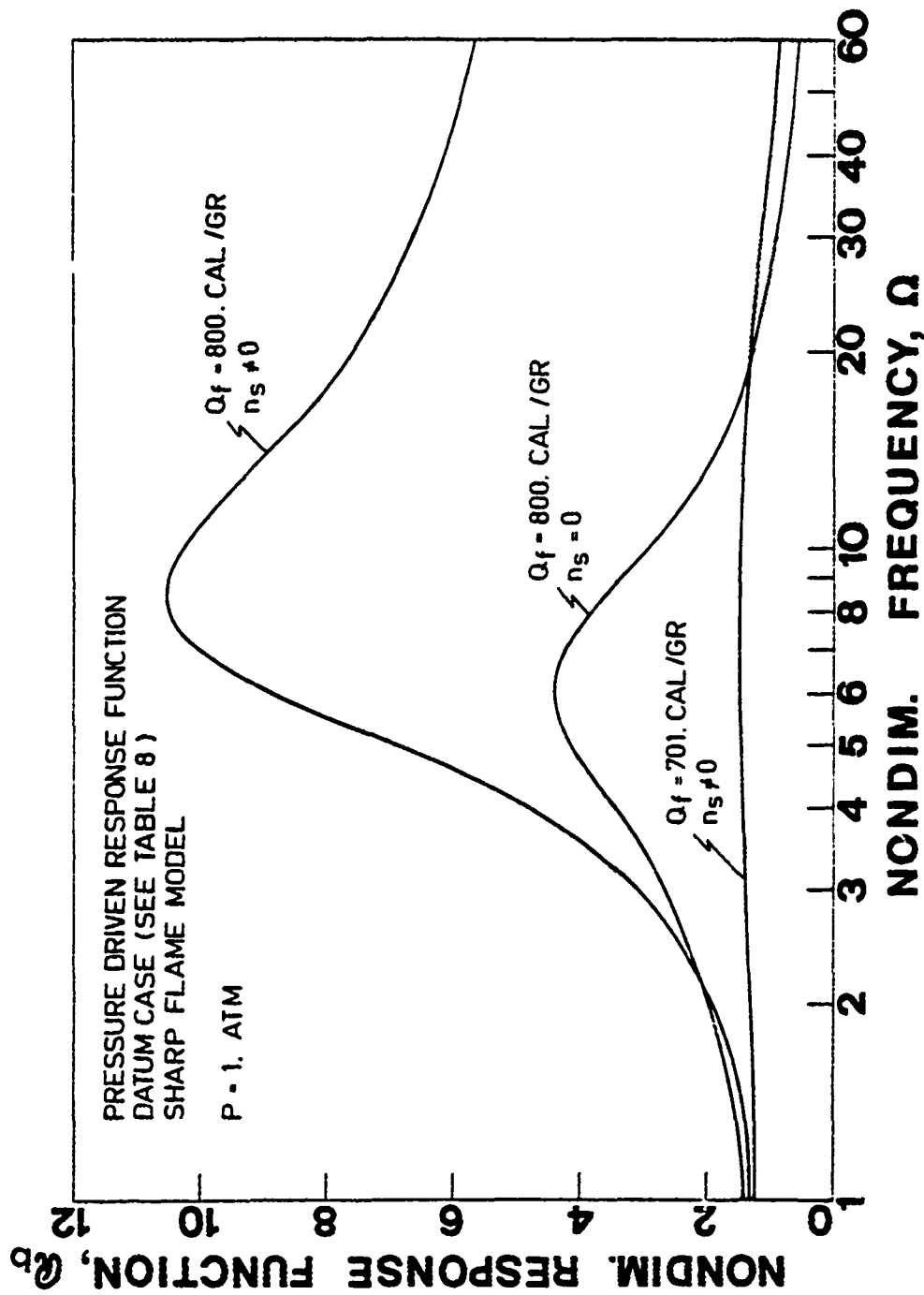


Fig. 28 Response function of a propellant strongly affected by the pressure dependence of surface pyrolysis law and by energy release in gas phase (sharp flame model).

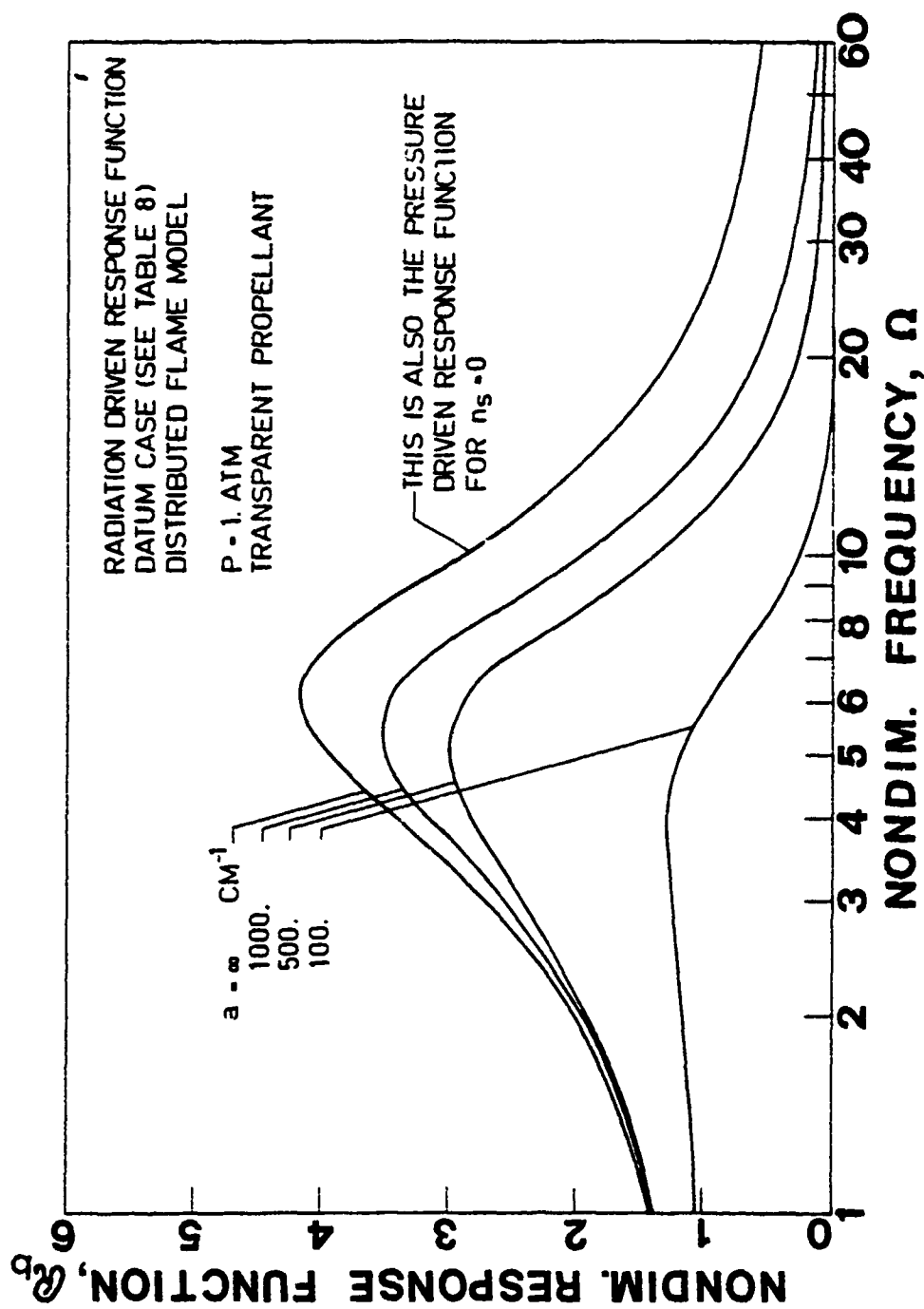


Fig. 29 Response function of a propellant showing that the pressure and radiation driven frequency behavior of an opaque propellant is the same for a distributed flame model.

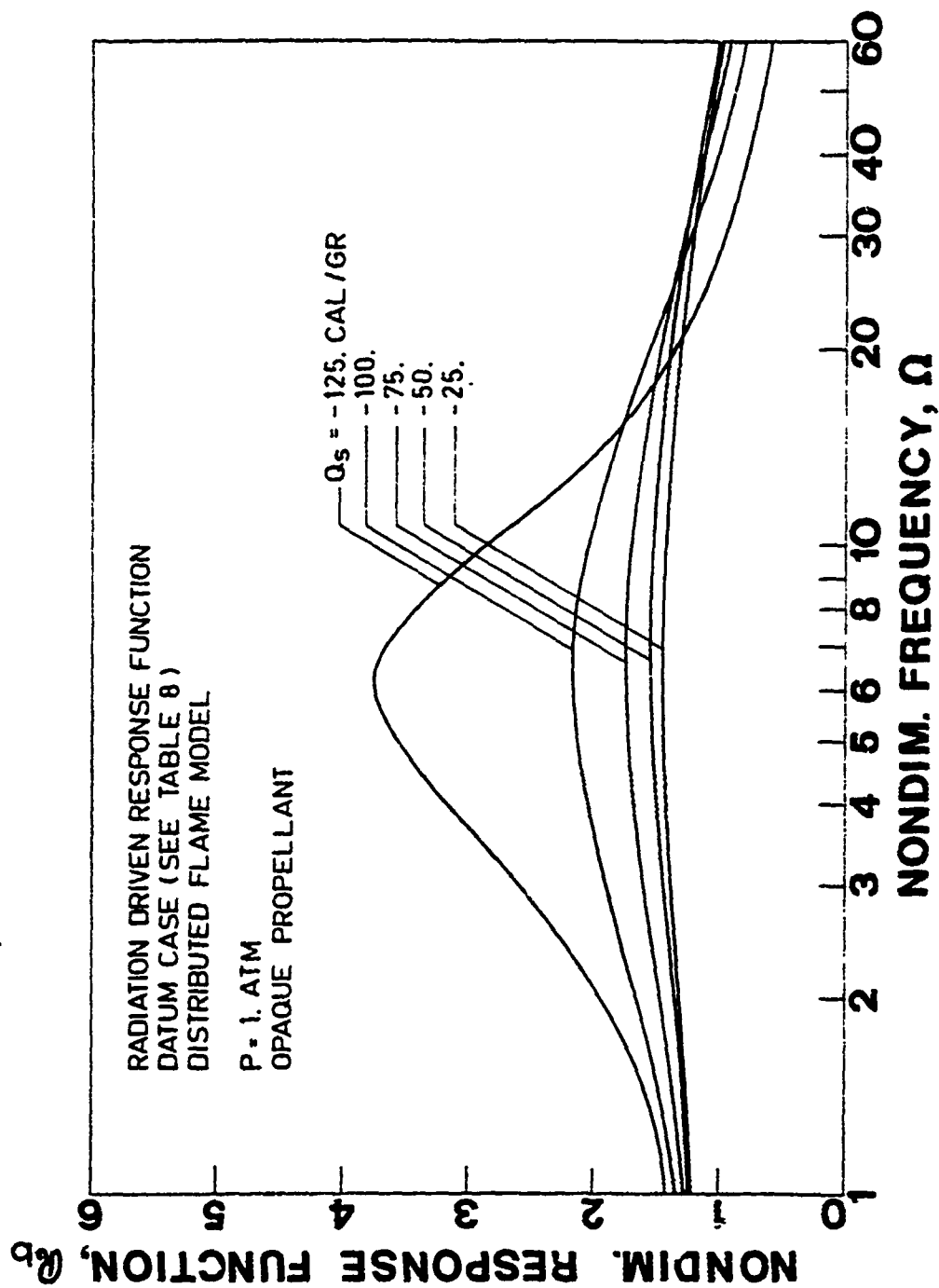


Fig. 30 Destabilizing effect of large surface energy release (distributed flame model).

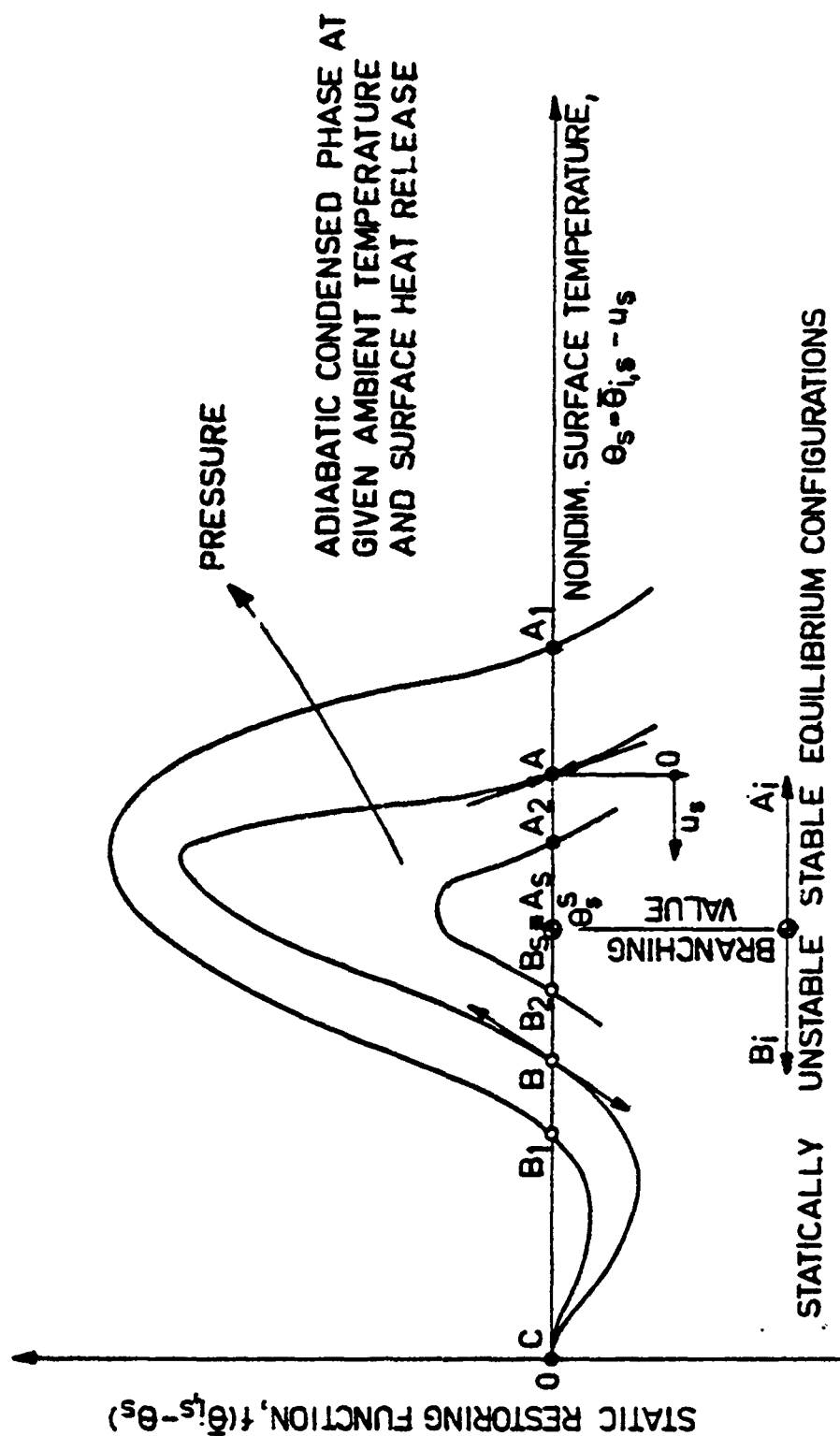


Fig. 31a Qualitative sketch of the nonlinear static restoring function, for different pressure values, illustrating the existence of three equilibrium configurations: A₁ and B₁ (for the reacting mode), C (for the unreacting mode). Roots B₁ are statically unstable.

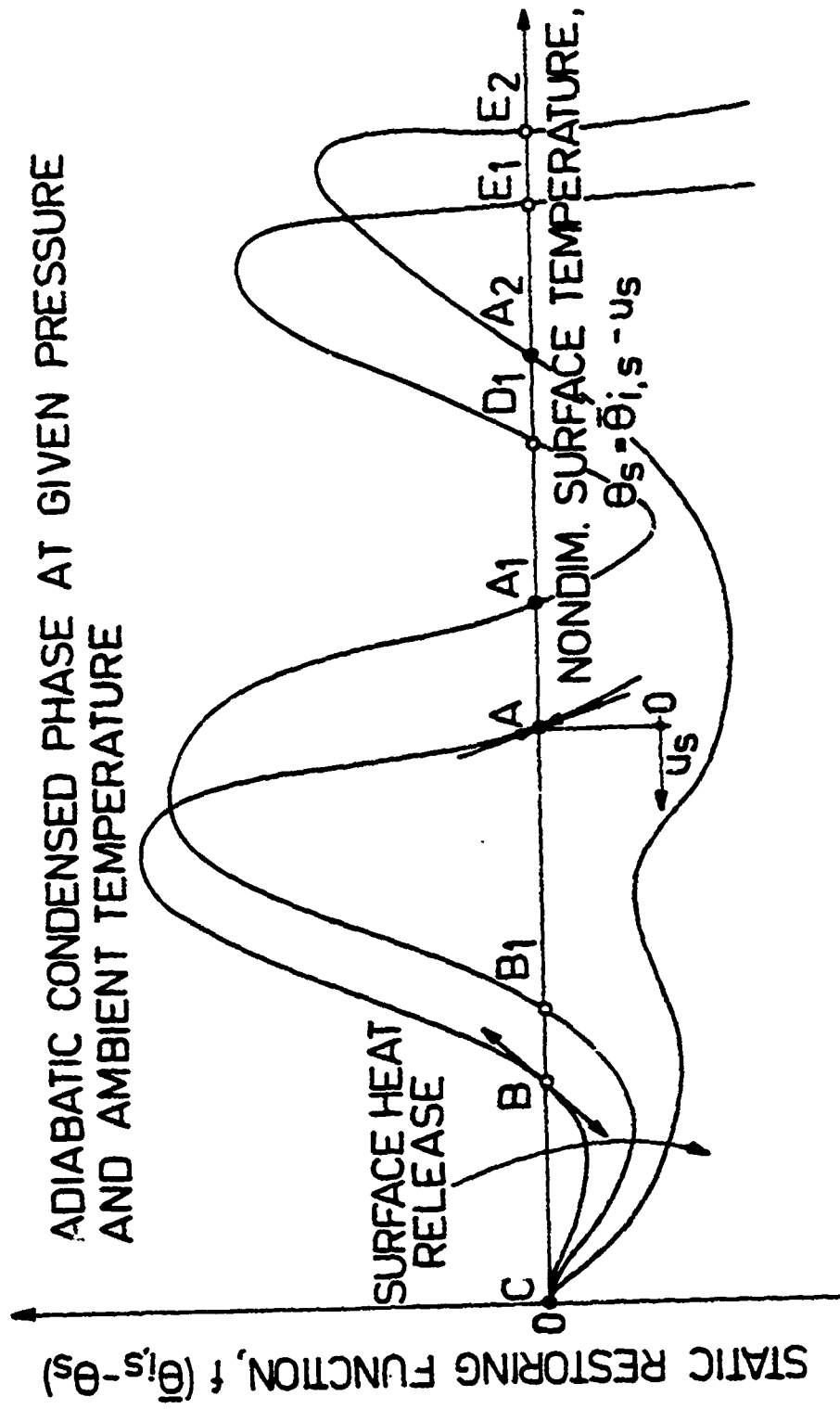


Fig. 31b Qualitative sketch of the nonlinear static restoring function, for increasing surface heat release values, illustrating the appearance of a second pair of roots, D and E, for the reacting mode (upper dynamic instability).

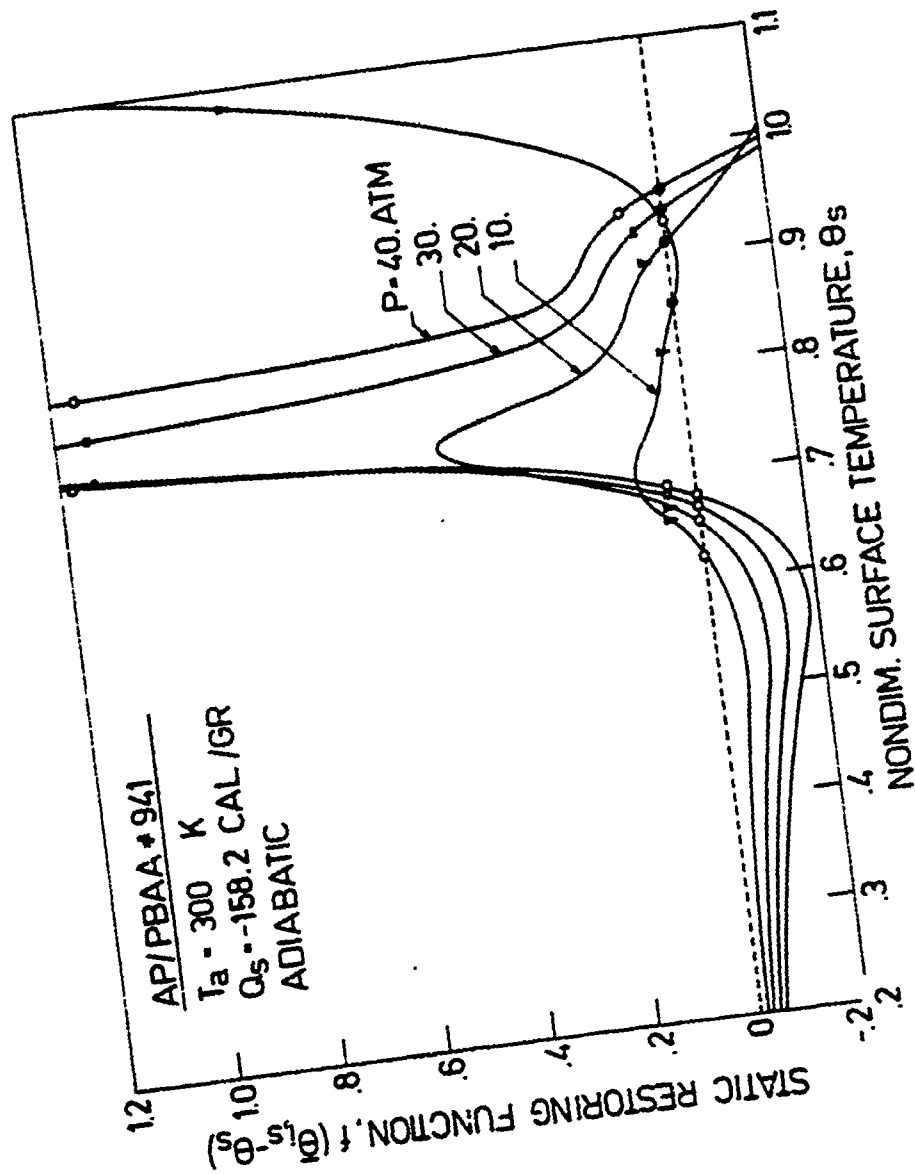


Fig. 32 Influence of pressure on nonlinear static restoring function for $Q_s = -158.2 \text{ cal/g}$ showing upper dynamic instability at $p = 10 \text{ atm}$.
 -181-

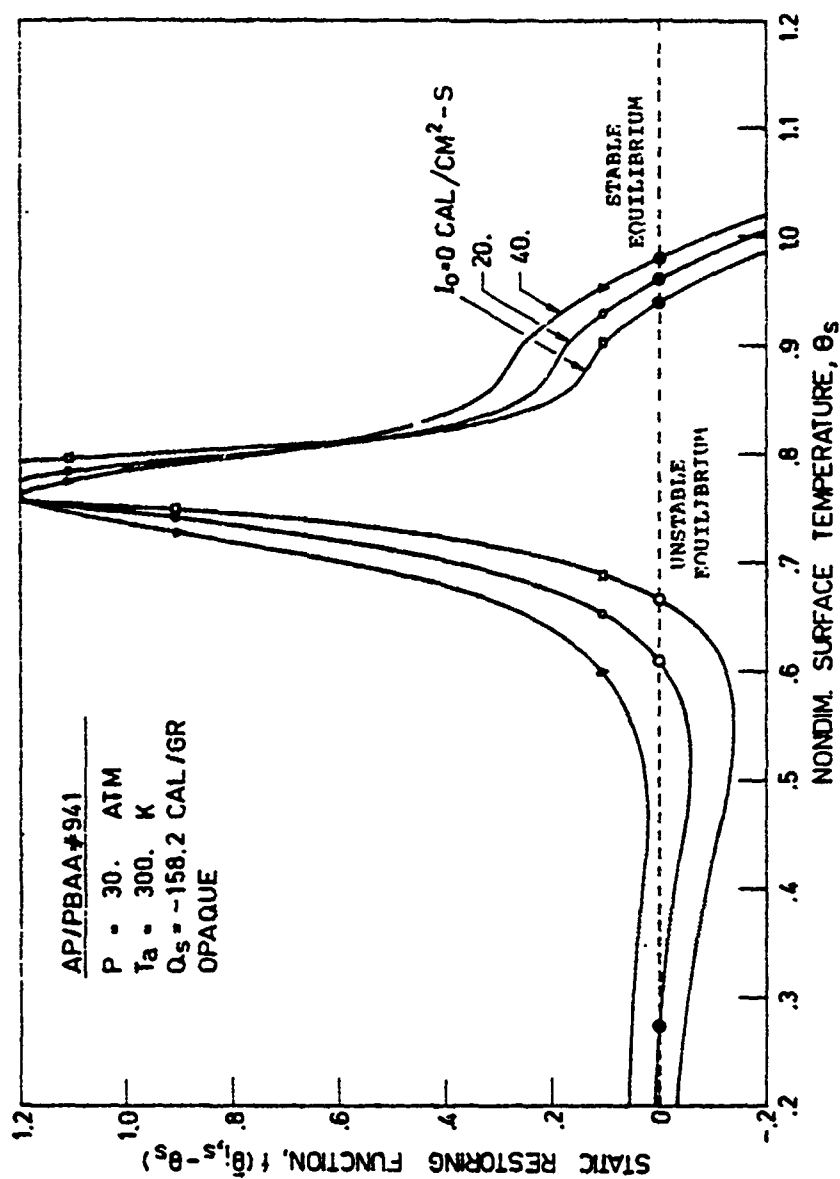


Fig. 33 Stabilizing effect of residual radiant flux intensity on lower dynamic stability boundary.

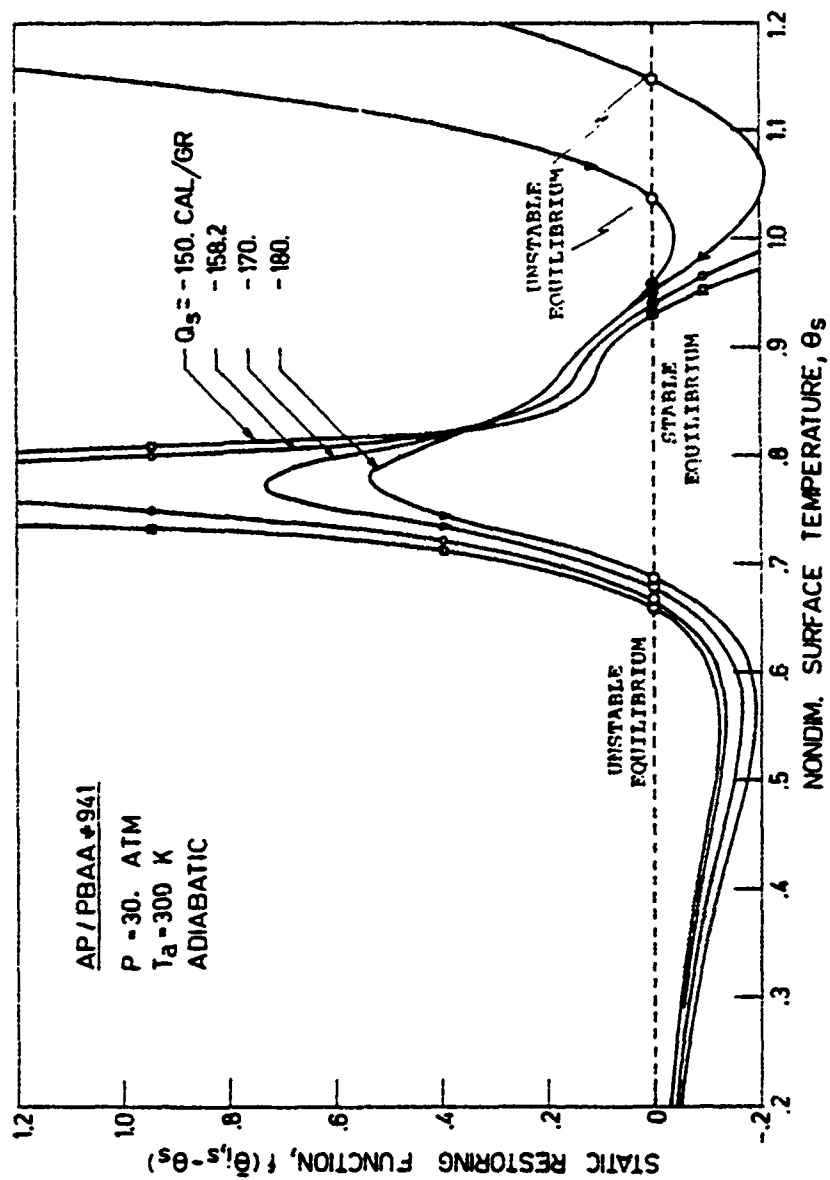


Fig. 34a Coalescence of A-D roots at $Q_s = -190$ cal/gr; the steady reacting mode is stationary for $|Q_s| < 190$ cal/gr and self-sustained oscillating for $|Q_s| > 190$ cal/gr. See Fig. 57.

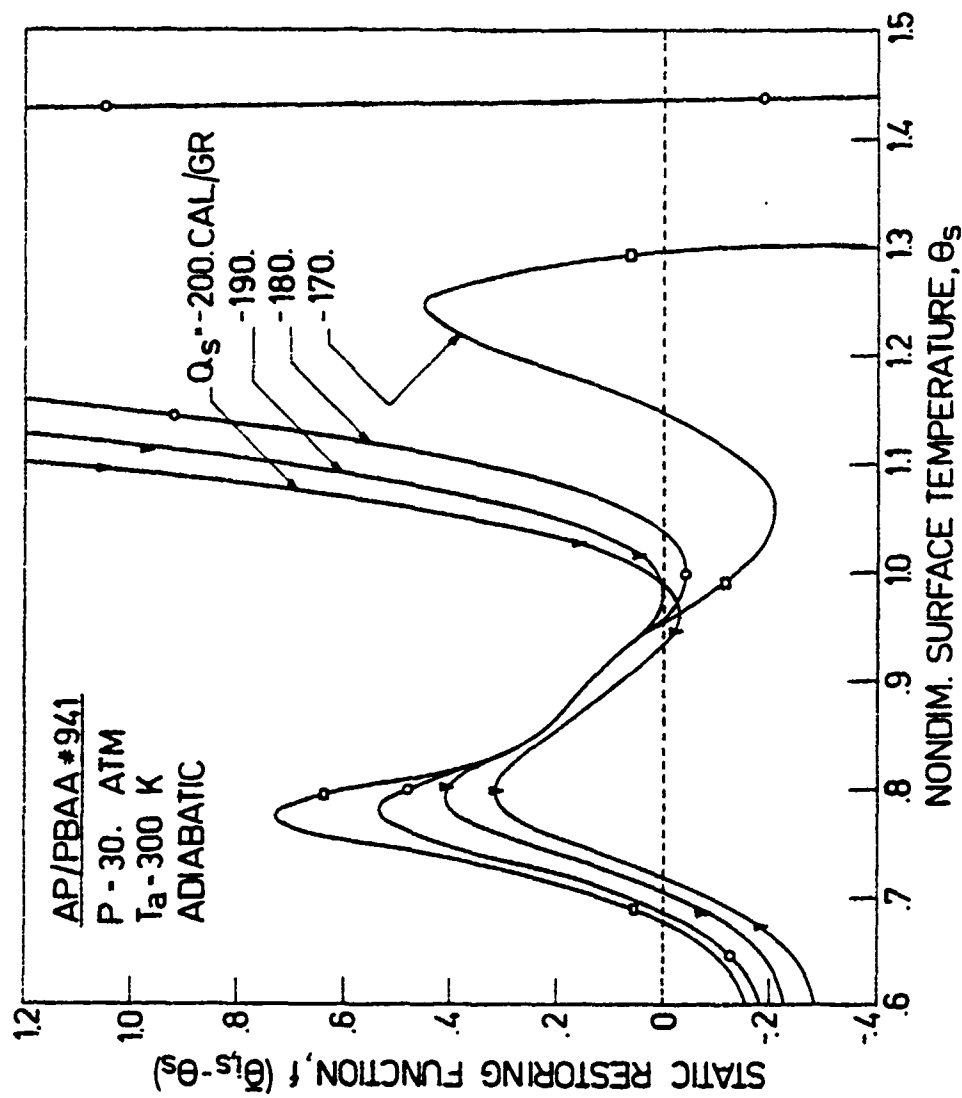


Fig. 34b Coalescence of λ -D roots at $Q_s = -190$ cal/g; the steady reacting mode is stationary for $|Q_s| < 190$ cal/g and self-sustained oscillating for $|Q_s| > 190$ cal/g. See Fig. 57.

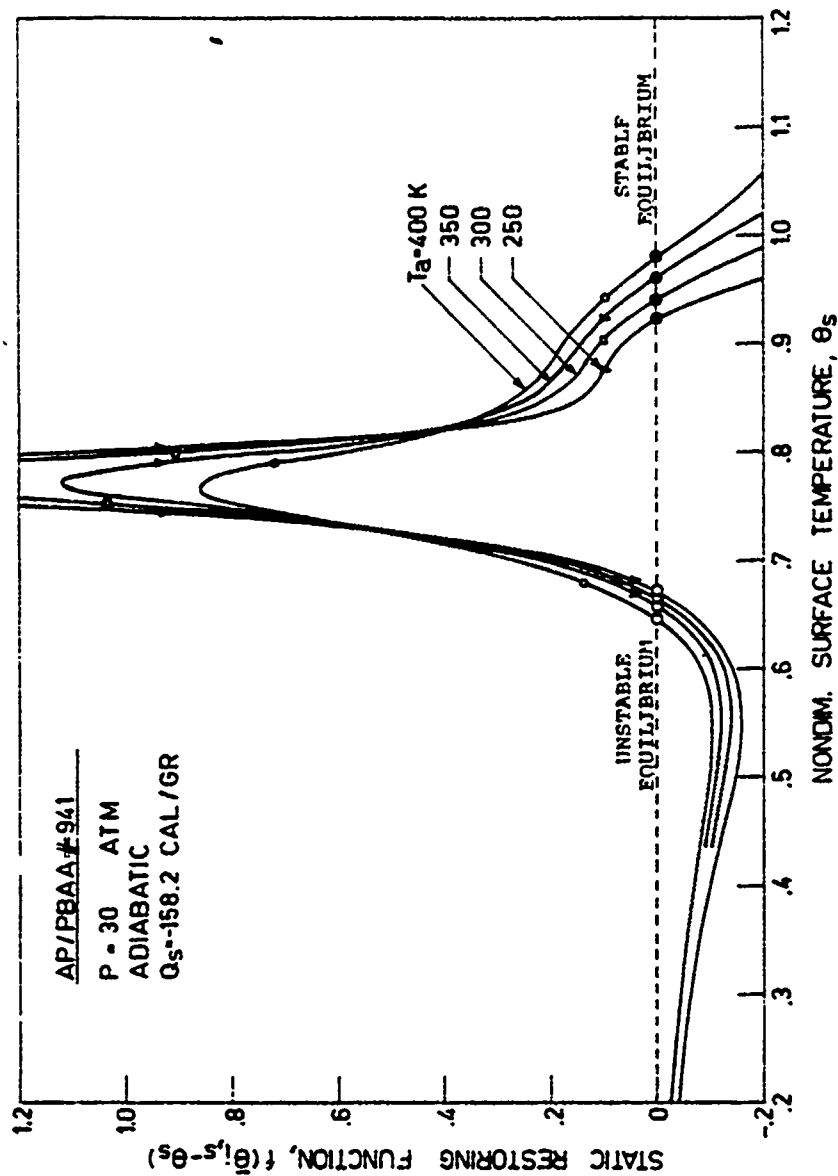


Fig. 35 Negligible influence of ambient temperature on non-linear static restoring function (for the indicated range of values).

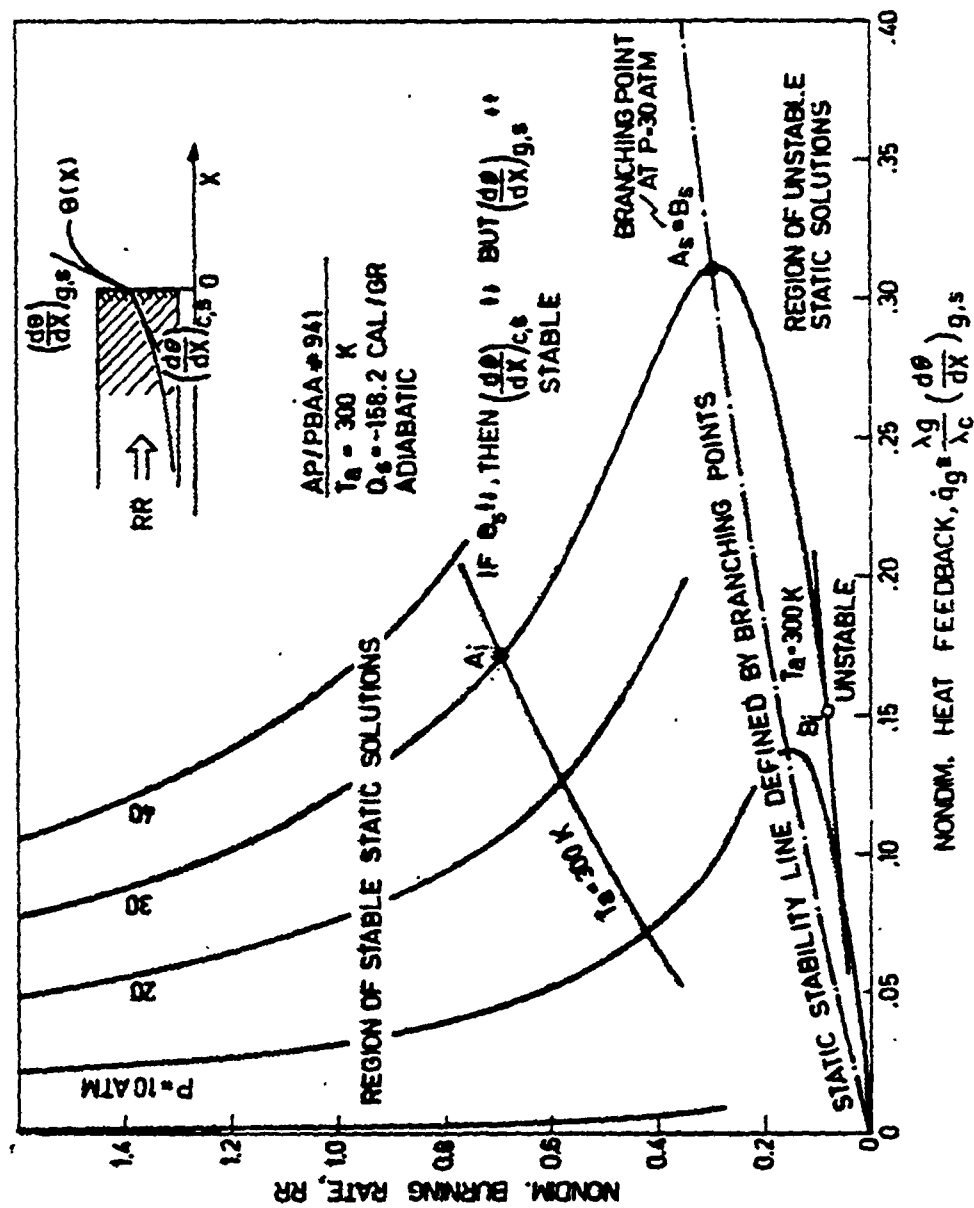


Fig. 36 Construction of the static stability line and its meaning.

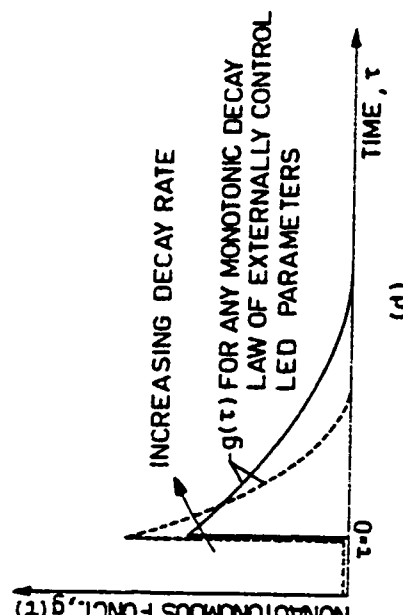
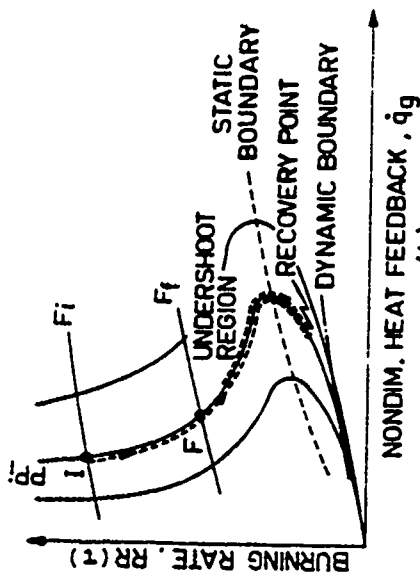
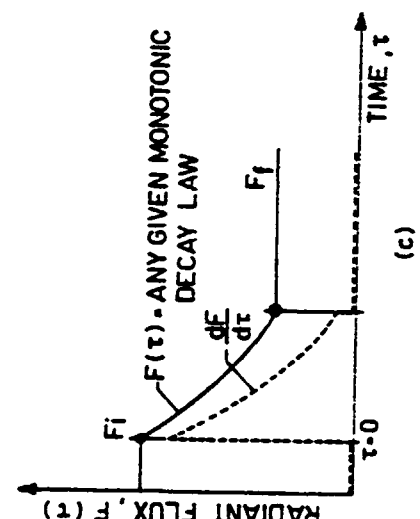
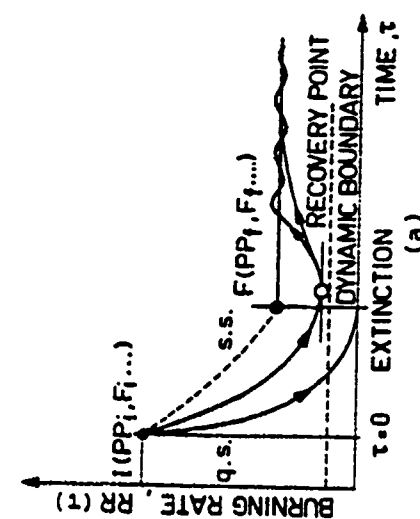


Fig. 37a Representative time histories of burning rate during deradiation showing possible occurrence of dynamic extinction.
 Fig. 37b Corresponding trajectories in burning rate vs heat feedback plane.
 Fig. 37c Nomenclature used for deradiation transients.
 Fig. 37d Nature of nonautonomous function considered in this study.

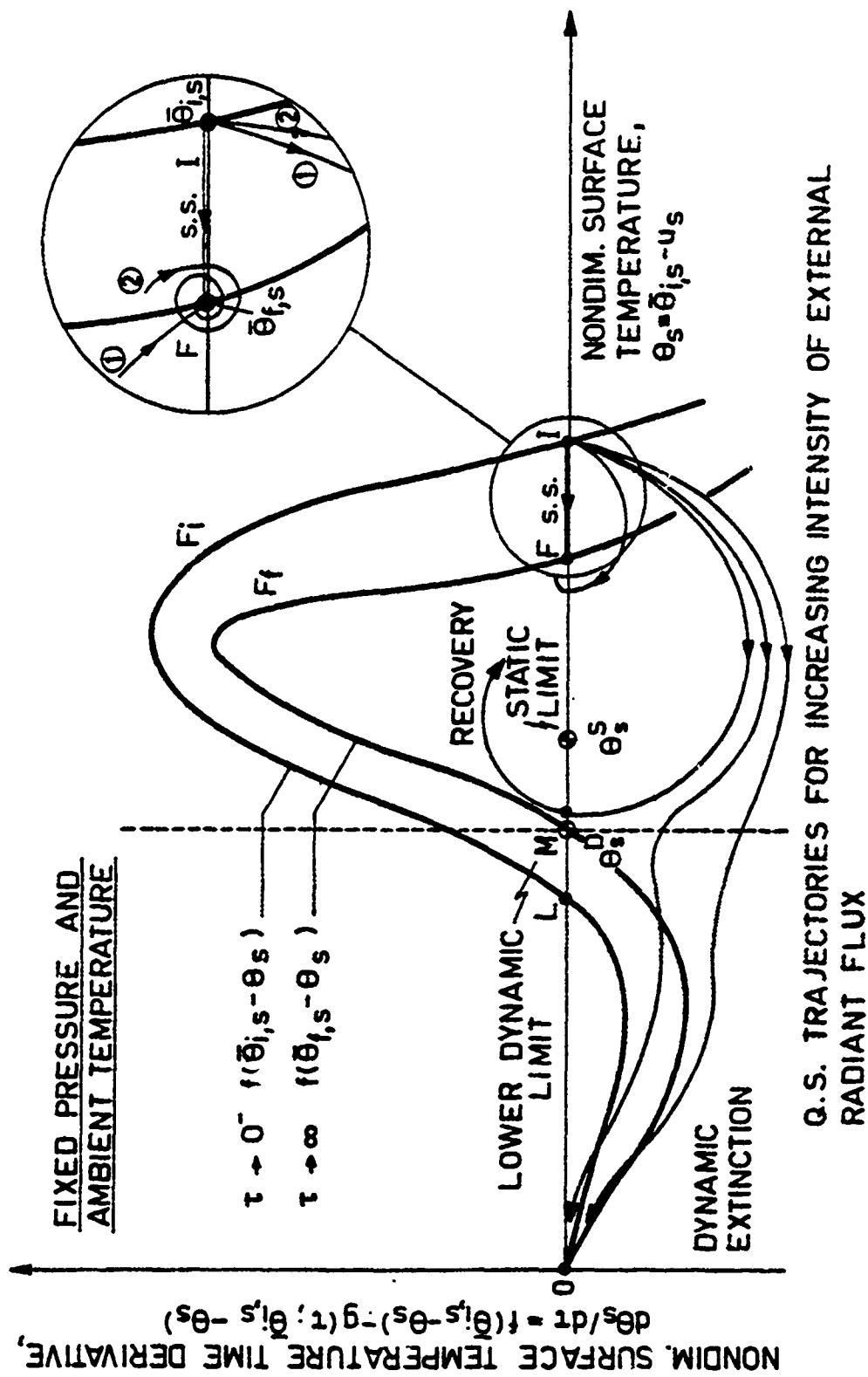


Fig. 38 The range of possible unstable equilibrium points in dynamic burning regime is limited by the no-return point M (the unstable root associated to the static restoring function for $\tau \rightarrow \infty$).

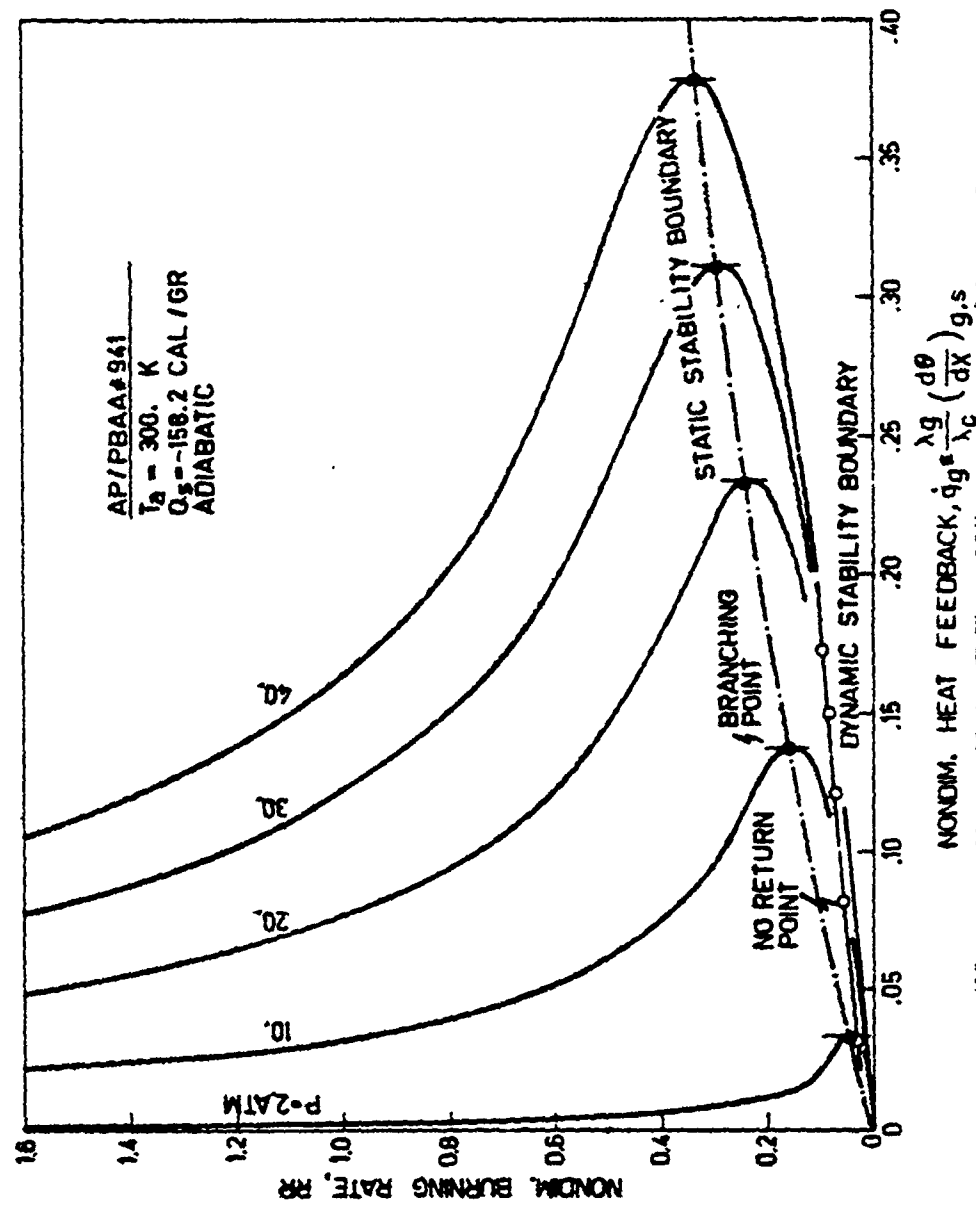
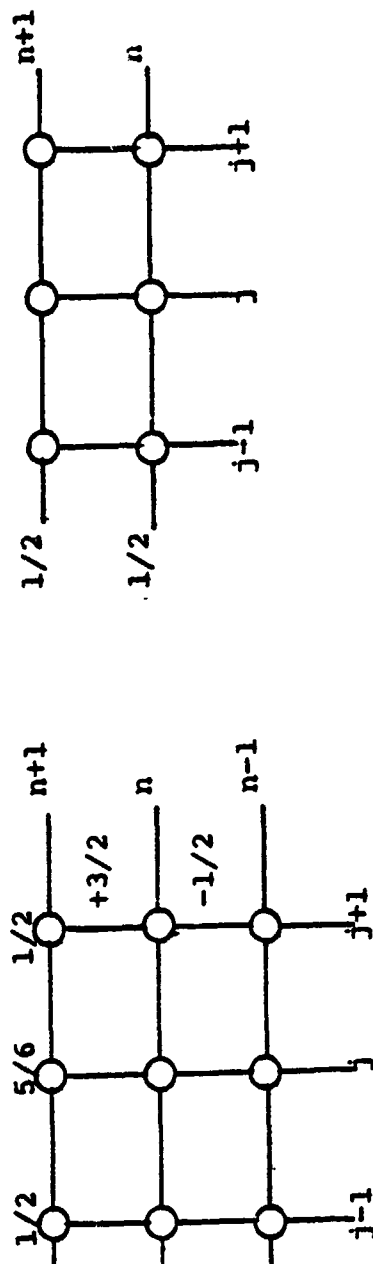


Fig. 39 Lower dynamic stability boundary on a burning rate vs heat feedback plane showing a sensible increase of burning region as compared with static burning regime. -189-

TIME VECTOR, $t = (n-1) \cdot \Delta t$



scheme # 13 from Ref. 16

scheme # 2 from Ref. 16
Crank-Nicholson

SPACE VECTOR, $x = (j-1) \cdot \Delta x$

Implicit, always stable (see §9.1)
error = $O[(\Delta t)^2] + O[(\Delta x)^4]$

Implicit, always stable (see §9.1)
error = $O[(\Delta t)^2] + O[(\Delta x)^2]$

FIG. 40 Numerical molecules used in the computer solution.

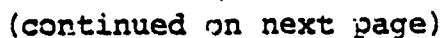
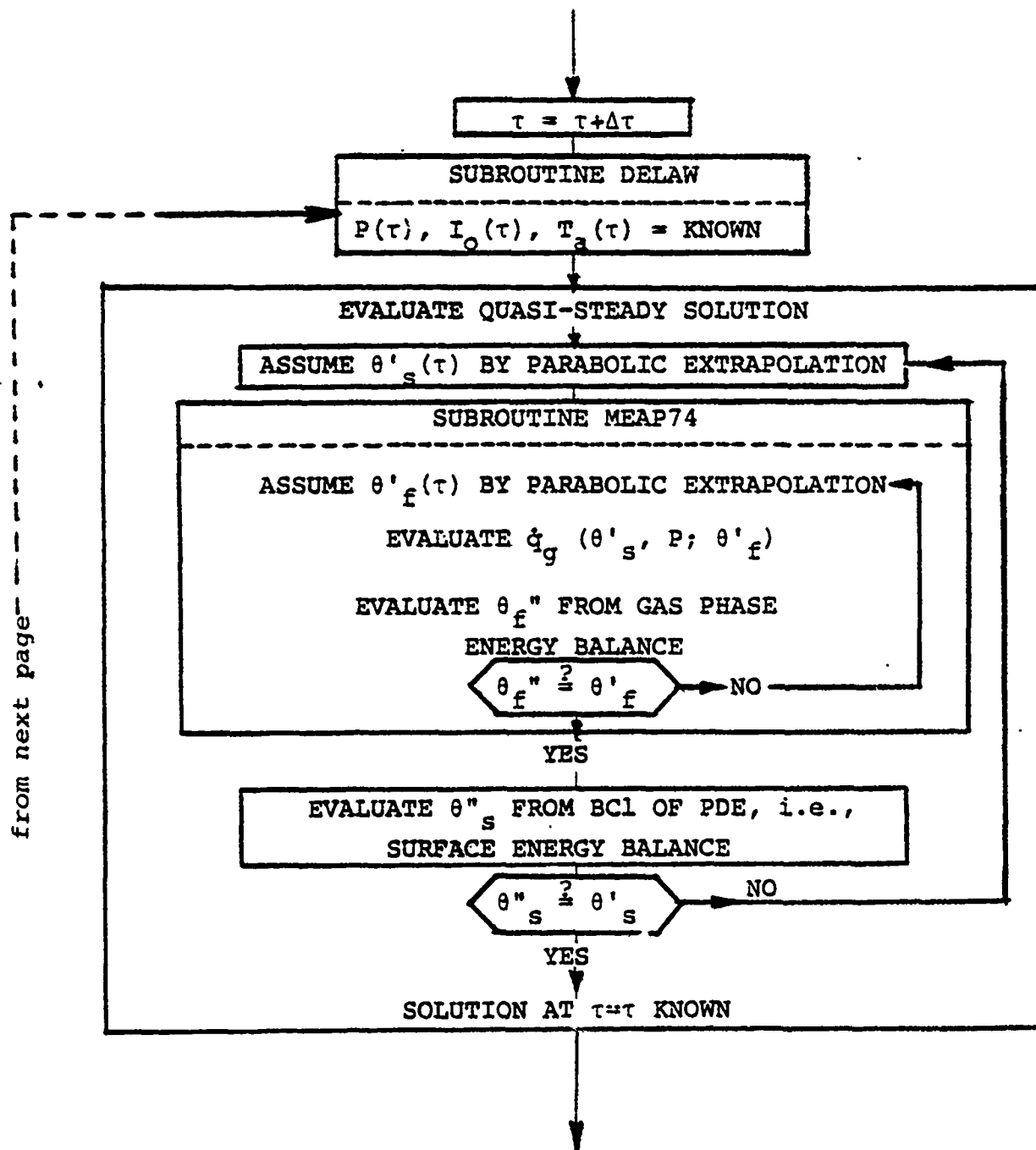


Fig. 41

(continued from previous page)



(continued on next page)

Fig. 41 (continued)

(continued from previous page)

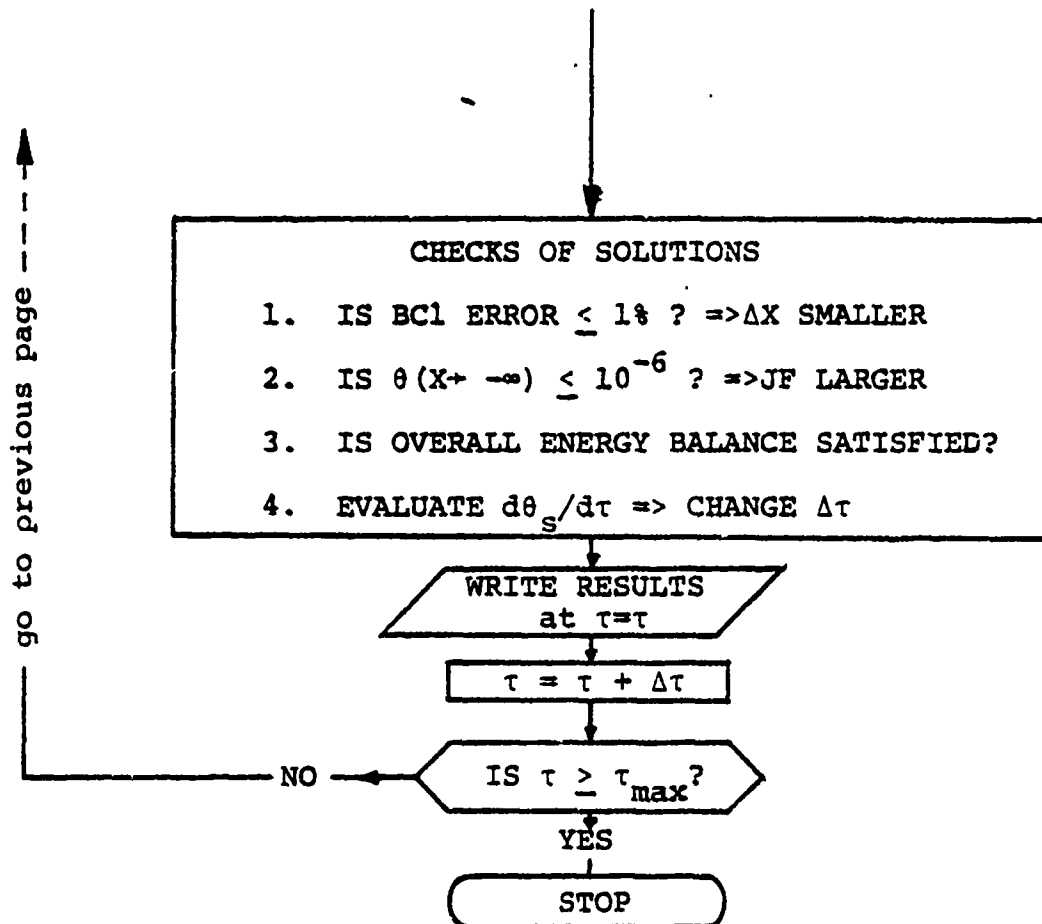


Fig. 41 (completed)

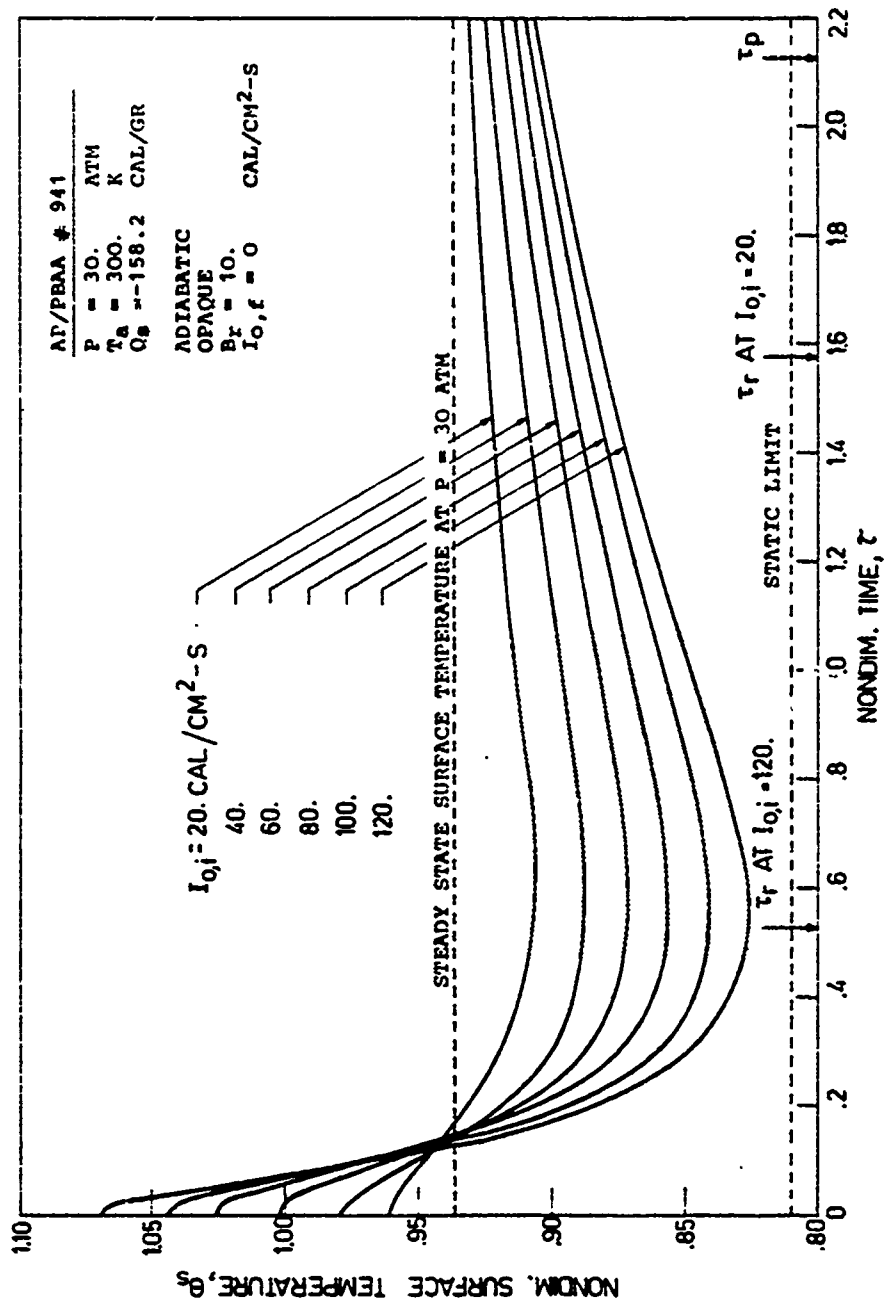


Fig. 42 Destabilizing effect of large initial radiant flux intensity on dynamic burning rate. (Cf. Fig. 46).

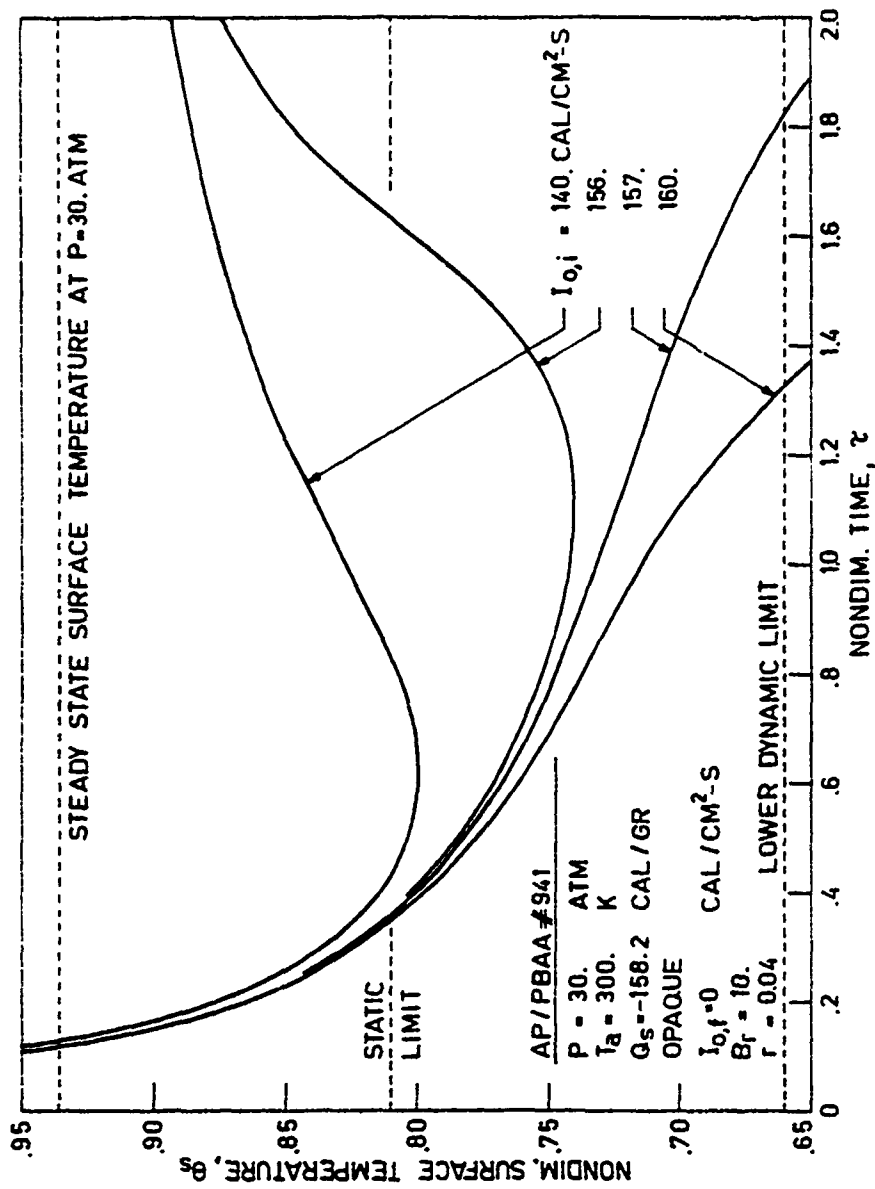


Fig. 43 Occurrence of dynamic extinction following fast deradiation. -195-

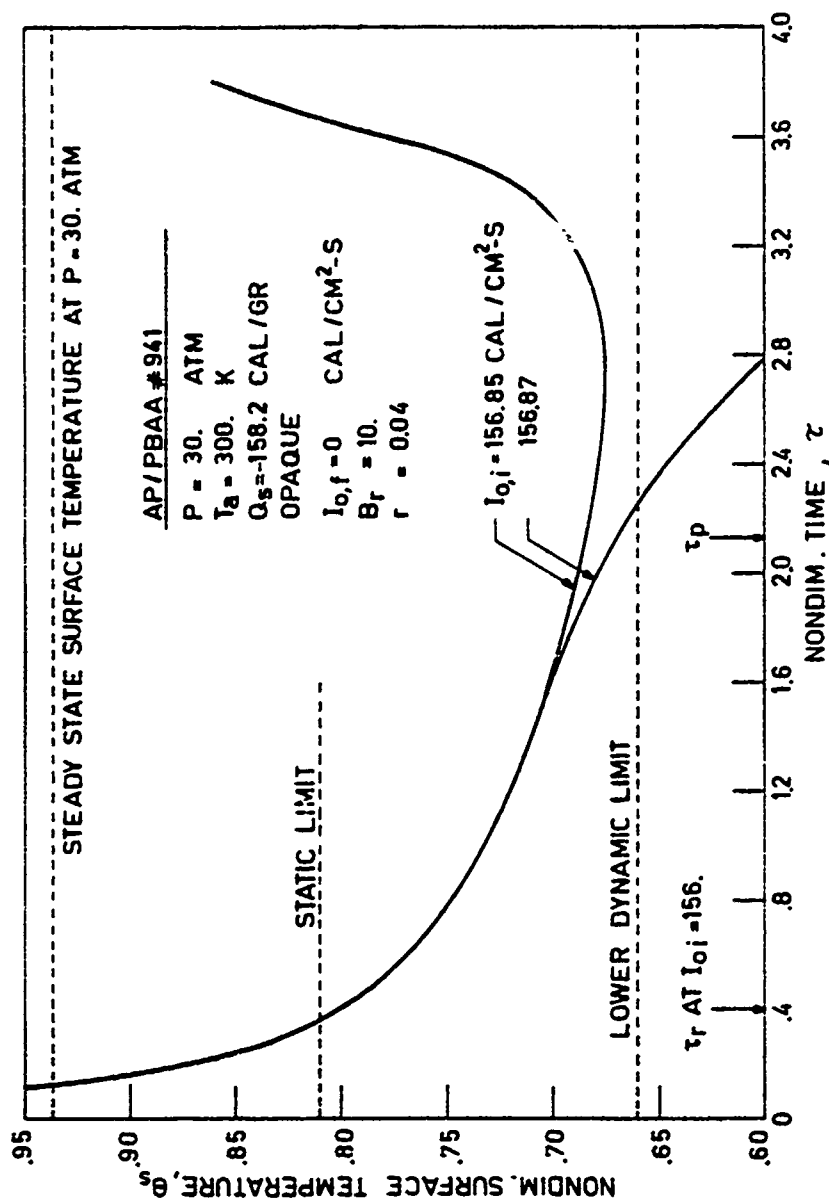


Fig. 44 Sensitivity of the burning propellant to the initial conditions in the region near the lower dynamic stability.

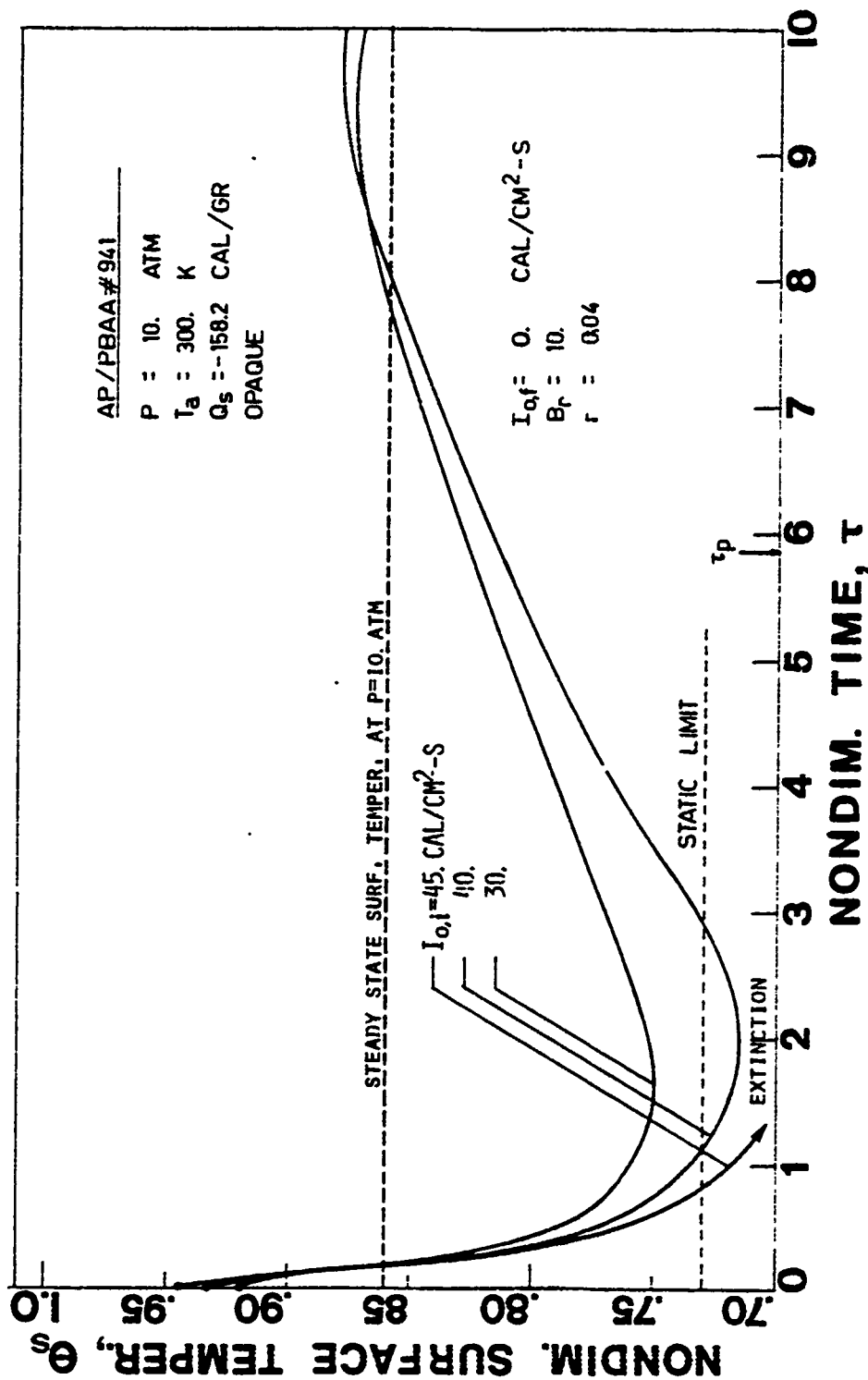


Fig. 45 Occurrence of damped oscillations in the dynamic burning rate following fast deradiation. (Cf. Fig. 47).

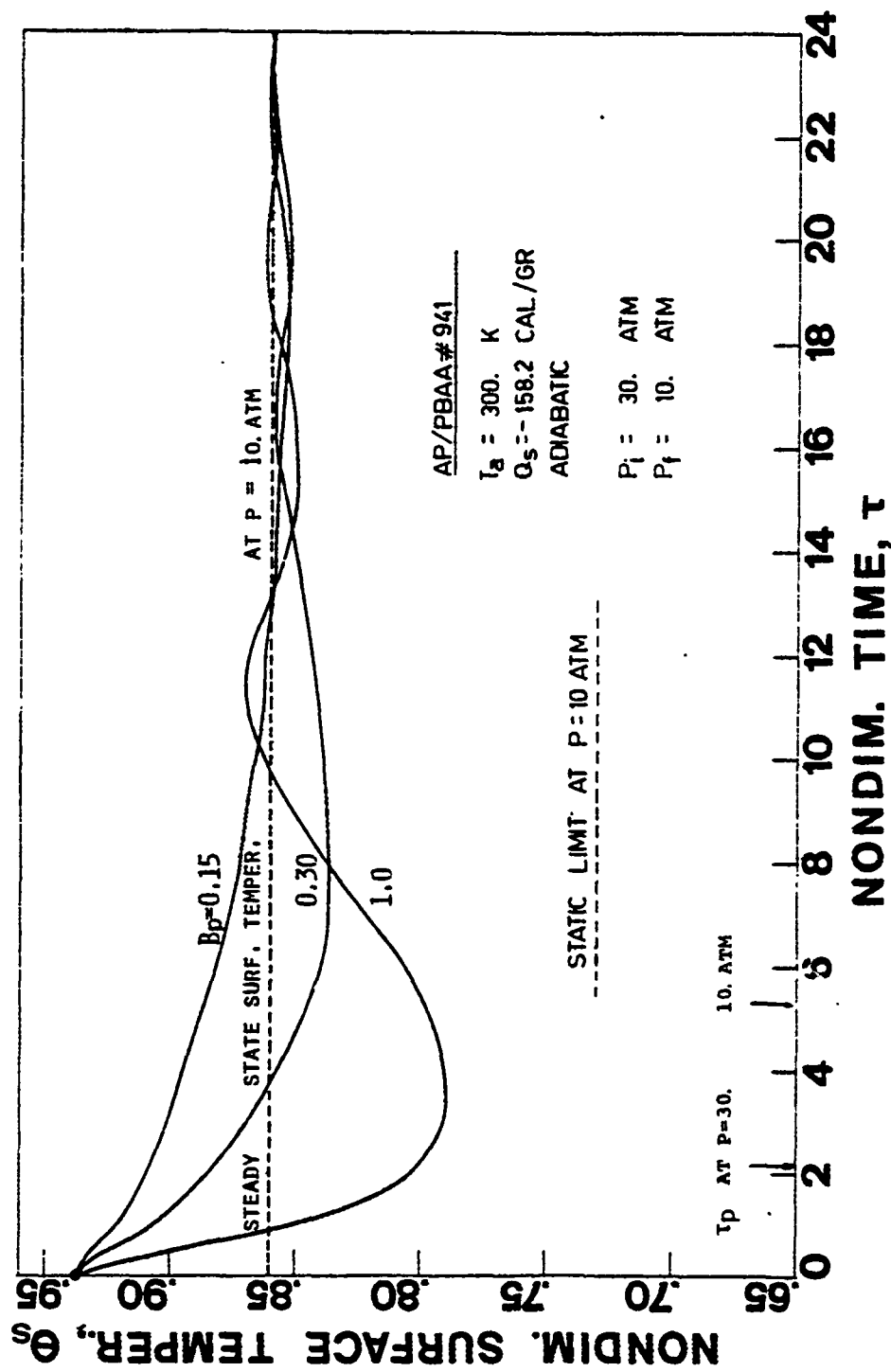


Fig. 46 Destabilizing effect of large depressurization rate on dynamic burning rate. (Cf. Fig. 42).

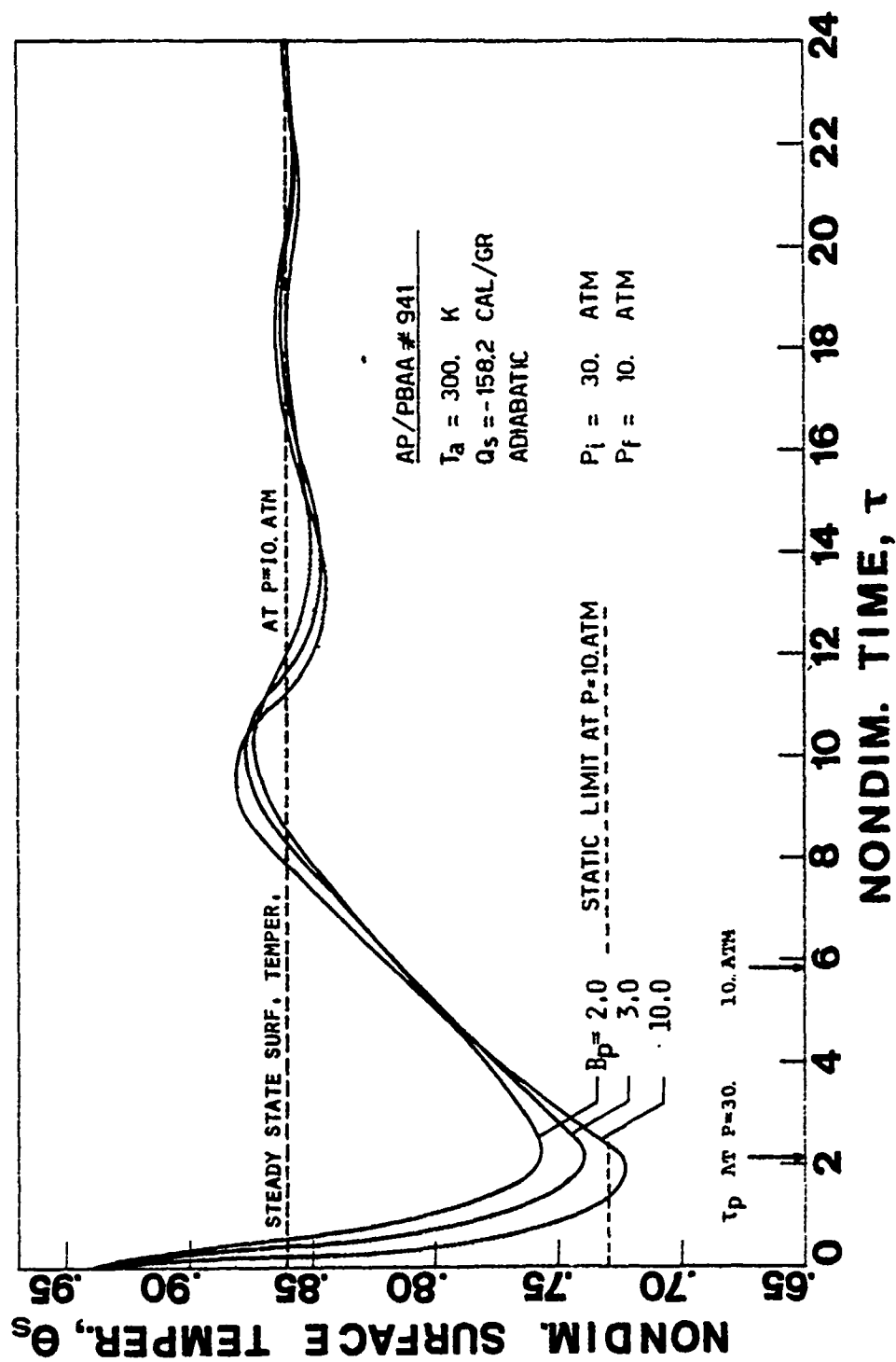


Fig. 47 Occurrence of damped oscillations in the dynamic burning rate following fast depressurization. (Cf. Fig. 45).

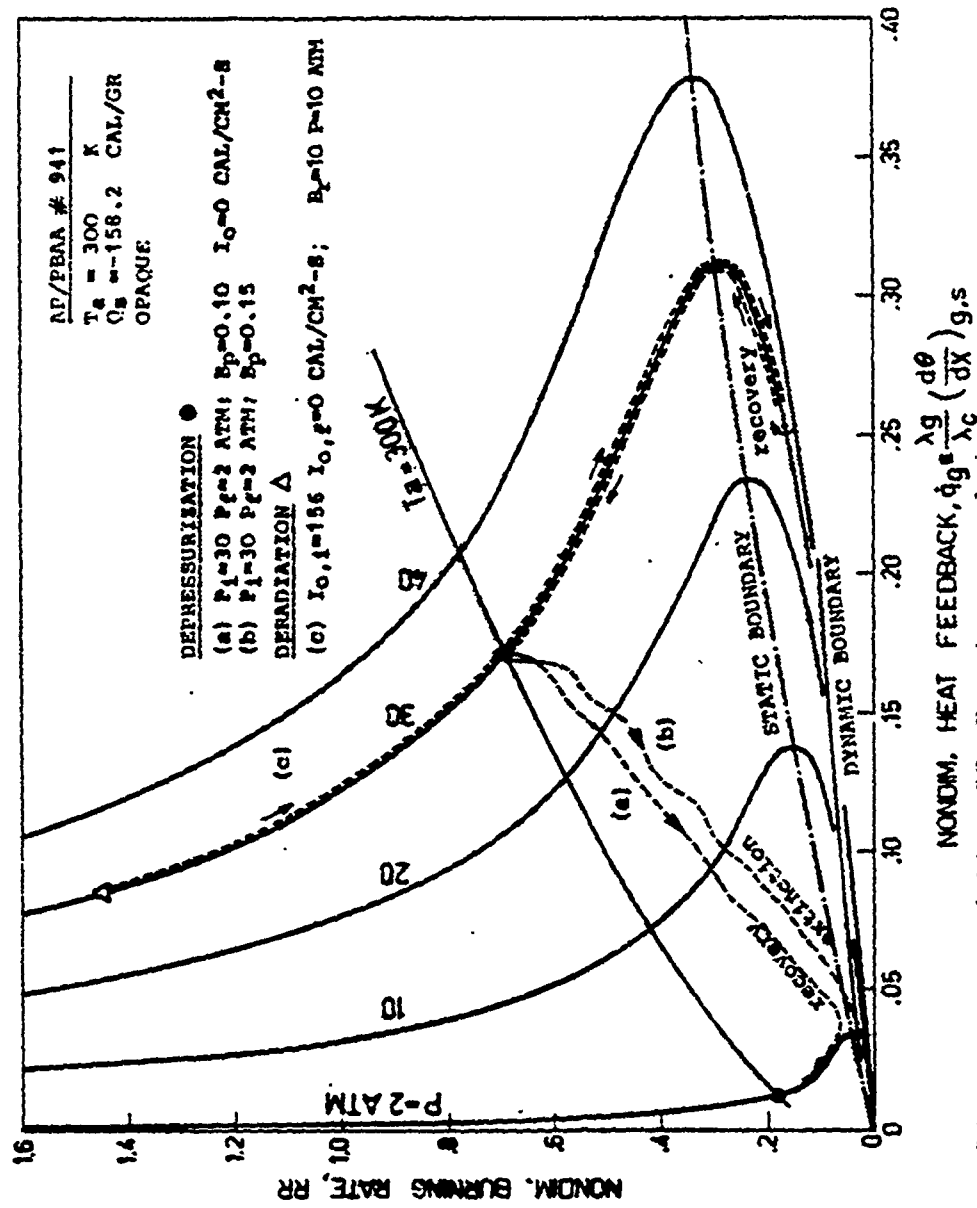


Fig. 48 Trajectories in the burning rate vs heat feedback (or MTS) plane showing that deradiation and depressurization transients follow different paths.

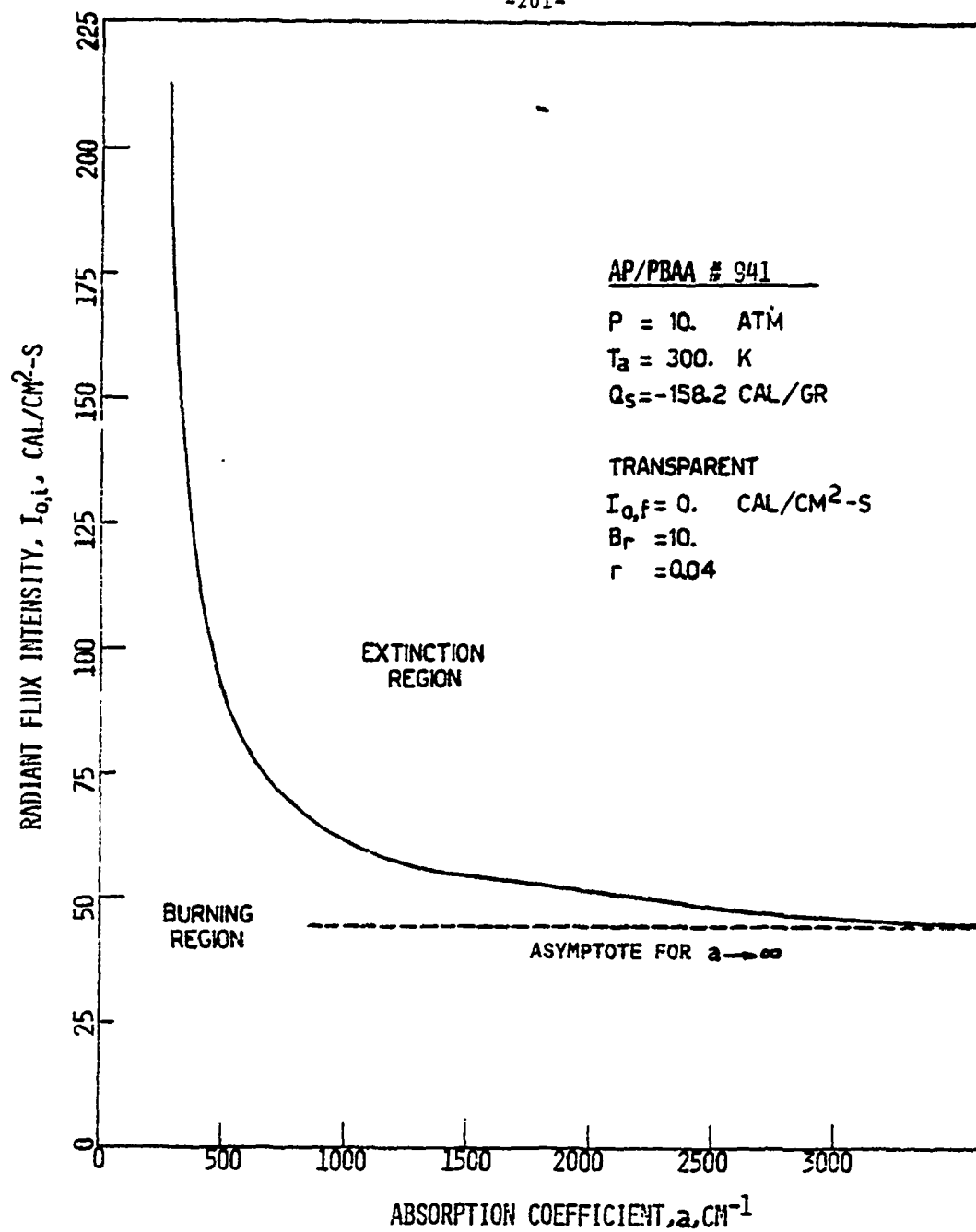


Fig. 49 Radiation penetration making more difficult dynamic extinction due to fast deradiation.

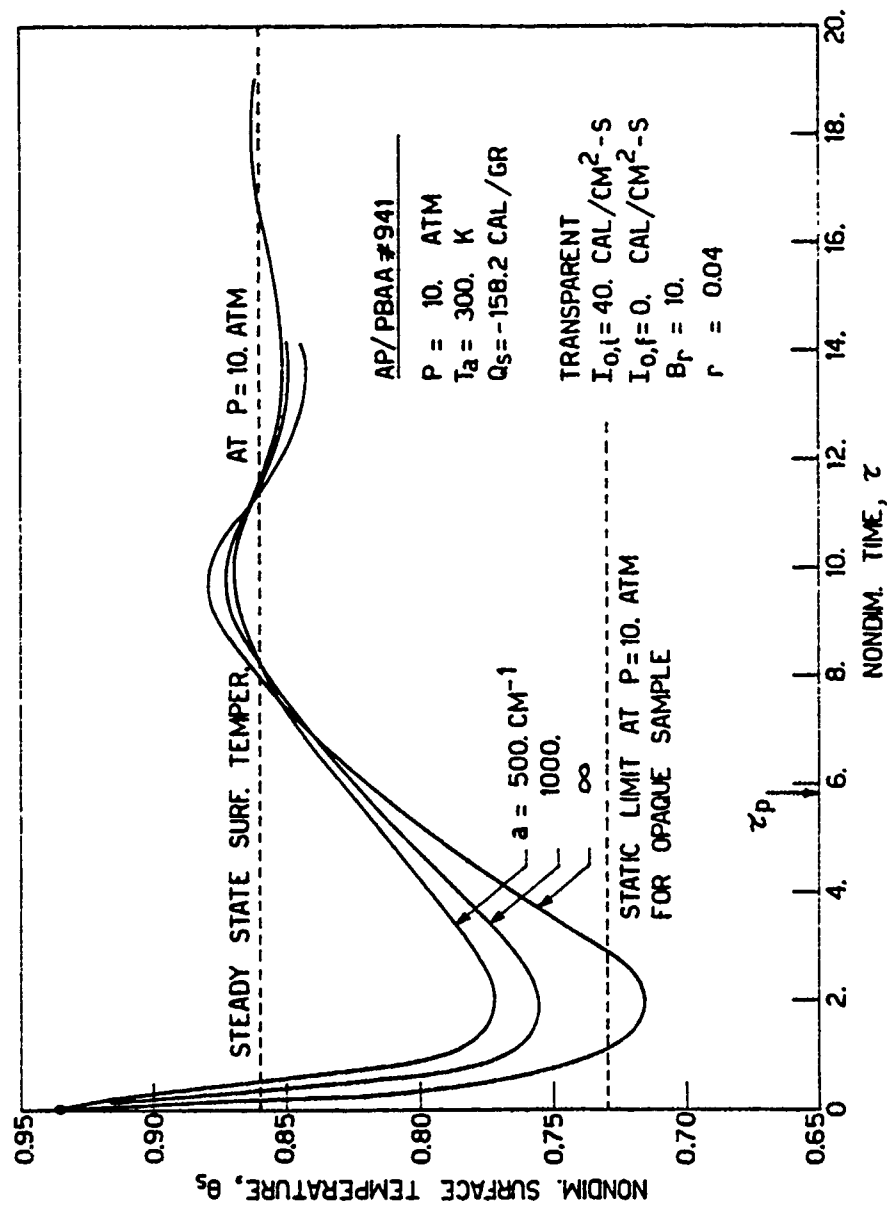


Fig. 50 Radiation penetration decreasing the intensity of the undershoot following fast deradiation.

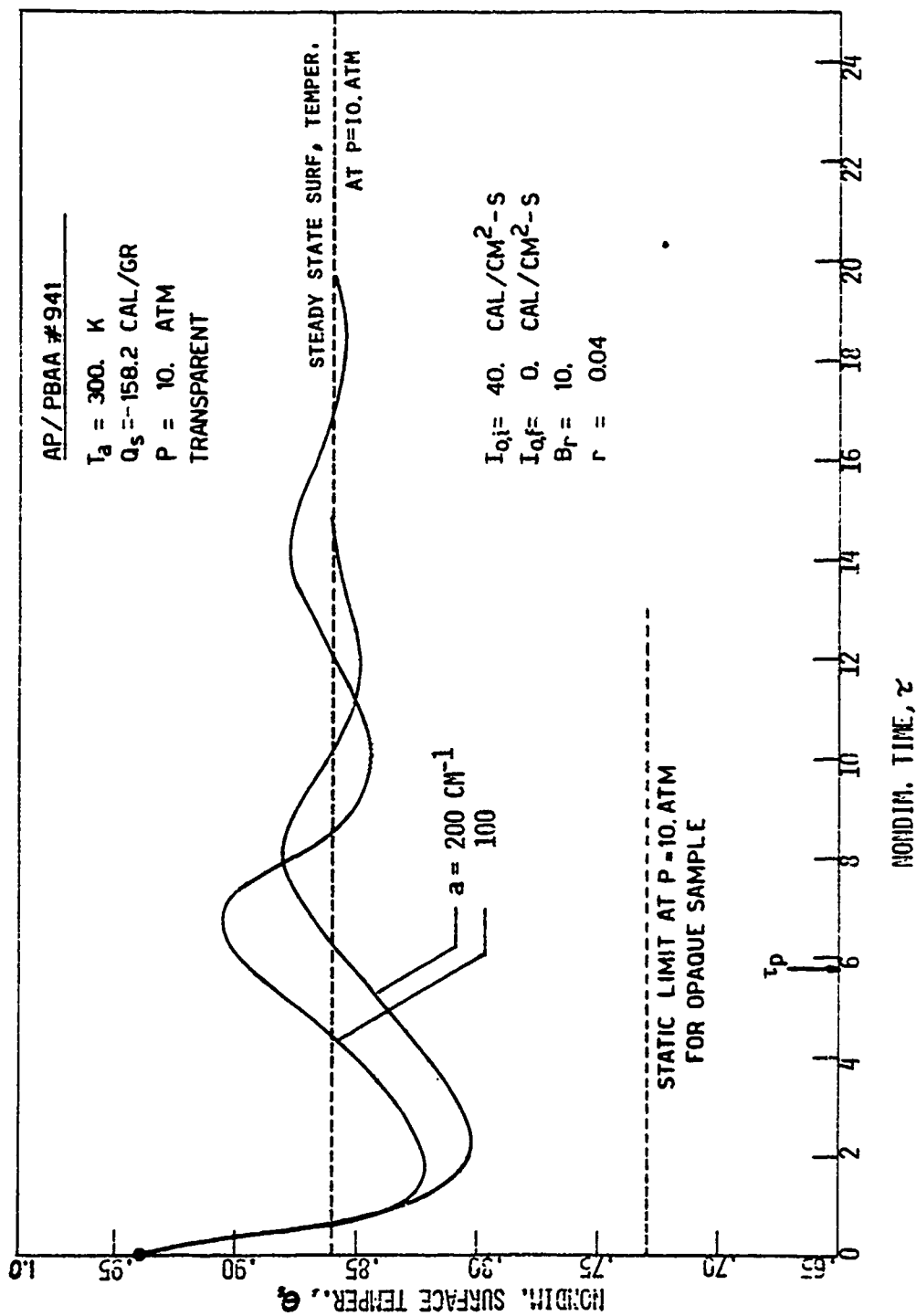


Fig. 51 Radiation penetration favoring damped oscillations
 of the dynamic burning rate following fast deradation.

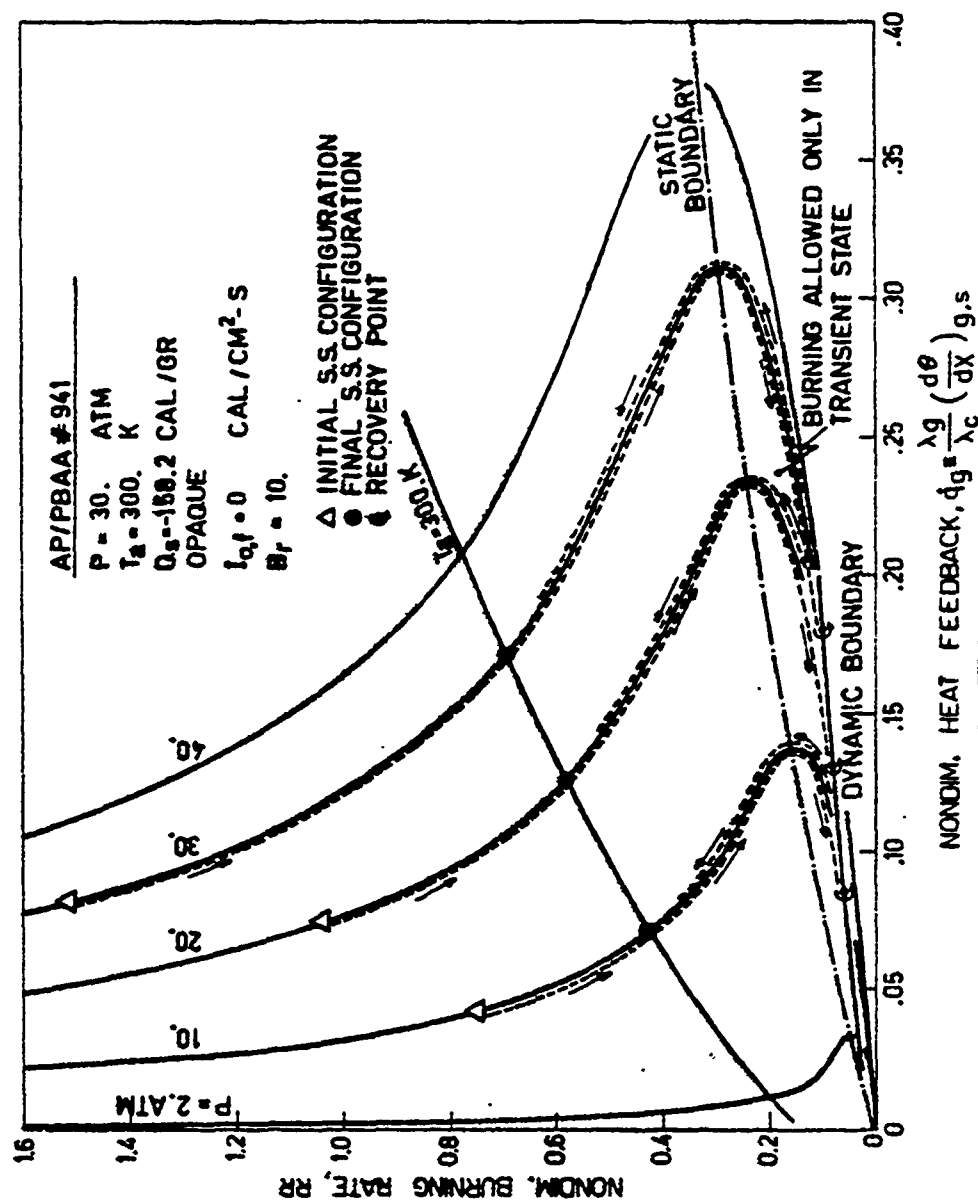


Fig. 52. Go/no-go computer simulated deradation tests showing very good agreement with the predicted lower dynamic stability boundary in the MTS plane.

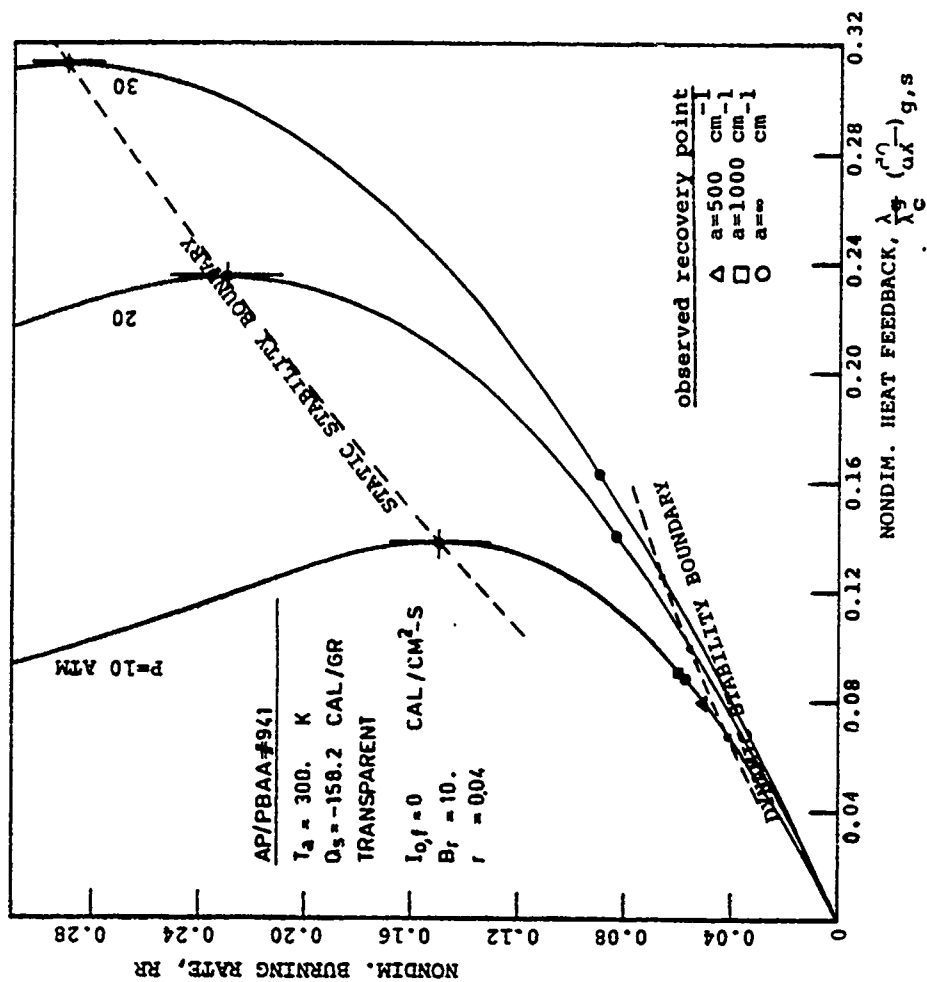


Fig. 53 Go/no-go computer simulated deradiation tests in the MTS plane showing that radiation penetration does not affect the lower dynamic stability boundary. See also Table 13 and Fig. 52.

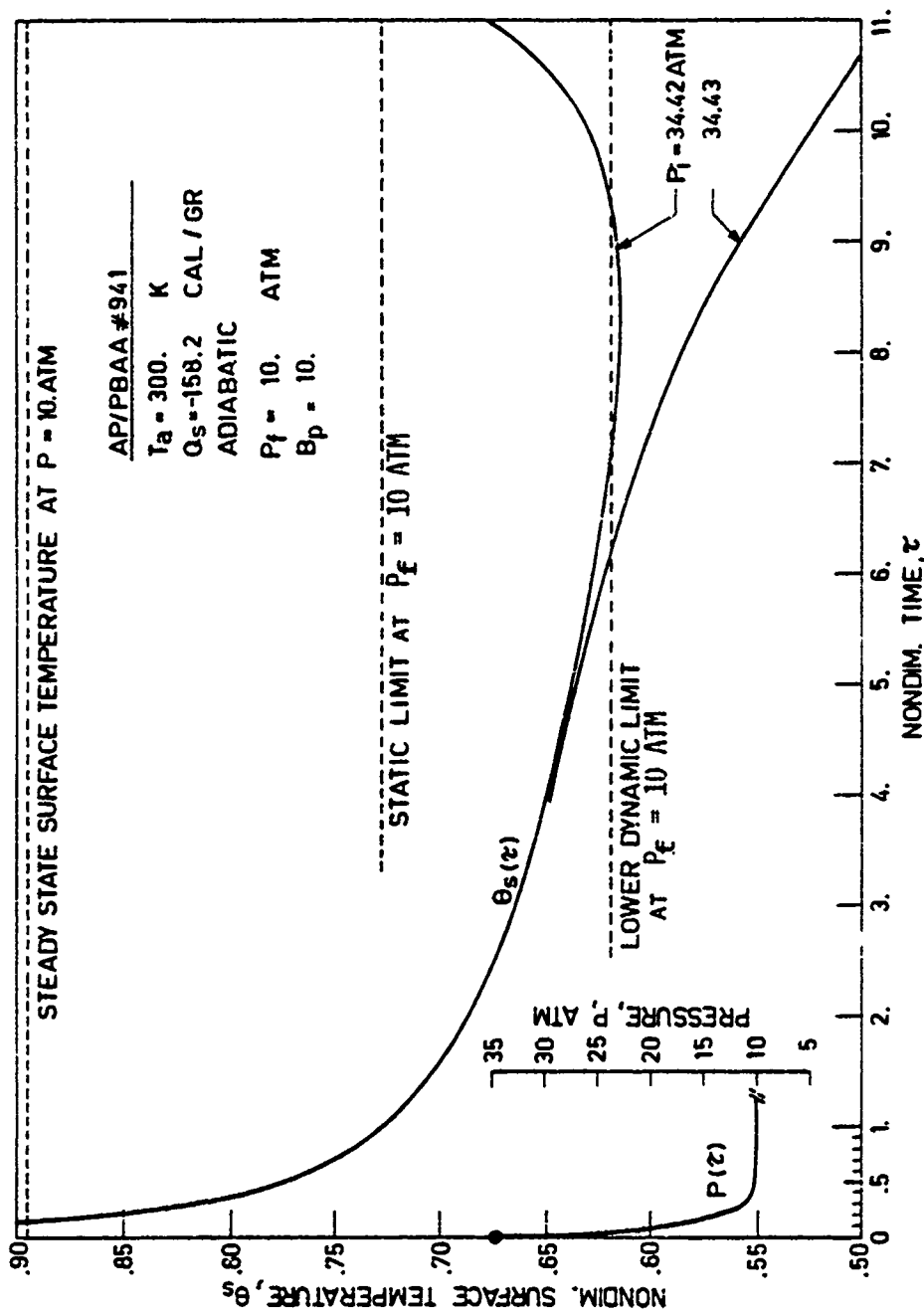


Fig. 54 Go/no-go computer simulated depressurization tests showing very good agreement with the predicted lower dynamic stability boundary. See also Table 13.

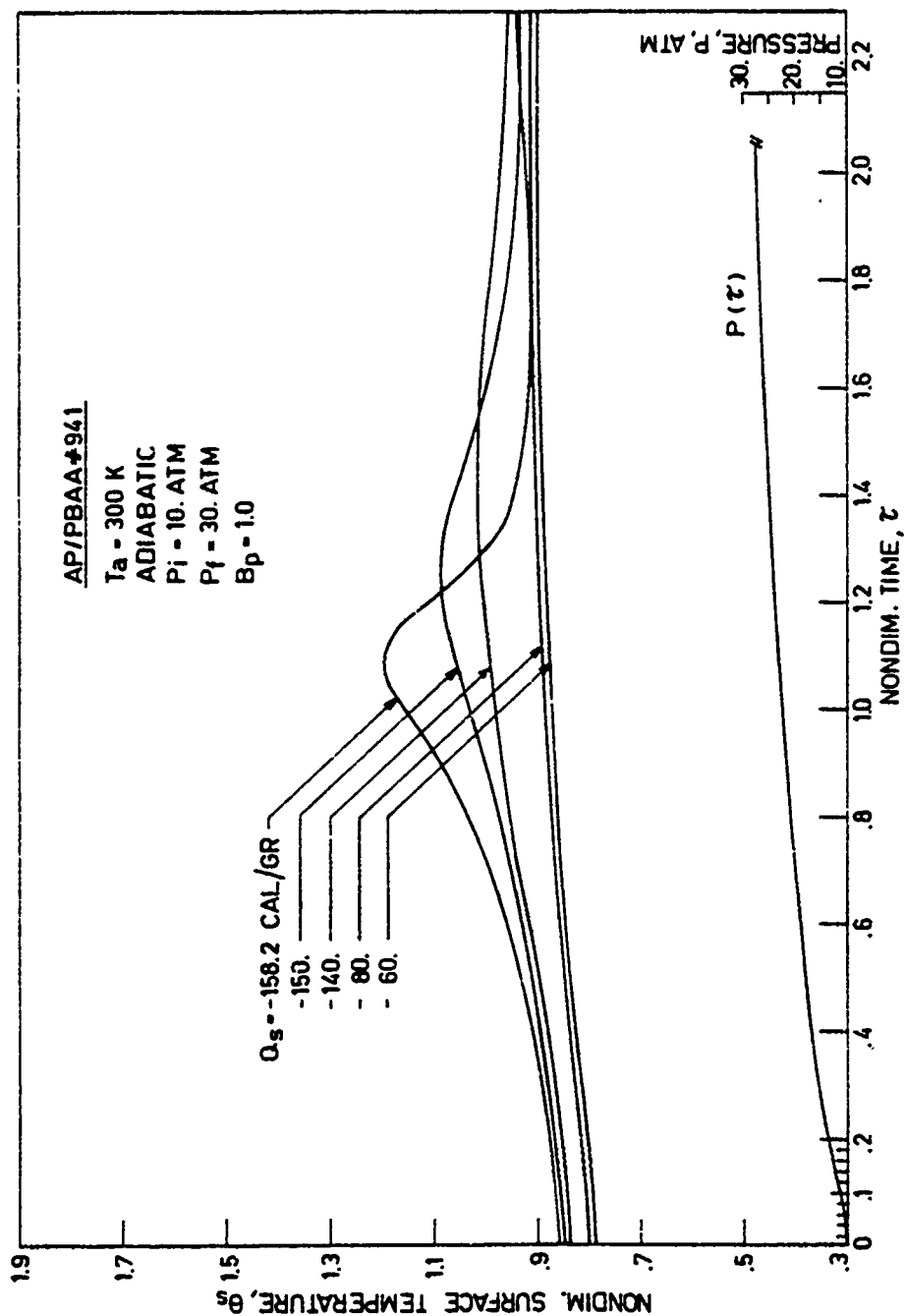


Fig. 55 Computer simulated pressurization tests showing no upper dynamic instability for $|Q_s| < 170\text{ cal/g}$. Cf. Tables 10 and 11.

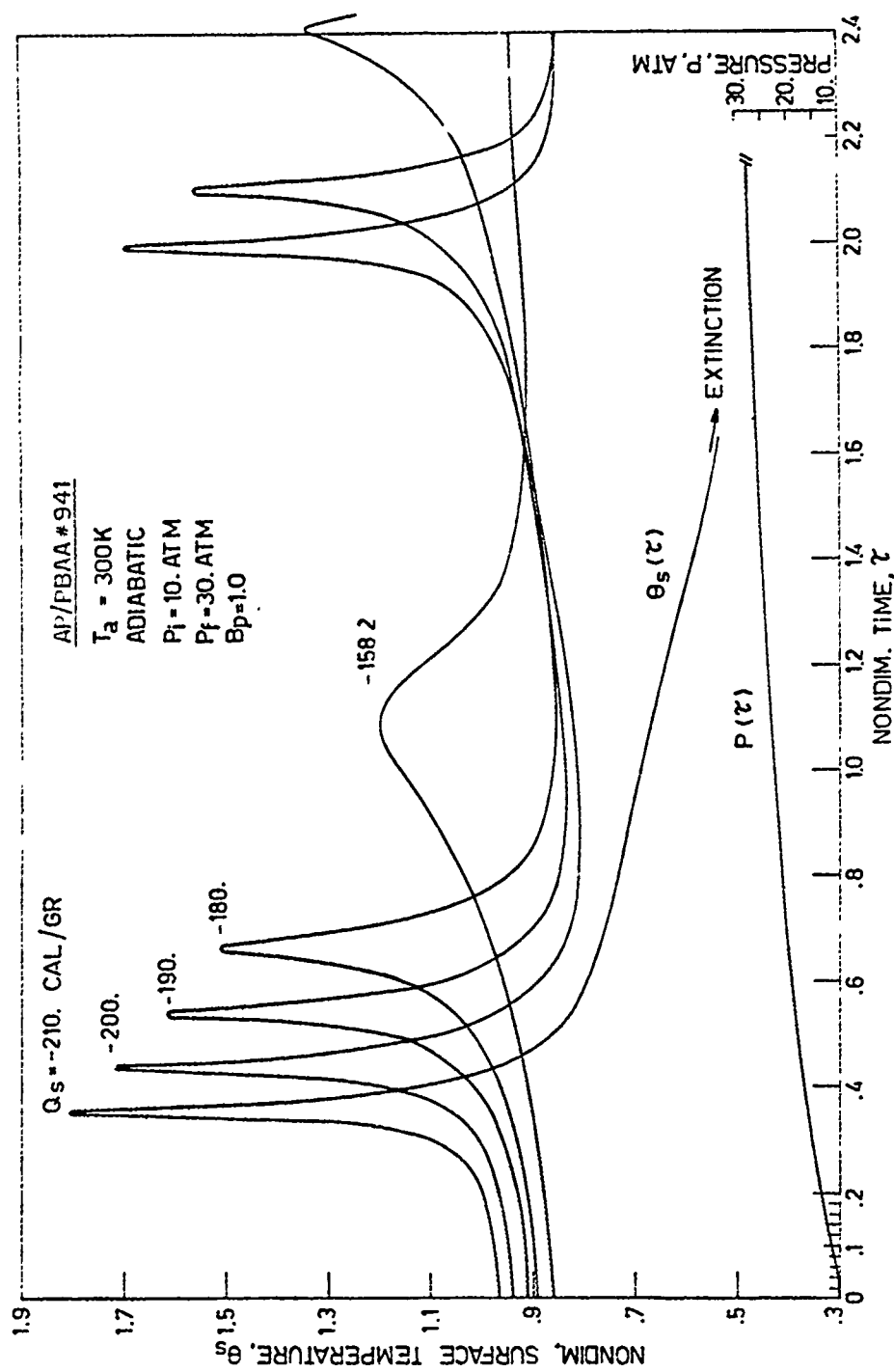


Fig. 56 Computer simulated pressurization tests showing upper dynamic instability for $|Q_s| > 170 \text{ cal/g}$. Cf. Tables 10-11.

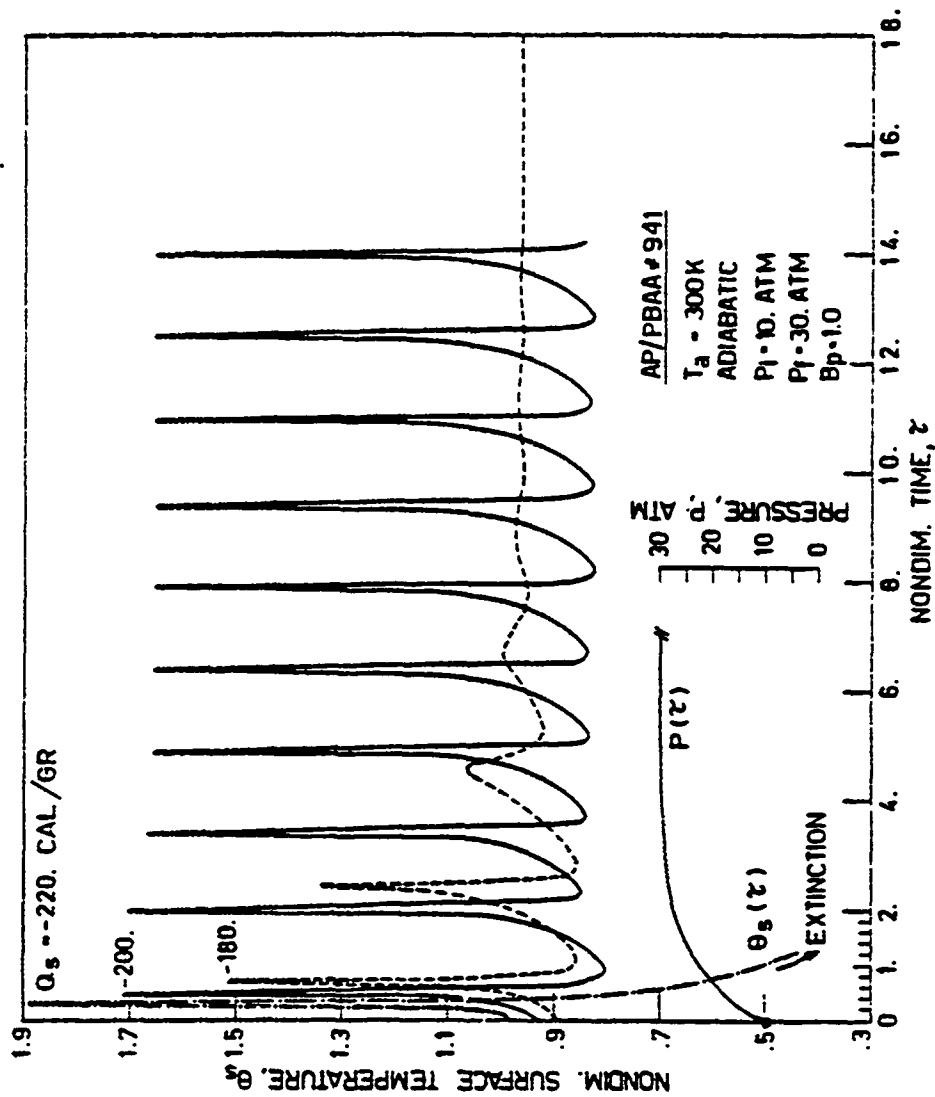


Fig. 57 Computer simulated pressurization tests showing self-sustained surface temperature oscillations. Cf. Tables 10 and 12.

APPENDIX A

THE INFLUENCE OF RADIATION ON THE STEADY CONDENSED PHASE THERMAL PROFILE AND THE QUASI-STEADY STATE GAS PHASE ASSUMPTION

In this appendix, first, a qualitative picture of the general problem of unsteady solid propellant combustion is given. Next, the effect of an external radiant flux on the stationary thermal profiles in the condensed phase is shown. Finally, the difficulties of dealing with unsteady processes are illustrated and the quasi-steady state gas phase assumption is introduced.

This appendix is meant to help the reader in understanding the theoretical developments of the thesis presented in Chapters 6-9. This appendix makes use of the main thesis nomenclature.

A.1 Qualitative Picture

With reference to Fig. 22a, let us consider the heterogeneous deflagration wave consuming a solid propellant subjected to a radiant flux impinging with intensity $(1-r) \cdot I_0$ at its surface. For the sake of simplicity, let us examine for the time being a steady state situation.

In general, a deflagration wave consists of a thermal wave and a simultaneous succession of a large number of endothermic or exothermic chemical reactions, which start somewhere in the subsurface region of the condensed phase and then proceed in the gas phase. Unfortunately, very little is known about the kinetics and the energetics of these reactions and, moreover, even if one knew all the details of the above processes, his task would be too cumbersome. Consequently, certain drastic but fruitful approximations are made. The first is the inert solid assumption, consisting in collapsing all reactions in the condensed phase and in concentrating at the surface their energy effects. Likewise, very little is known about the phase transformations occurring at the interface (condensed/gas). Again we admit our ignorance by making the approximation of a plane infinitesimally thin burning surface neatly separating the inert condensed phase from the reacting gas phase; the energy effects of the phase transformation are concentrated here. We emphasize that this is a pure abstraction, but a useful one, yielding useful predictions about real propellants.

Usually just one (essentially phenomenological) parameter Q_s , energy release at the surface in cal/g, is defined encompassing the energy effects due both to the distributed volumetric reaction collapsed to the surface and to the phase transformations. The qualitative picture we have so far of the deflagration wave consuming a solid propellant consists of a layer with no reactions (pure thermal layer) in the condensed phase and of a layer with reactions and mass diffusion in the gas phase. In order to proceed further, we need to put our discussion on a quantitative basis.

A.2 Stationary Thermal Profiles in Presence of Radiation

We wish to determine the temperature profile in the condensed phase of a strand, whose hot boundary temperature is T_s and whose cold boundary temperature is T_a , burning steadily, assisted by a constant radiant flux intensity in a closed vessel at temperature T_a and pressure P . The reference system, shown in Fig. 22a, has its origin anchored to the burning surface by moving the condensed phase toward the right with speed R . The following assumptions are made:

1. $1 - D$, semi-infinite strand
2. chemically inert condensed phase
3. infinitesimally thin plane surface
4. uniform and isotropic composition of condensed phase
5. constant properties of condensed phase
6. heat exchange only through the burning surface.

Therefore, it is possible to associate a unique temperature value to each station x included between the two boundaries. In order to give a less vague meaning to the expression "infinitely long strand", one has to verify that for all characteristic lengths δ_i of the condensed phase

$$\delta_i/L \ll 1$$

where L is the actual length of the strand.

Moreover, it is assumed that radiation is due only to some external source of known intensity and frequency. However, the radiant flux will suffer several interactions before getting to the surface of the burning strand. For the sake of simplicity, it is assumed that the radiant flux impinges perpendicularly to the burning surface with a constant known intensity I_0 and that a fraction, rI_0 , is reflected back. It is also assumed that the distribution of the radiation penetrating into the condensed phase may be described simply by an exponential decay (Beer's law):

$$(A.2.1) \quad I_x = I_0 \cdot e^{-ax}$$

where a , cm^{-1} is the absorption coefficient. The approximation of Beer's law is acceptable as long as the scattering of radiation in the condensed phase is negligible. Finally, since all optical properties depend on wavelength, the radiation is assumed monochromatic.

With reference to Fig. 23a, a local balance of energy leads to the following nondimensional energy equation:

$$(A.2.2) \quad \left\{ \begin{array}{l} RR \frac{d\theta}{dx} = \frac{d^2\theta}{dx^2} + (1-r) \frac{F}{l_{\text{rad}}} e^{x/l_{\text{rad}}} \\ \theta(x \rightarrow -\infty) = 0 \\ \theta(x = 0) = \theta_s \end{array} \right. \quad \begin{array}{l} \text{II ODE} \\ X = (0, -\infty) \\ \text{BC2} \\ \text{BC1} \end{array}$$

where $RR = R/R_{ref}$ is the nondimensional burning rate;

$X = x/x_{ref}$ is the nondimensional distance;

$\theta = (T - T_{ref}) / (T_{s,ref} - T_{ref})$ is the nondimensional temperature;

$F = I_0 / [\rho_c c_c R_{ref} (T_{s,ref} - T_{ref})]$ is the nondimensional radiant flux intensity;

$\ell_{rad} = (\ell/a)/x_{ref}$ is the nondimensional radiant layer thickness (for further information see §B.2).

Reference conditions are taken as follows:

$P_{ref} = 68 \text{ atm}$	refer. pressure
$R_{ref} = R(P_{ref})$	refer. burning rate
$X_{ref} = \alpha_c / R_{ref} \equiv \delta_{th,ref}$	refer. distance
$T_{s,ref} = T_s(P_{ref})$	refer. surface temperature

Notice that the reference length is the thickness of the thermal layer in the condensed phase at the reference conditions. The choice of this reference is obvious if one considers the properties associated with the condensed phase thermal layer both for steady and unsteady regimes.

The general solution of (Eq. A.2.2) is

$$A.2.3 \quad \theta(X) = C_1 + C_2 e^{X \cdot RR} + (1-r) \frac{F}{RR - 1/\ell_{rad}} e^{X/\ell_{rad}}$$

where C_1 and C_2 are defined by the two boundary conditions:

$$A.2.4 \quad \begin{cases} BC2 & \theta(X \rightarrow \infty) = C_1 = 0 \\ BC1 & \theta(X = 0) = C_2 + (1-r) \frac{F}{RR - 1/\ell_{rad}} = \theta_s \end{cases}$$

For a totally opaque propellant (in a sense to be specified) no forcing (radiation) term would appear in the ODE of Eq. A.2.2 and consequently no particular integral would be required in the general solution given by Eq. (A.2.3): the thermal profile would be totally conductive. But, in general, the non-dimensional temperature profile in the condensed phase of a steadily burning strand assisted by a radiant flux intensity F is, from Eqs. (A.2.3) and (A.2.4):

$$A.2.5 \quad \theta(X) = \theta_s e^{X \cdot RR} + (1-r) \frac{F}{RR - 1/\ell_{rad}} [e^{X/\ell_{rad}} - e^{X \cdot RR}]$$

In Fig. 23b the contribution due to conduction

$$\theta_{co}(X) = \theta_{s,co} e^{X \cdot RR}$$

and the contribution due to the radiation penetration

$$\theta_r(X) = (1-r) \frac{F}{RR - 1/\ell_{rad}} \left[\frac{RR}{\ell_{rad}} e^{X/\ell_{rad}} - e^{X \cdot RR} \right]$$

are shown graphically. The radiative thermal profile starts with zero slope, since the absorption of radiation is a volumetric process. The effect of the radiation penetration is to make the overall thermal profile less steep.

It is worthwhile to remark that the conductive thermal layer thickness:

$$l_{th} \equiv \frac{\alpha_c/R}{\delta_{th,ref}}$$

depends also on the operating pressure through the burning rate, while the radiant absorption layer thickness

$$l_{rad} \equiv \frac{(l/a)}{\delta_{th,ref}}$$

depends exclusively on the nature of the propellant. Notice that if $l_{th}/l_{rad} \gg 1$ the energy transfer by conduction dominates over the energy transfer by radiation; physically this corresponds to the limiting case of an opaque condensed phase. All this implies that, if a large pressure excursion occurs, the propellant response may be altered by the presence of radiation since it alters the thermal layer thickness in the condensed phase.

A.3 The Quasi-Steady State Gas Phase Assumption

The prediction of the burning rate evolution in time for arbitrary but independently assigned laws $P(t)$ and/or $I_0(t)$ and for a given set of initial values implies that the surface temperature (related to the burning rate through some law to be defined) is unknown. Therefore, the condensed phase thermal profile can no longer be determined in a straightforward way, as it was for the stationary case in the previous section. Indeed, the coupling between the condensed and the gas phases through the burning surface needs to be considered explicitly.

For a stationary configuration, the deflagration wave in the (chemically inert) condensed phase is defined by the thermal and radiant layer thicknesses. Since the gas phase is the site of a complicated pattern of chemical reactions with the appropriate diffusive and kinetic processes, we recognize that the analysis of a deflagration wave with these gas phase contributions in principle requires the knowledge of the thicknesses not only of the proper thermal and radiant layers but also of some diffusive, kinetic and reacting layers (to be defined). This is already a big problem, since very little is known about the details of the gas phase phenomena. In order to simplify our physical model, hopefully without losing the essential features of the overall system, the following assumptions are made for the gas phase:

1. emission of radiation is neglected;
2. any interaction with the external radiant flux is neglected;
3. Kinetic processes are approximated by a one step (typically second order) reaction.

Even with this simple model, we would still not know the final gas temperature. In order to make life simpler, we use the further (unnecessary) assumption of no energy losses from the gas phase; in this event, the final gas temperature is given for a stationary process by:

$$\theta(x \rightarrow +\infty) = \theta_f \equiv \frac{T_f - T_{ref}}{T_{s,ref} - T_{ref}}$$

where θ_f is the nondimensional adiabatic flame temperature. This hypothesis is justified by the fact that it has little impact on a model where several more serious approximations have been made.

Despite these assumptions, for a nonsteady case the problem of fully defining the deflagration wave is still very difficult. The shape of the thermal profile is a priori unpredictable since it depends on the full previous time history and on the arbitrary but given laws $P(t)$ and/or $I_0(t)$. It is obvious that the concept of a simple fixed thermal layer loses all its meaning. For the condensed phase, at least, we may overcome this difficulty by solving the full unsteady thermal problem. Unfortunately, this implies we must face the difficulties of a strongly nonlinear initial value problem expressed by a parabolic PDE. Things are much worse in the gas phase: not only does the concept of characteristic layers lose its validity, but we do not know how to deal properly with unsteady reacting processes including their diffusive and kinetic aspects.

At this point we invoke a powerful approximation: the quasi-steadiness assumption. This consists in considering the fully unsteady condensed phase portion of the deflagration wave coupled to a steady gas phase portion of the deflagration wave through the burning surface. In doing so, the gas phase is assumed to adjust itself instant by instant and infinitely fast to the conditions existing in the condensed phase (say, burning rate) and to the conditions imposed by the external parameters (say, pressure).

This assumption may be justified by consideration of the various characteristic times. Let the characteristic time for the conductive thermal processes in the condensed phase be in dimensional terms

$$(A.3.1) \quad t_{th,c} \equiv \delta_{th,c}/R = \alpha_c/R^2 .$$

This can be thought of as the time required by a particle traveling with (stationary) speed R to get across the conductive thermal layer. Likewise, the characteristic time associated with the conductive thermal layer in the gas phase in dimensional terms is

$$(A.3.2) \quad t_{th,g} \equiv \delta_{th,g}/U = \alpha_g/U^2$$

For consistency with the previous definitions, let the reference time be defined as

$$t_{ref} \equiv \delta_{th,ref} = \alpha_c/R_{ref}^2$$

from which the following nondimensional characteristic times are obtained

$$\begin{aligned} \tau_c &\equiv t_{th,c}/t_{ref} \\ \tau_g &\equiv t_{th,g}/t_{ref} . \end{aligned}$$

Say, now, that by some means we are able to define a characteristic time for the law of change of the controlling parameters; it is always possible to associate a certain t_{ext} to a depressurization transient (for example, see Ref. 92). In the same time scale used for the other characteristic times, let

$$\tau_{ext} \equiv t_{ext}/t_{ref}$$

be the nondimensional characteristic time measuring the rate of change of the external parameters. Whenever

$$(A.3.3) \quad \tau_c \ll \tau_{ext} \quad \text{and} \quad \tau_g \ll \tau_{ext}$$

the overall phenomenon may be considered as fully steady. Conversely, if

$$(A.3.4) \quad \tau_c \gg \tau_{ext} \quad \text{and} \quad \tau_g \gg \tau_{ext}$$

the overall phenomenon must be treated as fully unsteady. In general, we are able to cope easily with the first problem but we have considerable difficulties with the second one. If, however

$$\tau_c \gg \tau_{ext} \quad \text{but} \quad \tau_g \ll \tau_{ext}$$

then we have an intermediate case in which the gas phase may be thought of as being in equilibrium with the external parameters (say, pressure) while still nothing can be said about the condensed phase (except that, in general, it is not in equilibrium) and about the coupling to the gas phase.

At this point, a fundamental and simple result from the physics of heterogeneous combustion is of great help. Let us compare the two characteristic thermal times in condensed and gas phases; for sake of clarity in dimensional terms one gets

$$\frac{t_{th,g}}{t_{th,c}} = \frac{\alpha_g}{\alpha_c} \frac{R^2}{U^2}$$

Mass continuity in a steady state requires

$$\rho_c R = \rho_g U$$

from which

$$(A.3.5) \quad \frac{t_{th,g}}{t_{th,c}} = \frac{\tau_{th,g}}{\tau_{th,c}} = \frac{\lambda_g}{\lambda_c} \frac{C_c}{C_g} \frac{\rho_g}{\rho_c}$$

depending only on physical properties of the propellant. For usual cases a good estimate is

$$(A.3.6) \quad \frac{\tau_g}{\tau_c} = O(0.01)$$

This implies that whenever

$$\tau_g \ll \tau_{ext}, \text{ even though } \tau_c \gg \tau_{ext}$$

the gas phase is not only in equilibrium with the external parameters (say, pressure) but also with the instantaneous conditions existing in the condensed phase (say, burning rate).

In conclusion, the quasi-steady gas phase assumption holds true (for the kinds of heterogeneous flames considered in this work) if Eq. A.3.7 is satisfied. This implies that all time derivatives in the gas phase equations are small and can be dropped out; all PDE's are then reduced to ODE's. Therefore, the gas phase equations are immediately integrable (e.g. see Eq. 6.5.4 for the energy equation). However, the resulting quasi-steady integral relations are different from the corresponding steady state relations due to the unsteadiness of the boundary conditions at the condensed/gas interface. For a through discussion of this final point, the reader is referred to Refs. 90 and 115.

APPENDIX B

RADIATION SCATTERING: EFFECT OF DISTRIBUTION FUNCTION IN THE CONDENSED PHASE

A more general treatment of the fate of the external radiant flux impinging on the surface of a burning propellant is offered in this appendix. The assumption of no radiation scattering in the condensed phase is relaxed, while all of the other assumptions listed in §6.5 are retained. This important aspect of the physics of the radiation has often been neglected in the literature of heterogeneous flames. This neglect may affect both the validity of the experimental measurements of absorption coefficients and the qualitative behavior of a burning propellant assisted by radiation, mainly with regard to dynamic effects.

The excellent treatment by Kottler B.1, B.2 and discussion by Ohlemiller⁸ and⁷⁵ are followed here. Further comments on the effects of radiation on burning propellants can be found in Refs. 126 and B.3. The law found for the distribution of radiation in an absorbing and scattering medium can then be incorporated in the system of equations listed in §6.5. (This law contains certain phenomenological constants which in general must be measured experimentally; a possible procedure is discussed.) Such a more general model can be numerically integrated following the discussions of Chapter 9.

For the sake of clarity, dimensional quantities are used in this appendix. The passage to nondimensional variables is then performed according to the rules indicated in §6.5.

B.1 Description of the Physical Problem

Let us consider a slab of heterogeneous material (Fig. B.1a) consisting of a large number of particles embedded in a homogeneous matrix (absorbing-scattering medium). Let the slab for the time being have a finite thickness t and be illuminated at one side by a radiant beam of intensity I_0 . The beam emerging from the other end at $x = t$ will be less intense also due to the fact that some light is scattered to the side by the particles and thus removed from the direct beam. In Fig. B.1a a portrait of the complicated 3-D radiation intensity distribution in the absorbing-scattering medium is given: at any station x , the radiation intensity (flux/unit solid angle) depends not only on the depth of the station from the surface $x = 0$, but also on the specific direction considered.

We wish, in this section, to describe the above distribution of radiation intensity. This is, in general, a formidable problem and a certain number of assumptions are to be made. In order to exclude a wavelength dependence, let us consider for the time being a beam of monochromatic radiation. It is also assumed for the time being that the matrix of the medium has the same refractive index as the external ambient

medium. When this assumption of a neutral medium is not satisfied, reflection at the surface and refraction at the boundary (scattering/ambient media) should be accounted for. Finally, the impinging radiation is assumed unpolarized and the electromagnetic wave is assumed plane.

A fundamental parameter is the nondimensional ratio d/λ , where d is some typical average size of the particles embedded in the matrix of the scattering medium and λ is the wavelength of the impinging radiation. Whenever

$$d/\lambda \ll 1$$

the absorption effects are largely dominant over the scattering effects and the extinction of the impinging beam is practically due only to absorption. In this case the fate of the beam is correctly described by Beer's law and the results found in Chapter 9 do not need to be modified. Conversely, if

$$d/\lambda \gg 1$$

the scattering effects are substantial and the extinction of the impinging beam may be due in large part to scattering. In this case Beer's law is no longer valid and the results found in Chapter 9 are inaccurate. Finally if

$$d/\lambda \approx 1$$

both absorption and scattering effects are important and the extinction of the impinging beam is due to both mechanisms. In this general physical configuration, Beer's law is not sufficient for describing the fate of the radiation at the interior of the condensed phase of the burning propellant and more sophisticated theories are to be implemented. Qualitatively, one would expect the results found in Chapter 9 to be still valid but with a dependence on the impinging external radiant flux less pronounced to the extent in which the extinction of the beam is due to scattering.

By scattering is meant the combined effect of reflection, refraction and diffraction on a radiant flux interacting with a particle. Only when $d/\lambda \gg 1$ can the fate of the nonabsorbed portion of a plane electromagnetic wave interacting with a particle be described using the classical concepts of the geometrical optics (reflection and refraction). For $d/\lambda \sim 1$ is no longer possible to separate the contributions to the radiant flux intensity due to reflection, refraction, and diffraction. A drastic difference exists depending on whether the beam is impinging on isolated particles or on a cluster of particles of different size. For the former case the well established treatments by Rayleigh ($d/\lambda \ll 1$, scattering only) and Mie (d/λ arbitrary, scattering and absorption) apply. These theories may be extended to an assembly of particles having the same diameter subjected to illumination

by a monochromatic plane wave, and separated from each other by a distance large enough to avoid a succession of scattering events from the same beam pencil. This situation is defined as single scattering in a monodisperse assembly of particles. In the more general configuration of a cluster made of closely packed particles of various shapes and sizes, multiple scattering in a polydisperse assembly has to be considered. This is a very difficult task and no rigorous theory is available so far. Several phenomenological treatments have been proposed and they commonly resort to some statistical average values for the geometrical factors concerning the particles dispersed in the absorbing-scattering medium. This smooths down the dependence of the results on the shape and size of the individual particles. The behavior of the absorbing-scattering medium is globally characterized by two constants, experimentally determined, defining the absorption and scattering properties of the medium under examination. These are known as "two constant theories".

With reference to Fig. B.1b, let us fix a polar system of coordinates and let us consider only axial-symmetric cases by putting $\partial/\partial\phi = 0$ for all the relevant functions which will be met. An external radiant beam impinging with intensity I_0 at the boundary of the slab and traveling inside the medium is subjected to negative contributions (decrease of intensity) due to absorption and out scattering and positive contributions (increase of intensity) due to emission and in scattering. As usual, any emission of radiation which is not of thermal nature is neglected in this work. We define the volume absorption coefficient a , cm^{-1} so that the radiant flux intensity emitted within a solid angle $d\omega$ from a point source and lost by absorption along an arbitrary path of length $d\ell$ is

$$dI_{\text{abs}} = a I d\ell$$

Likewise, we define the volume scattering coefficient s , cm^{-1} so that the radiant flux intensity emitted within a solid angle $d\omega$ from point source and lost by scattering out along an arbitrary path of length $d\ell$ is

$$dI_{\text{sca. out}} = -s I d\ell$$

Obviously, the (total) volume extinction coefficient k , cm^{-1} is defined so that the radiant flux intensity emitted within a solid angle $d\omega$ from a point source suffers a total loss along an arbitrary path of length $d\ell$ given by

$$dI_{\text{loss}} = -k I d\ell$$

being

$$k = a + s$$

Due to Kirchoff's law, the radiant flux intensity emitted within a solid angle $d\omega$ from a point source distributed along an arbitrary path length $d\ell$ is

$$dF_{em} \approx a I_b d\ell$$

where I_b is the intensity of the black body radiation defined by Planck's law.

With reference to Fig. B.1b, it can be shown^{B4-B6} that the gain in intensity of the radiant flux along an arbitrary path $d\ell$ by scattering from all other bundles $d\omega'$ into the bundle $d\omega$ can be expressed as

$$dI_{sca.in} = s d\ell \int_{\omega'} P(\eta, \eta') I(x, \eta') d\omega'$$

where the phase function $P(\eta, \eta')$ gives the fraction of radiation incident from direction η' that is scattered into direction η . In all scattering processes it is assumed that no frequency change occurs in the re-emission of radiation. It follows that the radiative transfer equation which is an energy conservation statement on the differential element can be written as:

$$(B.1.1) \quad \frac{dI}{dx} = - (a+s) \frac{I}{\mu} + a I_b + \frac{s}{2\mu} \int_{-1}^{+1} P(\mu, \mu') I(x, \mu') d\mu'$$

where $I(x, \mu)$ is the radiant intensity at depth x in direction

μ to the inward normal of the boundary surface;

$\mu \equiv \cos \eta$

a is the volumetric absorption coefficient;

s is the volumetric scattering coefficient;

The solution of the above integro-differential equation for the general case of multiple scattering in a polydisperse cluster of particles is difficult to obtain. Even for those particular configurations for which rigorous solutions have been found, the use of the proper approximate solutions is preferable

Let us turn now to the specific case of a burning propellant. Due to the distribution and moderate level of temperature in the condensed phase, the emission of thermal radiation aI_b is assumed to be negligible compared to the external radiant flux. As due to the nature of the propellant, two typical situations may occur. If the composition is homogeneous on a molecular scale (e.g., some DB propellants), the scattering

effects are negligible. In this case the medium can be thought of as a pure absorbing one and the radiative transfer equation reduces to Beer's law for the limiting value of $s \rightarrow 0$. Whenever this occurs, the results as presented in Chapter 9 are valid. On the other hand, if the composition of the strand is not homogeneous on a molecular scale (e.g., a composite AP propellant), the full Eq. (B.1.1) needs to be considered and a model for the optical heterogeneity of the absorbing-scattering medium is required. Following Ohlemiller⁷⁵, a conventional composite propellant may be thought of as consisting of two phases: a first phase (25% by weight of the propellant) consisting of a polymeric fuel binder with additives and aluminum powder suspended in it and a second phase (75% by weight of the propellant) consisting of a controlled distribution of AP particles. Usually, additives and aluminum powder have a mean size of less than 10μ , whereas AP particles may range from 1μ to 100μ with a large fraction of particles of the order of 100μ in size. Therefore the fuel phase fills the interstices around the randomly distributed but rather closely packed AP particles.

In the arc image apparatus most of the radiation is absorbed by the polymeric fuel and then the heat is transmitted by conduction to the adjacent AP particles, which are quite transparent to the arc image radiation (0.3 to 1.5μ). Conversely, in the laser ignition apparatus the radiation (10.6μ) is absorbed both by the polymeric fuel and the AP particles. Note that Eq. B.1.1 has been derived on the assumption of a collection of absorbing and scattering particles distributed in a neutral medium. Obviously, this is not the case for the fuel phase since the medium absorbs as well as the particles. We can account for this fact by considering some mean absorption coefficient, a , depending on the composition of the fuel phase and a surface reflectivity coefficient, r . Due to the different refractive index of the polymeric fuel and AP particles, the reflectivity coefficient may vary on the surface of the propellant. Likewise, as mentioned, the absorption coefficient of the polymeric fuel and AP particles may sensibly differ from the average value. All this implies complicated 3-D interactions between the local deposition of radiation in depth and the heating of the propellant by conduction. The picture is made even more difficult by the chaotic change of direction of the light rays ("scattering") in the propellant. It is stressed that the wavelength dependence of the relevant optical properties accentuates these manifestations of heterogeneity in the arc image apparatus. Notice also that, in the case of arc image radiation, the polychromatic nature of the radiant beam should be accounted for. This is not a conceptual difficulty once we are able to deal with monochromatic radiation.

Subsequently, once the problem of the radiation distribution has been solved (see §B.2), the problem (possibly 3-D) of the heating of the propellant must be dealt with. This also is, in general, a very difficult matter and in this report we will just summarize the discussion by Ohlemiller⁸ and 75) in §B.2. As to the radiation scattering question, even considering all the assumptions and simplifications so far mentioned, the problem is still very difficult to solve. In order to avoid too cumbersome and unrewarding a task (recall the approximations listed in §6.5 for the heterogeneous deflagration wave in a solid propellant), we accept the further assumption of isotropic scattering. This amounts to putting for the phase function

$$P(\mu, \mu') = 1$$

Then the radiative transfer equation in dimensional terms in an absorbing and scattering medium may be written as

$$(B.1.2) \quad \frac{dI}{dx} = -(a+s) \frac{I}{\mu} + s \frac{J}{\mu}$$

where $J(x, \mu)$ is the source function at depth x in direction μ to the inward normal of the boundary surface and represents the contribution to radiation in direction μ by scattering from all other directions. It can be written as

$$(B.1.3) \quad J(x, \mu) = \frac{1}{2} \int_{-1}^{+1} P(\mu, \mu') I(x, \mu') d\mu' = \frac{1}{2} \int_{-1}^{+1} I(x, \mu') d\mu'$$

The radiative transfer equation will be used in the form of Eq. (B.1.2) throughout the remainder of the text. To assist the reader, the assumptions implicit in Eq. (B.1.2) are summarized as follows:

1. monochromatic radiation;
2. plane wave;
3. unpolarized radiation;
4. polydisperse cluster of particles;
5. multiple scattering;
6. isotropic scattering;
7. nonemitting scattering medium;
8. no frequency change in re-emission of radiation;
9. axial symmetric processes (no edge effects).

B.2 Approximate Solutions of the Radiative Transfer Equation

Within the framework of the assumptions listed in the previous section, Eq.(B.1.2) can be solved for two different configurations corresponding rather closely to the experimental set up of the arc image and of the laser tube. Obviously, the beam from the arc image can be treated as diffuse polychromatic radiation while the beam from the laser tube can be treated as collimated monochromatic radiation. Both cases, at this point easily solvable in principle, are still difficult in actual practice: the arc configuration requires an extension to polychromatic radiation and the laser configuration requires a proper treatment of the collimated nature of the beam.

B.2.1 Diffuse Irradiation in an Arc Image Furnace

We start by considering the case of monochromatic uniformly diffuse radiation (see Fig. B.2). In this case, a first approximation solution of Eq.(B.1.2) is obtained by the assumption of no angular dependence of the radiant flux intensity in each of two hemispheres. The original beam $I(x, \mu)$ is split conceptually into two parts; one $I^+(x)$ travels in the forward direction and the second $I^-(x)$ travels in the backward direction. Both radiant fluxes are considered independent of angular distribution within their respective hemispheres, which is nearly correct as long as $I(x, \mu)$ has a weak dependence on μ in Eq.(B.1.3). The following expressions are obtained (p. 14 of Ref. B.2):

$$(B.2.1) \quad \begin{cases} I^+(x) \equiv I(x, \mu > 0) = \left[\frac{I_0 e^{2\Gamma t}}{e^{2\Gamma t} - R_\infty^2} \right] e^{-\Gamma x} - \left[\frac{I_0 R_\infty^2}{e^{2\Gamma t} - R_\infty^2} \right] e^{+\Gamma x} \\ I^-(x) \equiv I(x, \mu < 0) = \left[\frac{I_0 R_\infty e^{2\Gamma t}}{e^{2\Gamma t} - R_\infty^2} \right] e^{-\Gamma x} - \left[\frac{I_0 R_\infty}{e^{2\Gamma t} - R_\infty^2} \right] e^{+\Gamma x} \end{cases}$$

where t is the thickness of the sample subjected to radiative heating:

$$\Gamma \equiv 2 \sqrt{a^2 + as}, \text{ cm}^{-1} \quad \text{is a constant}$$

$$R_\infty \equiv (2a + s - \Gamma)/s \quad \text{is a constant}$$

It will be noticed that the original integro-differential equation of radiative transfer is reduced in this simple case to a pair of ODE's. The above solution is called the Schuster-Kubelka or Schuster-Schwartzchild first approximation solution.

For a semi-infinite slab, in the sense that

$$e^{\Gamma t} \gg R_{\infty}^2$$

the Schuster-Kubelka solution may be written very simply as

$$(B.2.2) \quad \begin{cases} I^+(x) = I_0 e^{-\Gamma x} \\ I^-(x) = I_0 R_{\infty} e^{-\Gamma x} \end{cases}$$

From the second of the above relationships, for $x = 0$ one gets

$$(B.2.3) \quad R_{\infty} = \frac{I^-(x=0)}{I_0}$$

which defines the constant R_{∞} as the volume reflectance of a slab of infinite thickness subjected to uniformly diffuse illumination.

Since the illumination at the surface is uniformly diffuse, the path length at each direction $d\eta$ is $d\ell = dx/\cos \eta$ (Fig. B.2a). It can be shown (see p. 108 of Ref. B.4) that the average path length for η varying from 0 to $\pi/2$ is

$$(B.2.4) \quad \overline{d\ell} = 2dx$$

i.e., uniformly diffuse radiation is equivalent to a collimated beam of the same intensity at $\eta = 60^\circ$. It is interesting to note that the first of Eqs. (B.2.2) suggests that the radiant layer thickness in an absorbing - scattering medium subjected to uniform diffuse illumination may be defined as

$$(B.2.5) \quad \delta'_{\text{rad}} \equiv 1/\Gamma$$

In the case of uniform diffuse illumination on a pure absorbing medium ($d/\lambda \ll 1$), as considered in Chapter 9, the previous relationship reduces to

$$(B.2.6) \quad \delta'_{\text{rad}} = 1/2a$$

which differs by a constant from the corresponding definition given in §A.2; the factor 2 originates from the average path length of Eq. (B.2.4.).

An application of the Eqs. (B.2.2) is shown in Figs. B3 and B4 for the values of the parameters indicated. In Figs. B3 ($s/k = 0.1$) and B4 ($s/k = 0.9$) the forward $I^+(x)$ and backward $I^-(x)$ radiant fluxes evaluated according to Eqs. (B.2.2) are shown. The radiant flux $I_{\text{abs}}(x)$ absorbed in a

layer of thickness x is also shown; notice that $I_{\text{abs}}(x = 0) = 0$ since absorption is a volumetric process. Increasing the albedo ratio s/k from 0.1 to 0.9 makes much less effective the heating process, in that $I_{\text{abs}}(x)$ increases slowly and only up to a certain value depending on s/k , and makes Beer's law more and more erroneous. In Fig. B3 (weak scattering) the departure from Beer's law is due mainly to the diffuse illumination (factor 2 just mentioned); in Fig. B4 the departure is a result of strong scattering. The energy balance shown in Fig. B2.b is used as a check at each station x .

A more accurate solution of Eq. (B.1.2) accounting for the angular dependence of the two radiant intensities may be expressed for a slab of infinite thickness as ^{B.2}

$$\text{B.2.7} \quad \left\{ \begin{array}{l} I(x, \mu > 0) = e^{-(a+s)x/\mu} \left[1 - \frac{s(1+R_\infty)}{2(a+s-\Gamma\mu)} \right] I_0 + \\ \quad + e^{-\Gamma x} \cdot \frac{s(1+R_\infty)}{2(a+s-\Gamma\mu)} I_0 \\ I(x, \mu < 0) = e^{-\Gamma x} \frac{s(1+R_\infty)}{2(a+s-\Gamma\mu)} I_0 \end{array} \right.$$

This is the radiant intensity at a station x in the direction μ for uniformly diffuse illumination on the surface $x = 0$ of a semi infinite slab. The Eqs. (B.2.7) are the Schuster-Schwartzchild second approximation solution.

An application of Eqs. (B.2.7) is shown in Fig. B5 for the values of the parameters indicated. A polar diagram is used in order to describe the angular distribution $I(x, \mu > 0)$ and $I(x, \mu < 0)$ of the radiant flux intensities at some selected values of x . Notice that, as the thickness x increases, the radiant flux intensity decreases in each direction. By integration over η , the total space distribution $I^+(x)$ and $I^-(x)$ can be obtained; the difference from the corresponding solution of Fig. B4 found by the Schuster-Kubelka approach is within 3% in all the computations made.

In the actual configuration of the arc image apparatus the polychromatic nature of the radiation has to be accounted for. Knowledge of the spectral distribution of the surface reflectivity $r(\lambda)$, absorption coefficient $a(\lambda)$, scattering coefficient $s(\lambda)$ and of the radiant flux intensity $I_0(\lambda)$ is assumed (see Fig. B.6). In a narrow band of wavelengths $d\lambda$, the radiant flux intensity absorbed at depth x can be expressed as:

$$dI(x; \lambda) = [1 - r(\lambda)] \cdot a(\lambda) \cdot \frac{I_\lambda(\lambda)}{I_{\text{tot}}} \cdot [I^+(x) + I^-(x)] d\lambda$$

where $I_{\lambda}(\lambda)/I_{\text{tot}}$, cm^{-1} is the normalized spectral energy distribution of the radiation source and measures the fractional amount of flux contained in the narrow band $d\lambda$. It follows that the radiative term

$$(B.2.8) \quad N_t \frac{1-r}{\ell_{\text{rad}}} \cdot F \cdot e^{X/\ell_{\text{rad}}}$$

of Eq.(6.5.2) has to be replaced by

$$(B.2.9) \quad N_t \cdot F \cdot f(X)$$

where using Eq.(B.2.2)

$$(B.2.10) \quad f(x) \equiv \int_{\lambda_1}^{\lambda_2} \frac{1-r(\lambda)}{\ell_{\text{rad}}(\lambda)} \frac{I_{\lambda}(\lambda)}{I_{\text{tot}}} (1 + R_{\infty}) e^{X/\ell'_{\text{rad}}} d\lambda$$

is a property of the material and radiant source and does not vary in time. This computation, easy in principle, is difficult in practice and requires careful experiments and numerical techniques. Notice that $\ell_{\text{rad}} \equiv (1/2a)/x_{\text{ref}}$ is the familiar nondimensional (absorption) radiant layer thickness when Beer's law holds, while $\ell'_{\text{rad}} \equiv (1/\Gamma)/x_{\text{ref}}$ is the nondimensional radiant layer thickness for an absorbing-scattering medium already introduced in Eq.(B.2.5). Notice also that in Eq.(B.2.10) the simple Schuster-Kubelka solution has been employed, since we are not specifically interested in the angular distribution of the radiant flux.

However, a major difficulty arises at this point. The previous term(B.2.8) was determined in §A.2 in the framework of a monodimensional analysis. In a polydisperse absorbing-scattering medium, where particles of various shapes and sizes are closely packed, heat conduction from the fuel phase absorbing the radiation to the adjacent possibly transparent AP particles is inherently a 3-D process. Only when the physical heterogeneity of the medium fades out compared to the thickness of the conductive thermal wave (in the condensed phase) is the above approximation of 1-D in principle allowed. A characteristic length "measuring" the heterogeneity of the absorbing-scattering medium may be conveniently defined by the average size of the AP particles, which has to be compared to the characteristic length of the conduction layer. The problem is further complicated by the presence of a third characteristic layer associated with radiation penetration. For a detailed discussion of all possible cases, the interested reader might wish to consult the work by Ohlemiller (pp. 14-15 of Ref. 8a). In any event, non 1-D treatments are considered an unrewarding task.

In summary, in the case of the arc image ignition apparatus the substitution of the term(B.2.9) for the term(B.2.8) is enough, within the limits just discussed, to account for the

general configuration of a polychromatic uniformly diffuse beam impinging on an absorbing-scattering medium. Since the scattering diminishes the amount of energy actually transferred to the solid propellant sample (for a given intensity of the impinging radiant flux), a decreased sensitivity of the propellant burning rate on dynamic effects associated with radiation would be expected. In particular, dynamic extinction would be more and more difficult to occur with increasing albedo ratio.

B.2.2 Collimated Irradiation with a Laser

Let us consider briefly the more complicated case of collimated monochromatic radiation (more complex because both collimated and diffuse fluxes are present). For a slab of infinite thickness the Schuster-Kubelka solution for the diffuse intensities is (p. 23 of Ref. B.2):

$$I^+(x) = \frac{3s}{3a-s} I_0 [e^{-(a+s)x} - e^{-\Gamma x}] \quad (B.2.11)$$

$$I^-(x) = \frac{s}{3a-s} I_0 [e^{-(a+s)x} - 3R_\infty e^{-\Gamma x}]$$

where I_0 , cal/cm²-s is the intensity of the collimated radiation impinging on the surface ($x=0$). The more accurate Schuster-Schwartzchild second approximation solution for the diffuse intensities is:

$$(B.2.12) \quad \left\{ \begin{aligned} I(x, \mu > 0) &= I_0 e^{-(a+s)x/\mu} - \frac{s(1+R_\infty)}{2} \frac{3s}{3a-s} I_0 \frac{e^{-\Gamma x} - e^{-(a+s)x/\mu}}{a+s-\Gamma\mu} + \\ &\quad - \frac{s}{2} \frac{3}{3a-s} I_0 \frac{e^{-(a+s)x} - e^{-(a+s)x/\mu}}{(1-\mu)} \\ I(x, \mu < 0) &= - \frac{s(1+R_\infty)}{2} \frac{3s}{3a-s} I_0 \frac{e^{-\Gamma x}}{a+s-\Gamma\mu} - \frac{s}{2} \frac{3}{3a-s} I_0 \frac{e^{-(a+s)x}}{(1-\mu)} \end{aligned} \right.$$

where the last term of the first of Eqs. (B.2.12) should not be extended to the limit $\mu = 1$.

To the above diffuse intensities the collimated intensity $I''(x)$ must be added according to

$$(B.2.13) \quad I''(x) = I_0 \delta(1-\mu) e^{-(a+s)x}$$

where $\delta(1-\mu)$ is the Dirac delta function.

In this case, the difficulty arises mainly from the fact that the more complex Schuster-Schwartzchild solution has to be considered, since the radiant flux has to adjust itself from an initially collimated configuration to a final uniformly diffuse configuration. This implies that the dependence of the angular distribution of the radiant flux on the station x can no longer be neglected. It follows that Eqs.(B.2.12) have to be integrated over $\mu \equiv \cos \eta$ in order for one to evaluate the amount of radiation falling on a given station x . The radiant intensity obtained by adding the collimated intensity given by Eq.(B.2.13) can then be directly substituted in Eq.(6.5.2) with the same qualitative effects as discussed at the end of the previous section.

In summary, for the laser ignition apparatus the approximate evaluation of F and ℓ_{rad} quantities in the term(B.2.8) is enough to account for the general configuration of a monochromatic collimated beam impinging on an absorbing-scattering medium. Notice that in this case we do not worry about 3-D conductive processes, since (at least at 10.6μ) the absorptivity of AP is comparable to that of the polymeric binders (about 250 cm^{-1}). This can be considered as another advantage of the laser with respect to the arc image source.

B.3 Experimental Determination of Optical Properties

Consider a slab of propellant of finite thickness bounded by two parallel and optically plane surfaces and subjected to uniformly diffuse radiation of monochromatic nature (Fig. B.7). In general, the refractive index of the matrix of the heterogeneous propellant is different from the refractive index of the ambient medium, usually air. Therefore, measurements of the optical properties of such a slab of heterogeneous propellant performed in an integrating photometer furnish only total (surface + volume) values of the reflectance and transmittance. (Note: an integrating photometer is necessary to capture all reflected and transmitted light). Instead we are interested in evaluating the three phenomenological constants required for any multiple scatter theory, i.e., the volumetric absorption and scattering coefficients, and the internal surface reflectance (see Fig. B.7). This can be done by extending to the case of uniformly diffuse illumination the solution given by Stokes (p. 484 of Ref. B.1) for collimated incidence. It is assumed that the illumination is uniformly diffuse inside the plate also. For remarks concerning this assumption see Kottler (p. 485 of Ref. B.1) and Kortum (p. 127 of Ref. B.4).

With reference to Fig. B.7 and to the related list of symbols, the Stokes theory shows that the total reflectance and transmittance can be expressed as:

$$(B.3.1) \quad R_t = r_e' + t_e' T_i [R_v(1 - r_i' R_v) + r_i' T_v^2]/D$$

$$(B.3.2) \quad T_t = t_e t_i T_v / D$$

$$\text{where } D \equiv (1 - r_i R_v) (1 - r_i' R_v) - r_i' r_i T_v^2$$

Notice that the following parameters

$$(B.3.3) \quad R_t, T_t, r_e', r_e''$$

are measurable, whereas the following parameters

$$(B.3.4) \quad R_v, T_v, r_i', r_i''$$

cannot be directly measured. Therefore, we have so far four unknowns in Eq. (B.3.4) with two algebraic equations Eqs. (B.3.1 and B.3.2). In order to solve the problem we need two more relationships. The first just assumes that the front and rear surfaces are optically identical, so that

$$(B.3.5) \quad \left\{ \begin{array}{ll} r_i' = r_i'' = r_i & \text{diffuse internal surface reflectivity} \\ r_e' = r_e'' = r_e & \text{diffuse external surface reflectivity} \end{array} \right.$$

The second relationship is obtained from a further measurement performed in some specific condition so that one of the parameters is known. For example, it has been suggested to measure the reflectance R_t^b of the sample with its rear surface blackened. In this configuration, the surface reflectivity at the rear surface $r_i'' = 0$ in Eq. (B.3.1). Therefore, the complete problem is solved by using the following set of algebraic equations:

$$(B.3.6) \quad \left\{ \begin{array}{l} R_t = r_e + t_e t_i [R_v (1 - r_i R_v) + r_i T_v^2] / D \\ T_t = t_e t_i T_v / D \\ R_t^b = r_e + t_e t_i R_v (1 - r_i R_v) \end{array} \right.$$

$$\text{where } D \equiv (1 - r_i R_v)^2 - r_i^2 T_v^2$$

The unknowns are R_v, T_v and r_i while the parameters R_t, T_t, R_f, r_e are measured. Kottler (p. 486 of Ref. B.4), among other comments, suggests avoiding measurements on overly thick samples, i.e., those with negligible transmittance, in order to get reliable results.

In actual practice most of the spectrophotometers use a collimated incidence beam. The above results need, therefore, to be extended to the configuration of collimated incident radiation. This implies that the total transmittance T_t consists now of a specular portion emerging from the rear surface and of the diffuse portion already considered. Moreover, the external diffuse surface reflectivity r_e has to be replaced by the specular surface reflectivity r_s . Any other differences in the parameters may be neglected. However, in order to verify the assumption of diffuse light at the interior of the slab, only plates with no emerging specular transmittance from the rear surface will be considered. This requires either a plate of sufficient thickness or a concentration of scattering particles large enough to avoid the confusing presence of two specular fluxes in the interior of the slab. With these provisions, the volume absorption coefficient a and the volume backward scattering coefficient s_b may be evaluated once the algebraic system of Eqs. (B.3.6) has been solved. In the framework of the Schuster theory, one gets

$$B.3.7 \quad \begin{cases} (1 + R_v^2 - T_v^2)/2R_v = (a + s_b)/s_b \\ \log[(1 - R_\infty R_v)/T_v] = \sqrt{a^2 - 2as_b} \, t \end{cases}$$

where $R_\infty = a + s_b - \sqrt{a^2 + 2as_b}$

is the volume reflectance for uniformly diffuse illumination when the thickness $t \rightarrow \infty$; it has been defined already by the relationship (B.2.3). Some algebraic manipulations show that the two definitions are equivalent if we put

$$s = 2s_b$$

Indeed the (total) volume scattering coefficient s can be thought of as the sum of the volume backward scattering coefficient s_b and of the volume forward scattering coefficient s_f , so that in general

$$s = s_f + s_b$$

For very small particles, one has

$$s_f = s_b$$

and therefore

$$s = 2s_b$$

A final comment concerns the experimental measurement of the external surface reflectivity. This can be performed in a spectrophotometer equipped with an integrating sphere and with some minor adjustments both diffuse and specular reflectivity can be evaluated. A detailed discussion on the related problems is contained in Ref. B.4.

REFERENCES IN APPENDIX B

- B.1 Kottler, F., "Turbid Media with Plane Parallel Surfaces," Journal of the Optical Society of America, Vol. 50, May 1960, pp. 483-490.
- B.2 Kottler, F., "The Elements of Radiative Transfer," Progress in Optics, Vol. III, John Wiley & Sons, Inc., New York, 1964.
- B.3 Boehringer, J.C. and Spindler, R.J., "Radiant Heating of Semitransparent Materials", AIAA Journal, Vol. 1, No. 1, 1963, pp. 84-88.
- B.4 Kortum, G., Reflectance Spectroscopy: Principles, Methods, Applications, Springer-Verlag, New York 1969.
- B.5 Van de Hulst, J., Light Scattering by Small Particles, John Wiley & Sons, Inc., New York, 1957.
- B.6 Hottel, H. C. and Sarofim, A. F., Radiative Transfer, McGraw Hill Publishing Co., New York, 1967.

NOMENCLATURE FOR APPENDIX B

Except for the following, symbols have the same meaning as in the main text.

a	=	volume absorption coefficient, cm^{-1}
d	=	particle diameter, cm
D	=	quantity defined at p. 229
$f(x)$	=	function defined by Eq. (B.2.10)
I_b	=	black body radiant flux intensity, $\text{cal}/\text{cm}^2\text{-s}$
$J(x, \mu)$	=	source function (see Eq. B.1.3)
k	=	volume extinction coefficient, cm^{-1}
l	=	dimensional layer thickness, cm
l_{rad}	=	nondimensional radiant layer thickness for absorbing medium.
l'_{rad}	=	nondimensional radiant layer thickness for absorbing-scattering medium
$P(\mu, \mu')$	=	phase function (see p. 220)
r	=	reflectivity coefficient
R_t	=	total reflectance (see Fig. B.7)
R_v	=	volume reflectance (see Fig. B.7)
R_∞	=	volume reflectance of infinitely thick slab (see pp. 223-224)
s	=	volume scattering coefficient, cm^{-1}
s_f	=	volume forward scattering coefficient, cm^{-1}
s_b	=	volume backward scattering coefficient, cm^{-1}
t	=	dimensional thickness of slab, cm
T_t	=	total transmittance (see Fig. B.7)
T_v	=	volume transmittance (see Fig. B.7)

Greek Symbols

Γ	=	quantity defined at p. 223.
δ_{rad}	=	dimensional radiant layer thickness for absorbing medium, cm
δ'_{rad}	=	dimensional radiant layer thickness for absorbing-scattering medium, cm
η	=	angle (see Fig. B.1)
λ	=	wave length, μm
μ	=	$\cos \eta$
ϕ	=	angle (see Fig. B.1)
ω	=	solid angle (see Fig. B.1)

Abbreviations

abs = absorbed

em = emitted

sca = scattered

LIST OF FIGURES IN
APPENDIX B

Fig. No.	Title	Page
B1.a	Qualitative picture of radiation scattering in an optically heterogeneous medium showing 3-D nature of the phenomenon.	234
B1.b	Axial-symmetric reference system.	234
B2.a	Schematic of diffuse illumination study case.	235
B2.b	Integral balance check for the study case.	235
B3	Schuster-Kubelka solution of diffuse illumination configuration for $s/k = 0.1$ showing little effect of scattering.	236
B4	Schuster-Kubelka solution of diffuse illumination configuration for $s/k = 0.9$ showing large effect of scattering.	237
B5	Schuster-Schwartzchild solution of diffuse illumination configuration for $s/k = 0.9$ showing angular distribution of forward and backward radiant flux intensities.	238
B6	Schematic illustrating the optical properties to be accounted for in the case of polychromatic radiation.	239
B7	Schematic illustrating a possible approach for measuring the optical properties of an heterogeneous medium (see Ref. B2).	240

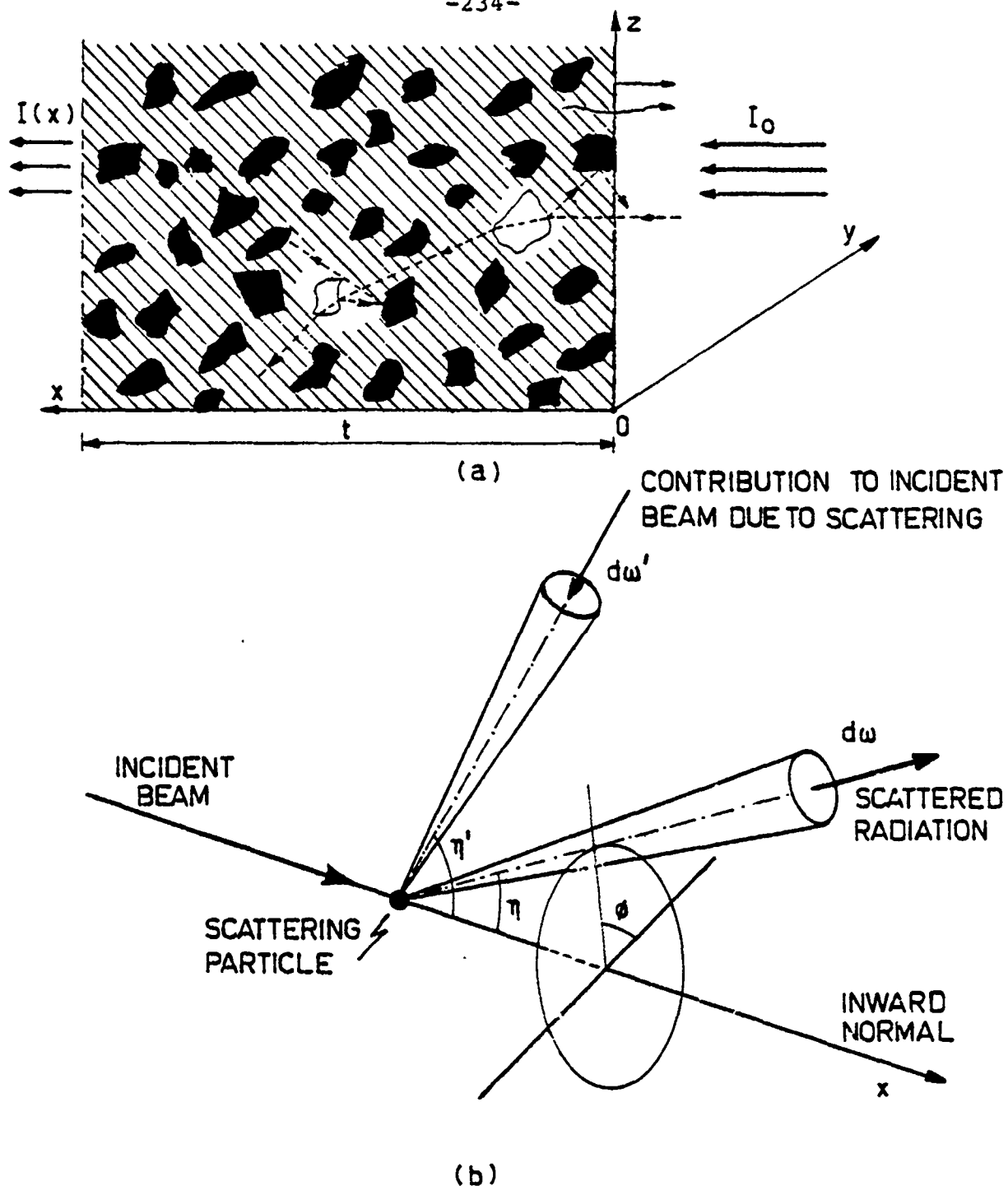


Fig. B1.a Qualitative picture of radiation scattering in an optically heterogeneous medium showing 3-D nature of the phenomenon.

Fig. B1.b Axial-symmetric reference system.

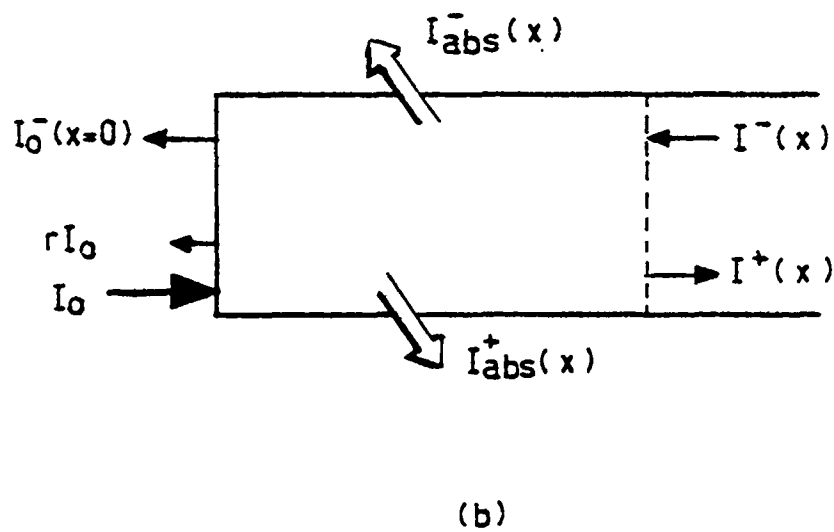
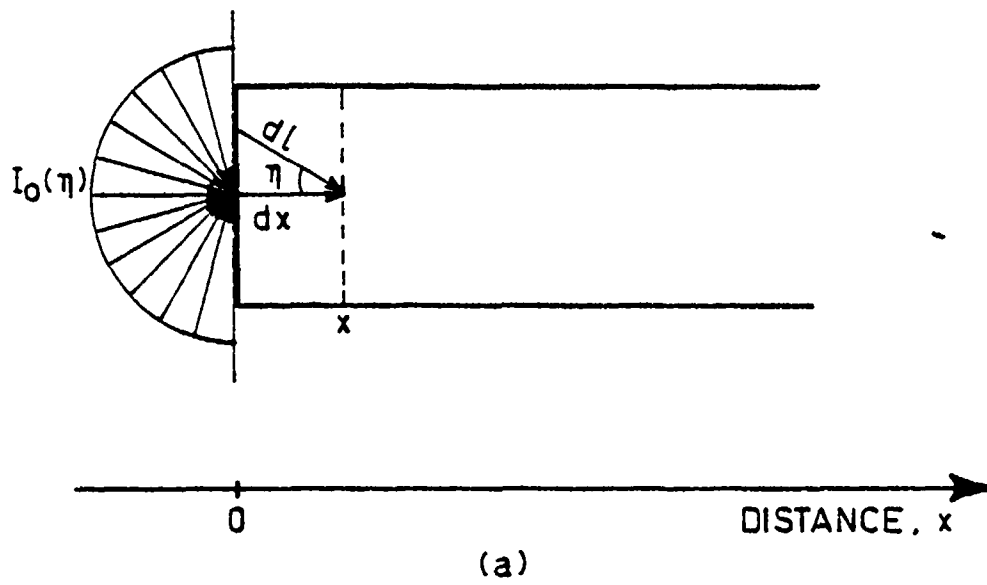


Fig. B2.a Schematic of diffuse illumination study case.

Fig. B2.b Integral balance check for the study case.

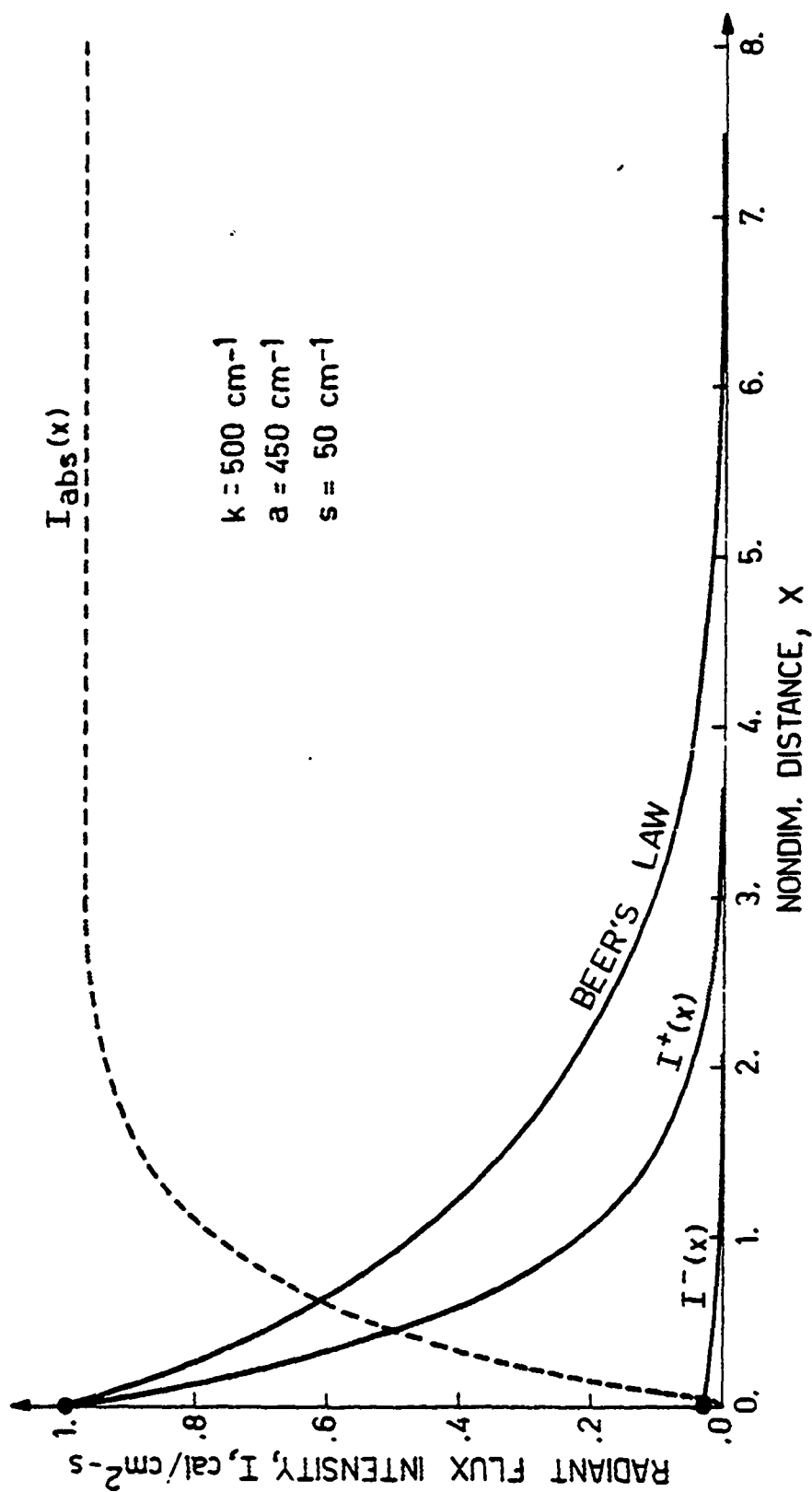


Fig. B3 Schuster-Kubelka solution of diffuse illumination configuration for $s/k=0.1$ showing little effect of scattering.

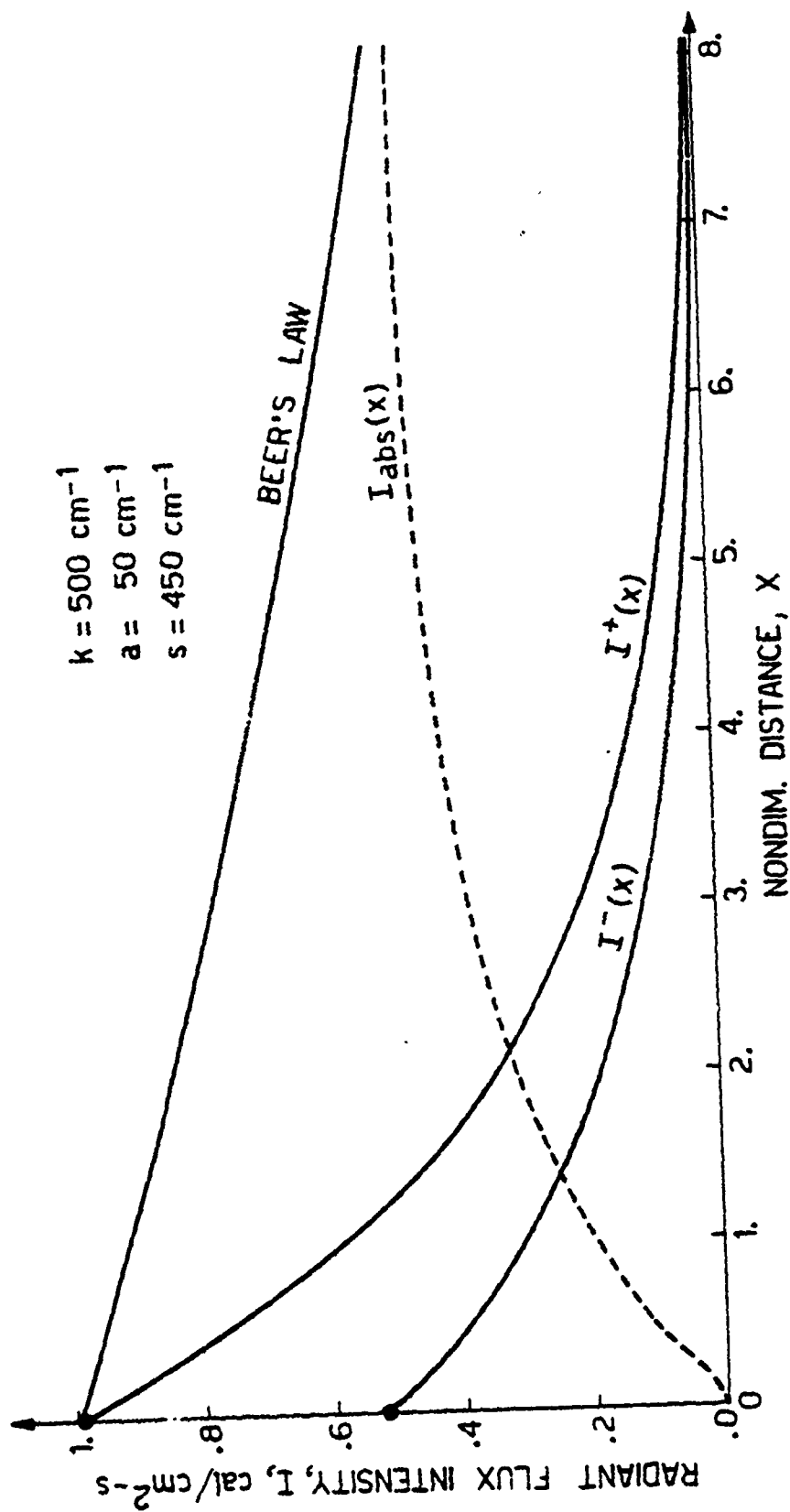


Fig. B4 Schuster-Kuelka solution of diffuse illumination configuration for $s/k=0.9$ showing large effect of scattering.

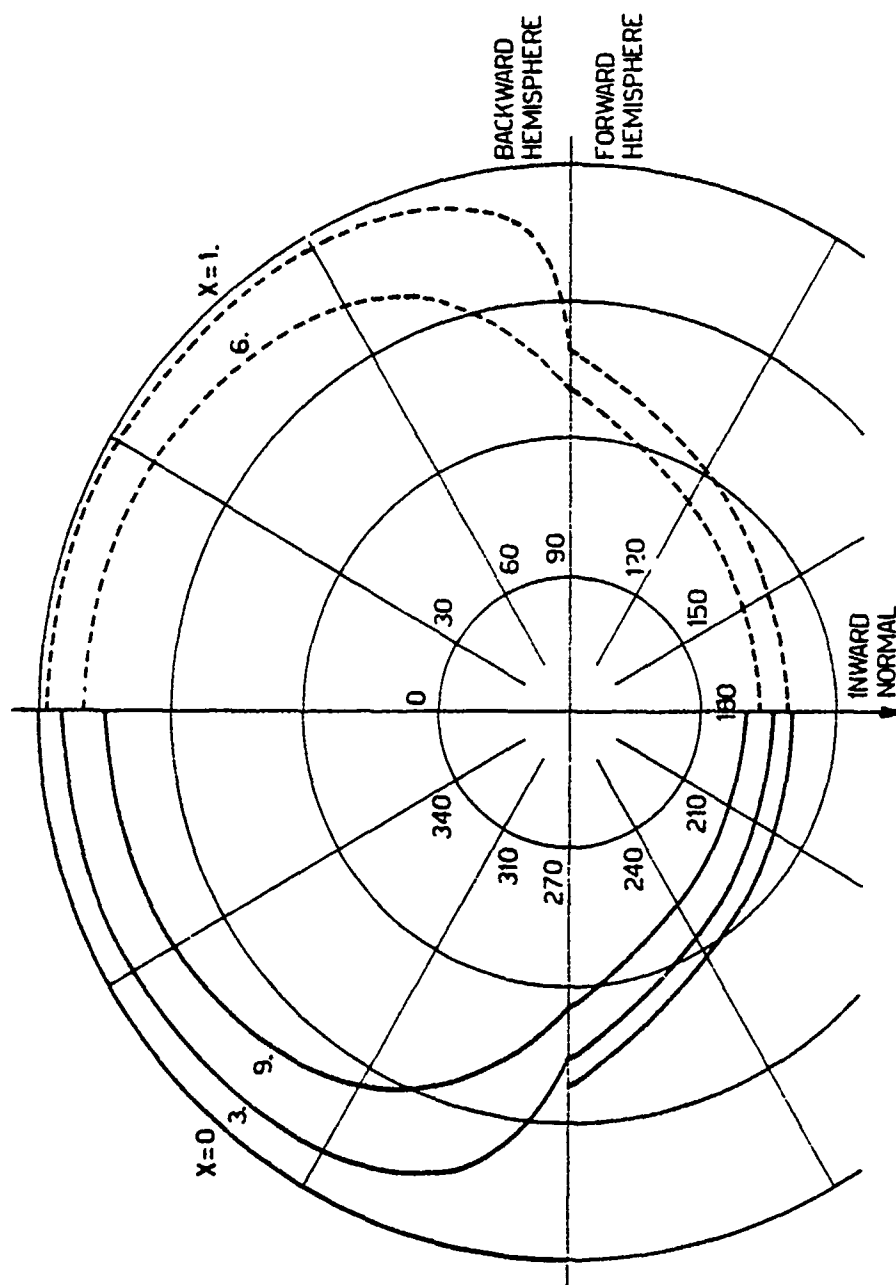


Fig. B5 Schuster-Schwartzchild solution of diffuse illumination configuration for $s/k=0.9$ showing angular distribution of forward and backward radiant flux intensities.

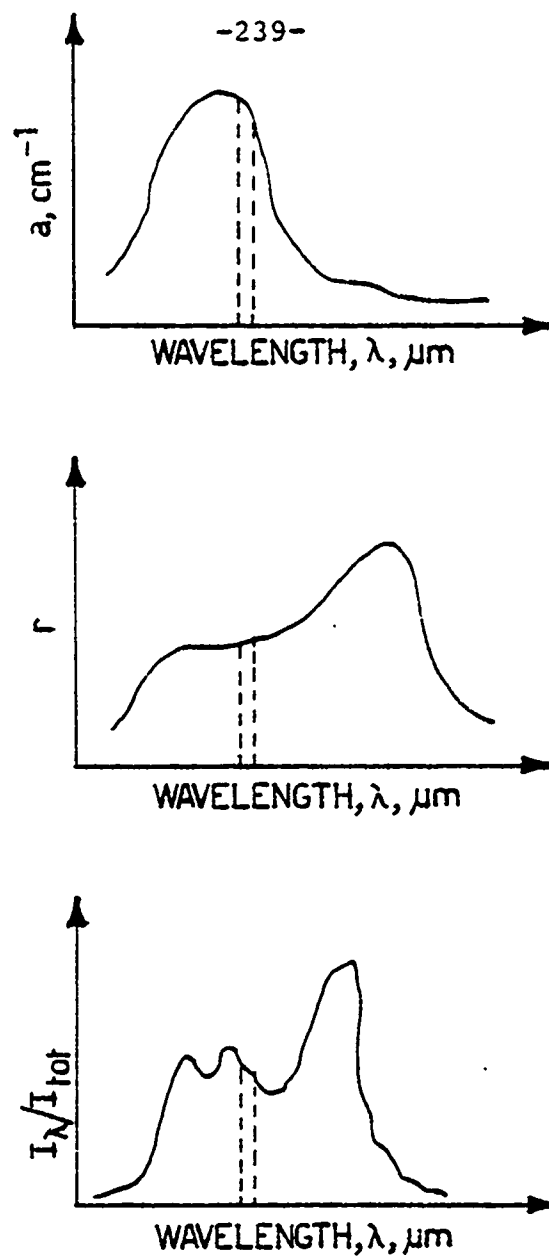
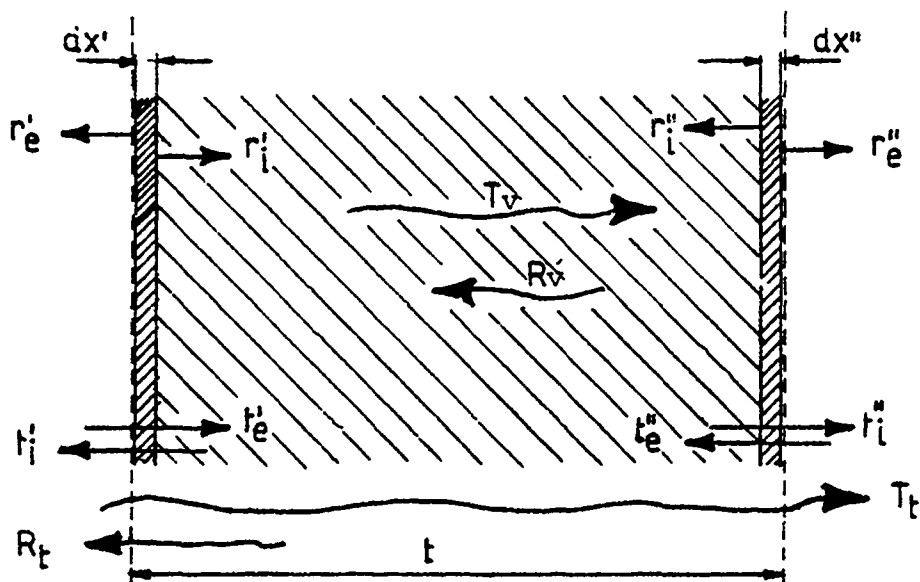


Fig. B6 Schematic illustrating the optical properties to be accounted for in the case of polychromatic radiation.



- r_e', r_e'' = external reflectance of the front, back surface
 t_e', t_e'' = external transmittance of the front, back surface
 r_i', r_i'' = internal reflectance of the front, back surface
 t_i', t_i'' = internal transmittance of the front, back surface
 R_v = pure volume reflectance
 T_v = pure volume transmittance
 R_t = total (front surface+back surface+volume) reflectance
 T_t = total (front surface+back surface+volume) transmittance

Fig. B7 Schematic illustrating a possible approach for measuring the optical properties of a heterogeneous medium (see Ref. B2).